

# **Characterization of trace amine transport properties across human intestinal epithelial cells**

by © Shreyasi Sarkar submitted

to the School of Graduate Studies in partial fulfillment of the  
requirements for the degree of

**Doctor of Philosophy, Department of Biochemistry, Faculty of Science**

Memorial University of Newfoundland

**June 2023**

St. John's, Newfoundland and Labrador

## ABSTRACT

Trace amines (TA), typified by *p*-tyramine (TYR) and 2-phenylethylamine (2-PE), function by activating trace amine-associated receptor 1 (TAAR1), a G protein-coupled receptor. TAAR1 is intracellularly localized and plays important physiological functions. Thus, it is important to know the mechanisms by which TA cellular levels can be controlled. TA can readily diffuse across synthetic lipid bilayers and Organic Cation Transporter 2 (OCT2; *Slc22A2*) was shown to transport TYR in synaptosomes. Whether a similar transporter regulates diet-derived TYR uptake across intestinal epithelial cells is unknown. In this study, I selected the Caco-2 human intestinal cell line to characterize TA transport properties across a Caco-2 monolayer. On studying TYR and 2-PE transport pattern, their transport across the apical membrane was shown to be mediated by a facilitated diffusion transporter which for TYR was decynium-22 ( $P = 0.0092$ ) and pentamidine sensitive ( $P = 0.001$ ), but not atropine (ATR) sensitive, suggesting it is OCT2. Conversely, across the basolateral membrane, Na<sup>+</sup>-dependent ( $P = 0.0174$ ) and ATR sensitive ( $P = 0.020$ ) active TYR transport was observed ( $P < 0.0001$ ), with a trend ( $P = 0.0714$ ) towards active 2-PE transport also observed. Kinetic parameters for the TYR active transporter were  $K_t = 33.1$  nM and  $V_{max} = 43.0$  nM/second. Protein purification by coupling TYR to a *N*-hydroxysuccinimide activated column led to isolation of 124 common TYR and ATR binding proteins from Caco-2 cells, although none of them were Na<sup>+</sup>-dependent transporters. Finally, TYR transport was modelled by developing ordinary differential equations in MATLAB using kinetic parameters of known TYR transport processes and compared to experimental data. Known TYR kinetics did not recapitulate experimental observations, suggesting the presence of additional transporters. Further simulations indicated that asymmetry in apical OCT2 transport ( $K_{t\_OCT2\_apicalto\text{cell}} = 110.4$  nM,  $K_{t\_OCT2\_\text{cell}to\text{apical}} = 1227.9$  nM), and an additional non-OCT2, symmetric, basolateral facilitated diffusion transporter ( $V_{max} = 6.0$  nM/s,  $K_t = 628.3$  nM) were required to recapitulate experimental parameters. In conclusion, OCT2 transports TYR across the apical Caco-2

membrane, while as yet unidentified Na<sup>+</sup>-dependent active transporter and symmetric facilitated diffusion transporter are responsible for TYR transport across Caco-2 basolateral membranes.

## LAY SUMMARY

Trace amines (TA) such as, *p*-tyramine (TYR) and 2-phenylethylamine (2-PE) are naturally occurring compounds that get their name due to their ‘trace’ concentrations. They are present in commonly consumed foods along with being produced by intestinal microbes. TA function by activating a protein known as trace amine-associated receptor 1 (TAAR1) which has been implicated in a variety of physiological functions and disease conditions. Since TAAR 1 is located inside cells, I was interested in determining how TA are transported into cells to provide access to TAAR1. TA can both diffuse through the cell membrane and can also be moved by transporter proteins. Of note, there is a transporter called Organic Cation Transporter 2 (OCT2) which transports TYR in nerve cells. In this thesis, I aimed to find if OCT2 also causes diet-derived TYR transport into intestinal epithelial cells using the Caco-2 human intestinal cell line which mimics the cells of the intestine. I have found distinct TYR transport processes for passage from inside the intestines (luminal) compared to passage from the blood (basolateral). Across the luminal membrane, I confirmed TYR transport to be taking place via OCT2, but across the basolateral membrane TYR was actively accumulated in cells, with the energy for this coming from a sodium gradient. Attempts to isolate and identify this protein were not successful. Finally, I used computer modelling techniques to examine whether there were any additional TYR transport processes occurring. The known TYR transport characteristics did not allow modelling of experimental observation suggesting the presence of additional TYR transporters. Further analysis identified the needed characteristics of this additional transporter. These transporters may serve as important therapeutic targets to modulate TA function and also increase our understanding of host-diet-microbe relationships in health and disease.

## CO-AUTHORSHIP STATEMENT

Parts of the work from this thesis have been published in the following journals:

1. Sarkar, S., and Berry, M.D., (2020). Involvement of Organic Cation Transporter 2 and a Na<sup>+</sup>-dependent active transporter in *p*-tyramine transport across Caco-2 intestinal cells. *Life Sci* 253, 117696. doi: 10.1016/j.lfs.2020.117696.

The contents from Sections 2.1, 2.3, 2.4, 2.6, 3.1, 3.2, 3.4 (except 3.4.1 and 3.4.4), 3.5 (except 3.5.1 and 3.5.2) and 4.2 have been published in this journal. My contributions for the paper included designing of the experiments and performing them, data analysis and interpretation, and preparation of the initial and final drafts of the manuscript with help from my supervisor, Dr. Berry.

2. Sarkar, S., Saika-Voivod, I., and Berry, M.D., (2022). Modelling of *p*-tyramine transport across human intestinal epithelial cells predicts the presence of additional transporters. *Front Physiol* 13, 1009320. doi: 10.3389/fphys.2022.1009320.

The contents from Sections 2.8, 3.7 and 4.4 have been published in this journal. My contributions for this paper included performing simulations, model development, data analysis and interpretation, and preparation of the initial and final drafts of the manuscript with help from Dr. Saika-Voivod and Dr. Berry.

Parts of the thesis that have not been published and are authored by me, with the guidance of my supervisor, include Chapter 1 (all sections), sections 2.2, 2.5, 2.7, 3.3, 3.4.1, 3.4.4, 3.5.1, 3.5.2, 3.6, 4.1, 4.3, 4.5 and 4.6.

## **ACKNOWLEDGEMENTS**

I would first like to thank my supervisor, Dr. Mark D. Berry for giving the opportunity to carry out this research project. I have learnt a lot during this journey through his guidance and support.

I would like to thank him for his patience and for all the help he provided.

I would next like to thank my Supervisory Committee members Dr. David H. Heeley and Dr. Jaeok Park, and my former committee members Dr. Sherri L. Christian and Dr. Margaret Brosnan, for their valuable suggestions and guidance regarding different aspects of my projects.

During COVID19 I had the opportunity to incorporate mathematical modelling into my research. This was made enjoyable and rewarding with all that I learned from Dr. Ivan Saika-Voivod from the Department of Physics and Physical Oceanography and I would like to thank him for his support.

I would also like to thank all my lab mates, colleagues, the faculty and the staff of the Department of Biochemistry for their support and company whenever needed.

Most importantly, my biggest help during my PhD have been my mother, father, sister and my best friend. Without them I would not have been able to gather the strength that was needed to meet all the expectations from my PhD. I would like to thank them immensely for their constant support, continuous patience, and words of motivation at every step of the way. This PhD was possible because of them.

Lastly, this work would not have been possible without my funding agencies, Natural Sciences and Engineering Research Council of Canada, Research and Development Corporation, NL and Memorial University of Newfoundland.

## **TABLE OF CONTENTS**

<b>CHARACTERIZATION OF TRACE AMINE TRANSPORT PROPERTIES ACROSS HUMAN INTESTINAL EPITHELIAL CELLS</b>	<b>I</b>
<b>ABSTRACT</b>	<b>II</b>
<b>LAY SUMMARY</b>	<b>IV</b>
<b>CO-AUTHORSHIP STATEMENT</b>	<b>V</b>
<b>ACKNOWLEDGEMENTS</b>	<b>VI</b>
<b>LIST OF TABLES</b>	<b>XIV</b>
<b>LIST OF FIGURES</b>	<b>XV</b>
<b>LIST OF ABBREVIATIONS</b>	<b>XIX</b>
<b>LIST OF SYMBOLS USED IN EQUATIONS</b>	<b>XXIV</b>
<b>LIST OF APPENDICES</b>	<b>XXVI</b>
<b>1 INTRODUCTION</b>	<b>1</b>
<b>1.1 An overview on trace amines</b>	<b>1</b>
<b>1.2 Vertebrate TA systems</b>	<b>4</b>

1.2.1 AADC-mediated synthesis of TA	4
1.2.2 TA from the diet	7
1.2.3 Microbiota-derived TA	7
1.2.4 Degradation of TA	8
1.2.5 Effects of TA	9
1.2.5.1 TA in the brain	9
1.2.5.2 TA in the periphery	11
1.2.6 TA-linked disorders	13
1.2.6.1 Central nervous system disorders	13
1.2.6.2 Disorders in the periphery	14
<b>1.3 Vertebrate TA receptors – TAARs</b>	<b>14</b>
1.3.1 TAAR subfamilies	16
1.3.2 TAAR1 - the best characterized member of the TAAR family	21
1.3.2.1 Subcellular localization of TAAR1	21
1.3.2.2 TAAR1 signalling cascades	22
1.3.2.3 Central expression and function	23
1.3.2.4 Peripheral expression and function	27
<b>1.4 Transport properties of vertebrate TA</b>	<b>30</b>
1.4.1 Uptake 1 transporters	31
1.4.2 Uptake 2 transporters	32
1.4.2.1 OCT Transporters	33

<b>1.5 Rationale</b>	<b>36</b>
1.5.1 Caco-2 human intestinal epithelial cell line	37
1.5.1.1 Transporter protein profile in Caco-2 cells	38
<b>1.6 Study hypothesis</b>	<b>39</b>
<b>1.7 Study objective</b>	<b>39</b>
<b>2 MATERIALS AND METHODS</b>	<b>41</b>
<b>2.1 Caco-2 cell culture</b>	<b>41</b>
2.1.1 Caco-2 subculture	41
2.1.2 Caco-2 subculture to 24 well Transwell® plate inserts	42
<b>2.2 Assessment of Caco-2 monolayer integrity</b>	<b>44</b>
2.2.1 Lucifer yellow rejection assay	44
2.2.2 Trans epithelial electrical resistance measurement	45
<b>2.3 Trace amine transport across Caco-2 monolayers</b>	<b>47</b>
2.3.1 Subcellular fractionation	47
2.3.2 Trace amine transcellular transport assay	49
2.3.3 Statistical analyses	50
<b>2.4 Characterizing TYR transporters</b>	<b>51</b>
2.4.1 Determination of the role of OCT2 in TYR transport	51
2.4.2 Statistical analyses	51

<b>2.5 Investigation of the presence of OCT2 in Caco-2 cells</b>	<b>52</b>
2.5.1 Preparation of Caco-2 cell lysate	52
2.5.2 Preparation of animal tissue homogenates	52
2.5.3 Preparation of synaptosomes	52
2.5.4 Bicinchoninic Acid (BCA) Protein Assay	53
2.5.5 Western Blot of OCT2	54
<b>2.6 Characterization of TYR active transporter in Caco-2 basolateral membranes</b>	<b>56</b>
2.6.1 Determination of transporter energy source	56
2.6.2 Determination of the kinetic parameters of the TYR active transporter in Caco-2 basolateral membranes	56
<b>2.7 Identification of the TYR active transporter in Caco-2 basolateral membrane</b>	<b>57</b>
2.7.1 Development of TYR affinity columns	57
2.7.2 Purification of TYR binding proteins from Caco-2 cells by affinity chromatography	61
2.7.3. Identification of TYR binding proteins isolated from Caco-2 cells	62
<b>2.8 Modelling of TYR transcellular transport across intestinal epithelial cells</b>	<b>63</b>
2.8.1 Development of mathematical models for known TYR transport processes	63
2.8.2 Development of ordinary differential equations for each compartment	63
2.8.3 Addition of further transporter processes to the Caco-2 membranes	66
2.8.4 Least squares determination of TYR transporter kinetics	72
2.8.4.1 Development of objective functions	73
2.8.4.2 Introduction of model order reduction	76
2.8.4.3 Comparison of modeled fits	78

<b>3 RESULTS</b>	<b>79</b>
<b>3.1 Investigation of TYR binding to the plasma membrane</b>	<b>79</b>
<b>3.2 Transcellular TYR passage</b>	<b>80</b>
3.2.1 Investigation of TYR transport across the apical Caco-2 membrane	80
3.2.2 Investigation of TYR transport across the basolateral Caco-2 membrane	81
<b>3.3 Transcellular 2-PE passage</b>	<b>83</b>
3.3.1 Investigation of 2-PE transport across the apical Caco-2 membrane	83
3.3.2 Investigation of 2-PE transport across the basolateral Caco-2 membrane	84
<b>3.4 Pharmacological characterization of the apical membrane transporter</b>	<b>86</b>
3.4.1 Effect of inhibition of all OCT isoforms on apical TYR transport	86
3.4.2 Effect of inhibition of OCT1 and 2 isoforms on apical TYR transport	88
3.4.3 Effect of inhibition of OCT1 on apical TYR transport	88
3.4.4 Investigation of the presence of OCT2 in Caco-2 cells	89
<b>3.5 Pharmacological characterization of the basolateral membrane transporter</b>	<b>92</b>
3.5.1 Effect of inhibition of all OCT isoforms on basolateral TYR transport	92
3.5.2 Effect of inhibition of OCT1 and OCT2 isoforms on basolateral TYR transport	93
3.5.3 Effect of inhibition of OCT1 on basolateral TYR transport	94
3.5.4 Effect of the replacing sodium on TYR transport	94
3.5.5 Kinetic characterization of the Na <sup>+</sup> -dependent, active transporter of TYR in Caco-2 basolateral membranes	96

<b>3.6 Identification of the basolateral membrane active transporter</b>	<b>97</b>
3.6.1 SDS PAGE isolation of proteins from TYR affinity columns	97
3.6.2 Protein identification	99
<b>3.7 Modelling of TYR transport kinetics across human intestinal epithelial cells</b>	<b>100</b>
3.7.1 Comparison of baseline simulation with experimental	100
3.7.2 Introduction of OCT2 in the basolateral membrane.	103
3.7.3 Introduction of a non-OCT2 facilitated diffusion transporter in the basolateral membrane	105
3.7.4 Introduction of asymmetry in facilitated diffusion transporters	107
3.7.5 Introduction of intracellular compartmentalization	109
<b>4 DISCUSSION</b>	<b>112</b>
<b>4.1 Caco-2 cells offer a suitable polarized model system for TA transport</b>	<b>112</b>
<b>4.2 There are distinct TA transport processes across apical and basolateral Caco-2 membranes</b>	<b>114</b>
4.2.1 TYR and 2-PE are transported by a diffusion-mediated process across the Caco-2 apical membrane	115
4.2.2 The apical TYR transporter is OCT2 in Caco-2 cells	115
4.2.3 TYR and 2-PE are transported via an active transport process across the basolateral membrane	118
4.2.4 TYR active transport is Na <sup>+</sup> -dependent	119
<b>4.3 TYR affinity column isolated proteins do not fit transporter selection criteria</b>	<b>122</b>

<b>4.4 Modelling of TYR transport predicts the presence of additional TYR transporters</b>	<b>124</b>
<b>4.5 Conclusions</b>	<b>132</b>
<b>4.6 Limitations and future directions</b>	<b>134</b>
<b>5. REFERENCES</b>	<b>136</b>
<b>6. APPENDIX</b>	<b>208</b>
<b>A. All common TYR and ATR binding proteins identified from Caco-2 cell</b>	<b>208</b>
<b>B. Codes used for MATLAB to investigate the presence of additional TYR transporters in Caco-2 cell</b>	<b>216</b>
B.i Solving baseline and plotting	216
B.ii Introducing OCT2 in the basolateral membrane at varying densities and plotting	225
B.iii Introducing a transporter with non-OCT2 kinetics in the basolateral membrane and plotting	240
B.iv. Solving for asymmetry and plotting	255
B.v. Solving for intracellular compartmentalization and plotting	280
<b>C. Copyright licences</b>	<b>313</b>
C.i Copyright licence for first paper	313
C.ii Copyright licence for second paper	314

## **LIST OF TABLES**

**Table 1.1: Functional human TAARs (hTAARs) and their endogenous TA substrates..... 16**

**Table 3.1: Classification of common TYR and ATR binding proteins. .... 100**

**Table 3.2: Kinetic parameters used for each model scenario. .... 102**

**Table 4.1: Required kinetic parameters to recapitulate experimental TYR transport..... 129**

## LIST OF FIGURES

<b>Figure 1.1: Structures of representative examples of endogenous TA .....</b>	<b>2</b>
<b>Figure 1.2: Metabolic pathways of TA.....</b>	<b>6</b>
<b>Figure 1.3: Subcellular localization of TAAR1 .....</b>	<b>22</b>
<b>Figure 1.4: Characterization of TA transport property across Caco-2 intestinal epithelial cells .....</b>	<b>40</b>
<b>Figure 2.1: Schematic representation of the Caco-2 cell monolayer culture system .....</b>	<b>43</b>
<b>Figure 2.2: Caco-2 monolayer development as a function of lucifer yellow exclusion .....</b>	<b>45</b>
<b>Figure 2.3: Development of a functional Caco-2 monolayer as a function of trans epithelial electrical resistance measurement .....</b>	<b>47</b>
<b>Figure 2.4: Sample radioisotope assay standard curve to determine picomoles of TYR in subcellular compartments .....</b>	<b>49</b>
<b>Figure 2.5: Sample BCA protein assay standard curve to determine amount of total protein .....</b>	<b>54</b>
<b>Figure 2.6: Absorption spectra of TYR and NHS.....</b>	<b>58</b>
<b>Figure 2.7: Absorption spectra of TYR and NHS in the presence of NaOH.....</b>	<b>59</b>
<b>Figure 2.8: Confirmation of TYR attachment to an NHS-column.....</b>	<b>60</b>
<b>Figure 2.9: Known TYR transport processes across Caco-2 cells representing the baseline simulation model .....</b>	<b>65</b>
<b>Figure 2.10: Known and predicted TYR transporters used for modelling transcellular passage in Caco-2 cells.....</b>	<b>67</b>

<b>Figure 2.11: Schematic representation of the Caco-2 model including an intracellular compartment for TYR sequestration .....</b>	<b>70</b>
<b>Figure 3.1: Subcellular distribution of TYR in Caco-2 cells.....</b>	<b>79</b>
<b>Figure 3.2: Transcellular [<sup>3</sup>H]TYR passage following addition to the apical compartment. ....</b>	<b>81</b>
<b>Figure 3.3: Transcellular [<sup>3</sup>H]TYR passage following addition to the basolateral compartment .....</b>	<b>82</b>
<b>Figure 3.4: Total transcellular transport across Caco-2 cells following apical and basolateral addition of [<sup>3</sup>H]TYR. ....</b>	<b>83</b>
<b>Figure 3.5: Transcellular [<sup>14</sup>C]2-PE passage following addition to the apical compartment. ....</b>	<b>84</b>
<b>Figure 3.6: Transcellular [<sup>14</sup>C]2-PE passage following addition to the basolateral compartment. ....</b>	<b>85</b>
<b>Figure 3.7: Total transcellular transport across Caco-2 cells following apical and basolateral addition of [<sup>14</sup>C]2-PE. ....</b>	<b>86</b>
<b>Figure 3.8: Total transcellular transport of TYR across Caco-2 cells following apical compartment loading in the presence and absence of decynium 22 .....</b>	<b>87</b>
<b>Figure 3.9: Total transcellular transport of TYR across Caco-2 cells following apical compartment loading in the presence and absence of pentamidine.....</b>	<b>88</b>
<b>Figure 3.10: Total transcellular transport of TYR across Caco-2 cells following apical compartment loading in the presence and absence of atropine.....</b>	<b>89</b>
<b>Figure 3.11: Western blot to look for the presence of OCT2 in Caco-2 cells.....</b>	<b>90</b>

<b>Figure 3.12 Western blot to look for the presence of OCT2 in Caco-2 cells with reversal of order of the use of primary antibodies.....</b>	<b>91</b>
<b>Figure 3.13: Total transcellular transport of TYR across Caco-2 cells following basolateral compartment loading in the presence and absence of decynium 22 .....</b>	<b>92</b>
<b>Figure 3.14: Total transcellular transport of TYR across Caco-2 cells following basolateral compartment loading in the presence and absence of pentamidine.....</b>	<b>93</b>
<b>Figure 3.15: Total transcellular transport of TYR across Caco-2 cells following basolateral compartment loading in the presence and absence of atropine.....</b>	<b>94</b>
<b>Figure 3.16: Total transcellular transport of TYR across Caco-2 cells following basolateral compartment loading in the presence and absence of choline chloride.....</b>	<b>95</b>
<b>Figure 3.17: Total transcellular transport of TYR across Caco-2 cells following apical compartment loading in the presence and absence of choline chloride.....</b>	<b>96</b>
<b>Figure 3.18: Kinetics of basolateral Caco-2 Na<sup>+</sup>-dependent active TYR transporter .....</b>	<b>97</b>
<b>Figure 3.19: Representative SDS PAGE image of the elution profile from TYR affinity columns .....</b>	<b>98</b>
<b>Figure 3.20: Representative SDS-PAGE of Caco-2 proteins eluted from TYR affinity columns .....</b>	<b>99</b>
<b>Figure 3.21: Comparison of the baseline model for TYR transport following basolateral loading to experimental findings .....</b>	<b>101</b>
<b>Figure 3.22: Comparison of the baseline model for TYR transport following apical loading to experimental findings.....</b>	<b>103</b>
<b>Figure 3.23: Comparison of TYR transport with the introduction of OCT2 to the Caco-2 basolateral membrane, following basolateral TYR loading, to experimental findings .....</b>	<b>104</b>

<b>Figure 3.24: Comparison of TYR transport with the introduction of OCT2 to the Caco-2 basolateral membrane, following apical TYR loading, to experimental findings.....</b>	<b>105</b>
<b>Figure 3.25: Comparison of TYR transport with the introduction of a non-OCT2 facilitated diffusion transporter to the Caco-2 basolateral membrane, following basolateral TYR loading, to experimental findings .....</b>	<b>106</b>
<b>Figure 3.26: Comparison of TYR transport with the introduction of a non-OCT2 facilitated diffusion transporter to the Caco-2 basolateral membrane, following apical TYR loading, to experimental findings .....</b>	<b>107</b>
<b>Figure 3.27: Comparison of TYR transport with the introduction of asymmetry in OCT2 and the facilitated diffusion transporter in the Caco-2 basolateral membrane, following basolateral TYR loading, to experimental findings .....</b>	<b>108</b>
<b>Figure 3.28: Comparison of TYR transport with the introduction of asymmetry in OCT2 and the facilitated diffusion transporter in the Caco-2 basolateral membrane, following apical TYR loading, to experimental findings.....</b>	<b>109</b>
<b>Figure 3.29: Comparison of TYR transport with the introduction of compartmentalization and symmetry in the facilitated diffusion transporter in the Caco-2 basolateral membrane, following basolateral TYR loading, to experimental findings .....</b>	<b>110</b>
<b>Figure 3.30: Comparison of TYR transport with the introduction of compartmentalization and symmetry in the facilitated diffusion transporter in the Caco-2 basolateral membrane, following apical TYR loading, to experimental findings.....</b>	<b>111</b>
<b>Figure 4.1: Binding of TYR to NHS-activated Sepharose column.....</b>	<b>122</b>
<b>Figure 4.2: Proposed TYR transport mechanisms across Caco-2 cells. ....</b>	<b>133</b>

## LIST OF ABBREVIATIONS

AADC: Aromatic amino acid decarboxylase

AMPA:  $\alpha$ -Amino-3-hydroxy-5-methyl-4-isoxazole propionic acid

AKT: Protein kinase B

ATR: Atropine

BSA: Bovine serum albumin

cAMP: Cyclic AMP

COMT: Catechol-O-methyl transferase

CREB: cAMP response element binding protein

DAT: Dopamine transporter

D $\beta$ H: Dopamine  $\beta$ -hydroxylase

D1R: Dopamine D1 receptor

D2R: Dopamine D2 receptor

DTC: Sodium diethyldithiocarbamate trihydrate

EC: Enzyme commission

GirK: G protein-coupled inwardly rectifying potassium

GPCR: G protein-coupled receptor

GLP-1: Glucagon-like peptide 1

GLUT1 : Glucose transporter 1

GLUT2 : Glucose transporter 2

GLUT3 : Glucose transporter 3

GLUT4 : Glucose transporter 4

GLUT5: Glucose transporter 5

GSK-3 $\beta$ : Glycogen synthase kinase 3 $\beta$

HBSS: Hank's balanced salt solution

HEPES: 4-(2-Hydroxyethyl)-1-piperazineethanesulfonic acid

5-HT<sub>1A</sub>: 5-Hydroxytryptamine 1A

5-HT<sub>1B</sub>: 5-Hydroxytryptamine 1B

5-HT<sub>2A</sub>: 5-Hydroxytryptamine 2A

IAA : Isoamylamine

INMT : Indolethylamine-*N*-methyltransferase

IL-1 $\beta$  : Interleukin 1 $\beta$

IL-6: Interleukin 6

3-IT: 3-iodothyronamine

KO: Knock-out

LC-MS/MS: Liquid chromatography tandem mass spectrometry

LY: Lucifer yellow

MAO: Monoamine oxidase

NET: Norepinephrine transporter

NMDA: N-methyl-D-aspartate

NHS: *N*-hydroxysuccinimide

NK: Natural killer

OA: Octopamine

OCT: Organic cation transporter

OCT1: Organic cation transporter 1

OCT2: Organic cation transporter 2

OCT3: Organic cation transporter 3

ODE: Ordinary differential equation

PAH: Phenylalanine hydroxylase

PBS: Phosphate buffered saline

PepT1: Peptide transporter 1

PHT1: Peptide/histidine transporter 1

PHT2: Peptide/histidine transporter 2

2-PE: 2-Phenylethylamine

PMAT: Plasma membrane monoamine transporter

PNMT: Phenylethanolamine-*N*-methyl transferase

PKA: Protein kinase A

PKC: Protein kinase C

PKG: Protein kinase G

PYY: Peptide YY

RMSD: Root mean square deviation

SDS: Sodium dodecyl sulphate

SDS PAGE: Sodium dodecyl sulphate polyacrylamide gel electrophoresis

SEM: Standard error of measurement

SERT : Serotonin transporter

SLC : Solute carrier

SYN : Synephrine

TA: Trace amines

TAAR: Trace amine-associated receptor

TBST: Tris buffered saline-Tween<sup>®</sup> 20

TEER: Trans epithelial electrical measurement

T<sub>h</sub>: T helper

TH: Tyrosine hydroxylase

TMA: Trimethylamine

TRP: Tryptamine

TNF $\alpha$ : Tumour necrosis factor  $\alpha$

TYR: *p*-Tyramine

## LIST OF SYMBOLS USED IN EQUATIONS

$A$ : surface area of the membrane

$F_{\text{blank}}$ : fluorescence of the assay buffer

$F_{\text{cell\_monolayer}}$ : fluorescence of basolateral compartment solutions derived from chambers containing Caco-2 cells

$F_{\text{LY}}$ : fluorescence of the LY solution

$K_{\text{t\_baso\_active}}$ :  $K_t$  of basolateral active transporter

$K_{\text{t\_baso\_new\_FD\_basotocell}}$ :  $K_t$  of new basolateral facilitated diffusion transporter

$K_{\text{t\_OCT2\_apicalto cell}}$ :  $K_t$  of new basolateral facilitated diffusion transporter

$K_{\text{t\_OCT2\_celltoapical}}$ :  $K_t$  of OCT2 in the cell to apical direction

$K_{\text{t\_new\_FD\_celltobaso}}$ :  $K_t$  of OCT2 in the cell to basolateral direction

$Q_A$ : Global objective function for apical

$Q_B$ : Global objective function for basolateral

$Q_{\text{apical}}$ : Objective function for apical compartment

$Q_{\text{cell}}$ : Objective function for cellular compartment

$Q_{\text{baso}}$ : Objective function for basolateral compartment

$Q_{\text{cell,apical}}$ : Objective function for apical compartment

$Q_{\text{cell,basolateral}}$ : Objective function for apical compartment

$p$  : permeability coefficient of TYR

$R_{\text{blank}}$ : electrical resistance across the Transwell<sup>®</sup> inserts containing no Caco-2 cells

$R_{\text{cell\_monolayer}}$ : electrical resistance across the Caco-2 monolayer

$R_{\text{insert}}$ : electrical resistance across the Transwell<sup>®</sup> inserts containing Caco-2 cells

$V_{\text{max\_OCT2}}$ :  $V_{\text{max}}$  of OCT2

$V_{\text{max\_baso\_active}}$ :  $V_{\text{max}}$  of basolateral active transporter

$V_{\text{max\_baso\_new\_FD}}$ :  $V_{\text{max}}$  of new basolateral facilitated diffusion transporter

$Vol_{\text{apical}}$ : Volume of apical compartment

$Vol_{\text{baso}}$ : Volume of basolateral compartment

$Vol_{\text{cell}}$ : Volume of cellular compartment

$X_1$ : concentration of TYR in the donor compartment

$X_2$ : concentration of TYR in the receiver compartment

## **LIST OF APPENDICES**

A. All common TYR and ATR binding proteins identified from Caco-2 cell

B. Codes used for MATLAB to investigate the presence of additional TYR transporters in Caco-2 cell

C. Copyright licences

# 1 INTRODUCTION

## 1.1 An overview on trace amines

Trace amines (TA) are a family of endogenous compounds that are responsible for regulating a myriad of physiological functions (Borowsky et al., 2001; Bunzow et al., 2001; Revel et al., 2011; Berry et al., 2017; Christian and Berry, 2018; Gainetdinov et al., 2018; Rutigliano et al., 2018; Nair et al., 2022). The name TA was deduced due to their relatively low concentration in mammalian tissues in comparison to the more abundant monoamine neurotransmitters dopamine, serotonin, epinephrine and norepinephrine to which TA are structurally and metabolically related (Berry, 2004; Farooqui and Farooqui, 2016; Gainetdinov et al., 2018). At 1-10 ng/g tissue, which is equivalent to a 10-100 nM endogenous concentration (Berry, 2004), TA represent less than 1% of the total biogenic amines which are synthesized in various cell types within the body (Berry, 2004; Gainetdinov et al., 2018). Classical examples of TA include *m*-, *o*- and *p*-tyramine (*m*-, *o*- and TYR), 2-phenylethylamine (2-PE), tryptamine (TRP), *m*- and *p*-octopamine (*m*- and OA), and synephrine (SYN) (Figure 1.1). Other more recently described TA include isoamylamine (IAA), trimethylamine (TMA), and 3-iodothyronamine (3-IT) (Figure 1.1).

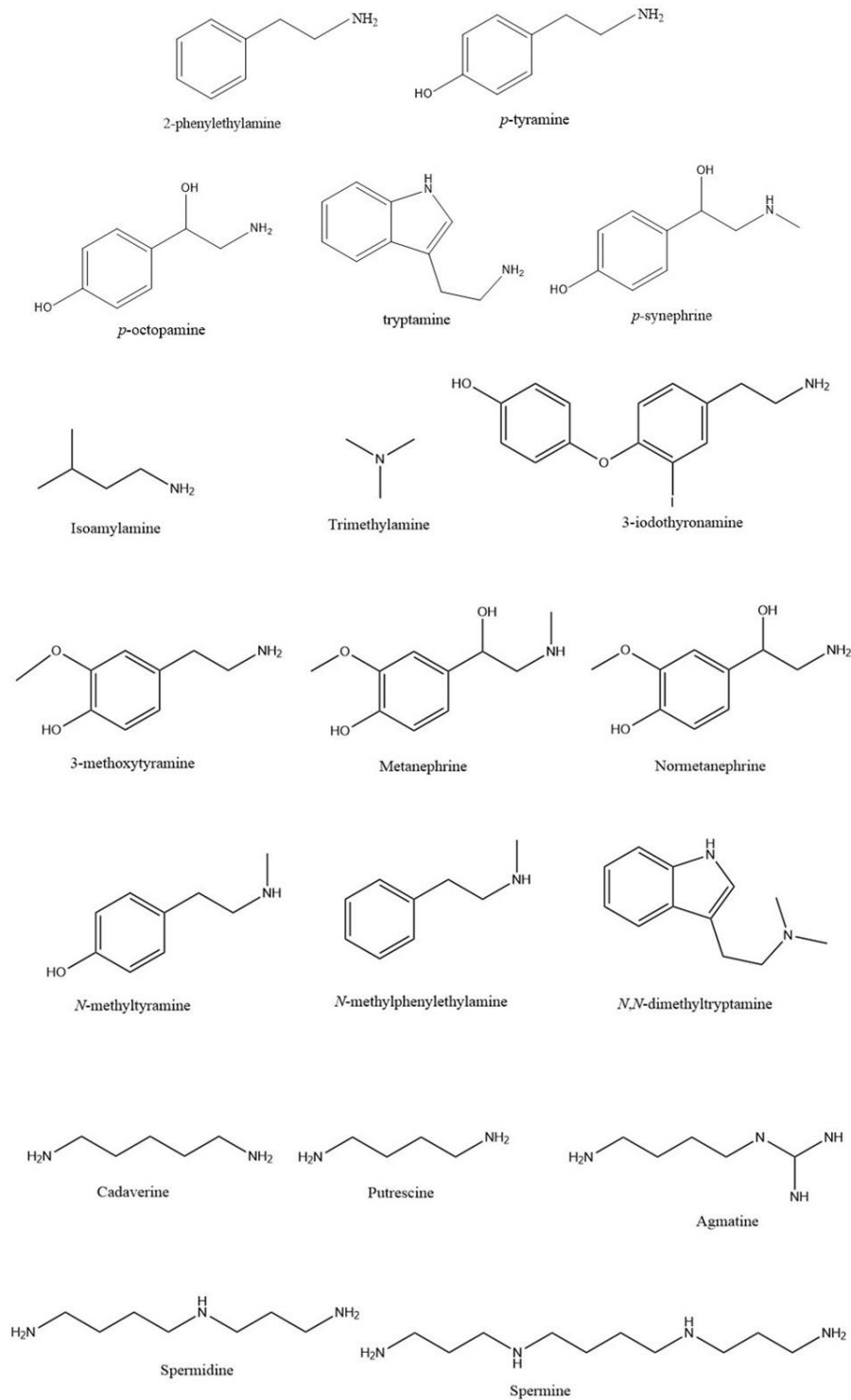


**Figure 1.1: Structures of representative examples of endogenous TA.** The figure was generated in ChemDraw 22.0.0.

The TA systems serve different functions in invertebrates and vertebrates. The invertebrate TA system primarily serves the role of monoaminergic neurotransmitters, involved in regulating a variety of behavioural and physiological processes (Downer et al., 1993; Roeder, 2005; Anton et al., 2007; Farooqui, 2007; Kononenko et al., 2009; Homberg et al., 2013). The vertebrate TA system, however, functions through unique G protein-coupled trace amine-associated receptors (TAARs), which regulate pre-existing signals in neuronal (Borowsky et al., 2001; Bunzow et al., 2001; Revel et al., 2011; Berry et al., 2017; Christian and Berry, 2018; Gainetdinov et al., 2018; Rutigliano et al., 2018; Alnefeesi et al., 2021; Nair et al., 2022), metabolic (Raab et al., 2016; Berry et al., 2017; Christian and Berry, 2018; Gainetdinov et al., 2018; Rutigliano et al., 2018; Batista-Lima et al., 2019; Cripps et al., 2020)), and immune (Babusyte et al., 2013; Harmeier et al., 2015; Jacobs et al., 2016; Berry et al., 2017; Santoru et al., 2017; Christian and Berry, 2018; Gainetdinov et al., 2018; Rutigliano et al., 2018) systems. Other TA such as certain *O*-methyl derivatives of monoamines including 3-methoxytyramine, metanephrine, and normetanephrine, and *N*-methyl metabolites of TA, such as *N*-methyltyramine, *N*-methylphenylethylamine and *N,N*-dimethyltryptamine, have also been shown to be TAAR ligands (Lindemann et al., 2005). In addition to these compounds, polyamines, such as cadaverine, putrescine, spermidine, spermine and agmatine can also act as TAAR ligands (Li et al., 2015). Further, the role of TAARs as a novel class of receptors for olfaction in pheromone and kairomone detection (Brahmachary and Dutta, 1979; Nishimura et al., 1989; Liberles, 2014) has also gained attention in vertebrate species. My thesis focusses on non-olfactory TA functions, and these are described in more detail below.

## 1.2 Vertebrate TA systems

TA are produced within the body by aromatic L-amino acid decarboxylase (AADC; EC 4.1.1.28) via decarboxylation of precursor amino acids (Boulton and Wu, 1972, 1973; Saavedra, 1974; Snodgrass and Iversen, 1974; Silkaitis and Mosnaim, 1976; Dyck et al., 1983). TA are also found in common dietary items (Coutts et al., 1986; Finberg and Gillman, 2011; An et al., 2015; Biji et al., 2016; Martin and Vij, 2016; Nalazek-Rudnicka and Wasik, 2017; Ohta et al., 2017; Liu et al., 2018; Park et al., 2019; Zhang et al., 2019; Chen et al., 2022). In addition, TA are synthesized by the intestinal microflora (Marcobal et al., 2006; Irsfeld et al., 2013; Williams et al., 2014; Zhu et al., 2014; Yang et al., 2015; Barbieri et al., 2019; Pretorius and Smith, 2020).

### 1.2.1 AADC-mediated synthesis of TA

The major pathway of TA synthesis in vertebrates is from the decarboxylation of amino acids by the enzyme AADC (Boulton and Wu, 1972, 1973; Snodgrass and Iversen, 1974; Silkaitis and Mosnaim, 1976; Dyck et al., 1983). AADC has been shown to exhibit broad substrate selectivity. Initially, L-5-hydroxytryptophan and L-DOPA were reported to be preferred substrates for AADC (Lovenberg et al., 1962; Christenson et al., 1970; Saavedra and Axelrod, 1973), producing serotonin and dopamine, respectively. L-phenylalanine can be converted to L-tyrosine by the action of phenylalanine hydroxylase (PAH) or tyrosine hydroxylase (TH). The decarboxylation of L-tyrosine results in the formation of TYR, decarboxylation of L-phenylalanine leads to the formation of 2-PE, and TRP is formed from the decarboxylation of L-tryptophan (Figure 1.2) (Boulton and Wu, 1972, 1973; Snodgrass and Iversen, 1974; Silkaitis and Mosnaim, 1976; Dyck et al., 1983). The AADC gene consists of fifteen exons located on human chromosome 7p12.1-12.3 (Sumi-Ichinose et al., 1995), with alternative splicing variants reported (Duan et al., 2004;

Bly, 2005; Lindemann et al., 2008; Xie et al., 2008). AADC is present in neuronal and glial cells (Li et al., 1992; Juorio et al., 1993; Xie et al., 2008), blood vessels (Li et al., 2014), intestine (Lauweryns and Van Ranst, 1988; Vieira-Coelho and Soares-da-Silva, 1993), kidney (Christenson et al., 1970; Aperia et al., 1990; Hayashi et al., 1990; Lancaster and Sourkes, 2011), liver (Bouchard and Roberge, 1979; Ando-Yamamoto et al., 1987; Dominici et al., 1987), lungs (Lauweryns and Van Ranst, 1988; Linnoila et al., 1993), pancreas (Lindstrom and Sehlin, 1983; Furuzawa et al., 1994; Rorsman et al., 1995) and stomach (Lichtenberger et al., 1982), which are therefore possible sites of TA synthesis. In addition, reports of the presence of AADC but not TH or tryptophan hydroxylase in mammalian D-neurons suggests that these enzymes may form a dedicated neuronal TA system (Jaeger et al., 1983, 1984; Fetissoff et al., 2009; Kitahama et al., 2009). These locations of AADC largely mirror the known location of TA and TAARs (Regard et al., 2007; Ito et al., 2009; Revel et al., 2013; Gainetdinov et al., 2018) hence, it is likely that localized formation occurs in such regions. Further, as can be seen from Figure 1.2, OA and SYN can be formed from TYR by the action of dopamine  $\beta$ -hydroxylase (D $\beta$ H; EC 1.14.17.1) and phenylethanolamine-*N*-methyl transferase (PNMT; EC 2.1.128) (Boulton and Wu, 1972, 1973). The action of PMNT and indolethylamine *N*-methyltransferase (INMT; EC 2.1.1.49) results in the *N*-methylation of TA which gives rise to the production of additional TAAR ligands, *N*-methylphenylethylamine, *N*-methyltyramine, and *N*-methyltryptamine (Saavedra and Axelrod, 1972; Lindemann et al., 2005; Zucchi et al., 2006) (Figure 1.2). The enzyme catechol-*O*-methyl transferase (COMT; EC 2.1.1.6) converts dopamine to 3-methoxytyramine, which is also a TAAR ligand (Bunzow et al., 2001; Sotnikova et al., 2010).

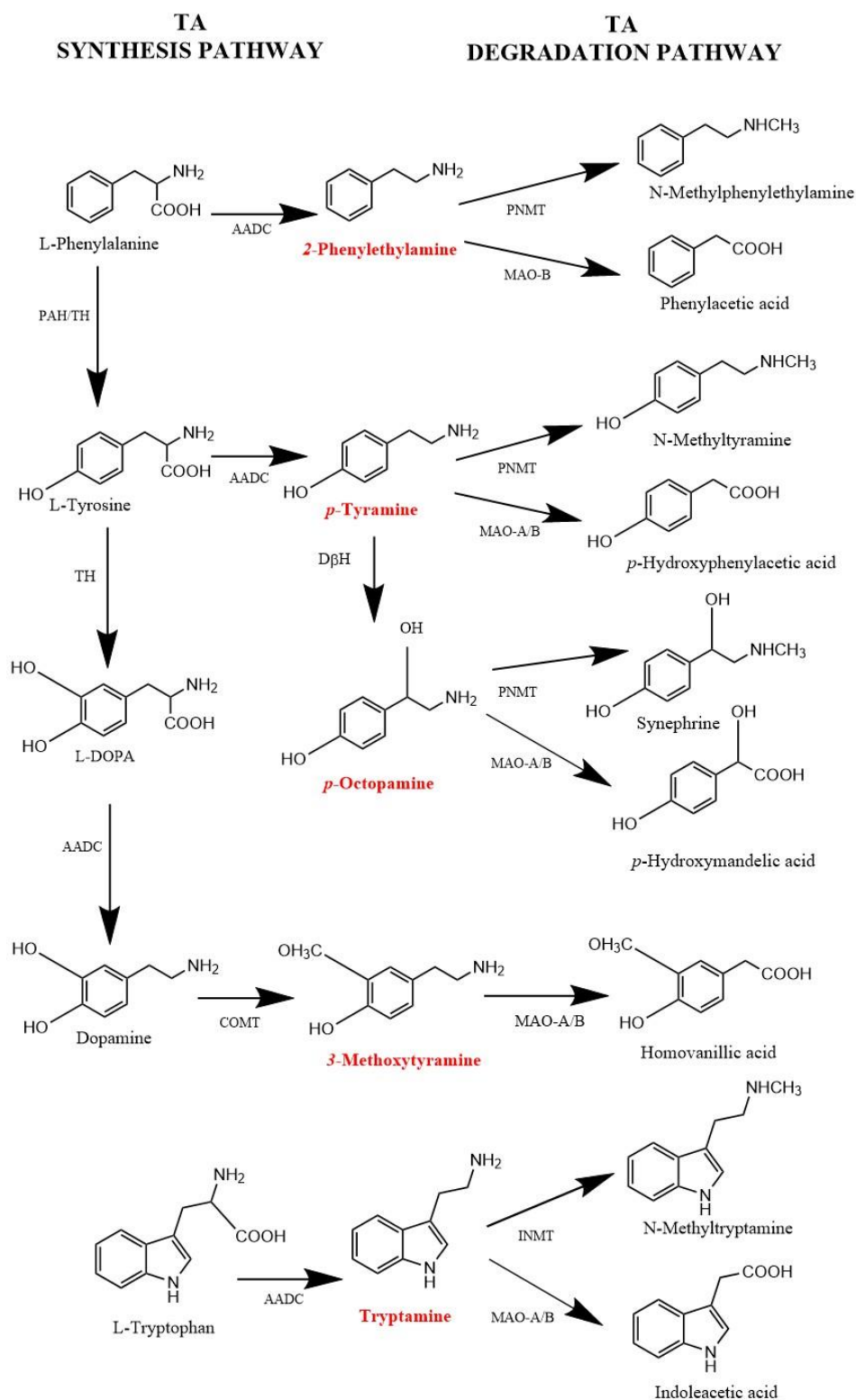


**Figure 1.2: Metabolic pathways of TA.** Pathways showing synthesis, degradation, and interconversion of TA. Traditional TA are denoted in red. Figure was generated in ChemDraw 22.0.0.

### 1.2.2 TA from the diet

Common dietary items have long been reported to contain abundant levels of TA such as TYR, 2-PE and TRP (Coutts et al., 1986). Reported sources of TA include aged cheeses, fermented food products such as meat, red wine, soy products, and chocolate (Coutts et al., 1986). Seafood sources that include molluscs, crustaceans and fish, have been shown to be a rich source of various TA, such as 2-PE, OA, TRP and TYR (An et al., 2015; Biji et al., 2016; Chen et al., 2022). Various herbal extracts used as medicine in different cultures such as, Ginkgo biloba (Könczöl et al., 2016), Chinese herbal medicines (Zhang et al., 2016) and Indian herbal brews (Leonti and Casu, 2014) have also been reported to contain TA.

Adverse reactions to TA rich food such as cheese, wine and seafood have been reported (Finberg and Gillman, 2011b; Biji et al., 2016). For example, a condition known as the ‘cheese effect’ has been reported with increased TYR accumulation seen in patients prescribed monoamine oxidase (MAO; EC 1.4.3.4) inhibitors (Sabelli and Mosnaim, 1974; Sabelli et al., 1996) following ingestion of high TYR containing foods, which results in increased blood norepinephrine levels and leads to hypertensive crisis, migraine and death (Price and Smith, 1971; Stratton et al., 1991; Anderson et al., 1993; Shalaby, 1996; Finberg and Gillman, 2011).

### 1.2.3 Microbiota-derived TA

It has been well-established that there is a clear association between diet, gastrointestinal microbiota, and health (Dinan and Cryan, 2015; Honda and Littman, 2016; Thaïss et al., 2016; Alexander et al., 2017; Brunkwall and Orho-Melander, 2017; Fung et al., 2017; Luo et al., 2017; Roy and Trinchieri, 2017). TA have been reported to be produced by the intestinal microbiota due to the presence of decarboxylase enzymes that include L-amino acids in their substrate profile.

Among them, *Enterococcus faecium* produces 2-PE and TYR from L-phenylalanine and L-tyrosine, respectively (Marcobal et al., 2006; Bugda Gwilt et al., 2020). Further, *Enterococcus faecalis* (Connil et al., 2002), *Lactobacillus brevis* (Lucas et al., 2003), *Carnobacterium divergens* (Coton et al., 2004), and *Lactococcus lactis* (Fernández et al., 2004) have been reported to contain selective tyrosine decarboxylase enzymes. L-phenylalanine decarboxylation has also been reported in *Lactobacillus brevis* (Bover-Cid et al., 2001; Gardini et al., 2001; Moreno-Arribas and Lonvaud-Funel, 2001). In addition, *Clostridium sporogenes* and *Ruminococcus gnavus* produce TA via the decarboxylase enzymes CLOSO\_02083 and RUMGNA\_01526 (Williams et al., 2014). Interestingly, microbiota dysbiosis linked with increased levels of 2-PE have been reported in patients with Crohn's disease (Jacobs et al., 2016; Santoru et al., 2017) and elevated TYR levels have been reported in ulcerative colitis through metabolomics studies (Santoru et al., 2017). Additionally, variable TRP levels associated with differential gut virome presence has been linked to depression (Duan et al., 2022). Outside of the gastrointestinal environment, in the genitourinary system, TA such as TYR, putrescine and cadaverine are produced by the vaginal microbiota that include *Dialister*, *Prevotella*, *Parvimonas*, *Megasphaera*, *Peptostreptococcus*, and *Veillonella sp.* (Nelson et al., 2015). Overall, the production of TA by the microbiota provides a possible mechanism through which constitutive microbiota is linked to host health.

#### 1.2.4 Degradation of TA

The enzyme MAO is involved in the metabolism of TA much like the metabolism of classical monoamine neurotransmitters. TYR is metabolized by MAO type A and B (Philips and Boulton, 1979; Durden and Philips, 1980), while 2-PE is a selective MAO type B substrate (Yang and Neff, 1973). MAO can convert TYR to *p*-hydroxyphenylacetic acid, 2-PE to phenylacetic acid, OA to

*p*-hydroxymandelic acid, and TRP to indoleacetic acid (Grimsby et al., 1997) (Figure 1.2). The enzymes INMT and PNMT convert TRP and TYR or 2-PE to their *N*-methyl derivatives (Lindemann et al., 2005), such as *N*-methylphenylethylamine (from 2-PE), *N*-methyltyramine (from TYR) and synephrine (from OA) (Figure 1.2). The *N*-methyl derivatives can also act on one or more TAARs in a species-specific manner (Simmler et al., 2016). There have also been reports of metabolism of TA via cytochrome P450 isozymes (Yu et al., 2003; Niwa et al., 2011) and semicarbazide-sensitive amine oxidase (E.C. 1.4.3.21) (Elliott et al., 1989). Finally, 2-PE can be acted upon by DβH to generate phenylethanolamine, which has been reported to be a weak agonist of TAAR1 (Wainscott et al., 2007), and TYR can also be acted upon by DβH to produce OA (Saavedra and Axelrod, 1973; Danielson et al., 1977).

### 1.2.5 Effects of TA

The effects of TA have not always been clearly linked to TAAR, with some reported effects pre-dating the discovery of TAAR in 2001 (Borowsky et al., 2001; Bunzow et al., 2001). In this section, the reported effects of TA that are either TAAR-independent or of unknown molecular basis are described.

#### 1.2.5.1 TA in the brain

TYR is one of the well-studied members of the vertebrate TA family. In addition to the *para* form (TYR), *meta* and *ortho* forms of tyramine are also present but have rarely been studied and are present in lower quantities than the *para*-form (Boulton, 1976; Davis, 1989). TYR and 2-PE have been shown to exhibit indirect sympathomimetic, amphetamine-like effects (Fuxe et al., 1967; Borison et al., 1975; Raiteri et al., 1977; Parker and Cubeddu, 1988; Janssen et al., 1999;

Baker et al., 2011). Further indirect sympathomimetic effect includes displacement of classical monoamine neurotransmitters (Jones and Boulton, 1980; Jones, 1983) from their presynaptic stores have been reported with the administration of TYR, although this has only been shown to occur when TYR levels reach at least 100-fold higher than their physiological concentrations (Dourish, 1982; Stoff et al., 1984; Berry, 2004). OA has also been suggested to exhibit indirect sympathomimetic responses, in the same manner as TYR and 2-PE (Raiteri et al., 1977; Parker and Cubeddu, 1988), as demonstrated by an increase in dopamine and dihydroxyphenylacetic acid efflux following OA administration in striatal slices (Parker and Cubeddu, 1988).

Effects that are independent of indirect sympathomimetic effects include enhancement of neuronal dopamine and noradrenaline activity which have been reported with the administration of TYR and 2-PE (Jones and Boulton, 1980; Paterson, 1988, 1993; Paterson and Boulton, 1988). The effect of TRP on regulating electrophysiological responses has also been demonstrated with TRP reducing excitatory responses in cortical neurons, followed by a long-lasting decrease in basal firing (Jones, 1982). Further, dopamine-mediated effects on membrane fluidity are potentiated by the administration of 2-PE (Harris et al., 1988). 2-PE can also induce a downregulation in D1R (dopamine D1 receptor) and  $\beta$ 1- and  $\beta$ 2-adrenergic receptors (Paetsch and Greenshaw, 1993; Paetsch et al., 1993). The polyamine agmatine has been shown to bind to NMDA receptors (Yang and Reis, 1999) and serotonin 5-HT<sub>2</sub> $\alpha$  receptors (Taksande et al., 2009). All these reports provide an understanding of the role of vertebrate TA in modulating neurotransmission which are independent of indirect sympathomimetic responses.

Other TA such as, IAA, TMA, 3-IT have also been reported to play important physiological roles. IAA is present in male mouse urine with links to its possible function as a pheromone that

may induce puberty in female mice (Nishimura et al., 1989). Similarly, TMA has been proposed to be a male pheromone in mice (Li et al., 2013).

#### *1.2.5.2 TA in the periphery*

Interestingly, TA effects have also been documented in tissues associated with the GI tract and nutrient metabolism. TYR, 2-PE, TRP, IAA and the polyamine can all stimulate secretion of gastrin from the G cells of the stomach in rats (Dial et al., 1991). In addition, IAA can inhibit the amplitude of gastrointestinal contractions in a tetrodotoxin-sensitive manner (Sánchez et al., 2017), suggesting a neuron-mediated function. TYR can also regulate the integrity of the intestinal epithelial layer with increased expression of tight junction protein (claudin-1 and ZO-1), along with reported inflammatory properties (Pretorius and Smith, 2022, 2023). Additionally, TYR at high doses has been reported to exhibit dose-dependent antilipolytic effects (Carpéné et al., 2018), including stimulating uptake of glucose into human adipocytes (Carpéné et al., 2022). Furthermore, OA and SYN have been reported to reduce adipogenic marker proteins in mouse preadipocyte cells while also reducing total cholesterol levels and bodyweight in mice fed high fat diet (Lee et al., 2022), suggestive of a role of these TA in counteracting obesity. In this context, OA has also been reported as a potential marker in non-alcoholic fatty liver disease (Brial et al., 2019). When it comes to 3IT, its administration has been shown to increase lipolysis (Mariotti et al., 2014). In addition, an important role of 3IT in thermoregulation has been demonstrated where it can induce hypothermia (Scanlan et al., 2004; Doyle et al., 2007; Braulke et al., 2008).

Moving to cardiovascular effects, it has been shown that when TYR is consumed in high amounts, it can exert cardiovascular effects (Berry, 2004; Varounis et al., 2017; Burns and Kidron, 2022). One of the major issues of concern is the hypertensive crisis that is caused upon ingestion

of very high amounts of TYR, otherwise known as ‘the cheese effect’ (as explained previously in section 1.2.2) in patients taking monoamine oxidase inhibitors, which is due to the previously described indirect sympathomimetic effects (Price and Smith, 1971; Stratton et al., 1991; Anderson et al., 1993; Shalaby, 1996). Such hypertensive crisis can lead to end-organ damage such as intracranial bleeds, retinal haemorrhages, pulmonary edema, or renal failure (Varounis et al., 2017). Additionally, increased levels of TRP, 2-PE and TYR have been found in patients with MAO-A/B deficiency disorders, with these patients having increased cardiovascular disorders (Lenders et al., 1996). Increased amounts of TYR in blood also exerts a vasopressor response, where it is taken by up the norepinephrine reuptake transporter and eventually releasing high quantities of norepinephrine into circulation, by displacing norepinephrine from its pre-synaptic storage vesicle (Broadley, 2010; Trupin, 2017; Burns and Kidron, 2022). In this respect, 2-PE has also been shown to increase aortic blood pressure (Liang and Sprecher, 1979). In addition, TYR, 2-PE, OA and synephrine have been shown to exhibit direct actions on  $\alpha$ 1-adrenoreceptors (Brown et al., 1988; Hibino et al., 2009; Varma et al., 2011; Koh et al., 2019) and weak  $\beta$ <sub>1</sub>-adrenoreceptor agonist effects in cardiac tissues (Jordan et al., 2011; Kleinau et al., 2011).

In terms of the immune system, early studies have reported effects of TYR on leukocyte and erythrocyte chemotaxis and aggregation (Wolf, 1921, 1923). Further, activated platelets have been shown to release TYR and 2-PE (D’Andrea et al., 2003), where the TA have been suggested to exhibit chemotactic responses of leukocytes (Christian and Berry, 2018). *N*-methyl metabolites of TA such as, *N,N*-dimethyltryptamine has been reported to inhibit the production of pro-inflammatory cytokines (IL-1 $\beta$ , IL-6, TNF $\alpha$ ) while increasing the secretion of anti-inflammatory cytokine (Szabo et al., 2014; Szabo, 2015). Very recently, anti-inflammatory properties of TRP were also reported in mouse macrophages (Agista et al., 2022). In addition, polyamines such as,

cadaverine, putrescine, spermidine, spermine and agmatine (Figure 1.1) have long been known to influence cell proliferation and growth and cellular stress responses (Miller-Fleming et al., 2015; Pegg, 2016).

#### 1.2.6 TA-linked disorders

As seen from the earlier sections, TA effects within the body are widespread and they have been implicated in different disorders which will be explained in the following sections.

##### *1.2.6.1 Central nervous system disorders*

Increased levels of 2-PE have been reported in urine samples from schizophrenia patients (Janssen et al., 1999) and patients showing mania symptoms (Karoum et al., 1982; Davis, 1989; Sabelli and Javaid, 1995). Links to 2-PE and the pathogenesis of drug abuse/dependence disorder are also supported by the report of 2-PE involvement in brain reward and reinforcement pathways (Greenshaw, 1984; Shannon and Thompson, 1984). In addition, in patients suffering from depression (Wolf and Mosnaim, 1983) or attention deficit hyperactivity disorder (Baker et al., 1991), decreased urinary levels of 2-PE have been reported, whereas high urinary levels of 2-PE were reported in patients with stress (Paulos and Tessel, 1982; Snoddy et al., 1985; Grimsby et al., 1997). Furthermore, TYR has also been suggested to play a role in pediatric-onset multiple sclerosis (Solmaz et al., 2022). Other TA such as, *N,N*-dimethyltryptamine has been reported to exhibit hallucinogenic properties (Carbonaro and Gatch, 2016). Dysregulation of the polyamine agmatine, has been implicated in affective disorder such as, depressive disorder, cognitive disorders such as, Alzheimer's dementia, substance/drug abuse, addiction and metabolic disorders as well (Piletz et al., 2013).

### *1.2.6.2 Disorders in the periphery*

TA have also been linked to immune-related disorders, where elevated TYR levels have been reported in fecal samples from patients suffering from ulcerative colitis (Nagao-Kitamoto et al., 2016; Santoru et al., 2017) and celiac disease (Di Cagno et al., 2011; De Angelis et al., 2016). This observation is in line with earlier studies reporting a change in L-tyrosine metabolism in inflammatory bowel disorder pathophysiology (Burczynski et al., 2006; Jansson et al., 2009). Elevated levels of 2-PE were reported in fecal samples from Crohn's disease patients (Jacobs et al., 2016; Santoru et al., 2017) and have been correlated to disease progression and symptoms. In addition, elevated 2-PE levels due to phenylalanine hydroxylase (EC 1.14.16.1) deficiency (Reynolds and Gray, 1978) has been reported in patients with phenylketonuria. Finally, TYR has been reported as a marker for Sjogren syndrome (Han et al., 2022) , and has been suggested to be involved in psoriasis (Ramessur et al., 2022). Several recent studies have further highlighted the important roles of agmatine in the treatment of atherosclerosis and fatty liver disease (Wiśniewska et al., 2021), and also in the diagnosis of prostate cancer (Coradduzza et al., 2022).

All in all, the role of TA in the body is physiologically widespread, where TA exhibit important psychiatric, metabolic and immune-related functions and point to the importance of controlling TA levels within different cells and tissues throughout the body.

### **1.3 Vertebrate TA receptors – TAARs**

TAARs are a family of G protein-coupled receptors (GPCR) which are rhodopsin-like, type A receptors and found only in vertebrates (Borowsky et al., 2001; Bunzow et al., 2001; Gloriam et al., 2005; Lindemann et al., 2005). The first evolutionary evidence of the emergence of TAAR-like protein appears to be in lamprey (Gloriam et al., 2005; Hashiguchi and Nishida, 2007; Libants

et al., 2009; Eyun et al., 2016), with a conserved TAAR signature motif emerging after the divergence of jawed vertebrates from jawless fish (Hashiguchi and Nishida, 2007; Eyun et al., 2016). Different studies have reported species-specific evolution in these genes resulting in large variations in the total number of functional TAARs present between species, along with the emergence of various species-specific isoforms (Lindemann et al., 2005; Vallender et al., 2010; Eyun et al., 2016). The highest number of TAARs observed so far is in the zebrafish with a total of 112 functional genes (Hashiguchi and Nishida, 2007; Hashiguchi et al., 2008; Hussain et al., 2009; Tessarolo et al., 2014; Gao et al., 2017). The bottlenose dolphin, however, is the only known vertebrate to not contain any functional TAAR genes, with all three genes pseudogenized (Eyun et al., 2016). All TAARs, except TAAR1, appear to be expressed in the olfactory epithelium (Liberles and Buck, 2006; Hashiguchi and Nishida, 2007; Gliem et al., 2009; Horowitz et al., 2014; Syed et al., 2015). Evolution and profiling of the TAAR genes strongly suggest dependence on changes in habitation and adaptation (Berry et al., 2017).

Among mammals, TAARs segregate to nine sub-families (TAAR1-9) (Eyun et al., 2016) with TAAR1-4 directed towards recognition of primary amines and evolving under negative selection pressures (Ferrero et al., 2012), while TAAR5-9 are tuned towards tertiary amines and/or diamines as determined through phylogenetic analysis and TAAR functional assays, which appear to have evolved under positive selection pressures (Eyun et al., 2016). Humans have six functional members of the TAAR family, TAAR1, 2, 5, 6, 8 and 9, and three pseudogenes TAAR3, 4 and 7, with all genes located on chromosome 6q23.2 (Borowsky et al., 2001; Bunzow et al., 2001). Each TAAR gene consists of a single exon, except TAAR2 which contains two exons (Lindemann et al., 2005). The expression levels of TAARs are very low, making their further characterization difficult with a well-validated anti-human antibody only available for TAAR1 (Raab et al., 2015),

which has made TAAR1 a less challenging isoform to study when compared to the other human TAARs. All human TAARs located in the olfactory epithelium couple to the G<sub>olf</sub> cascade to stimulate cAMP (cyclic AMP) production (Liberles and Buck, 2006). Known endogenous ligands for human TAAR are shown in Table 1.1.

**Table 1.1: Functional human TAARs (hTAARs) and their endogenous TA substrates.**

Functional hTAARs	Endogenous TA agonists
TAAR1	TYR <sup>a</sup> , 2-PE <sup>a</sup> , TRP <sup>a</sup> , OA <sup>b</sup> , 3MT <sup>c</sup>
TAAR2	Unknown
TAAR5	TMA <sup>c</sup> , dimethylethylamine <sup>b</sup> , 3IT <sup>d</sup>
TAAR6	Diamine binding pocket <sup>e</sup>
TAAR8	Cadaverine <sup>f</sup> , diamine binding pocket <sup>e</sup>
TAAR9	Unknown

a: Liberles and Buck (2006) ; b: Wallrabenstein et al., 2013 ; c: Li et al., 2015 ; d: Dinet, Mulhaus, Wienchol et al., 2015 ; e: Li et al., 2015 ; f: Kovacs et al., 2019

### 1.3.1 TAAR subfamilies

TAAR1 is by far the best characterized and most studied among the TAARs. TAAR1 is well conserved among mammals, avians and amphibians (Hussain et al., 2009) with 97% homology between humans and cynomolgus monkeys, and 77% between rats and mice (Gainetdinov et al., 2018). Unlike most GPCRs, TAAR1 has an intracellular localization in all cell types studied (Lindemann et al., 2005; Barak et al., 2008; Raab et al., 2015; Pei et al., 2016; Pitts et al., 2019; Barnes et al., 2021), which is further explained in Section 1.3.2.1. The cellular distribution of TAAR1 generally mirrors the previously described locations of AADC (Regard et al., 2007; Ito et

al., 2009; Revel et al., 2013; Gainetdinov et al., 2018) and is described fully in subsequent sections (Sections 1.3.2.3 and 1.3.2.4). Agonists for TAAR1 include TYR and 2-PE, (Liberles and Buck, 2006; Simmler et al., 2016; Bonner et al., 2019) (Table 1.1), which are the best characterized so far. TAAR1 has been reported to play important roles in regulating monoaminergic neurotransmission in the brain (Lindemann et al., 2008; Xie et al., 2008; Revel et al., 2011, 2013), controlling nutrient-induced hormone secretion in the periphery (Adriaenssens et al., 2015; Raab et al., 2015) and in regulating various immune functions (D'Andrea et al., 2003; Nelson et al., 2007; Wasik et al., 2012; Babusyte et al., 2013; Barnes et al., 2021, 2022).

In addition to being present in the olfactory epithelium (Liberles and Buck, 2006), TAAR2 presence in limbic brain areas in mice where it regulates dopaminergic activity and adult neurogenesis has been recently reported (Efimova et al., 2022). In the immune system, TAAR2 shows a similar expression pattern as TAAR1, being present in B lymphocytes, monocytes, NK cells and T lymphocytes in humans and mice (Nelson et al., 2007; Babusyte et al., 2013). Further, TAAR2 can heterodimerize with TAAR1 (Babusyte et al., 2013), which plays a role in the chemotactic response to 2-PE (not a TAAR2 ligand), suggesting the need for a functional interaction between TAAR1 and 2. This chemotactic response has also been shown to be dependent on  $G_i$  signalling (Malki et al., 2015). The expression of TAAR2 has also been reported in the mucosal cells of the duodenum in mice (Ito et al., 2009), and in the heart (Chiellini et al., 2007) and the testes in rats (Chiellini et al., 2012). Even though ligands for TAAR2 have not been identified (Table 1.1), primary amines have been suggested to activate TAAR2 (Ferrero et al., 2012).

TAAR3 is a pseudogene in humans (Lindemann and Hoener, 2005), however it plays a role as a functional receptor in the olfactory system in other species studied such as mice (Nishimura

et al., 1989) and sac winged bats (Santos et al., 2016). IAA has been reported to be an endogenous agonist of mouse TAAR3 (Liberles and Buck, 2006; Liberles, 2015), and proposed to act as a mouse pheromone (Nishimura et al., 1989). In addition, TAAR3 has also been reported to be expressed in kidney (Ruiz-Hernández et al., 2020) and pancreatic  $\beta$  cells (Cripps et al., 2020) in rats.

TAAR4 is also a pseudogene in humans (Lindemann and Hoener, 2005) but is functional in other mammalian species such as mice and rats (Fehler et al., 2010; Dewan et al., 2013). TAAR4 has an overlapping pharmacological profile with that of TAAR1 (Liberles and Buck, 2006; Dewan et al., 2013). Additionally, 2-PE activation of TAAR4 in the olfactory epithelium induces innate avoidance behaviour in mice and may be involved in predator detection and avoidance (Dewan et al., 2013).

TAAR5 has been shown to be present in various regions of the mouse brain (Dinter et al., 2015; Kalinina et al., 2021; Efimova et al., 2022), including the purkinje cells of the cerebellum and medial vestibular nucleus, where it has been shown to regulate sensorimotor activities (Kalinina et al., 2021). The involvement of TAAR5 in regulating dopaminergic activity and adult neurogenesis, much like TAAR2 in mice, has also been reported in the limbic areas of the brain (Efimova et al., 2022). Outside the brain, low level expression has been reported in leukocyte populations in mice (Babusyte et al., 2013). In addition, TAAR5 expression has been reported in the spinal cord (Gozal et al., 2014) and the testes (Chiellini et al., 2012) in rats. There has been another report of a possible link of altered TAAR5 expression to the development of diabetic neuropathy in male Wistar rats (Ruiz-Hernández et al., 2020). TAAR5 has been shown to couple to  $G_s$  (Wallrabenstein et al., 2013),  $G_{q/11}$  (Dinter et al., 2015) and  $G_{12/13}$  dependent MAP kinase (Dinter et al., 2015) pathways. TAAR5 has long been known to be tuned towards tertiary amines

(Ferrero et al., 2012), the best characterized of which is TMA, which has been shown in multiple species including humans (Liberles and Buck, 2006; Wallrabenstein et al., 2013; Zhang et al., 2013). Dimethylamine has also been reported to act as a partial agonist of TAAR5 (Wallrabenstein et al., 2013) (Table 1.1).

TAAR6 is highly expressed in the dendrites and perinuclear components of olfactory neurons and in the glomeruli of the olfactory bulbs (Liberles and Buck, 2006; Fleischer et al., 2007; Johnson et al., 2012; Yoon et al., 2015). Recent transcriptomic data meta-analysis has confirmed low levels of expression of TAAR6 in prefrontal cortex and nucleus accumbens in human and mouse (Vaganova et al., 2022), expression patterns that coincide with the brain areas involved in the pathogenesis of schizophrenia and bipolar affective disorders (Vaganova et al., 2022). Tumour-specific expression of TAAR6 in melanoma samples has been reported (Vaganova et al., 2022), suggesting a possible role for TAAR6 in melanoma pathogenesis. Localization in human kidney (Borowsky et al., 2001) and leukocytes (D'Andrea et al., 2003; Babusyte et al., 2013), and rat spinal cord (Gozal et al., 2014) have also been reported. Signal transduction cascades with respect to TAAR6 have not yet been identified. As is the case for TAAR2, there have been no reports of any ligands for TAAR6 even though it has been suggested to be tuned towards tertiary amines (Ferrero et al., 2012; Guo et al., 2022) and also contain a putative diamine binding site (Li et al., 2015).

Similar to TAAR3 and 4, TAAR7 is a pseudogene in humans (Lindemann et al., 2005). TAAR7 is the main locus for variation in TAAR gene subtypes between different mammalian species, due to species-specific expansions (Borowsky et al., 2001; Lindemann and Hoener, 2005; Lindemann et al., 2005; Eyun et al., 2016). Physiological effects of TAAR7 have not yet been reported.

Expression of TAAR8 has been reported in human astrocytes (D'Andrea et al., 2012), amygdala, kidney (Borowsky et al., 2001) and leukocytes (D'Andrea et al., 2003). The possible involvement of TAAR8 in ameliorating the aggressiveness of breast cancer, through the action of cadaverine (as a putative endogenous ligand), by reversal of endothelial-to-mesenchymal transition and reduction of mitochondrial oxidation has also been reported (Kovács et al., 2019). TAAR8 couples to the G<sub>i</sub> cascade (Mühlhaus et al., 2014) and like TAAR6, contains a diamine binding domain as was studied through structural modelling and sequence alignment studies (Li et al., 2015).

TAAR9 has been suggested to play a role in regulating cholesterol levels, with a significant decrease in total cholesterol and low-density lipoprotein levels reported in TAAR9-KO (knock-out) rats (Murtazina et al., 2021). Additionally, TAAR9 along with TAAR8, was shown to be involved in the reversal of endothelial-to-mesenchymal transition of breast cancer cell lines and reduction of mitochondrial oxidation, (Kovács et al., 2019) thus potentially being a target to decrease the aggressiveness of breast cancer. TAAR9 has also been reported to be present in human leukocytes (D'Andrea et al., 2003; Babusyte et al., 2013). A role in diabetic nephropathy was suggested, where altered TAAR9 expression was observed in rat kidneys, along with TAAR3 and 5 expression (Ruiz-Hernández et al., 2020). Further, expression in mouse gastrointestinal tract (Ito et al., 2009), the spleen (Regard et al., 2008), skeletal muscle and pituitary gland (Vanti et al., 2003) have also been reported. There is currently no information on the TAAR9 signaling cascade.

### 1.3.2 TAAR1 - the best characterized member of the TAAR family

Studies have reported the widespread localization of TAAR1 and its implications in a variety of physiological functions. This section will discuss in detail its localization, signalling and effects across different cells and tissues.

#### *1.3.2.1 Subcellular localization of TAAR1*

Even though TAAR1 belongs to the GPCR family, it has been shown to have an intracellular subcellular localization (Bunzow et al, 2001; Lindemann and Hoener, 2005; Miller et al., 2005; Revel et al., 2013; Raab et al., 2015; Pei et al., 2016) (Figure 1.3). This has been suggested to be due to the absence of *N*-terminal glycosylation sites (Barak et al., 2008). TAAR1 intracellular localization was shown to be in intracellular puncta (Miller et al., 2005 and 2011), endoplasmic reticulum and golgi apparatus (Barak et al., 2008; Raab et al., 2016), secretory vesicles (Barak et al., 2008), and the nucleus (Pitts et al., 2019; Barnes et al., 2021). Rare plasma membrane expression of TAAR1 has also been reported (Borowsky et al., 2001; Miller et al., 2005; Xie et al., 2007; Underhill et al., 2021). TAAR1 heterodimerizes with D2-like dopamine receptors, in particular the D2R-long isoform, which promotes TAAR1 appearance at the plasma membrane (Espinoza et al., 2011; Harmeier et al., 2015). In MCF-7, MDA-MB-468 and SKBR3 breast cancer cell lines, TAAR1 protein expression was reported to be nuclear (Pitts et al., 2019), although this was not the case in other breast cancer cell lines such as, T47D, MDA-MB-231 and BT-474, suggesting no association of subcellular localization with breast cancer subtype. Similar nuclear localization of TAAR1 has also been shown in human macrophages (Barnes et al., 2021) which was dependent on the activation state of the macrophages. The variable subcellular localization of TAAR1 in different activation states is suggestive of variable TAAR1 function. Given a primarily

intracellular localization, it is important to study how TAAR1 ligands are transported across the plasma membrane into cells to allow binding to TAAR1 and this is a central component for this thesis work.

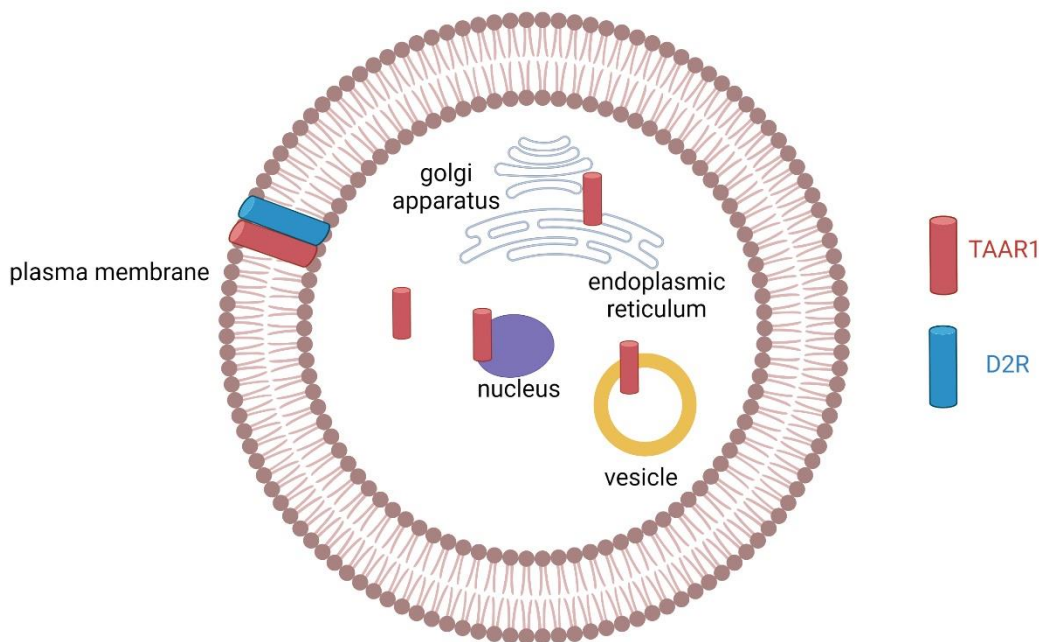


**Figure 1.3: Subcellular localization of TAAR1.** TAAR1 has been reported to have an intracellular localization. Localization in the endoplasmic reticulum, golgi apparatus, vesicular membrane, nucleus, with rare plasma membrane expression (upon heterodimerization with D2R receptor) have been reported. The figure was generated in BioRender.

### 1.3.2.2 TAAR1 signalling cascades

TAAR1, a  $G_s$ -coupled receptor, functions via stimulation of adenylyl cyclase with subsequent stimulation of cAMP production (Borowsky et al., 2001; Bunzow et al., 2001; Lindemann and Hoener, 2005; Reese et al., 2007; Wainscott et al., 2007; Barak et al., 2008; Hu et al., 2009; Espinoza et al., 2011; Revel et al., 2011; Liu et al., 2014). Consistent with this,

demonstrations of TAAR1-dependent phosphorylation of protein kinase A (EC 2.7.11.11) and C (EC 2.7.11.13) have been reported in HEK-293 cells, rhesus monkey B cells and lymphocytes (Panas et al., 2012), with downstream activation of transcription factors, cAMP response element binding protein (CREB) and nuclear factor of activated T cells (Panas et al., 2012). Furthermore, TAAR1 downstream activation targets have been identified in pancreatic  $\beta$ -cells, which include exchange protein activated by cAMP, inositol triphosphate receptor, calcium/calmodulin-dependent protein kinase II (EC 2.7.11.17) and CREB (Michael et al., 2019). In addition, TAAR 1 induces an activation of G protein-coupled inwardly rectifying potassium (GirK) channels (Bradaia et al., 2009; Revel et al., 2011), resulting in inhibition of neuron firing frequency.

TAAR1 can also heterodimerize with D2R, and this heterodimerization appears to promote  $\beta$ -arrestin signalling through TAAR1 but promotes  $G_i$  signalling through D2R (Espinoza et al., 2011; Harmeier et al., 2015). When TAAR1 heterodimerizes with D2R, an increase in TAAR1 interactions with  $\beta$ -arrestin 2 is seen, followed by a reduction in activation of GSK 3 $\beta$  signalling (Harmeier et al., 2015). This may be particularly relevant to the development of psychotherapeutics, since  $\beta$ -arrestin-mediated GSK 3 $\beta$  and AKT signalling have been linked to psychiatric disorders such as schizophrenia, bipolar disorder, and depression (Beaulieu et al., 2009).

### *1.3.2.3 Central expression and function*

TAAR1 has a heterogenous expression in the brain primarily associated with the brain nuclei and projection areas of the dopaminergic, serotonergic and glutamatergic systems (Borowsky et al., 2001; Lindemann et al., 2008). Expression in the amygdala, basal ganglia, frontal cortex, limbic areas, substantia nigra, and ventral tegmental area have been confirmed (Borowsky et al.,

2001; Lindemann et al., 2008). Further expression in the spinal cord (Borowsky et al., 2001; Lindemann et al., 2008; Gozal et al., 2014) and astrocytes (Cisneros and Ghorpade, 2014) have also been shown. In dopaminergic cells, TAAR1 activation can downregulate dopaminergic neurotransmission (Lindemann et al., 2008), consistent with increased dopaminergic transmission when TAAR1 is knocked-out (Lindemann et al., 2008). Further, 2-PE (Xie and Miller, 2008) modulates dopamine transporter function via both TAAR1 and D2 autoreceptors. In addition, TAAR1 agonists inhibit the dopamine-dependent hyperactivity seen in dopamine transporter-KO mice (Revel et al., 2011, 2013). At both pre- (Bradaia et al., 2009) and post-synaptic D2R (Espinoza et al., 2015), TAAR1-mediated effects can be observed, most likely due to TAAR1 and D2R heterodimerizing (Espinoza et al., 2011).

With respect to serotonin function, 2-PE can modulate serotonin transporter function via TAAR1 and 5-HT<sub>1A</sub>/5-HT<sub>1B</sub> autoreceptors (Xie et al., 2008). A synthetic TAAR1 agonist, RO5166017, has been reported to inhibit the firing rate of dorsal raphe nuclei serotonergic neurons (Revel et al., 2011). Furthermore, in a transgenic TAAR1 over-expressing mouse line, an increased serotonin level in prefrontal cortex was found with increased firing rates of dorsal raphe nuclei serotonergic neurons (Revel et al., 2013).

TAAR1 regulation of glutamatergic transmission has been observed with improvement in prefrontal cortical hypoglutamatergic activity seen in pharmacological magnetic resonance imaging studies after the administration of TAAR1 agonists (Revel et al., 2013). In line with this, a role of TAAR1 in preventing hypoglutamatergic states has been further confirmed in the striatum of TAAR1-KO mice (Sukhanov et al., 2016). Through another study it was observed that activation of TAAR1 in human astrocytes by methamphetamine, results in decreased in glutamate clearance because of downregulation of excitatory amino acid transporter 2 (Cisneros and

Ghorpade, 2014). Additionally, upregulation of TAAR1 leads to reduced excitatory amino acid transporter 2 expression and consequently reduced glutamate clearance in astrocytes (Ding et al., 2017).

In terms of the behavioural effects of TAAR1, agonists provide potential pharmacotherapeutic benefits against a myriad of psychiatric disorders. With respect to schizophrenia, TAAR1 has the unique ability to normalize both dopamine hyper-reactivity and hypoglutamatergic states in mice (Revel et al., 2011). TAAR1 agonists, including a mixed 5-HT<sub>1A</sub>/TAAR1 (ulotaront) agonist from Sunovion Pharmaceutical Inc, have shown beneficial effects in several pre-clinical animal models of schizophrenia, including prepulse inhibition of startle and PCP-induced hyperactivity (Nazimek J et al., 2017). TAAR1 agonists also improve the accuracy of object retrieval in Cynomolgus monkeys, which is suggestive of the improvement in cognitive abilities via TAAR1 (Revel et al., 2013). Clinical trials have confirmed these potential beneficial effects with ulotaront (SEP-363856) (Dedic et al., 2019; Koblan et al., 2020; Begni et al., 2021; Correll et al., 2021) and ralmitaront (NCT03669640, 2018; NCT04512066, 2020), two TAAR1 synthetic agonists that are currently under phase III (Koblan et al., 2020; Correll et al., 2021) and II (NCT03669640, 2018; NCT04512066, 2020) clinical trials in patients with schizophrenia, respectively.

Beneficial effects of TAAR1 agonists have also been seen in various animal models of depression. A dose-dependent reduction in the time of immobility in the forced swim test, with the administration of TAAR1 partial agonists was observed (Revel et al., 2013). Further, a differential reinforcement of low response rate test in cynomolgus monkeys showed that TAAR1 agonists increased the number of reinforcers obtained (Revel et al., 2013), which is consistent with

responses seen to known antidepressants like MAO inhibitors, serotonin reuptake inhibitors and tricyclic antidepressants (McGuire and Seiden, 1980; O'Donnell and Seiden, 1983).

The effect of TAAR1 in regulating sleep has also been demonstrated. TAAR1 partial agonists can cause an increase in wakefulness and reduced latency to sleep in rats and mice (Revel et al., 2013; Schwartz et al., 2016; Black et al., 2017). Furthermore, over expression of TAAR1 levels has been shown to cause increase in wakefulness, and TAAR1 agonism resulted in reduction in both non-rapid eye movement and rapid eye movement sleep (Schwartz et al., 2016; Hopkins et al., 2021). In another study, TAAR1 agonism was shown to reduce cataplexy in mouse narcolepsy models (Black et al., 2017), and this result further supports TAAR1 effects in maintaining sleep architecture.

TAAR1 has also been shown to have anti-craving and anti-dependence effects in various animal models of addiction (Gainetdinov et al., 2018). When it comes to cocaine-mediated effects, reduction in drug-taking behaviours and hyperactivity (Revel et al., 2011, 2013), retention in reward memory (Liu et al., 2016), self-administration (Pei et al., 2015) and sensitization (Thorn et al., 2014), and withdrawal-induced drug seeking (Pei et al., 2014) behaviours have been observed with TAAR1 agonists. Similarly, TAAR1 agonists decrease nicotine-induced hyperactivity (Liu et al., 2018; Sukhanov et al., 2018), sensitization, self-administration and demand (Liu et al., 2018), while knocking out TAAR1 enhances nicotine-seeking behaviours (Liu et al., 2018). Furthermore, chronic nicotine administration selectively decreases TAAR1 expression in the nucleus accumbens (Liu et al., 2018). Additionally, TAAR1 synthetic agonist RO5256390 showed prevention of binge-eating of highly palatable foods in rodents (Ferragud et al., 2016).

TAAR1 is also expressed in areas that are involved in regulation of feeding behaviour, such as the cortex, hypothalamus and limbic systems, and TAAR1 agonists decrease food intake in diet-

induced obese mice (Raab et al., 2015), with improvements seen in weight loss and insulin sensitivity (Raab et al., 2015). In line with this, TAAR1 agonists have been shown to prevent olanzapine treatment-associated weight gain (Revel et al., 2013).

Finally, TAAR1 mRNA was also shown to be decreased in monocytes from multiple sclerosis patient samples, while increased TAAR1 expression in macrophage/microglia was observed in the area surrounding lesions in multiple sclerosis, suggesting a link between TAAR1 and neuroinflammation (Barnes et al., 2021).

#### *1.3.2.4 Peripheral expression and function*

In the gastrointestinal system TAAR1 appears to be involved in regulating hormone secretion in response to nutrient intake. Expression in stomach D cells (Regard et al., 2007; Chiellini et al., 2012; Revel et al., 2013; Adriaenssens et al., 2015; Raab et al., 2015), pancreatic  $\beta$ -cells (Regard et al., 2007; Revel et al., 2013; Raab et al., 2015), and neuroendocrine intestinal enterochromaffin cells (Kidd et al., 2008; Ito et al., 2009; Revel et al., 2013; Raab et al., 2015) have been reported. TAAR1 coexpression was further reported with glucagon-like peptide 1 (GLP-1) and peptide YY (PYY) in human duodenal sections (Raab et al., 2015).

TAAR1 has been reported to be present in pancreatic  $\beta$  cells where studies with TAAR1 agonists have shown increases in glucose-stimulated insulin secretion (Raab et al., 2015; Michael et al., 2019; Cripps et al., 2020). Decreased insulin secretion was observed with glucolipotoxic downregulation of TAAR1, which was shown not to be due to loss of  $\beta$  cells, further strengthening potential links of TAAR1 and type 2 diabetes pathophysiology (Cripps et al., 2020). In addition, single nucleotide polymorphisms of TAAR1 have been reported in patients with disturbed insulin secretion (Mühlhaus et al., 2014). As previously described, TAAR1 agonists can also induce

significant loss of body weight in diet-induced obese mice (Raab et al., 2015), which appeared to have both central and peripheral components with both a delay in gastric emptying and also decreased food intake (Raab et al., 2015). In addition, TAAR1 has been shown to increase somatostatin release from stomach D-cells (Adriaenssens et al., 2015) and plasma levels of GLP-1, PYY (Raab et al., 2015) which suggests that TAAR1 regulates nutrient-induced hormone secretion. TAAR1 has also been suggested to elicit gastric contractile behaviour (Batista-Lima et al., 2019).

In the immune system, TAAR1 expression has been shown in human leukocytes (D'Andrea et al., 2003), including peripheral mononuclear cells (Nelson et al., 2007), B lymphocytes (Wasik et al., 2012; Babusyte et al., 2013), monocytes (Babusyte et al., 2013; Barnes et al., 2021), macrophages (Barnes et al., 2022), polymorphonuclear leukocytes (Babusyte et al., 2013), NK (natural killer) cells (Babusyte et al., 2013) and T lymphocytes (Babusyte et al., 2013; Sriram et al., 2016). TAAR1 leukocyte expression is increased upon activation (Nelson et al., 2007; Wasik et al., 2012) and endogenous ligands for TAAR1 are both positive chemotactic signals for leukocytes (Babusyte et al., 2013) and can be released from activated platelets (D'Andrea et al., 2003). Activation of TAAR1 appears to regulate T helper (T<sub>h</sub>) cell differentiation, particularly directing it away from T<sub>h</sub>1 (pro-inflammatory) and toward T<sub>h</sub>2 (anti-inflammatory) phenotypes (Babusyte et al., 2013). TAAR1 agonists also increase interleukin (IL)-4 and decreases IL-2 secretion in leukocytes (Babusyte et al., 2013). The differentiation of T<sub>h</sub> cell to the T<sub>h</sub>2 phenotype may cause increased activation of B lymphocytes (Babusyte et al., 2013; Christian and Berry, 2018). Further, an increase in B cell secretion of immunoglobulin E has also been reported in response to TAAR1 agonists (Babusyte et al., 2013). Very recently, TAAR1-mediated regulation of purinergic signalling was also reported in mouse bone marrow-derived macrophages (Barnes et

al., 2022). As such, TAAR1 may be a target for pharmacotherapy in situations of inappropriate immune system activation. Interestingly, TAAR1 has been linked to several immune-related disorders (Vattai et al., 2017; Christian and Berry, 2018; Barnes et al., 2021, 2022; Vaganova et al., 2022). TAAR1 ligands have been directly linked to the pathology of inflammatory bowel disease (Jacobs et al., 2016; Santoru et al., 2017), Crohn's Disease (Jacobs et al., 2016; Santoru et al., 2017), ulcerative colitis (Santoru et al., 2017) and celiac disease (Di Cagno et al., 2011; De Angelis et al., 2016).

High expression of TAAR1 in placental syncytiotrophoblasts, cytotrophoblast, decidua and glands has been reported in patients suffering from recurrent miscarriages (Stavrou et al., 2018). Furthermore, the placenta and umbilical cord contain semicarbazide sensitive amine-oxidase/vascular adhesion protein-1, which is an enzyme that includes endogenous TAAR1 agonists in its substrate profile (Sikkema et al., 2002). Together these studies are suggestive of TAAR1-directed ligands being a novel treatment strategy for miscarriages.

The expression of TAAR1 in breast cancer cell lines has been demonstrated (Pitts et al., 2019). Also, a positive correlation of TAAR1 expression and human epidermal growth factor receptor 2 positivity (Vattai et al., 2017) has been reported, however, initial reports of the linkage were not able to be verified (Pitts et al., 2019). Further, a drastic decrease in the expression of TAAR1 was reported in melanoma samples (Vaganova et al., 2022).

Even though there have been reports of TAAR1 being expressed in thyroid gland epithelial cells (Szumska et al., 2015), adipose tissue, blood vessels, heart, kidney, liver, lung and testes (Borowsky et al., 2001; Chiellini et al., 2007, 2012; Regard et al., 2008; Fehler et al., 2010), further validation studies are lacking. Due to the links between TAAR1 and various aspects of the periphery, this further calls attention to a putative role in pharmacotherapy. How its agonists have

access to TAAR1 given its subcellular localization is intracellular remains an unknown question. In the following sections known transport properties of TA across cell membranes will be described.

#### **1.4 Transport properties of vertebrate TA**

It has previously been shown that TA can more readily diffuse across synthetic lipid bilayers than the classical monoamine neurotransmitters because TA are less polar, with their diffusion half-lives being fifteen seconds or less (Berry et al., 2013). In line with this, TYR was seen to be transported across rabbit erythrocytes by non-saturable simple diffusion (Blakeley and Nicol, 1978) and transport across rat intestinal sacs and rat intestinal segments was also suggested to occur by simple diffusion (Tchercansky et al., 1994). Further, following *in vivo* bolus administration of 2-PE, transport across the blood-brain barrier was observed to take place by simple diffusion by studying the brain-uptake index (Mosnaim et al., 2013).

A number of studies have examined the characteristics of TA release from neurons. Studies have shown a lack of depolarization induced release of TA (Durden and Philips, 1980; Henry et al., 1988; Juorio et al., 1988; Dyck, 1989; Berry et al., 2013). This observation is, however, not consistent with simple diffusion across membranes, as from Nernstian kinetics it is expected that as the membrane potential becomes less negative, there should be a decrease in the intracellular:extracellular concentration ratio (Berry et al., 2016). The fact that this is not seen with 2-PE, TRP or TYR, suggests that transporters may be involved in membrane passage. In this regard, 2-PE (1.1  $\mu\text{M}$ ) passage across Caco-2 monolayer was seen to occur by  $\text{H}^+$ -dependent transporter systems (Fischer et al., 2010). Further, TYR clearance (2  $\mu\text{M}$ ) across blood-cerebrospinal fluid barriers has also been reported to involve a  $\text{H}^+$ -dependent transport system (Akanuma et al., 2018).  $\text{Na}^+$ -dependent membrane passage of 2-PE (10 nM) in rabbit erythrocytes

(Mason et al., 1983), and at concentrations up to 200  $\mu\text{M}$  in isolated rat lung (Ben-Harari and Bakhle, 1980) has been shown. In addition, TYR transport (100 nM) across native neuronal membrane preparations has subsequently been reported to involve a transporter with the pharmacological characteristics of Organic Cation Transporter 2 (OCT2; *Slc22A2*; see Section 1.4.2.1; Berry et al., 2016). In summary, although TA can readily diffuse across cell membranes, in at least some preparations they appear to be transported by one or more transporters.

#### 1.4.1 Uptake 1 transporters

Uptake 1 transporters are high-selectivity, low-capacity,  $\text{Na}^+$ -dependent (Iversen, 1973; Bönisch et al., 1985; Eisenhofer, 2001), secondary active transporters, where the transport of their substrates is mediated by co-transport of  $\text{Na}^+$  ions down their electrochemical gradient from the extracellular to intracellular medium (Cheng and Bahar, 2019). Representative examples of uptake 1 transporters include dopamine transporter (DAT, *Slc6A3*), norepinephrine transporter (NET, *Slc6A3*) and serotonin transporter (SERT, *Slc6A4*). These transporters are localized in the corresponding monoaminergic neurons with projections to the neocortex, basal ganglia and limbic forebrain areas (Lin et al., 2011), localizations that correspond with the reported functions of monoamine transporters in regulating mood, learning, cognition, sleep-wake cycle and appetite (Aggarwal and Mortensen, 2017). These transporters are considered as the primary transport mechanism for clearance of released neurotransmitters from the synapse (Duan and Wang, 2010). Outside the central nervous system, SERT have been reported to be present in the lung (Paczkowski et al., 1996), intestine (Gordon and Barnes, 2003), blood platelets (Gordon and Barnes, 2003), lymphocytes (Faraj et al., 1994; Gordon and Barnes, 2003), and adrenal chromaffin cells (Schroeter et al., 1997). NET is also expressed outside the central nervous system in locations

such as the adrenal glands, vas deferens and placenta (Schroeter et al., 2000; Jayanthi et al., 2002; Sung et al., 2003). All uptake 1 transporters contain 12 alpha-helical transmembrane domains with intracellular and extracellular loops and an S1 binding site. The S1 binding site binds the substrate with one or two Na<sup>+</sup> ions, and comprises of a hydrophobic region to bind to the aromatic groups of the substrates and a hydrophilic region to interact with the amino groups of the substrates for uptake 1 transporters. TA have long been reported to be substrates for uptake 1 transporters (Raiteri et al., 1977; Danek Burgess and Justice, 1999; Liang et al., 2009; Berry et al., 2016).

#### 1.4.2 Uptake 2 transporters

Uptake 2 transporters are classified as polyspecific, low-affinity, high-capacity, Na<sup>+</sup>- and Cl<sup>-</sup>-independent transporters (Iversen, 1973; Bönisch et al., 1985; Eisenhofer, 2001) that consist of the Slc family of transporters which further consists of 65 distinct families of facilitated diffusion or secondary active transporters (Yee and Giacomini, 2021). Their capacity of uptake is much greater than uptake 1 transporters (Iversen, 1971). They were initially characterized as transporters for synaptic clearance of neurotransmitters when uptake 1 transporters become saturated (Couroussé and Gautron, 2015). There have been further reports however, reporting the active involvement of uptake 2 transporters in the monoaminergic system (Duan and Wang, 2010). Uptake 2 transporters are also present in the periphery, with the first demonstration in the heart (Iversen, 1965). Other areas, such as the liver and intestines, (Boenisch, 1980; Gebauer et al., 2021) have been reported to express uptake 2 transporters. Out of the 65 families, the *Slc22* family, which is also known as the organic ion transporter family, is the largest containing 28 members that transport organic anions and cations (Yee and Giacomini, 2021). The OCT family belongs to the *Slc22* group of transporters. TA have been shown to be substrates for a number of Slc transporters

in particular the OCT sub-family and Plasma Membrane Monoamine Transporter (PMAT; *Slc29A4*) (Breidert et al., 1998; Gründemann et al., 1998; Engel and Wang, 2005; Schömig et al., 2006; Nies et al., 2011; Berry et al., 2016; Gebauer et al., 2021).

#### *1.4.2.1 OCT Transporters*

The OCT sub-family constitutes OCT1 (encoded by the *Slc22A1* gene), OCT2 (encoded by *Slc22A2* gene), OCT3 (encoded by *Slc22A3* gene), organic cation/carnitine transporter 1 (encoded by *Slc22A4* gene) and 2 (encoded by *Slc22A5* gene), and OCT6 (encoded by *Slc22A16* gene) (Koepsell, 2013), which are all facilitated diffusion transporters. *Slc22A15* is an additional member that clusters with other OCT members, but no substrate has yet been identified for *Slc22A15* (Eraly and Nigam, 2002; Drake et al., 2014; Okada et al., 2019; Zhu et al., 2019). The inclusion of TA, notably TYR and 2-PE, as substrates for OCTs 1-3 has been reported (Gozal et al., 2014; Berry et al., 2016; Gebauer et al., 2021), with at least OCTs 1 and 2 shown to have nanomolar affinity for TYR (Iseki et al., 1993; Breidert et al., 1998; Berry et al., 2016), suggesting they may play a role in endogenous TA membrane passage. Interestingly, TAAR1 and OCT transporters have also been implicated in similar disorders as will be discussed in the later part of this section.

The genes encoding OCTs in the human genome are located on chromosome 6 (Koehler et al., 1997; Song et al., 2019). In terms of amino acid identity, OCTs 1-3 contain between 543-557 amino acids (Giacomini et al., 2010), with OCT1 and OCT2 having 70% identity with each other (Sala-Rabanal et al., 2013; Maier et al., 2021) and around 50% identity with OCT3 (Gorboulev et al., 1997; Zhang et al., 1997; Gründemann et al., 1998). *N*-glycosylation sites are present on the first extracellular loop, and a large intracellular loop is also present between transmembrane domains six and seven which contains phosphorylation sites for PKA, PKC, protein kinase G (EC

2.7.11.12) and tyrosine kinases (Koepsell, 2020b). The current understanding of the mechanisms of transport by OCTs 1-3 is largely based on computational homology modelling and characterization of structure-function relationships through uptake measurements, as no crystal structures have been resolved. The binding pocket within the outward-open binding cleft contains binding sites (Schmitt et al., 2009) and following binding to the substrate, conformational changes are seen, through which the substrate is released into the cytosol. After release, the transporter, either in the empty state or containing a substrate bound to the inward conformation, again switches back to the outward-open conformation. Evidence through tracer flux measurements of varying substrates have shown that OCTs 1 and 2 transport cations in both directions across the plasma membrane (Nagel et al., 1997; Busch et al., 1998; Budiman et al., 2000).

All OCTs are expressed in the kidney (Karbach et al., 2000; Wu et al., 2000a), brain (Gorboulev et al., 1997; Busch et al., 1998; Gründemann et al., 1998; Wu et al., 1998, 2000a; Vialou et al., 2004; Gasser et al., 2017), placenta (Gorboulev et al., 1997; Kekuda et al., 1998; Bottalico et al., 2004; Sata et al., 2005), basolateral membrane of trophoblasts (Sata et al., 2005), intestinal enterocytes (Gorboulev et al., 1997; Karbach et al., 2000; Slitt et al., 2002; Müller et al., 2005; Koepsell et al., 2007; Han et al., 2013), and in the luminal membrane of lung epithelial cells (Lips et al., 2005). For OCT2, expression has also been reported in the pancreas (Schorn et al., 2021). Strong expression of OCT3 has been reported in the liver (Nies et al., 2009), skeletal muscle, and heart (Wu et al., 2000). This distribution is not dissimilar to that reported for TAAR1 (see Sections 1.3.2.3 and 1.3.2.4), which suggests a similar expression profile between TAAR1 and the OCT transporters. In this context, it is also interesting to note that there is an overlap in the list of substrates for OCTs 1-3 and TAAR1, including TA such as TYR, 2-PE, OA, TRP, synephrine, *N*-methylphenylethylamine, and *N*-methyltryptamine (Braidert et al., 1998; Schömig

et al., 2006; Gozal et al., 2014; Berry et al., 2016; Gebauer et al., 2021), as well as the classical monoamines such as dopamine, serotonin and norepinephrine (Breidert et al., 1998a; Busch et al., 1998; Gründemann et al., 1998; Wu et al., 2000).

OCT1 has been implicated in various aspects of fat utilization and storage (Liang et al., 2018), including reduced-function polymorphisms of OCT1 associated with high plasma total cholesterol and LDL levels (Liang et al., 2018). Further, increased expression of OCT1 has been reported in adipocytes of morbidly obese individuals (Moreno-Navarrete et al., 2011; Suhre et al., 2011; Kim et al., 2017; Liang et al., 2018). Together, these observations may suggest a role for an OCT1 substrate in fat metabolism.

The role of OCT2 in mediating serotonin and norepinephrine clearance was reported when there was reduction observed in the levels of these monoamines in several brain regions of OCT2-KO mice (Jonker et al., 2003). OCT2-KO mice also showed a depression-like phenotype (Bacq et al., 2012), suggesting a role of OCT2 in psychiatric disorders including depression, anxiety and stress-related behaviours (Bacq et al., 2012). An association has been recently reported in the differential expression of OCT2 and overall survival in patients with renal cell carcinoma (Whisenant and Nigam, 2022), and in oxaliplatin sensitivity in pancreatic ductal adenocarcinoma (Chiu et al., 2022).

Reduction in OCT3 functional alleles have been shown to be associated with increased basal metabolic rate in white adipocytes (Song et al., 2019), suggesting a role of OCT3 in metabolic disorders. OCT3 has also been implicated in type 2 diabetes (Mahrooz et al., 2017). Additionally, absence of OCT3 has been reported to lead to liver fibrosis (Vollmar et al., 2019) and hepatocarcinogenesis progression (Vollmar et al., 2017). Further, OCT3 is overexpressed in colorectal cancer cells (Yokoo et al., 2008) and is implicated in prostate cancer (Chen et al., 2013).

The similarities in expression, substrate profile of TAAR1 and OCTs 1-3 and in their implications in similar diseases provide an important perspective of the role of the OCTs in the regulation of the ligands of TAAR1 in such conditions. This is suggestive of OCTs1-3 to be important targets in controlling the TA system that could be implicated in a variety of psychiatric, metabolic and immune-related diseases as explained previously, and as such the link between these systems should be studied closely.

## **1.5 Rationale**

Since TAAR1 is intracellular, the process by which its agonists are transported across cellular membranes is an important question. In addition, TA are found in commonly consumed food items and produced by the intestinal microbiota (see Section 1.2.2.2). Additionally, there have been several associations of TA systems with intestinal disorders such as Crohn's disease, ulcerative colitis, irritable bowel disease, and celiac disease (Section 1.2.2.2). Although transport of TA across the intestinal cell layer has been studied at supraphysiological levels (Tchercansky et al., 1994; Fischer et al., 2010), the transport properties of nanomolar (physiological) levels of TA across the intestinal cell layer have not. Further, with the aforementioned similarities in the expression, substrate profile and disease incidence observed between the TA system and OCT transporters, I aimed to determine whether similar transport processes such as, OCT2, regulate physiological TA concentration passage across intestinal epithelial cells as those previously observed with nanomolar levels of TYR transport in neurons (Berry et al., 2016). For this, I selected the Caco-2 human intestinal epithelial cell line, as a suitable model.

### 1.5.1 Caco-2 human intestinal epithelial cell line

Caco-2 cells (human colorectal adenocarcinoma epithelial adherent cell line) are widely used for permeability studies of different compounds and are an accepted *in vitro* model system for drug transport studies due to their ability to mimic the physiological situation (Hidalgo et al., 1989; Hilgers et al., 1990; Wilson et al., 1990; Artursson and Karlsson, 1991). The Caco-2 cell line was developed by Jorgen Fogh in 1977 at Sloan-Kettering Institute for Cancer Research (Fogh et al., 1977). Even though the cells originate from a colon adenocarcinoma, after confluency, they differentiate to resemble polarized foetal ileal epithelial cells (Lea, 2015). This colonic to small intestine differentiation in culture has been further confirmed through proteome analysis (Stierum et al., 2003). These cells show a cylindrical morphology and form polarized monolayers on culturing with distinct apical and basolateral membranes (Lea, 2015), exhibiting features such as, microvilli, brush border membrane-associated hydrolyzing enzymes (such as dipeptidyl dipeptidase, alkaline phosphatase, sucrase isomaltase, and lactase), and a wide variety of transporter systems (Christensen, 1990; Hilgers et al., 1990; Sood et al., 1992; Mahraoui et al., 1994b, 1994a; Ferrer-Martinez et al., 1995; Glahn et al., 1996; Hosoya et al., 1996; Gunshin et al., 1997; Yee, 1997; Mailleau et al., 1998; Perdikis et al., 1998; Bleasby et al., 2000; Costa et al., 2000; Martel et al., 2001; Thwaites et al., 2002; Goto et al., 2003; Kipp et al., 2003; Maulén et al., 2003; Sambuy et al., 2005; Maubon et al., 2007; Horie et al., 2011; Tai et al., 2013; Gerasimenko et al., 2016; Jochems et al., 2018; Koepsell, 2020a). Full morphological differentiation is associated with the presence of polarized nuclei and cell height similar to that of normal human intestinal epithelium cells (Sambuy et al., 2005). To obtain these physiological conditions, Caco-2 cells are grown on permeable filter supports to allow for passage of nutrients and ions on both sides of a cell monolayer. Here, the apical membrane represents the luminal side of the epithelial cell, whereas the basolateral side represents the side of the cell in closest contact with the blood

vessels. To confirm the tightness of the monolayers for drug permeation/transport studies, trans epithelial electrical resistance (TEER) measurements and/or proliferation rate can be monitored (Srinivasan et al., 2015). Several studies have reported high correlation between Caco-2 permeability coefficients and *in vivo* absorption (Artursson and Karlsson, 1991; Glahn et al., 1996; Cheng et al., 2008; Sun et al., 2008). The Caco-2 system has been used to screen the transport of a wide variety of molecular and ionic species including cadmium (Gerasimenko et al., 2016), caffeine and glycine (Yee, 1997), urea, glucose and testosterone (Hilgers et al., 1990), and synthetic drugs such as azithromycin and diazepam (Yee, 1997), among others.

#### *1.5.1.1 Transporter protein profile in Caco-2 cells*

Caco-2 cells express a variety of transporter proteins from different families that are known to be important in intestinal transport *in vivo*. Specific intestinal transporters for sugars, amino acids, peptides, vitamins, bile acids and micronutrients have all been reported in Caco-2 cells (Jochems et al., 2018). The Na<sup>+</sup>/glucose co-transporters SGLT1 (*Slc5A1*) (Mahraoui et al., 1994; Kipp et al., 2003; Koepsell, 2020a), glucose facilitated transporters GLUT1-3 (*Slc2A1-3*) (Mahraoui et al., 1994a; Koepsell, 2020a), and the fructose transporter GLUT5 (*Slc2A5*) (Mahraoui et al., 1994a, 1994; Gouyon et al., 2003; Koepsell, 2020a) are all expressed in Caco-2 cells. Further, the presence of Na<sup>+</sup>/H<sup>+</sup> antiporter NHE 3 has also been confirmed (Thwaites et al., 2002). A number of ATP-binding cassette (ABC) transporters, including cystic fibrosis transmembrane conductance regulator, a Cl<sup>-</sup> channel, (Sood et al., 1992; Mailleau et al., 1998) and the P-glycoprotein multidrug resistance efflux pump are also expressed (Hosoya et al., 1996; Goto et al., 2003). Furthermore, amino acid transporter systems supporting the uptake of essential amino acids (Jochems et al., 2018) as well as L-glutami-e-B<sub>0</sub> transporter (Christensen, 1990; Costa et al.,

2000) and L-glutamate - X<sub>AG</sub><sup>-</sup> transporter; (Ferrer-Martinez et al., 1995) have been reported. Likewise, peptide transporters such as PepT1 (*Slc15A1*), PHT2 (*Slc15A3*) and PHT1 (*Slc15A4*) have been confirmed in Caco-2 cells (Tai et al., 2013; Jochems et al., 2018), along with transporters for various micronutrients such as the vitamin transporter SVCT1- (*Slc23A1*) (Maulén et al., 2003), and the Fe<sup>2+</sup>, Zn<sup>2+</sup>, Mn<sup>2+</sup> divalent metal ion transporter *Slc11A2* (Gunshin et al., 1997). Among the uptake 1 transporters, SERT (Vieira-Coelho et al., 1998; Martel et al., 2003) and NET (Zhang et al., 2020) are present in Caco-2 cells. Finally, of most potential relevance to TA, the expression of all three OCTs have also been shown (Bleasby et al., 2000; Martel et al., 2001; Maubon et al., 2007; Horie et al., 2011). Together, these observations make the Caco-2 cell line a relevant, suitable physiological model for studying TA transport properties in the gastrointestinal tract.

## 1.6 Study hypothesis

I hypothesize that OCT2 is responsible for transporting endogenous levels of TYR and 2-PE (best-characterized TAAR1 endogenous agonists) across Caco-2 cells, as was seen with native neuronal preparations. In addition to OCT2-mediated transport across Caco-2 cells, I also hypothesize that there are additional TYR and 2-PE transporters in the Caco-2 cell.

## 1.7 Study objective

The overall objective of this study is to characterize the transport of endogenous levels of TA across intestinal epithelial cells (Figure 1.4). Specifically, this study will address the following objectives:

- i) Characterize TYR and 2-PE transport at endogenous levels across the Caco-2 intestinal epithelial cell layer and determine if OCT2 is responsible for such transport.
- ii) Identify and characterize any additional TYR transport processes present.

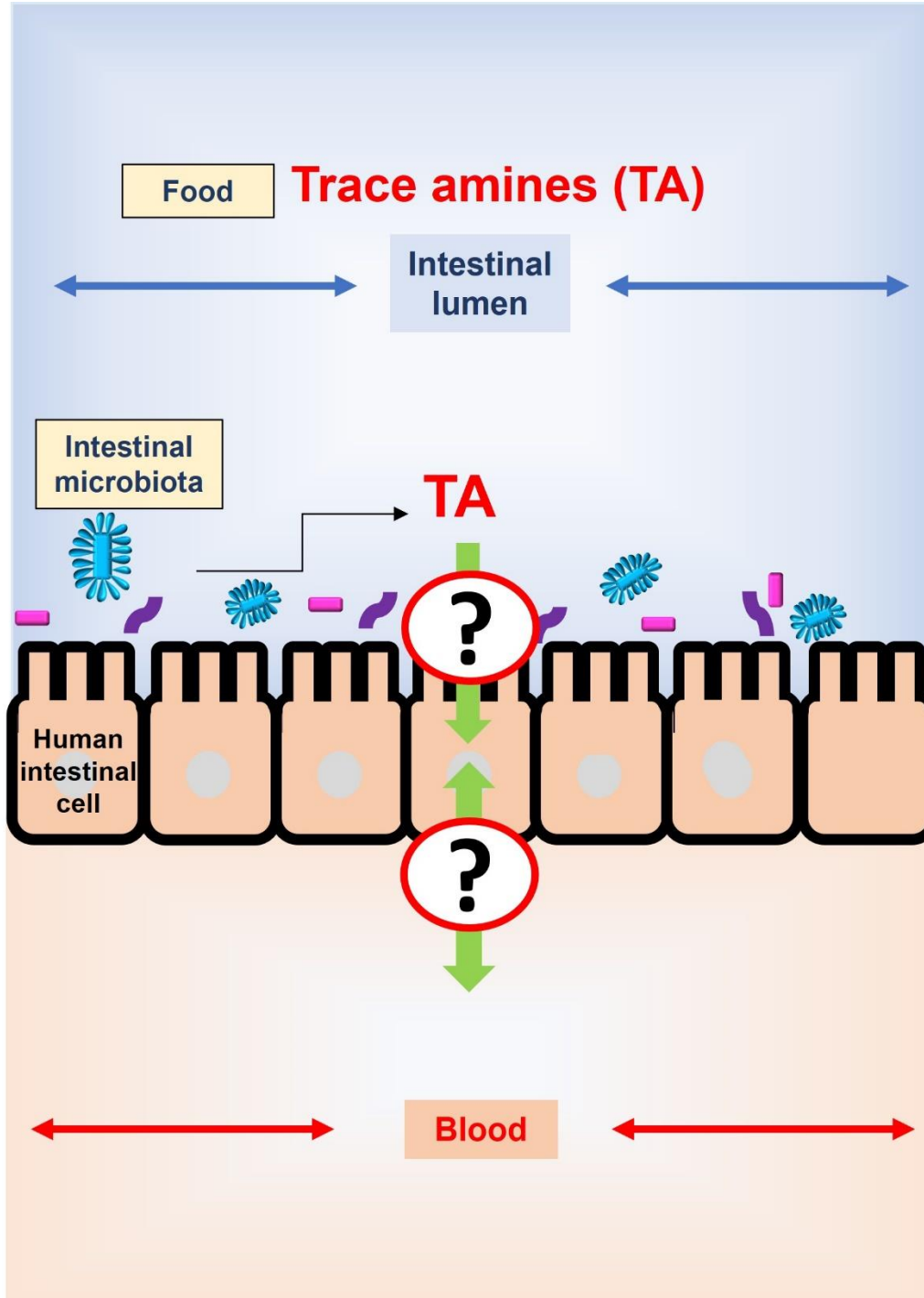


**Figure 1.4: Characterization of TA transport property across Caco-2 intestinal epithelial cells.** The objective for the current study is to investigate if TYR and 2-PE transport across human intestinal Caco-2 cells takes place via OCT2, a facilitated diffusion transporter, as found in rat brain synaptosomes. The figure was generated in MS PowerPoint.

## **2 MATERIALS AND METHODS**

### **2.1 Caco-2 cell culture**

The Biosafety ethics clearance reference number for all the processes undertaken was BC-003. The Caco-2 human intestinal epithelial cell line (American Type Culture Collection, Manassas, VA; passage numbers 18-49) was maintained in Corning® 75cm<sup>2</sup> U-Shaped canted neck cell culture flasks with vent cap (Corning Life Sciences, Tewksbury, MA) at 37°C under 5% CO<sub>2</sub>. The cells were grown in 15 mL of complete Dulbecco's Modified Eagle's Medium (Sigma Aldrich, Oakville, ON) supplemented with 10% fetal bovine serum (ThermoFisher Scientific, Ottawa, ON), 1% non-essential amino acids (ThermoFisher Scientific, Ottawa, ON), 44.04 mM NaHCO<sub>3</sub> (ACP Chemicals Inc, Montreal, QC) and 50 U/mL penicillin + streptomycin (Sigma Aldrich, Oakville, ON), pH 7.4.

#### **2.1.1 Caco-2 subculture**

Once the cells were 70-80% confluent, they were subcultured. The cells were washed with 4 mL of phosphate buffered saline (PBS; Sigma Aldrich, Oakville, ON) solution containing 0.01 M phosphate buffer, 0.0027 M potassium chloride and 0.137 M sodium chloride, pH 7.4, at 25 °C. The cells were then treated with 2 mL of 0.25 % sterile-filtered trypsin-EDTA solution (Sigma Aldrich, Oakville, ON) for 5 minutes at 37°C under 5% CO<sub>2</sub>. After this trypsinization, cells were collected in a 15 mL centrifuge tube (Fisher Scientific, Ottawa, ON) and the action of trypsin was stopped with 9 mL of Caco-2 growth medium. The cell suspension was centrifuged at 150 X g for 5 minutes at room temperature, the supernatant discarded, and the pellet was resuspended in 1 mL of growth medium. Equal aliquots of the suspension were added to Corning® 75cm<sup>2</sup> U-Shaped

Canted Neck Cell Culture Flasks with Vent Cap containing 14.5 mL of Caco-2 growth medium for further subculturing (Corning Life Sciences, Tewksbury, MA).

#### 2.1.2 Caco-2 subculture to 24 well Transwell® plate inserts

At 70-80% confluency cells were harvested as described in Section 2.1.1. Following resuspension in 1 mL of Caco-2 growth medium, Trypan Blue exclusion was performed using 90 µL of cell suspension and 10 µL of Gibco™ 0.4% Trypan Blue solution (ThermoFisher Scientific, Ottawa, ON) to determine the total number of viable cells using a haemocytometer. For counting, four quadrants were counted and the average was determined. To determine the number of cells per ml, the dilution factor (x 10) and the hemocytometer factor (x 10,000) was multiplied with the average cell count. The cells were seeded at  $1 \times 10^5$  cells per polycarbonate Transwell® insert (6.5 mm diameter, 0.4 µm pore size, 0.33 cm<sup>2</sup> membrane area), supported in Corning® 24 well Transwell® multi-well plates. This allows a three-compartment system (apical, cellular and basolateral; Figure 2.1) mimicking the physiological situation of intestinal epithelial cells (Altay et al., 2019) to be established. Here, the apical compartment represents the luminal space and the basolateral compartment represents the blood.

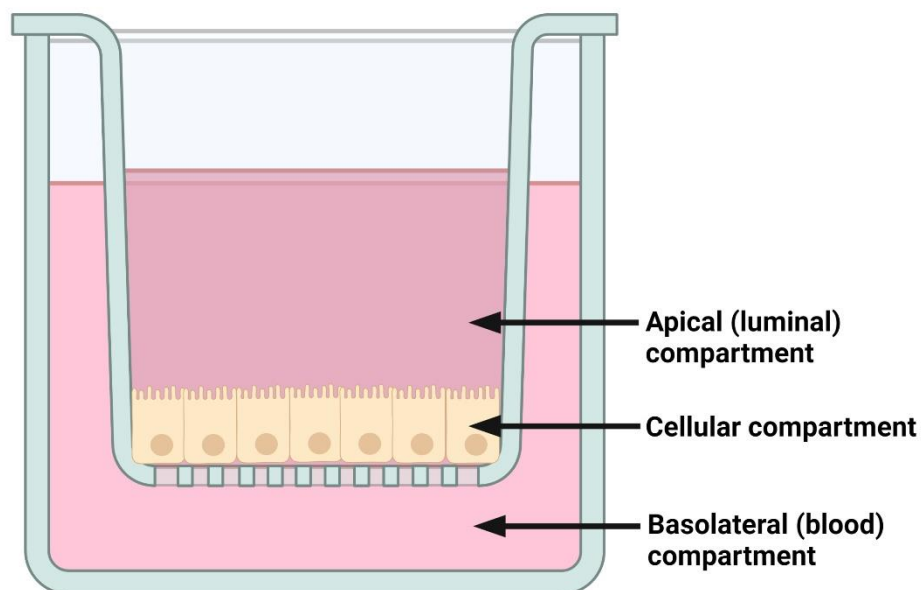


**Figure 2.1: Schematic representation of the Caco-2 cell monolayer culture system.** The Transwell<sup>®</sup> inserts allowed the physiological environment of the intestinal epithelial cells to be recreated in a culture system, with the apical compartment representing the luminal side of the intestinal epithelial cells and the basolateral compartment representing the blood side. Figure was generated in BioRender.

Caco-2 growth medium was added as a 100  $\mu\text{L}$  volume to the apical compartment and 600  $\mu\text{L}$  volume to the basolateral compartment. Transwell<sup>®</sup> cultures were incubated at 37°C under 5%  $\text{CO}_2$  and the media from both compartments changed every second day until a uniform cell monolayer was formed.

## 2.2 Assessment of Caco-2 monolayer integrity

### 2.2.1 Lucifer yellow rejection assay

The growth medium in the apical compartment was replaced with 100  $\mu\text{L}$  of 0.1 mg/mL of lucifer yellow (LY; Sigma Aldrich, Oakville, ON), dissolved in assay buffer, consisting of Hank's Balanced Salt Solution (HBSS) containing 136.89 mM NaCl, 5.30 mM KCl, 0.44 mM  $\text{KH}_2\text{PO}_4$ , 5.55 mM glucose, 0.34 mM  $\text{Na}_2\text{HPO}_4 \cdot 7\text{H}_2\text{O}$ , 4.17 mM  $\text{NaHCO}_3$ , and 10 mM 4-(2-hydroxyethyl)-1-piperazineethanesulfonic acid (HEPES), pH 7.4 at room temperature, and the basolateral compartment was replaced with 600  $\mu\text{L}$  of assay buffer. Culture plates were covered with aluminium foil and incubated for 1 hour at 37°C under 5%  $\text{CO}_2$ . After incubation, 90  $\mu\text{L}$  of each basolateral compartment solution was transferred to individual wells of a Nunc™ F96 Microwell™ black polystyrene plate (ThermoFisher Scientific, Ottawa, ON). Fluorescence was measured in each well at an excitation wavelength = 485 nm and emission wavelength = 535 nm using a Synergy Mx Fluorescent Plate Reader (Biotek, Winooski, VT) and the percent LY permeability determined using Equation 1.

$$\%LY \text{ permeability} = [(F_{\text{cell\_monolayer}} - F_{\text{blank}})/(F_{\text{LY}} - F_{\text{blank}})] * 100 \quad (\text{Equation 1})$$

Where  $F_{\text{cell\_monolayer}}$  is the fluorescence of basolateral compartment solutions derived from chambers containing Caco-2 cells,  $F_{\text{LY}}$  is the fluorescence of the LY solution, and  $F_{\text{blank}}$  is the fluorescence of the assay buffer. A functional Caco-2 monolayer was defined as a percent LY permeability less than 3% (Debebe et al., 2012; Rastogi et al., 2013). Culturing for 23 days was found to consistently provide a LY permeability <3% (Figure 2.2).

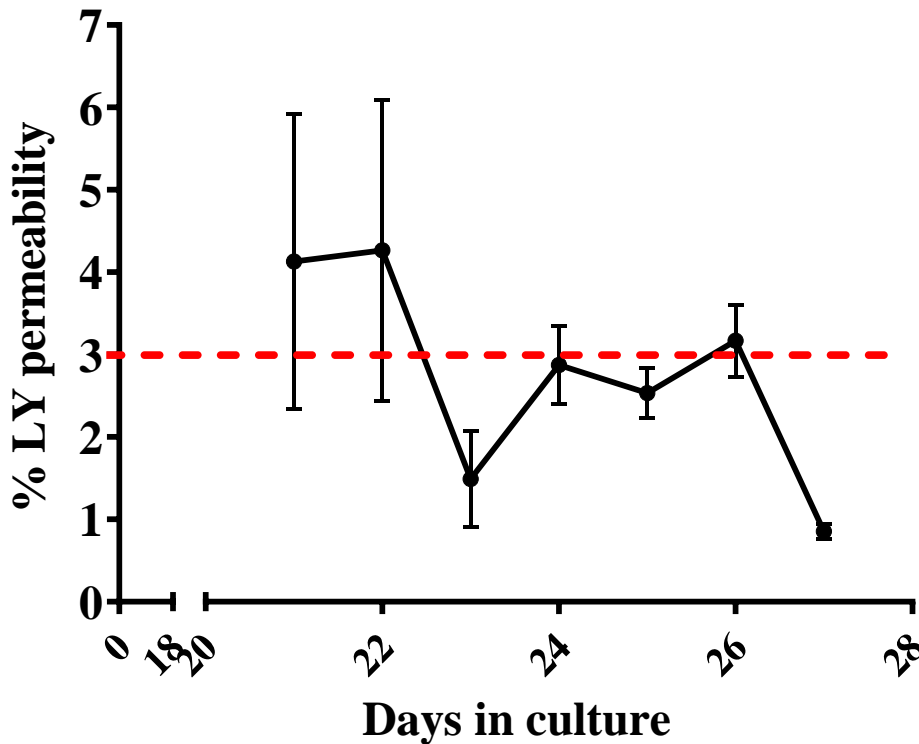


**Figure 2.2: Caco-2 monolayer development as a function of lucifer yellow exclusion.** Lucifer yellow at 0.1 mg/mL, dissolved in assay buffer, was added to the apical compartment of cultured Caco-2 cells and incubated for 1 hour at 37°C under 5% CO<sub>2</sub>. After incubation, fluorescence of the basolateral compartment solution was measured at excitation wavelength = 485 nm and emission wavelength = 535 nm. %LY permeability was determined from Equation 1. Data represents mean ± SEM, n = 3 cultures from 3 independent experiments, except day 23 for which there were n = 7 cultures from 7 independent experiments (for further confirmation, 4 additional experiments were performed). Figure was generated in GraphPad Prism v6.0.

### 2.2.2 Trans epithelial electrical resistance measurement

At various days following plating, the medium was removed from both compartments which were then washed three times with assay buffer (see Section 2.2.1). Cells were then incubated in assay buffer for 30 minutes at 37°C under 5% CO<sub>2</sub> and a Millicell ERS-2 epithelial volt-ohm meter (Millipore Sigma, Burlington, MA) used to measure the electrical resistance across the Transwell<sup>®</sup> inserts containing Caco-2 cells ( $R_{\text{insert}}$ ), along with a blank Transwell<sup>®</sup> insert containing no cells ( $R_{\text{blank}}$ ). The resistance of the cell monolayer was then determined using Equation 2.

$$R_{cell\_monolayer} = R_{insert} - R_{blank} \quad (\text{Equation 2})$$

The unit area resistance for each monolayer was then calculated using Equation 3.

$$\text{Unit area resistance} = R_{cell\_monolayer} \times \text{Effective membrane area} \quad (\text{Equation 3})$$

Where the effective membrane area was taken as the area of the Transwell<sup>®</sup> insert membrane (0.33 cm<sup>2</sup>).

Optimization studies revealed that 23 days in culture corresponded to a TEER measurement of >45 Ωcm<sup>2</sup> (Figure 2.3). For all subsequent experiments only 23-day old cultures showing TEER >45 Ωcm<sup>2</sup> were used.

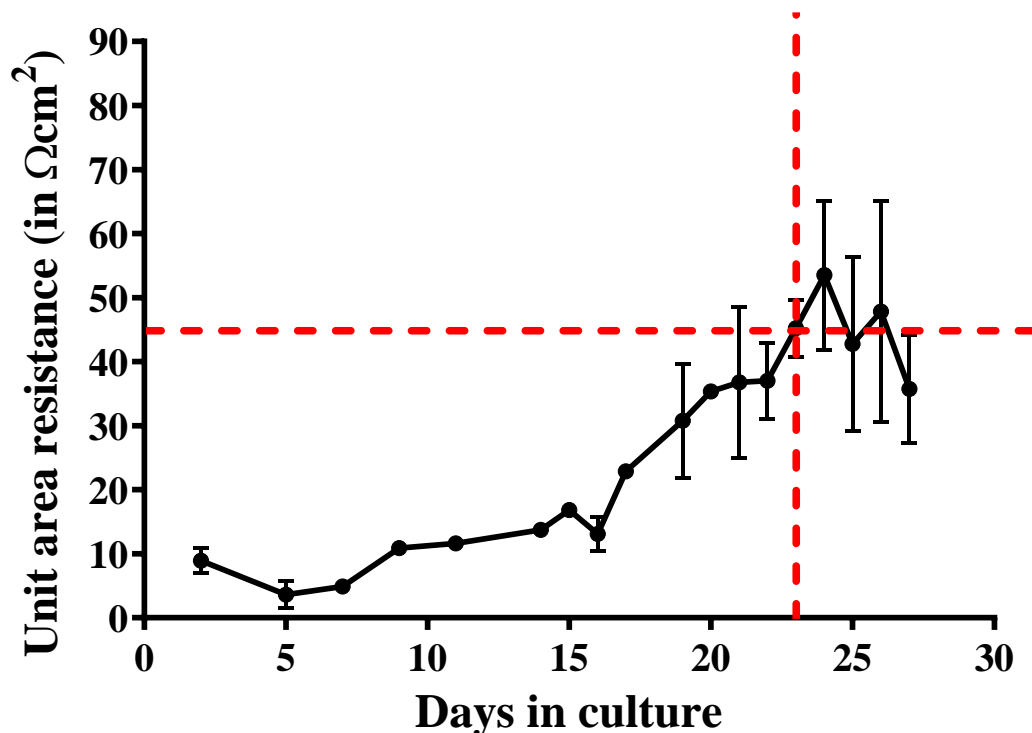


**Figure 2.3: Development of a functional Caco-2 monolayer as a function of trans epithelial electrical resistance measurement.** Cultured Caco-2 cells on Transwell® inserts were incubated in assay buffer for 30 minutes at 37°C under 5% CO<sub>2</sub>. After incubation, the electrical resistance across the Transwell® inserts was measured using a Millicell ERS-2 epithelial volt-ohm meter. The resistance of the Caco-2 cell monolayer was then determined using Equation 2. Data represents mean  $\pm$  SEM, n = 3 cultures from 3 independent experiments, except day 23 for which there were n = 7 cultures from 7 independent experiments (for further confirmation, 4 additional experiments were performed). Figure was generated in GraphPad Prism v6.0.

## 2.3 Trace amine transport across Caco-2 monolayers

### 2.3.1 Subcellular fractionation

Since it has been suggested that TYR can non-specifically interact with the plasma membrane (Tejwani and Anderson, 2008) the amount of TYR in different subcellular compartments was determined. The medium from Caco-2 cells grown to 70-80% confluency in T75 flasks was removed, 15 mL of assay buffer (Section 2.2.1) with TA degrading enzyme inhibitors to prevent metabolism (10  $\mu\text{M}$  pargyline [MAO-A and -B], 2.5  $\mu\text{M}$  OR-486 [catechol-

O-methyl transferase], 100  $\mu$ M sodium diethyldithiocarbamate trihydrate (DTC [dopamine- $\beta$ -hydroxylase]) was added, and the cells were incubated for 30 minutes at 37°C under 5% CO<sub>2</sub>. Then, 100 nM (corresponding to 1500 pmol) of [<sup>3</sup>H]TYR (American Radiolabelled Chemicals Inc., St. Louis, MO) was added to the cells and incubated for 30 minutes at 37°C under 5% CO<sub>2</sub>. After incubation, the assay buffer was removed, and cells were washed with 10 mL of PBS (pH 7.4). Following the wash, the cells were harvested as previously described in Section 2.1.1. The resultant suspension was then transferred to a 15 mL centrifuge tube and was centrifuged at 150 X g for 5 minutes at room temperature. The supernatant was removed, and the cell pellet resuspended in 15 mL of ice-cold hypotonic buffer, pH 7.5, consisting of 10 mM NaCl, 1.5 mM MgCl<sub>2</sub>, and 10 mM Tris-HCl. Cells were disrupted with a Wheaton® Dounce Tissue Grinder (DWK Life Sciences, Millville, NJ, USA) using 15 up-and-down strokes with a loose-fitting pestle and 25 up-and-down strokes with a tight-fitting pestle. The suspension was then transferred to an ultracentrifuge tube and centrifuged at 17,000 X g for 15 minutes at 4°C using a L60K ultracentrifuge (Beckman Coulter, Brea, California, United States). The supernatant (S1) was recovered and kept aside for further use. ScintiVerse™ BD cocktail (Thermo Fisher Scientific, Ottawa, ON) was added to pellet (P1) corresponding to the crude mitochondrial fraction (Rangel et al., 2013) for liquid scintillation counting using a Tri-Carb 2810TR liquid scintillation analyzer (PerkinElmer, Waltham, MA). The S1 supernatant was centrifuged at 80,000 X g for 1 hour at 4°C. The resulting supernatant constitutes the ribosome and cytosol fraction (Rangel et al., 2013), while the pellet represents the plasma membrane fraction (Rangel et al., 2013). Both were collected and transferred to individual scintillation vials containing scintillation fluid for liquid scintillation counting. The counts per minute values obtained were converted to picomoles of TYR by comparison to a standard curve constructed for each independent experiment (Figure 2.4).

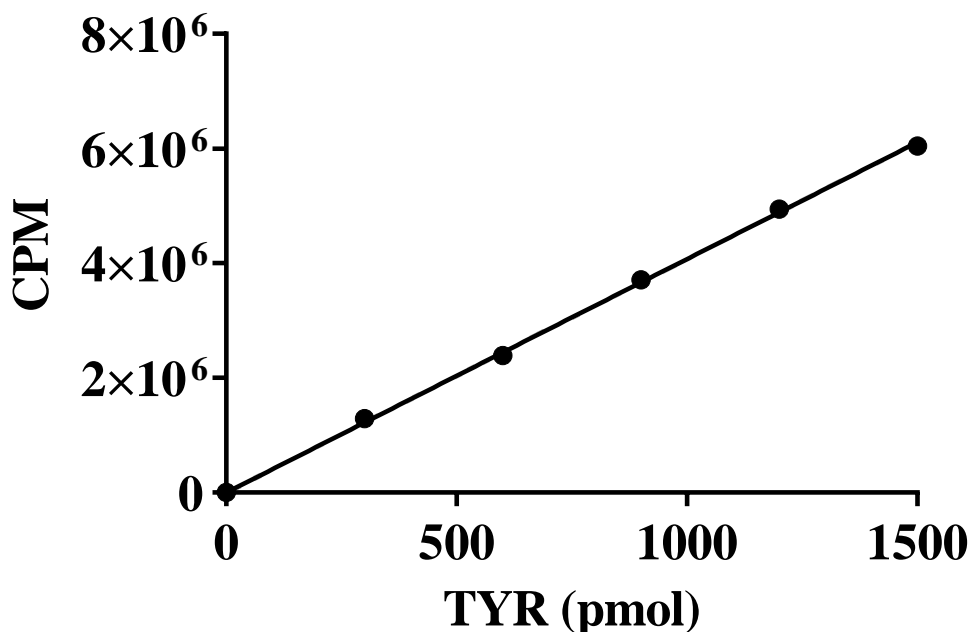


**Figure 2.4: Sample radioisotope assay standard curve to determine picomoles of TYR in subcellular compartments.** The unknown picomole amounts of TYR were determined by interpolation of the CPM values of TYR from the linear regression curve determined by GraphPad Prism v6.0.

### 2.3.2 Trace amine transcellular transport assay

Tight Caco-2 monolayers were defined based on TEER measurements. From the tight, functional Caco-2 monolayers, medium was removed from both compartments which were then washed three times with assay buffer containing TA degrading enzyme inhibitors (see Section 2.2.2) to prevent metabolism. After washing, either 90 (trace amine treated) or 100  $\mu\text{L}$  of assay buffer (blank controls) was added to the apical compartment, and either 590 or 600  $\mu\text{L}$  of assay buffer added to the basolateral compartment, and cells incubated for 30 minutes at 37°C under 5%  $\text{CO}_2$ . After incubation a 10  $\mu\text{L}$  aliquot of either [<sup>3</sup>H]TYR (American Radiolabeled Chemicals Inc.,

St. Louis, MO) or [<sup>14</sup>C]2-PE (Perkin Elmer, Waltham, MA) containing TA degrading enzyme inhibitors was added to either the apical or the basolateral compartment to give a final concentration of 100 nM, and cells incubated for varying time points (0, 5, 10, 15, 20, 25, 30 minutes). At the given time points, the apical and basolateral compartments were collected and transferred to individual scintillation vials containing ScintiVerse™ BD cocktail for liquid scintillation counting using a Tri-Carb 2810TR liquid scintillation analyzer. The cell fractions were lysed in 100 µL of NP-40 lysis buffer (20 mM Tris-HCl, 137 mM NaCl, 10% [v/v] glycerol, 1% [v/v] NP-40, 2 mM EDTA; pH 8.0) by incubating for 20 minutes at 37°C under 5% CO<sub>2</sub> before transferring the lysate to scintillation vials containing ScintiVerse™ BD cocktail. Picomoles of TA were determined by comparison to standard curves performed with every experiment and converted to molar concentrations using the known volumes of the apical (100 µL) and basolateral (600 µL) compartments. The volume for the Caco-2 cell monolayer was calculated based on literature information that the volume of a Caco-2 cell monolayer is 11.56 µL for 24 mm insert membranes with a growth area of 4.67 cm<sup>2</sup> (Sun and Pang, 2008). From this information, the height of the Caco-2 cell monolayer was calculated to be 0.0025 cm with the assumption of the cell monolayer being a cylinder (volume of a cylinder =  $\pi r^2 h$ ) since the monolayer is columnar. Using this the volume of Caco-2 cell monolayer for this study was calculated to be 0.817 µL.

### 2.3.3 Statistical analyses

All results are represented as mean  $\pm$  standard error of the mean (SEM). Distribution of TYR between the subcellular compartments was compared by one-way ANOVA with Tukey's multiple comparison post-hoc analysis. Time-dependent accumulation of TYR and 2-PE in different

compartments was compared by two-way ANOVA with Sidak's multiple comparison post-hoc analysis. All analyses and graphing were performed using GraphPad Prism v6.0.

## **2.4 Characterizing TYR transporters**

### **2.4.1 Determination of the role of OCT2 in TYR transport**

Since well-validated OCT2 specific inhibitors have not been reported, a pharmacological subtractive approach was taken to determine the role of OCT2 in TYR transport as described previously (Berry et al., 2016), where the effect of inhibitors of varying selectivity towards the OCT family on TYR transport were tested. Experiments were conducted as described in Section 2.3.2. with assay buffer also including one of 1  $\mu\text{M}$  decynium-22 (pan-OCT inhibitor), 200  $\mu\text{M}$  pentamidine (OCT1 and OCT2 inhibitor), or 10  $\mu\text{M}$  atropine (ATR; OCT1 inhibitor).

### **2.4.2 Statistical analyses**

All results are represented as mean  $\pm$  SEM. Statistical analysis was performed using two-way ANOVA with Sidak's post-hoc analysis to compare the time-dependent accumulated concentrations of TYR in different compartments, in the presence or absence of inhibitors with varying selectivity towards the OCT-family. All analyses were performed using GraphPad Prism v6.0.

## **2.5 Investigation of the presence of OCT2 in Caco-2 cells**

### **2.5.1 Preparation of Caco-2 cell lysate**

Confluent Caco-2 cells were harvested as described in Section 2.1.1. The supernatant was discarded and the cell pellet was resuspended in 100  $\mu$ L of NP-40 lysis buffer and incubated for 20 minutes at 37°C under 5% CO<sub>2</sub>. The lysate was then stored on ice until further use.

### **2.5.2 Preparation of animal tissue homogenates**

All procedures were performed in accordance with Canadian Council on Animal Care guidelines and were approved by Memorial University Animal Care Committee. The animals used for this study were 8 weeks old, male, Sprague Dawley rats, housed on a 12-hour light-dark cycle, and fed a standard chow diet. For tissue collection, the rats were euthanized using CO<sub>2</sub>, followed by decapitation after which the brain, intestines and the kidneys were removed. From the brain, the frontal cortex and the striata were isolated. The frontal cortex was used for preparation of synaptosomes (see Section 2.5.3). The striata, intestines and the kidney were individually diced, homogenized in 10 volumes of NP-40 lysis buffer, and kept on ice until further use.

### **2.5.3 Preparation of synaptosomes**

The frontal cortex was diced and then homogenized in 10 volumes of 0.32 M sucrose using a Wheaton<sup>®</sup> Dounce Tissue Grinder with 10 up-and-down strokes of a loose pestle. After homogenization, the suspension was centrifuged at 1,000 X g for 10 minutes at 4°C using a Thermo Sorvall<sup>™</sup> ST 16R centrifuge (ThermoFisher Scientific, Ottawa, ON). Following centrifugation, the pellet was discarded, and the supernatant centrifuged at 10,000 X g for 20

minutes at 4°C. The supernatant was removed and the crude synaptosomal pellet was resuspended in 100 µL of NP-40 lysis buffer and incubated for 20 minutes at 37°C. Lysed synaptosomes were kept on ice until further use.

#### 2.5.4 Bicinchoninic Acid (BCA) Protein Assay

Total protein was determined in tissue preparations by the Pierce BCA Protein Assay Kit (ThermoFisher Scientific, Ottawa, ON). The protein samples and the standards were added to Corning™ clear polystyrene 96-well microplates at a volume of 10 µL, in duplicate. To these, 200 µL of BCA working reagent was added and mixed using a Fisherbrand™ multi-platform shaker for 30 seconds followed by incubation for 30 minutes at 37°C. After incubation, the absorbance for each well was measured at 562 nm using a Biotek Powerwave XS UV/Vis microplate spectrophotometer (Winooski, VT). Protein content was determined by comparison to a standard curve of bovine serum albumin (BSA) in the concentration range of 0-20 µg/10 µL (Figure 2.5) that was prepared for each experiment, using GraphPad Prism v6.0.

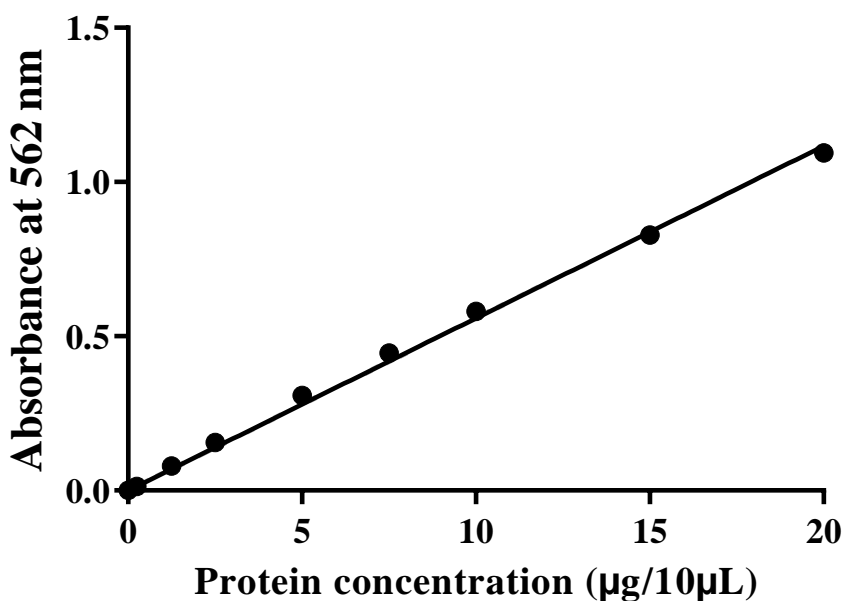


**Figure 2.5: Sample BCA protein assay standard curve to determine amount of total protein.** Baseline correction was performed using a blank. The unknown amount of total protein ( $\mu\text{g}/10\ \mu\text{L}$ ) was determined by interpolation of the absorbance values measured at 562 nm from the linear regression curve determined by GraphPad Prism v6.0.

#### 2.5.5 Western Blot of OCT2

Tissue samples containing 20  $\mu\text{g}$  of protein were used to perform sodium dodecyl sulphate polyacrylamide gel electrophoresis (SDS PAGE) using a Mini gel tank (ThermoFisher Scientific, Ottawa, ON) with Bolt™ 4-12% bis-tris plus gels (ThermoFisher Scientific, Ottawa, ON) at 200 V for 32 minutes. After SDS PAGE, the proteins were transferred onto a nitrocellulose membrane using iBlot®2 transfer stacks (ThermoFisher Scientific, Ottawa, ON) for an iBlot®2 gel transfer device (ThermoFisher Scientific, Ottawa, ON) set to 20-25 V for 7 minutes. Either the anti-SLC22A2 polyclonal primary antibody (Elabscience®, Houston, Texas; catalogue number: E-AB-62923) at 1:200 dilution in 1X iBind™ solution (ThermoFisher Scientific, Ottawa, ON), or anti-SLC22A2 Picoband™ primary antibody (Boster Biological Technology, Pleasanton, CA;

catalogue number: PB9394) at 1:400 dilution in 1X iBind™ solution were used to identify OCT2 using the Invitrogen™ iBind™ western device (ThermoFisher Scientific, Ottawa, ON) with an overnight incubation at 4 °C. The membrane was then washed once with 1X iBind™ solution and incubated with goat anti-rabbit (H+L) horseradish peroxidase conjugated secondary antibody (Bio-Rad, Mississauga, ON; catalogue number: 1706515) at 1:600 dilution in 1X iBind™ solution at 4 °C. Bands were visualized by chemiluminescence using Clarity™ Western ECL substrate (Bio-Rad, Hercules, CA, USA) and molar masses estimated by comparison to a SeeBlue™ Plus2 pre-stained protein standard (ThermoFisher Scientific, Ottawa, ON). Bands were imaged using an ImageQuant LAS 4000 gel documentation system (GE Healthcare, Chicago, IL).

To confirm if the same proteins were identified with each of the primary antibodies, membranes were stripped and re-probed with the other primary antibody. Mild membrane stripping was performed by incubating membranes twice for 10 mins at 37°C, pH 2.2 with 0.2 M glycine, 3.46 mM SDS, 1% (v/v) Tween 20 (mild stripping buffer), with constant shaking on a Fisherbrand™ multi-platform shaker (ThermoFisher Scientific, Ottawa, ON). This was followed by two washes with PBS (pH 7.4) and two washes with tris buffered saline-Tween 20 (TBST; containing 137 mM NaCl, 2.7 mM KCl, 19 mM tris, 0.1% Tween 20). Harsh stripping was performed by incubating membranes in 2% (w/v) SDS; 0.0625 M tris HCl, pH 6.8; 0.8% (v/v) 2-mercaptoethanol for 1 hour at 50°C with shaking on a Fisherbrand™ multi-platform shaker, followed by one wash each with water and TBST.

## 2.6 Characterization of TYR active transporter in Caco-2 basolateral membranes

### 2.6.1 Determination of transporter energy source

Experiments were conducted as described in Section 2.3.2, except that NaCl in the assay buffer was replaced on an equimolar basis by choline chloride to determine the sodium dependence of the basolateral active transporter.

### 2.6.2 Determination of the kinetic parameters of the TYR active transporter in Caco-2 basolateral membranes

[<sup>3</sup>H]TYR at varying concentrations (200, 100, 50, 10, 5 and 1 nM), in the presence of inhibitors of TA degrading enzymes (10 μM pargyline, 2.5 μM OR-486 and 100 μM DTC), was added to the basolateral compartment, and the cellular compartment was collected at various time points (0, 10, 20, 30, 45, 60, 180, 300 and 600 seconds) after addition, and radioactivity and TYR concentration determined as previously described (Section 2.3.2).

For Michaelis-Menten analysis the initial velocity ( $V_0$ ) at each concentration was determined from the initial linear phase of the TYR concentration versus time plots. Total TYR transport was defined as that obtained in regular assay buffer, while non-specific (non-transporter-mediated) transport was defined as that present in assay buffer containing choline chloride instead of NaCl. Transporter-specific passage was then defined as the difference between the two and used to obtain the  $K_t$  and  $V_{max}$  from plots of  $V_0$  versus substrate concentration using GraphPad Prism v6.0 as described previously (Berry et al., 2016).

## 2.7 Identification of the TYR active transporter in Caco-2 basolateral membrane

### 2.7.1 Development of TYR affinity columns

*N*-hydroxysuccinimide (NHS)-activated Sepharose 4 Fast Flow (GE Healthcare, Chicago, IL), an agarose matrix, was used to couple to TYR to prepare TYR affinity columns. TYR attaches to the column by displacing the NHS group. NHS-activated Sepharose 4 Fast Flow in 100% isopropanol (0.4 mL; 1 matrix volume) was centrifuged at 1,000 X g for 1 minute at 4°C using a Thermo Sorvall™ ST 16R centrifuge. The supernatant was removed, and the pellet was washed with 10 matrix volumes of cold 1 mM hydrochloric acid by centrifuging at 1,000 X g for 1 minute at 4° C using a Thermo Sorvall™ RC 6+ centrifuge (ThermoFisher Scientific, Ottawa, ON). The supernatant was discarded, and the pellet was further washed in 10 matrix volumes of coupling buffer (0.2 M NaHCO<sub>3</sub>, 0.5 M NaCl, pH 8.3) by centrifuging at 1000 X g for 1 minute at 4°C. The supernatant was discarded, and the matrix was resuspended in one half matrix volume of 0.023 M TYR (Alfa Aesar, Haverhill, MA) in coupling buffer and mixed by shaking. The tube was sealed with parafilm and incubated at 4°C with continuous shaking using a Fisherbrand™ multi-platform shaker for 16 hours. After incubation, the coupling efficiency to the column was determined.

To determine the coupling efficiency, the coupled matrix was centrifuged at 1000 X g for 1 minute at 4°C using a Thermo Sorvall™ RC 6+ centrifuge. The supernatant was recovered and the pellet was resuspended in 3X matrix volumes of coupling buffer, centrifuged at 1000 X g for 1 minute at 4°C, and repeated a further two times. The original supernatant was equally divided between two tubes 'a and b'. Equivalent blank tubes containing only coupling buffer were also prepared. Pure TYR shows two absorbance peaks at 235 nm and 275 nm (Figure 2.6) one of which coincides with the 235 nm absorbance peak of NHS (Figure 2.6) (Lucas et al., 2006; Klykov and Weller, 2015; Spasojevic et al., 2019). To differentiate between the absorbance peak of the NHS

group and uncoupled TYR, NaOH was added to tube ‘b’ (flowthrough + NaOH; Figure 2.7) and incubated for 30 minutes at room temperature to provide a separation between NHS and TYR peaks. After incubation, the pH for the ‘b’ tubes were checked to ensure all the ‘b’ solutions had a basic pH of at least pH 11, and the absorption spectra determined using a NanoDrop™ 2000 spectrophotometer (Figure 2.7). This allowed a complete separation of spectra due to auto-oxidation of TYR at basic pH (Figure 2.7), and an absorbance was seen at 300 nm following NaOH treatment with TYR but not NHS solutions.

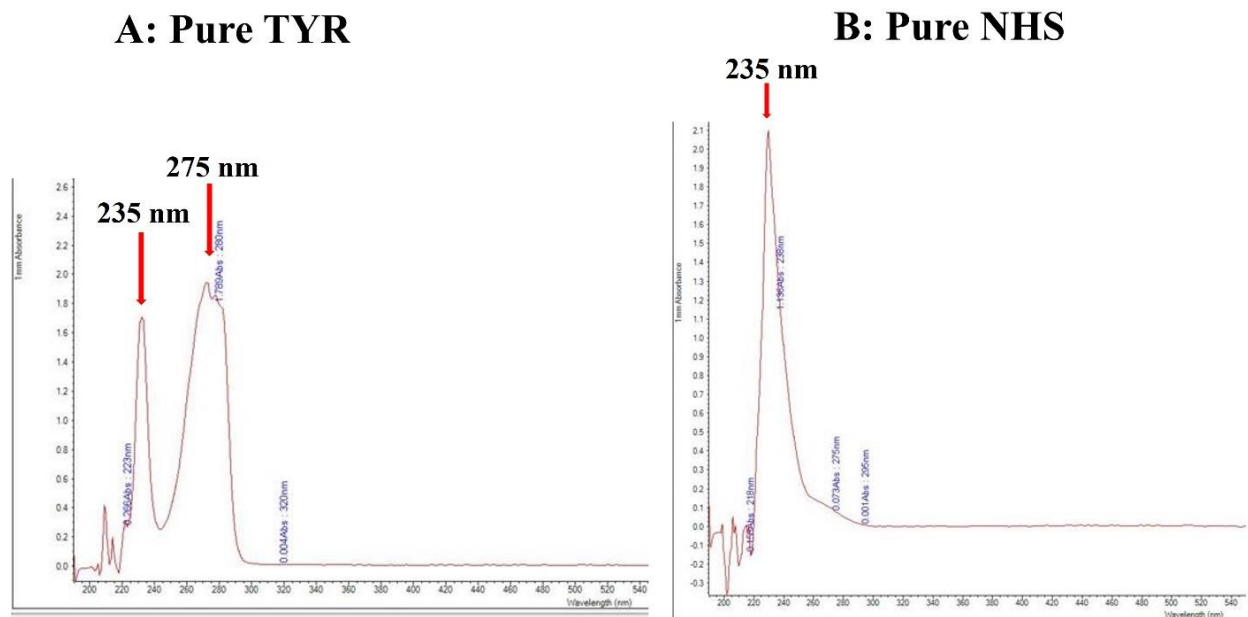
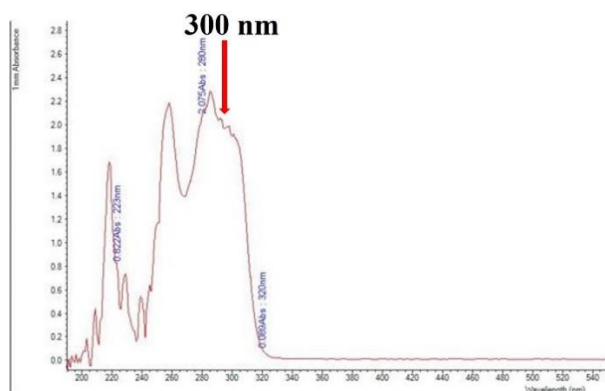


**Figure 2.6: Absorption spectra of TYR and NHS.** A – Spectral absorbance of pure TYR; and B – spectral absorbance of pure NHS at pH 8.3.

### A: Pure TYR+ NaOH



### B: Pure NHS + NaOH

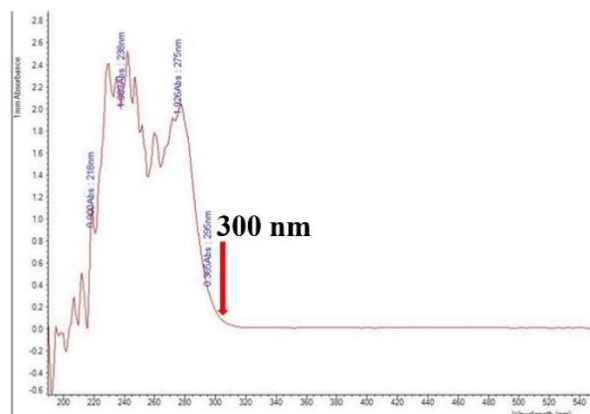


**Figure 2.7: Absorption spectra of TYR and NHS in the presence of NaOH.** A – Spectral absorbance of pure TYR+NaOH; and B – spectral absorbance of pure NHS+NaOH at pH 11.

A 40% reduction in absorbance of the flowthrough solution compared to the input solution was consistently seen (paired t-test,  $P < 0.0001$  Figure 2.8) indicating successful coupling of TYR to the NHS column.

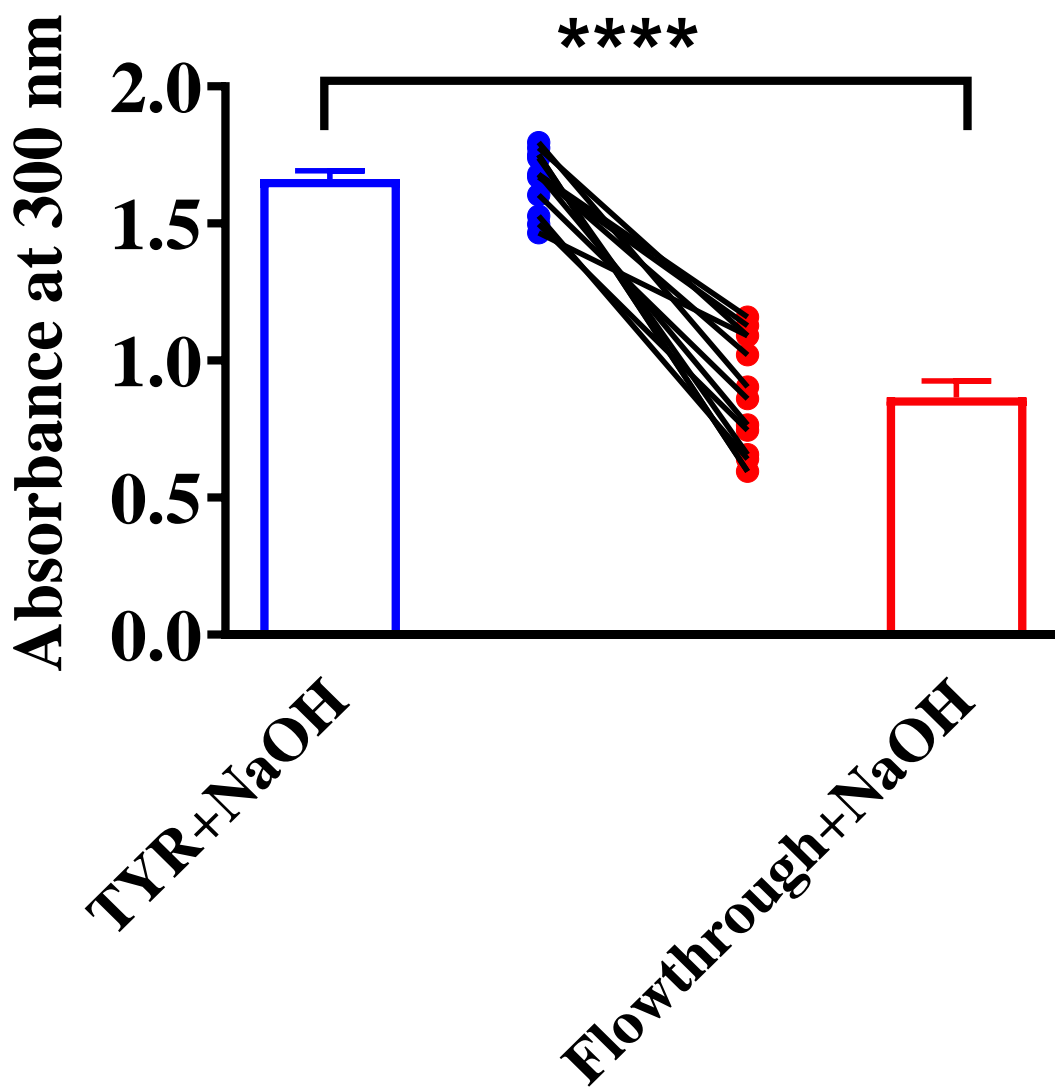


**Figure 2.8: Confirmation of TYR attachment to an NHS-column.** Successful coupling was observed with TYR being retained by the NHS affinity column. Data represents mean  $\pm$  SEM,  $n=13$ . Analysis was made between different fractions using GraphPad Prism version 6 by paired t-test,  $P < 0.0001$ . Bars represent the mean absorbance for the two groups, while the points represent each of the absorbance readings that were recorded for independent preparations.

TYR-coupled matrices were resuspended in 2 matrix volumes of blocking buffer (0.1 M tris-HCl, pH 8.5), sealed with parafilm and incubated at 4°C for 2 hours with continuous shaking using a Fisherbrand™ multi-platform shaker. After 2 hours, the matrix was centrifuged at 1000 X g for 1 minute at 4°C using a Thermo Sorvall™ RC 6+ centrifuge, the supernatant was discarded, and

the pellet was washed alternately with ice cold 0.1 M tris buffer (pH 8.5) and acetate buffer (0.1 M CH<sub>3</sub>COONa, 0.5 M NaCl; pH 4.5), for six times.

#### 2.7.2 Purification of TYR binding proteins from Caco-2 cells by affinity chromatography

Caco-2 cells were grown to full confluency in three Corning® 75cm<sup>2</sup> U-Shaped canted neck cell culture flasks with vent cap. Once confluent, the medium was removed, and the cells washed with 4 mL of sterile PBS (pH 7.4) per flask. Cells were harvested by trypsinization as described in Section 2.1.1, the supernatants discarded, and pellets pooled by resuspending in 0.8 mL of NP-40 lysis buffer containing Halt™ Protease Inhibitor Cocktail (1X; ThermoFisher Scientific, Ottawa, ON) and 1 mM phenylmethanesulfonyl fluoride (Sigma Aldrich, Oakville, ON). The suspension was incubated for 20 minutes at 37°C and the resultant solution used for purification of TYR binding proteins by affinity chromatography.

The Caco-2 lysate was loaded onto the blocked TYR-matrix in a microcentrifuge tube, sealed with parafilm, and incubated for 16 hours at 4°C with continuous shaking using a Fisherbrand™ multi-platform shaker. Following incubation, the matrix+lysate solution was centrifuged at 1000 X g for 1 minute at 4°C. The pellet was resuspended in 1X matrix volume of assay buffer and centrifuged again at 1000 X g for 1 minute at 4°C, with the resuspension and centrifugation repeated a further four times. After the final wash, TYR binding proteins were eluted by resuspending the pellet in either 1.15 M TYR in assay buffer, or 100 µM ATR in assay buffer. Tubes were sealed with parafilm and incubated for 1 hour at room temperature with constant shaking using a Fisherbrand™ multi-platform shaker. After incubation, the tube was centrifuged at 1000 X g for 1 minute at 4°C and the supernatant collected, as the first TYR-binding protein fraction. The pellet was resuspended in one half matrix volume of either TYR or ATR elution solution, incubated for 1 hour at room temperature with constant shaking using a Fisherbrand™

multi-platform shaker, and centrifuged again at 1000 X g for 1 minute at 4°C. This was repeated one more time and during each step, the supernatants were collected giving the second and third TYR-binding protein fractions.

Proteins in fractions isolated from affinity columns were separated by SDS-PAGE as previously described in Section 2.5.5. Proteins were visualized by incubating the gel in staining solution containing 0.25% (w/v) Coomassie Brilliant Blue R-250 (BioRad, Hercules, CA), 50% (v/v) 95% ethanol and 10% (v/v) glacial acetic acid, for 40 minutes at room temperature with constant shaking, followed by destaining (0.8 L deionised water, 0.1 L 95% ethanol, and 0.1 L glacial acetic acid) for 2 hours at room temperature to remove non-selective dye accumulation. Protein bands were then digitally recorded using a Biorad Chemidoc system (Hercules, CA).

### 2.7.3. Identification of TYR binding proteins isolated from Caco-2 cells

Protein bands that were common between different samples were excised from gels with a scalpel. After cutting the gel bands, they were transferred to microcentrifuge tubes with a hole placed in the caps. Tubes were incubated in a desiccator overnight to dry the excised gel. Dried, excised bands were shipped to the Biological Mass Spectrometry Core Facility at Dalhousie University for protein digestion, followed by liquid chromatography with tandem mass spectrometry analysis of the protein digests. From these digests, peptide hits were identified using the Proteome Discoverer Software, and protein identification and grouping based on the presence of common peptide fingerprints among the protein digests. The inclusion criteria for putative TYR transporters were i) membrane proteins, ii) transporter proteins, iii) active transporters, iv) Na<sup>+</sup>-dependent active transporters, and v) TYR being a known substrate.

## 2.8 Modelling of TYR transcellular transport across intestinal epithelial cells

### 2.8.1 Development of mathematical models for known TYR transport processes

Known TYR transport processes were modelled using previously described transporter modelling techniques (Friedman, 2008). Equations 4 and 5 represent generalized equations for facilitated diffusion and active transport, respectively, assuming Michaelis-Menten kinetics for all transporter mediated membrane passage. In this instance  $X_1$  represents the concentration of TYR in the donor compartment and  $X_2$  the concentration in the receiver compartment.

$$\frac{dX_1}{dt} = -\frac{V_{max}X_1}{K_t+X_1} + \frac{V_{max}X_2}{K_t+X_2} \quad (\text{Equation 4})$$

$$\frac{dX_1}{dt} = -\frac{V_{max}X_1}{K_t+X_1} \quad (\text{Equation 5})$$

For non-transporter mediated processes (simple diffusion), a one-phase exponential decay function was used (Equation 6), where  $p$  is the TYR permeability coefficient of  $22.6 \pm 4.3 \text{ \AA/s}$  (Berry et al., 2013) and  $A$  represents the surface area of the membrane.

$$\frac{dX_1}{dt} = -p \times A (X_1 - X_2) \quad (\text{Equation 6})$$

Equations 4-6 were used in the development of additional equations as explained in the next section.

### 2.8.2 Development of ordinary differential equations for each compartment

Using the above equations, a set of ordinary differential equations (ODEs) for the known TYR transport processes across each membrane were developed for the apical (Equation 7), cellular (Equation 8) and basolateral (Equation 9) compartments (Figure 2.9) to model the rate of change of TYR concentration within each compartment for both luminal-to-blood and blood-to-

luminal transcellular passage. In all equations, text in blue corresponds to simple diffusion terms, text in green corresponds to OCT2 mediated facilitated diffusion transport, and purple text to a basolateral membrane Na<sup>+</sup>-dependent active transporter. The  $\alpha$  term represents a constant which is the product of  $p$  and A. The volumes of the apical, cellular, and basolateral compartments are represented as  $Vol_{apical}$ ,  $Vol_{cell}$ ,  $Vol_{baso}$ .

$$\frac{dX_{apical}}{dt} = \left[ -\left(\frac{\alpha}{Vol_{apical}}\right) \times (X_{apical} - X_{cell}) \right] + \left[ -\left(\frac{Vol_{cell}}{Vol_{apical}}\right) \times \left(\frac{V_{max\_OCT2}X_{apical}}{K_{t\_OCT2}+X_{apical}} - \frac{V_{max\_OCT2}X_{cell}}{K_{t\_OCT2}+X_{cell}}\right) \right] \quad (\text{Equation 7})$$

$$\frac{dX_{cell}}{dt} = \left[ -\left(\frac{\alpha}{Vol_{cell}}\right) \times (X_{cell} - X_{apical}) \right] + \left[ -\left(\frac{\alpha}{Vol_{cell}}\right) \times (X_{cell} - X_{baso}) \right] + \left(\frac{V_{max\_OCT2}X_{apical}}{K_{t\_OCT2}+X_{apical}} - \frac{V_{max\_OCT2}X_{cell}}{K_{t\_OCT2}+X_{cell}}\right) + \left(\frac{V_{max\_baso\_active}X_{baso}}{K_{t\_baso\_active}+X_{baso}}\right) \quad (\text{Equation 8})$$

$$\frac{dX_{baso}}{dt} = \left[ -\left(\frac{\alpha}{Vol_{baso}}\right) \times (X_{baso} - X_{cell}) \right] + \left[ -\left(\frac{Vol_{cell}}{Vol_{baso}}\right) \times \left(\frac{V_{max\_baso\_active}X_{baso}}{K_{t\_baso\_active}+X_{baso}}\right) \right] \quad (\text{Equation 9})$$

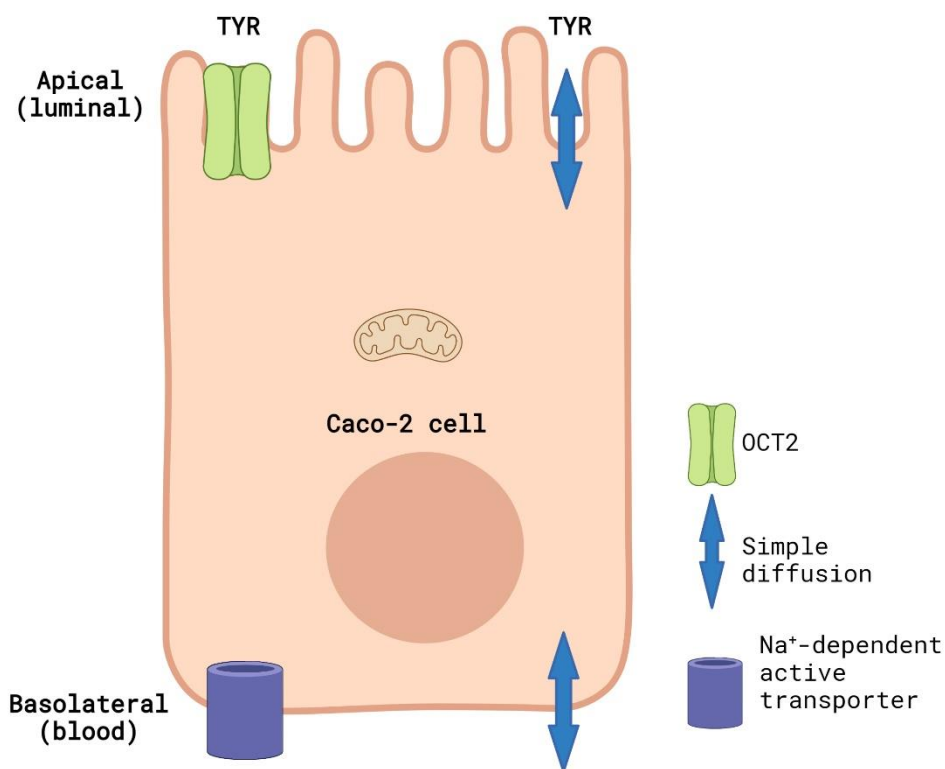


**Figure 2.9: Known TYR transport processes across Caco-2 cells representing the baseline simulation model.** This figure represents the baseline model of known TYR transport processes in the Caco-2 intestinal cell line, where TYR can cross Caco-2 plasma membranes by simple diffusion, be transported across the apical membrane by the bi-directional facilitated diffusion transporter OCT2, or actively accumulated within the cell from the basolateral compartment by an unidentified  $\text{Na}^+$ -dependent active transporter. This image was generated in BioRender and adapted from Sarkar et al., 2022.

The value for the OCT2  $V_{\max}$  from previous synaptosome studies (30.2 fmol/mg protein/s; (Berry et al., 2016) was converted to nM/s (0.11 nM/s) using the known protein content of individual synaptosomal preparations in those studies (Berry et al., 2016). Compartment concentrations for apical and basolateral additions were those experimentally determined in Section 2.3.2. The start point at the donor compartment was set to the average concentration

obtained at 10 seconds after compartment loading. Predicted concentration-time relationships in each compartment were compared to that experimental data using MATLAB (vR2021a).

### 2.8.3 Addition of further transporter processes to the Caco-2 membranes

In an attempt to better recapitulate experimental data, a facilitated diffusion transporter with the kinetic characteristics of OCT2 was added to the basolateral membrane (Figure 2.10) and is represented by the red text in Equations 10 and 11 for cellular and basolateral compartments respectively.

$$\begin{aligned} \frac{dX_{cell}}{dt} = & \left[ -\left(\frac{\alpha}{Vol_{cell}}\right) \times (X_{cell} - X_{apical}) \right] + \left[ -\left(\frac{\alpha}{Vol_{cell}}\right) \times (X_{cell} - X_{baso}) \right] + \\ & \left( \frac{V_{max\_OCT2}X_{apical}}{K_t_{OCT2}+X_{apical}} - \frac{V_{max\_OCT2}X_{cell}}{K_t_{OCT2}+X_{cell}} \right) + \left( \frac{V_{max\_baso\_active}X_{baso}}{K_t_{baso\_active}+X_{baso}} \right) \\ & + \left( \frac{V_{max\_baso\_new\_FD}X_{baso}}{K_t_{baso\_new\_FD}+X_{baso}} - \frac{V_{max\_baso\_new\_FD}X_{cell}}{K_t_{baso\_new\_FD}+X_{cell}} \right) \end{aligned} \quad \text{(Equation 10)}$$

$$\begin{aligned} \frac{dX_{baso}}{dt} = & \left[ -\left(\frac{\alpha}{Vol_{baso}}\right) \times (X_{baso} - X_{cell}) \right] + \left[ -\left(\frac{Vol_{cell}}{Vol_{baso}}\right) \times \left(\frac{V_{max\_baso\_active}X_{baso}}{K_t_{baso\_active}+X_{baso}}\right) \right] + \\ & \left[ -\left(\frac{Vol_{cell}}{Vol_{baso}}\right) \times \left(\frac{V_{max\_baso\_new\_FD}X_{baso}}{K_t_{baso\_new\_FD}+X_{baso}} - \frac{V_{max\_baso\_new\_FD}X_{cell}}{K_t_{baso\_new\_FD}+X_{cell}}\right) \right] \end{aligned} \quad \text{(Equation 11)}$$

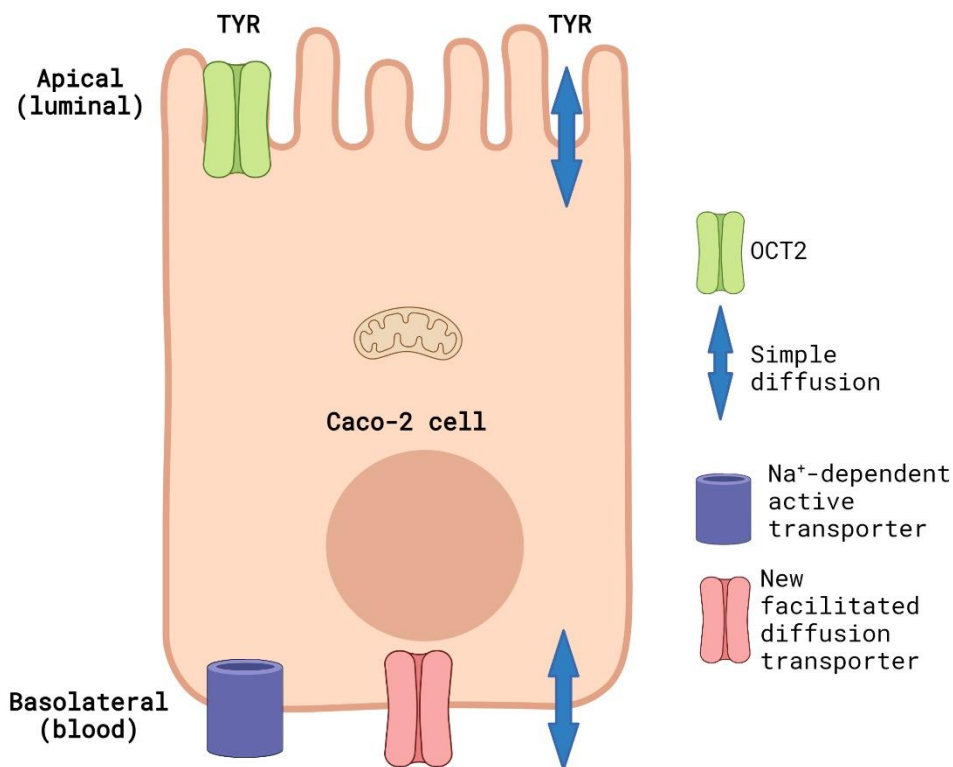


**Figure 2.10: Known and predicted TYR transporters used for modelling transcellular passage in Caco-2 cells.** This figure represents the model where an additional facilitated diffusion transporter in the basolateral membrane has been added and optimal kinetic parameters that maximized consistency with experimental concentration-time relationships determined. This image was generated in BioRender and adapted from Sarkar et al., 2022.

To allow for possible density differences of OCT2 in the Caco-2 basolateral membrane as compared to the apical compartment, when solving Equations 10 and 11 the  $V_{\max\_baso\_new\_FD}$  was allowed to vary from 0.1-20 X the experimental  $V_{\max}$  of OCT2. In addition, the role of a non-OCT2, facilitated diffusion transporter in the Caco-2 basolateral membrane was investigated by allowing both the  $K_{t\_baso\_new\_FD}$  and  $V_{\max\_baso\_new\_FD}$  terms to vary from the values utilized for OCT2.

Results from these models suggested that one or more of the facilitated diffusion transporters may be unequally bi-directional. To model this asymmetry equations were modified to allow different  $K_t$  values for each direction of transport for the facilitated diffusion transporters in both the apical and the basolateral Caco-2 membranes (Equations 12-14). Here,  $K_{t\_OCT2\_apicalto\text{cell}}$  represents the  $K_t$  of OCT2 in the apical to cellular direction (Equations 12 and 13);  $K_{t\_OCT2\_cellto\text{apical}}$  the  $K_t$  of OCT2 in the cellular to apical direction (Equations 12 and 13);  $K_{t\_baso\_new\_FD\_baso\text{to}\text{cell}}$  the  $K_t$  of the unknown basolateral membrane facilitated diffusion transporter in the basolateral to cellular direction (Equations 13 and 14); and  $K_{t\_baso\_new\_FD\_cell\text{to}\text{baso}}$  for the same transporter in the cellular to basolateral direction (Equations 13 and 14).

$$\frac{dX_{\text{apical}}}{dt} = \left( \frac{\alpha}{Vol_{\text{apical}}} \right) \times (X_{\text{cell}} - X_{\text{apical}}) + \left( \frac{Vol_{\text{cell}}}{Vol_{\text{apical}}} \right) \times \left( \frac{V_{\text{max\_OCT2}}X_{\text{cell}}}{K_{t\_OCT2\_cellto\text{apical}} + X_{\text{cell}}} - \frac{V_{\text{max\_OCT2}}X_{\text{apical}}}{K_{t\_OCT2\_apicalto\text{cell}} + X_{\text{apical}}} \right) \quad (\text{Equation 12})$$

$$\frac{dX_{\text{cell}}}{dt} = \left[ \left( \frac{\alpha}{Vol_{\text{cell}}} \right) \times (X_{\text{apical}} - X_{\text{cell}}) + \left( \frac{\alpha}{Vol_{\text{cell}}} \right) \times (X_{\text{baso}} - X_{\text{cell}}) \right] + \left[ \left( \frac{V_{\text{max\_baso\_active}}X_{\text{baso}}}{K_{t\_baso\_active} + X_{\text{baso}}} \right) \right] \\ \left( \frac{V_{\text{max\_OCT2}}X_{\text{apical}}}{K_{t\_OCT2\_apicalto\text{cell}} + X_{\text{apical}}} - \frac{V_{\text{max\_OCT2}}X_{\text{cell}}}{K_{t\_OCT2\_cellto\text{apical}} + X_{\text{cell}}} \right) + \left( \frac{V_{\text{max\_baso\_new\_FD}}X_{\text{baso}}}{K_{t\_baso\_new\_FD\_baso\text{to}\text{cell}} + X_{\text{baso}}} - \frac{V_{\text{max\_baso\_new\_FD}}X_{\text{cell}}}{K_{t\_baso\_new\_FD\_cell\text{to}\text{baso}} + X_{\text{cell}}} \right) \quad (\text{Equation 13})$$

$$\frac{dX_{\text{baso}}}{dt} = \left[ - \left( \frac{\alpha}{Vol_{\text{baso}}} \right) \times (X_{\text{baso}} - X_{\text{cell}}) \right] + \left[ - \left( \frac{Vol_{\text{cell}}}{Vol_{\text{baso}}} \right) \times \left( \frac{V_{\text{max\_baso\_active}}X_{\text{baso}}}{K_{t\_baso\_active} + X_{\text{baso}}} \right) \right] + \\ \left[ - \left( \frac{Vol_{\text{cell}}}{Vol_{\text{baso}}} \right) \times \left( \frac{V_{\text{max\_baso\_new\_FD}}X_{\text{baso}}}{K_{t\_baso\_new\_FD\_baso\text{to}\text{cell}} + X_{\text{baso}}} - \frac{V_{\text{max\_baso\_new\_FD}}X_{\text{cell}}}{K_{t\_baso\_new\_FD\_cell\text{to}\text{baso}} + X_{\text{cell}}} \right) \right] \quad (\text{Equation 14})$$

As an alternative to asymmetry of the facilitated diffusion transporters, potential intracellular compartmentalization of TYR was also modelled (Figure 2.11). Initially, a compartmentalization

factor ‘z’ was introduced to restrict the amount of intracellular TYR that was available for transport out of Caco-2 cells (Equations 15-17), where  $0 \leq z \leq 1$  (Equations 15-17).

$$\frac{dX_{apical}}{dt} = \left[ -\left(\frac{\alpha}{Vol_{apical}}\right) \times (X_{apical} - z * X_{cell}) \right] + \left[ -\left(\frac{Vol_{cell}}{Vol_{apical}}\right) \times V_{max\_OCT2} \left( \frac{X_{apical}}{K_{t\_OCT2\_apicalto cell} + X_{apical}} - \frac{z * X_{cell}}{K_{t\_OCT2\_cellto apical} + z * X_{cell}} \right) \right] \quad (\text{Equation 15})$$

$$\begin{aligned} \frac{dX_{cell}}{dt} = & \left[ -\left(\frac{\alpha}{Vol_{cell}}\right) \times (z * X_{cell} - X_{apical}) \right] + \left[ -\left(\frac{\alpha}{Vol_{cell}}\right) \times (z * X_{cell} - X_{baso}) \right] + \\ & V_{max\_OCT2} \left( \frac{X_{apical}}{K_{t\_OCT2\_apicalto cell} + X_{apical}} - \frac{z * X_{cell}}{K_{t\_OCT2\_cellto apical} + z * X_{cell}} \right) \\ & + \left( \frac{V_{max\_baso\_active}}{K_{t\_baso\_active} + X_{baso}} \right) + V_{max\_baso\_new\_FD} \left( \frac{X_{baso}}{K_{t\_baso\_new\_FD\_basotocell} + X_{baso}} - \right. \\ & \left. \frac{z * X_{cell}}{K_{t\_baso\_new\_FD\_celltobaso} + z * X_{cell}} \right) \end{aligned} \quad (\text{Equation 16})$$

$$\begin{aligned} \frac{dX_{baso}}{dt} = & \left[ -\left(\frac{\alpha}{Vol_{baso}}\right) \times (X_{baso} - z * X_{cell}) \right] + \left[ -\left(\frac{Vol_{cell}}{Vol_{baso}}\right) \times \right. \\ & \left. \left( \frac{V_{max\_baso\_active}}{K_{t\_baso\_active} + X_{baso}} \right) + \left[ -\left(\frac{Vol_{cell}}{Vol_{baso}}\right) \times V_{max\_baso\_new\_FD} \left( \frac{X_{baso}}{K_{t\_baso\_new\_FD\_basotocell} + X_{baso}} - \right. \right. \right. \\ & \left. \left. \left. \frac{z * X_{cell}}{K_{t\_baso\_new\_FD\_celltobaso} + z * X_{cell}} \right) \right] \right] \end{aligned} \quad (\text{Equation 17})$$

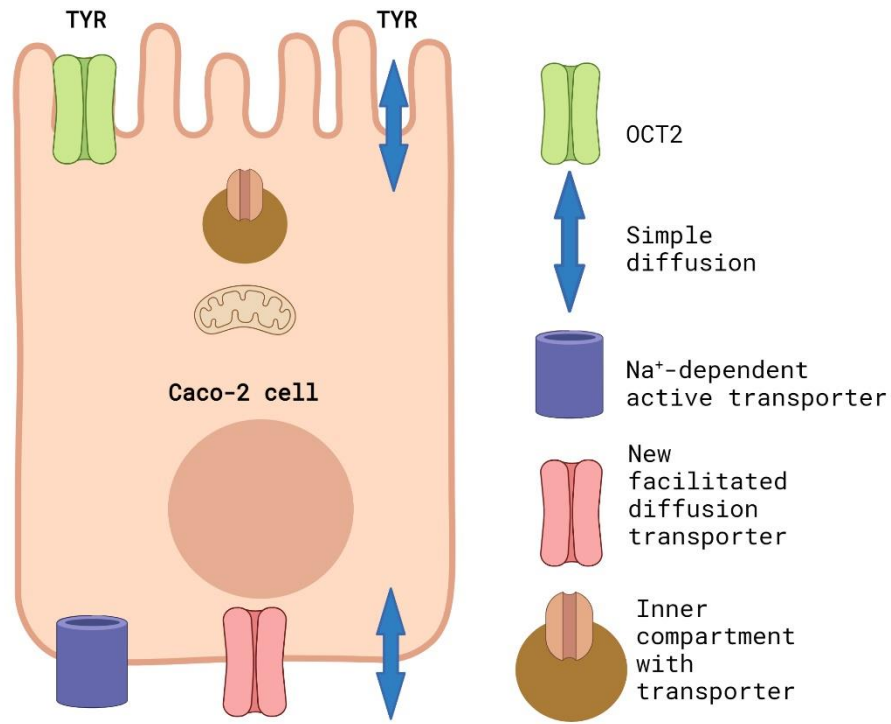


**Figure 2.11: Schematic representation of the Caco-2 model including an intracellular compartment for TYR sequestration.** To test if addition of a new compartment could remove the need for asymmetry of transporters, a compartment within the cell with separate kinetic properties was introduced. This image was generated in BioRender and adapted from Sarkar et al., 2022.

To further characterize the possibility of compartmentalization of TYR within the cells, Michaelis-Menten terms were introduced to define the kinetic parameters for the necessary transporter associated with compartmentalization (brown text, Equation 19), which by definition required the transport to be active (Equations 18-21). Equation 21 is represented in light brown to show the inner compartment component. The volume of the intracellular compartment ( $Vol_{inner}$ )

was set at 10% of the total volume of the cell, as an estimate of an average volume for an intracellular compartment.

$$\frac{dX_{apical}}{dt} = - \left[ \left( \frac{\alpha}{Vol_{apical}} \right) \times (X_{apical} - X_{cell}) + \left( \frac{Vol_{cell}}{Vol_{apical}} \right) \times V_{max\_OCT2} \left( \frac{X_{apical}}{K_{t\_OCT2\_apicalto\ cell} + X_{apical}} - \frac{X_{cell}}{K_{t\_OCT2\_cellto\ apical} + X_{cell}} \right) \right] \quad (\text{Equation 18})$$

$$\begin{aligned} \frac{dX_{cell}}{dt} = & \left[ - \left( \frac{\alpha}{Vol_{cell}} \right) \times (X_{cell} - X_{apical}) \right] + \left[ - \left( \frac{\alpha}{Vol_{cell}} \right) \times (X_{cell} - X_{baso}) \right] + \\ & V_{max\_OCT2} \left( \frac{X_{apical}}{K_{t\_OCT2\_apicalto\ cell} + X_{apical}} - \frac{X_{cell}}{K_{t\_OCT2\_cellto\ apical} + X_{cell}} \right) \\ & + \left( \frac{V_{max\_baso\_active\_transporter} X_{baso}}{K_{t\_baso\_active\_transporter} + X_{baso}} \right) + \\ & V_{max\_baso\_new\_FD\_transporter} \left( \frac{X_{baso}}{K_{t\_baso\_new\_FD\_baso\ to\ cell\_transporter} + X_{baso}} - \right. \\ & \left. \frac{X_{cell}}{K_{t\_baso\_new\_FD\_cell\ to\ baso\_transporter} + X_{cell}} \right) - \left( \frac{V_{max\_i} X_{cell}}{K_{t\_i} + X_{cell}} \right) \end{aligned} \quad (\text{Equation 19})$$

$$\begin{aligned} \frac{dX_{baso}}{dt} = & \left[ - \left( \frac{\alpha}{Vol_{baso}} \right) \times (X_{baso} - X_{cell}) \right] + \left[ - \left( \frac{Vol_{cell}}{Vol_{baso}} \right) \times \left( \frac{V_{max\_baso\_AT} X_{baso}}{K_{baso\_AT} + X_{baso}} \right) \right] + \left[ - \left( \frac{Vol_{cell}}{Vol_{baso}} \right) \times \right. \\ & \left. V_{max\_baso\_FD\_new} \left( \frac{X_{baso}}{K_{t\_baso\_FD\_new\_baso} + X_{baso}} - \frac{X_{cell}}{K_{t\_baso\_FD\_new\_cell} + X_{cell}} \right) \right] \end{aligned} \quad (\text{Equation 20})$$

$$\frac{dX_i}{dt} = \left[ \left( \frac{Vol_{cell}}{Vol_{inner}} \right) \times \left( \frac{V_{max\_i} X_{cell}}{K_{t\_i} + X_{cell}} \right) \right] \quad (\text{Equation 21})$$

#### 2.8.4 Least squares determination of TYR transporter kinetics

The kinetic terms for the unknown additional transporter described in the previous sections were determined by deriving objective functions and using a least squares minimization technique to minimize the squared difference between the experimentally obtained results and the needed kinetics of the unknown transporter(s) using Mathematica (v12.1.1). To estimate transporter parameters from experimental data, e.g., the various  $V_{\max}$  and  $K_t$  values on the right-hand side (RHS) of Equations 12, 13 and 14, two least-squares fitting procedures were utilized that are described in detail below.

In the first instance the fitting procedure for determining model parameters considered the rate of change of the concentration. As an illustrative example, consider fitting  $V_{\max\_OCT2}$  and  $K_{t\_OCT2}$  in the model comprising Equations 12, 13 and 14. Note that compartmental volumes and  $\alpha$  are known constants and are therefore not fit parameters. Linear regression analysis was performed on the experimental concentration-time relationships to determine the rate of change of TYR concentration in each of the apical, cellular, and basolateral compartments following both apical and basolateral compartment TYR loading. In all cases, the data were well described by constant rates of change (concentrations changing linearly in time). Thus, all the experimental data could be described by six “slopes”.

The second procedure involved solving the ODEs at each iteration of the fitting procedure and comparing model and experimental concentrations. As the fits of several parameters were non-linear, choices for the initial values of the parameters used in the fitting procedures were determined by considering the constraints on parameter values implied by the model given the experimental data. This allowed reducing of the computational time and power needed for exhaustive searches over initial parameter values.

### 2.8.4.1 Development of objective functions

Equations 12-14 were rearranged so that all experimentally known quantities including the determined rate, appear on the RHS and terms with parameters to be solved appear on LHS (Equations 22-24 respectively).

$$-\left(\frac{Vol_{cell}}{Vol_{apical}}\right) \times \left(\frac{V_{max\_OCT2}X_{apical}}{K_{t\_OCT2}+X_{apical}} - \frac{V_{max\_OCT2}X_{cell}}{K_{t\_OCT2}+X_{cell}}\right) = \frac{dX_{apical}}{dt} + \left(\frac{\alpha}{Vol_{apical}}\right) \times (X_{apical} - X_{cell})$$

(Equation 22)

$$\frac{V_{max\_OCT2}X_{apical}}{K_{t\_OCT2}+X_{apical}} - \frac{V_{max\_OCT2}X_{cell}}{K_{t\_OCT2}+X_{cell}} + \frac{V_{max\_baso\_active}X_{baso}}{K_{t\_baso\_active}+X_{baso}} = \frac{dX_{cell}}{dt} + \left(\frac{\alpha}{Vol_{cell}}\right) \times (X_{cell} - X_{apical}) + \left(\frac{\alpha}{Vol_{cell}}\right) \times (X_{cell} - X_{baso})$$

(Equation 23)

$$-\left(\frac{Vol_{cell}}{Vol_{baso}}\right) \times \left(\frac{V_{max\_baso\_active}X_{baso}}{K_{t\_baso\_active} + X_{baso}}\right) = \frac{dX_{baso}}{dt} + \left(\frac{\alpha}{Vol_{baso}}\right) \times (X_{baso} - X_{cell})$$

(Equation 24)

This rearrangement allows using the LHSs to define fitting functions  $F_{apical}$ ,  $F_{cell}$  and  $F_{baso}$  (Equations 25-27).

$$F_{apical}(V_{max\_OCT2}, K_{t\_OCT2}; X_{apical}, X_{cell}, X_{baso}) = -\left(\frac{Vol_{cell}}{Vol_{apical}}\right) \times \left(\frac{V_{max\_OCT2}X_{apical}}{K_{t\_OCT2}+X_{apical}} - \frac{V_{max\_OCT2}X_{cell}}{K_{t\_OCT2}+X_{cell}}\right)$$

(Equation 25)

$$F_{cell}(V_{max\_OCT2}, K_{t\_OCT2}; X_{apical}, X_{cell}, X_{baso}) = \left( \frac{V_{max\_OCT2} X_{apical}}{K_{t\_OCT2} + X_{apical}} - \frac{V_{max\_OCT2} X_{cell}}{K_{t\_OCT2} + X_{cell}} \right) + \frac{V_{max\_baso\_active} X_{baso}}{K_{t\_baso\_active} + X_{baso}} \quad (\text{Equation 26})$$

$$F_{baso}(V_{max\_OCT2}, K_{t\_OCT2}; X_{baso}) = - \left( \frac{Vol_{cell}}{Vol_{baso}} \right) \times \left( \frac{V_{max\_baso\_active} X_{baso}}{K_{t\_baso\_active} + X_{baso}} \right) \quad (\text{Equation 27})$$

Since the compartmental concentrations were determined experimentally from  $t = 0$  to  $t = 30$  minutes at intervals of 5 minutes, these three functions can be written as functions of time, e.g. Equation 28.

$$F_{apical}(V_{max\_OCT2}, K_{t\_OCT2}; t) = F_{apical}(V_{max\_OCT2}, K_{t\_OCT2}; X_{apical}(t), X_{cell}(t)) \quad (\text{Equation 28})$$

The RHSs of the Equations 22-24 were used to define known, time-dependent quantities for each compartment,  $f_{apical}(t)$ ,  $f_{cell}(t)$  and  $f_{baso}(t)$ , respectively. This ‘f’ term contains small diffusive terms and derivatives of TYR concentration with respect to time ( $dX/dt$ ). Since all TYR concentration data were described by linear relationships, the  $dX/dt$  components of the ‘f’ terms become constant and, as such, the ‘f’ terms have only a very weak time dependence which is solely dependent on the very small diffusive terms.

Objective functions (Q) were then defined for each compartment as shown in Equations 29-31 and represent the squared differences between  $F$  and  $f$  calculated at each time point  $t$ .

$$Q_{apical} = \sum_{t=0}^T (F_{apical}(V_{max\_OCT2}, K_{t\_OCT2}; t) - f_{apical}(t))^2 \quad (\text{Equation 29})$$

$$Q_{cell} = \sum_{t=0}^T (F_{cell}(V_{max\_OCT2}, K_{t\_CT2}; t) - f_{cell}(t))^2 \quad (\text{Equation 30})$$

$$Q_{baso} = (F_{baso}(V_{max\_OCT2}, K_{t\_OCT2}; t) - f_{baso}(t))^2 \quad (\text{Equation 31})$$

Global objective functions for the entire system can then be written for apical ( $Q_A$ ) and basolateral ( $Q_B$ ) loading as the sum of the individual compartment objective functions following either apical or basolateral loading respectively (Equations 32 and 33).

$$Q_A = Q_{apical,apical\_addition} + Q_{cell,apical\_addition} + Q_{baso,apical\_addition} \quad (\text{Equation 32})$$

$$Q_B = Q_{apical,baso\_addition} + Q_{cell,baso\_addition} + Q_{baso,baso\_addition} \quad (\text{Equation 33})$$

$Q_A$  and  $Q_B$  can then be minimized simultaneously by defining an overall function  $Q$  (Equation 34), providing a least-squares minimized solution for the individual kinetic terms in Equations 22-24.

$$Q = Q_A + Q_B \quad (\text{Equation 34})$$

In order to complement and validate the above fitting procedure, the  $F$  functions in Equations 29-31 were redefined to be the solutions to Equations 22-24. For example,  $F_{apical}(V_{max\_OCT2}, K_{t\_OCT2}; t) = X_{apical}(t)$ . Here,  $X_{apical}(t)$  comes from the numerical solution to Equations 22-24. The quantities  $f$  in Equations 29-31 were simply redefined to be the compartmental concentrations

determined from experiment e.g.  $f_{\text{apical}} = X_{\text{apical}}(t)$ . As the cellular concentrations were generally much larger than in the other two compartments, I reduced both  $Q_{\text{cell,apical\_addition}}$  and  $Q_{\text{cell,basolateral\_addition}}$  in  $Q_A$  and  $Q_B$ , respectively, by a constant factor  $w$ . The value of  $w$  affects the results, and I empirically found that a value of 1000 worked well. The dependence of the fitting procedure on  $w$  was mitigated by choosing good initial parameter values, as described in the following section.

#### 2.8.4.2 Introduction of model order reduction

Non-linear fitting with many fit parameters can be difficult: there are in general many local minima of the objective functions in parameter space, meaning similar fits can be achieved with very different parameter values. As such, results depend on the initial parameter values chosen when minimizing the objective function. In this final step, approximations were introduced to decrease the number of parameters that needed to be solved simultaneously, thereby simplifying the computational complexity. This allowed ranges of parameter values to be explored interactively and thus determine reasonable starting values. The procedure was based on approximating experimental concentrations as constant values or as being linear in time and on simplifying the model ODEs. For example, for the model represented by Equations 15-16,  $K_{t\_OCT2\_celltoapical}$  was approximated as follows.

Considering Equation 15, since simple diffusion is negligible compared to the other transporter-mediated processes it was assumed  $\alpha \approx \mathbf{0}$ , which allowed Equation 15 to be simplified to Equation 35,

$$\frac{dX_{\text{apical}}}{dt} \cong \left[ - \left( \frac{Vol_{\text{cell}}}{Vol_{\text{apicl}}} \right) \times V_{\text{max\_OCT2}} \left( \frac{X_{\text{apical}}}{K_{t\_OCT2\_apicalto\text{cell}} + X_{\text{apical}}} - \frac{z \cdot X_{\text{cell}}}{K_{t\_OCT2\_cellto\text{apical}} + z \cdot X_{\text{cell}}} \right) \right]$$

(Equation 35)

For basolateral addition at timepoint  $t = 0$  second, the following experimental parameters were substituted into the Equation: at  $t = 0$  second,  $X_{apical} = 0$  nM,  $X_{cell} \approx 500$  nM and  $dX_{apical}/dt = 0.3168$  nM/min =  $0.00528$  nM/second (the slope of the linear fit of the experimental data). This allows Equation 35 to be reduced to Equation 36.

$$0.00528 \cong \left[ 0.0082 V_{max\_OCT2} \left( \frac{500z}{K_{t\_OCT2\_celltoapical} + 500z} \right) \right] \quad (\text{Equation 36})$$

Rearranging Equation 36 to Equation 37 allows  $K_{t\_OCT2\_celltoapical}$  to be expressed as a function of other variables. For solutions where no intracellular compartment was modelled  $z$  was set to 1.

$$K_{t\_OCT2\_celltoapical} = (-500 + 768.65V_{max\_OCT2})z \quad (\text{Equation 37})$$

Similar approximation techniques were also used for expressing:

- $K_{t\_OCT2\_apicalto cell}$  in relation to  $V_{max\_OCT2}$  and  $z$
- $K_{t\_baso\_new\_FD\_cellto baso}$  in relation to  $V_{max\_baso\_new\_FD}$
- $K_{t\_baso\_active\_transporter}$  in relation to  $V_{max\_OCT2}, V_{max\_baso\_new\_FD\_transporter}, K_{t\_baso\_new\_FD\_basotocell}$  and  $z$

Constraints were not used when minimizing the objective function(s) because of the approximate nature of such constraints.

#### 2.8.4.3 *Comparison of modeled fits*

The root mean square deviation (RMSD) was determined to compare the predicted models of asymmetry (Equations 12-14) and compartmentalization (Equations 15-17). For each of the predicted models, there were a set of constant values for apical, cellular and basolateral compartments for both additions. The square root of the second sample moment of these values and the experimentally observed values gave the RMSD. The RMSD was calculated for the apical, cellular, and basolateral compartments for both additions using MATLAB.

### 3 RESULTS

#### 3.1 Investigation of TYR binding to the plasma membrane

From my subcellular fractionation study, approximately 97.7% of added TYR was associated with the ribosome + cytosolic compartment (Figure 3.1), with only 1.8% associated with the mitochondrial fraction and 0.5% associated with the plasma membrane. This observation confirms that cellular TYR in subsequent experiments is intracellular and represents transmembrane transport.

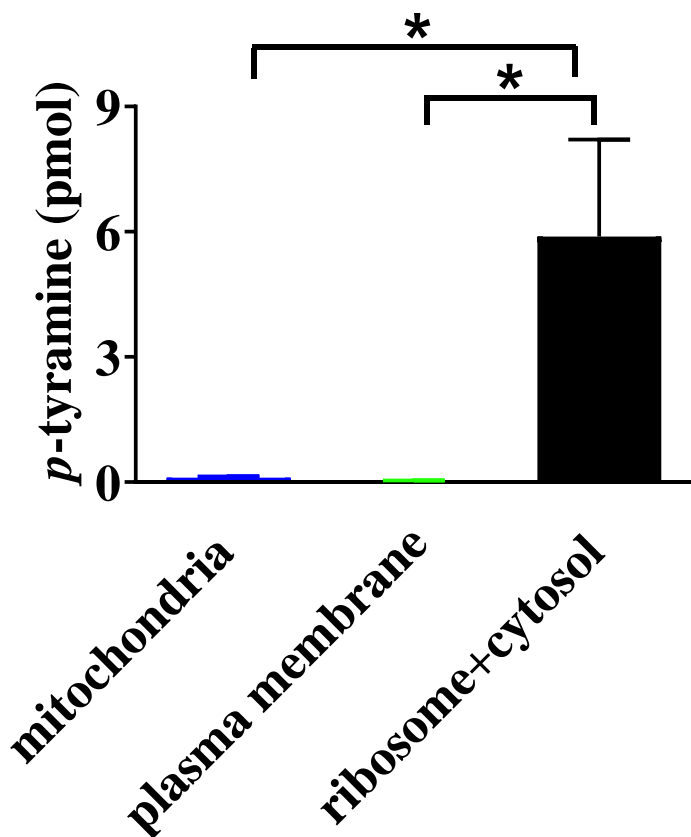


**Figure 3.1: Subcellular distribution of TYR in Caco-2 cells.** [<sup>3</sup>H]TYR (100 nM; corresponding to 1500 pmol TYR) was added to the cells and incubated for 30 minutes at 37°C under 5% CO<sub>2</sub>. After incubation, cells were washed with PBS and cells harvested. Subcellular fractions were collected by differential centrifugation. The counts per minute values obtained were converted to pmoles of TYR by comparison to a standard curve constructed for each independent experiment. Data represents mean ± SEM, n = 3. Comparisons were made between different fractions using

GraphPad Prism version 6 by one-way ANOVA with Tukey's multiple comparison post-hoc analysis. \* $P < 0.05$ . This figure was adapted from Sarkar et al., 2020.

### **3.2 Transcellular TYR passage**

#### 3.2.1 Investigation of TYR transport across the apical Caco-2 membrane

Following apical addition there was a significant main effect of compartment (two-way ANOVA,  $P < 0.0001$ , compartment;  $P = 0.6130$ , time;  $P = 0.4105$ , compartment x time; Figure 3.2), suggesting differences in TYR concentration in the different compartments. Sidak's multiple comparison post-hoc analysis, however, indicated no significant difference in TYR concentration between apical and cellular compartments at any time point, with the exception of at 25 minutes ( $P = 0.0012$ ).

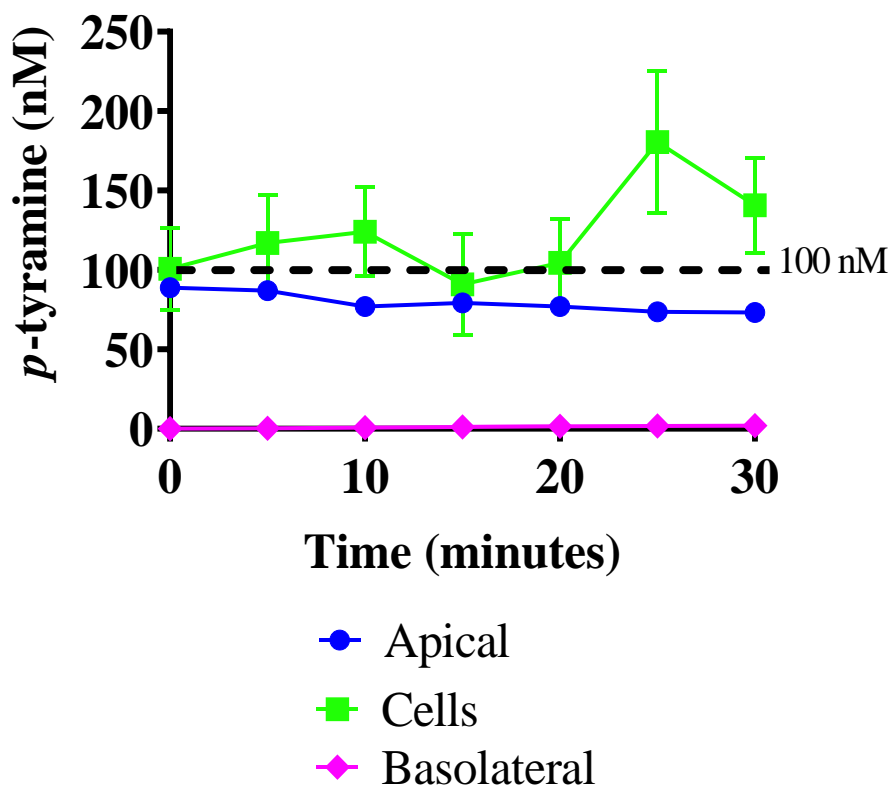


**Figure 3.2: Transcellular [<sup>3</sup>H]TYR passage following addition to the apical compartment.** [<sup>3</sup>H]TYR was added at 100 nM in the apical compartment and the transport was monitored for varying time points by liquid scintillation counting and the concentration of TYR in each compartment obtained by comparison to standard curves. The “zero” time point represents 100 nM of TYR (represented by broken black lines) added to the apical compartment and transport immediately quenched (approximately 10 seconds), which was the shortest time frame at which the experiment could be reliably performed. The data is represented as mean ± SEM, n = 9-10 cultures from 10 independent experiments. Comparisons were made between different compartments using GraphPad Prism version 6 by two-way ANOVA. This figure was adapted from Sarkar et al., 2020.

### 3.2.2 Investigation of TYR transport across the basolateral Caco-2 membrane

Basolateral TYR addition resulted in cellular concentrations 5-10 fold higher than those added to the basolateral compartment (two-way ANOVA;  $P < 0.0001$ , compartment;  $P = 0.5673$ , time;  $P = 0.6636$ , compartment x time). Sidak’s multiple comparison post-hoc analysis between cellular and basolateral compartments showed significant differences at the 10<sup>th</sup> ( $P = 0.0171$ ), 15<sup>th</sup>

( $P = 0.0009$ ), and 30<sup>th</sup> ( $P = 0.0166$ ) minute, with a trend towards significance observed for the 20<sup>th</sup> minute:  $P = 0.0652$ ; Figure 3.3), indicating the presence of an active transporter in the basolateral membrane. This also resulted in greater apical concentrations of TYR following basolateral addition, than basolateral TYR concentrations following apical addition (two-way ANOVA;  $P < 0.0001$ , direction;  $P = 0.0002$ , time;  $P = 0.0610$ , direction x time; Figure 3.4).

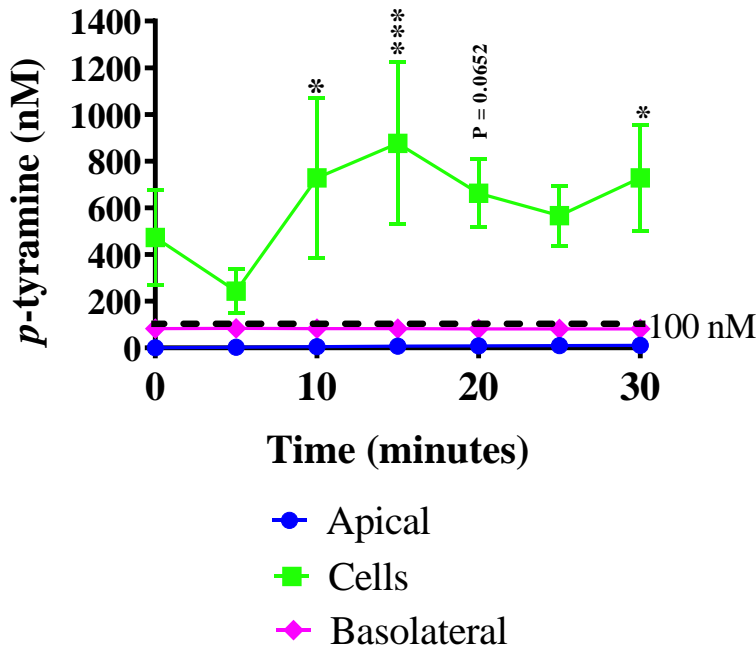


**Figure 3.3: Transcellular [<sup>3</sup>H]TYR passage following addition to the basolateral compartment.** [<sup>3</sup>H]TYR was added at 100 nM in the basolateral compartment and the transport was monitored for varying time points. At each time point, the radioactivity in each compartment was determined and the concentration of TYR obtained by comparison to standard curves. The “zero” time point represents 100 nM of TYR (represented by broken black lines) added to the basolateral compartment and transport immediately quenched (approximately 10 seconds), which was the shortest time frame at which the experiment could be reliably performed. The data is represented as mean  $\pm$  SEM,  $n = 9-10$  cultures from 10 independent experiments. Comparisons were made by Sidak’s multiple comparison post-hoc analysis between cellular and basolateral compartments on GraphPad Prism version 6. \* $P = 0.0171$  (10<sup>th</sup> minute), \*\*\* $P = 0.0009$  (15<sup>th</sup> minute), \* $P = 0.0166$  (30<sup>th</sup> minute). This figure was adapted from Sarkar et al., 2020.

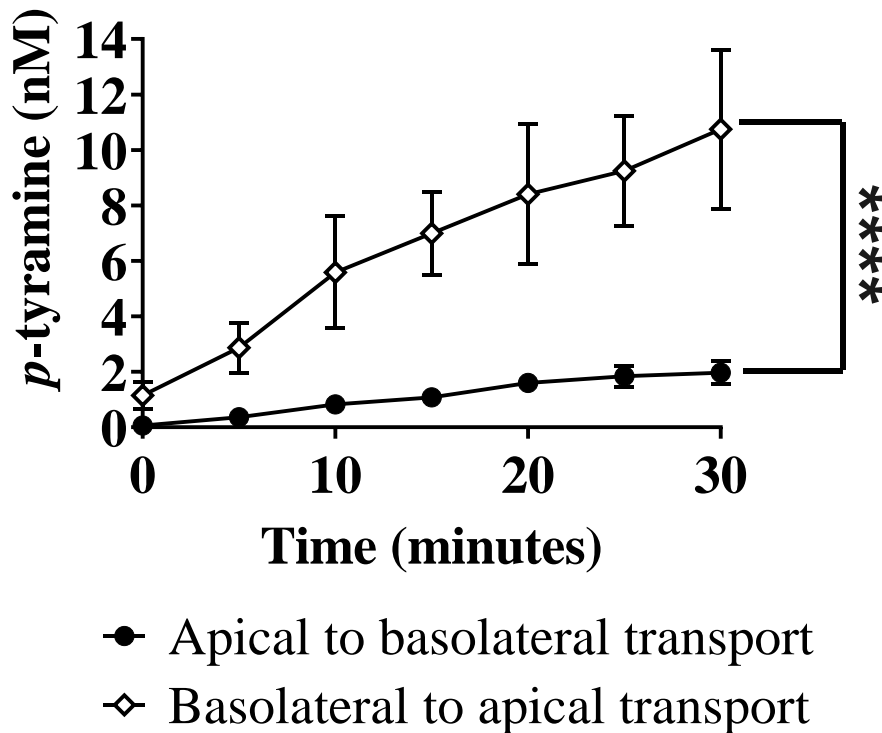


**Figure 3.4: Total transcellular transport across Caco-2 cells following apical and basolateral addition of [<sup>3</sup>H]TYR.** [<sup>3</sup>H]TYR (100 nM) was added to the assay buffer in either the apical or the basolateral compartment as described in previous figures. Data represents TYR concentration in the basolateral (following apical addition) and apical (following basolateral addition) compartments. Results are mean ± SEM, n = 9-10 cultures from 10 independent experiments. Comparisons were made between different compartments using GraphPad Prism version 6 by two-way ANOVA, \*\*\*\**P* < 0.0001. Reprinted from Sarkar et al., 2020.

### 3.3 Transcellular 2-PE passage

#### 3.3.1 Investigation of 2-PE transport across the apical Caco-2 membrane

With apical 2-PE addition, there was a significant effect of compartment observed (two-way ANOVA; *P* < 0.0001, compartment; *P* = 0.9432, time; *P* = 0.9848, compartment x time) suggesting differences in 2-PE concentration in the different compartments. Sidak's multiple comparison post-hoc analysis, however, indicated no significant difference in TYR concentration between apical and cellular compartments at any time point Figure 3.5.

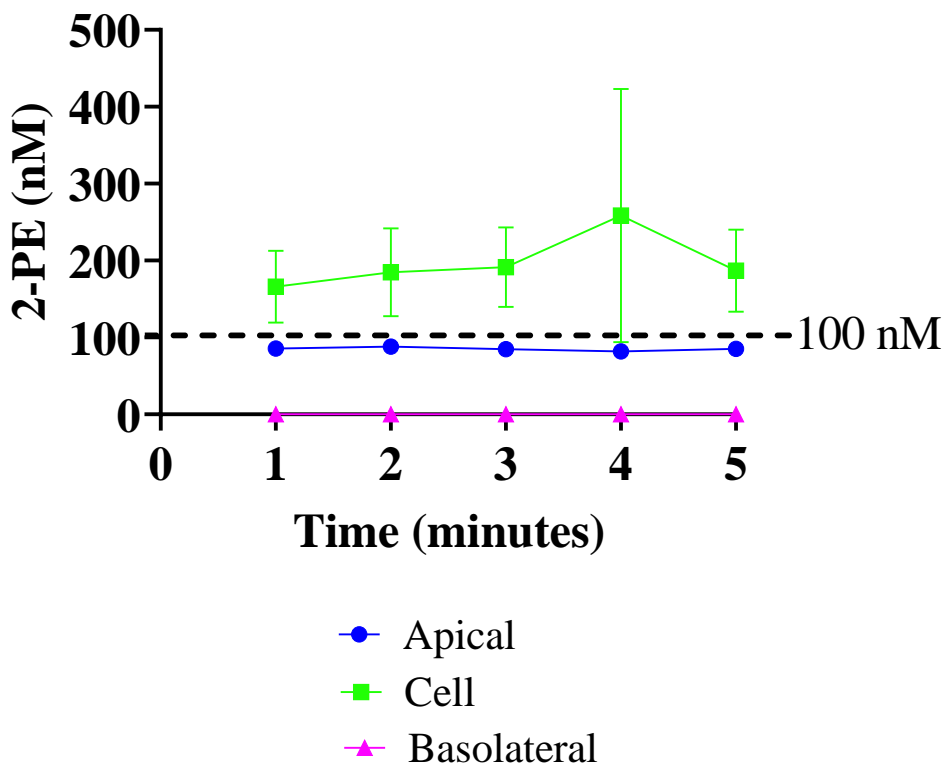


**Figure 3.5: Transcellular [<sup>14</sup>C]2-PE passage following addition to the apical compartment.** [<sup>14</sup>C]2-PE was added at 100 nM in the apical compartment and the transport was monitored for varying time points. After transport, the radioactivity was counted and the concentration of 2-PE in each compartment obtained by comparison to standard curves. The data is represented as mean ± SEM, n = 2-3 cultures from 3 independent experiments. Comparisons were made between different compartments using GraphPad Prism version 6 by two-way ANOVA.

### 3.3.2 Investigation of 2-PE transport across the basolateral Caco-2 membrane

Basolateral 2-PE addition showed a significant main effect of compartment (two-way ANOVA;  $P < 0.0001$ , compartment;  $P = 0.9531$ , time;  $P = 0.9931$ , compartment x time), suggesting different 2-PE concentrations in the different compartments. Sidak's multiple comparison post-hoc analysis, however, showed no difference between the cellular and basolateral compartments with only a trend towards significance observed at the 2<sup>nd</sup> minute ( $P = 0.0714$ ;

Figure 3.6). A greater transcellular movement of 2-PE following basolateral addition than following apical addition was, however, observed (two-way ANOVA;  $P < 0.0001$ , direction;  $P = 0.0247$ , time;  $P = 0.0302$ , direction x time; Figure 3.7).

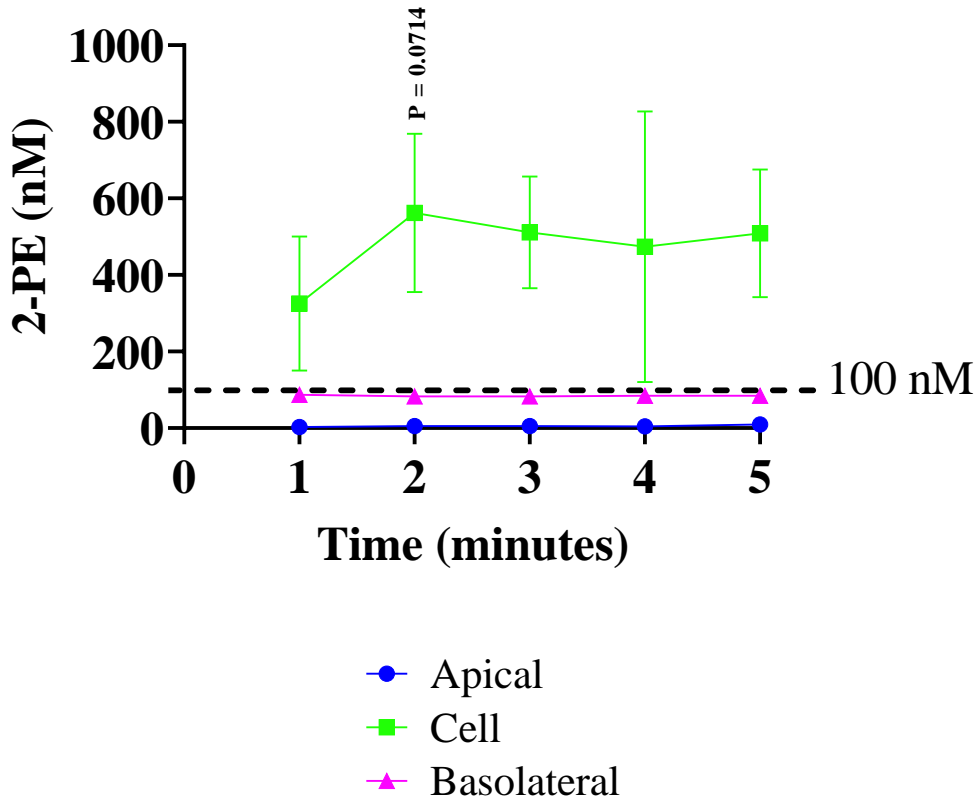
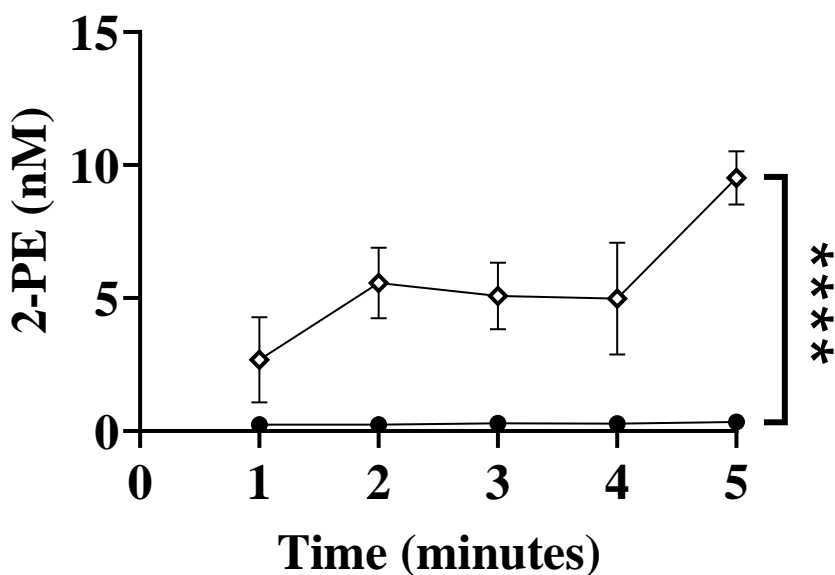


**Figure 3.6: Transcellular [ $^{14}\text{C}$ ]2-PE passage following addition to the basolateral compartment.** [ $^{14}\text{C}$ ]2-PE was added at 100 nM in the basolateral compartment and the transport was monitored for varying time points. After transport, the radioactivity was counted and the concentration of 2-PE in each compartment obtained by comparison to standard curves. The data is represented as mean  $\pm$  SEM,  $n = 2-3$  cultures from 3 independent experiments. Comparisons were made by Sidak's multiple comparison post-hoc analysis between cellular and basolateral compartments on GraphPad Prism version 6.



- Apical to basolateral transport
- ◇ Basolateral to apical transport

**Figure 3.7: Total transcellular transport across Caco-2 cells following apical and basolateral addition of [<sup>14</sup>C]2-PE.** [<sup>14</sup>C] 2-PE (100 nM) was added to the assay buffer in either the apical or the basolateral compartment as described in previous figures. Data represents 2-PE concentration in the basolateral (following apical addition) and apical (following basolateral addition) compartments. Results are mean ± SEM, n = 2-3 cultures from 3 independent experiments. Comparisons were made using GraphPad Prism version 6 by two-way ANOVA, \*\*\*\**P* < 0.0001.

### 3.4 Pharmacological characterization of the apical membrane transporter

#### 3.4.1 Effect of inhibition of all OCT isoforms on apical TYR transport

To investigate if the facilitated diffusion of TYR across the apical membrane involved OCT isoforms as previously reported in neuronal membranes (Berry et al., 2016), 1 μM decynium-22, a pan-OCT and PMAT inhibitor, was used with same principle of combinatorial pharmacological approach since well-validated OCT2 inhibitors were not available. Decynium-22 significantly

decreased TYR accumulation in the cellular compartment (two-way ANOVA;  $P = 0.0092$ , treatment;  $P = 0.8589$ , time;  $P = 0.3842$ , treatment x time; Figure 3.8B) indicating the involvement of one or more OCT isoforms (or PMAT) in the apical membrane.

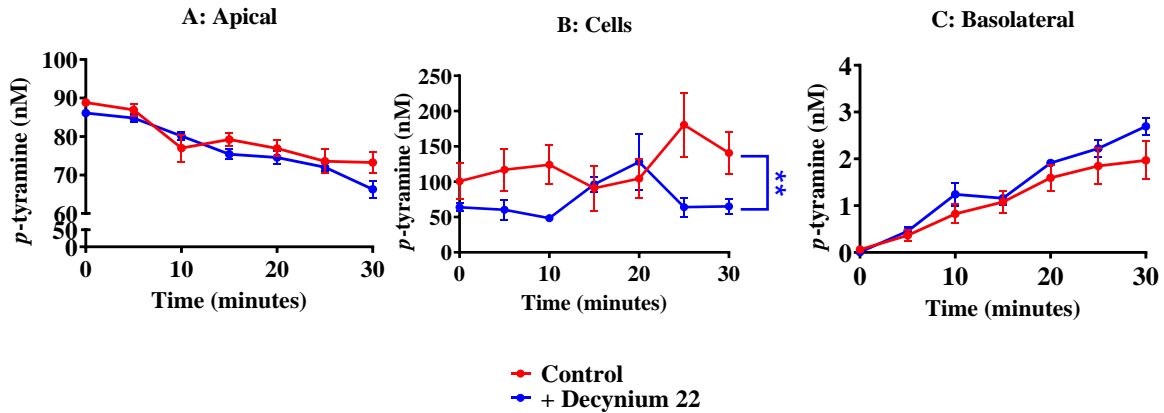


**Figure 3.8: Total transcellular transport of TYR across Caco-2 cells following apical compartment loading in the presence and absence of decynium 22.** [ $^3\text{H}$ ]TYR was added at 100 nM in the apical compartment and the transport was monitored for varying time points. After transport, the radioactivity was counted, and the concentration of TYR was obtained from standard curves. The “zero” time point represents 100 nM of TYR added to the apical compartment and removed at 10 seconds, which was the shortest time frame at which the experiment could be reliably performed. The data represents mean  $\pm$  SEM,  $n = 9-10$  cultures from 10 independent experiments for control, and  $n = 4-5$  from 5 independent experiments for decynium 22. Comparisons were made between different compartments using GraphPad Prism version 6 by two-way ANOVA,  $**P = 0.0092$ .

### 3.4.2 Effect of inhibition of OCT1 and 2 isoforms on apical TYR transport

Pentamidine (200  $\mu\text{M}$ ), an OCT1 and OCT2 inhibitor (Jung et al., 2008), decreased TYR accumulation in the cellular (two-way ANOVA;  $P = 0.001$ , treatment;  $P = 0.857$ , time;  $P = 0.740$ , treatment x time; Figure 3.9B), and basolateral (two-way ANOVA;  $P = 0.05$ , treatment;  $P < 0.0001$ , time;  $P = 0.985$ , treatment x time; Figure 3.9C) compartments following apical TYR loading.

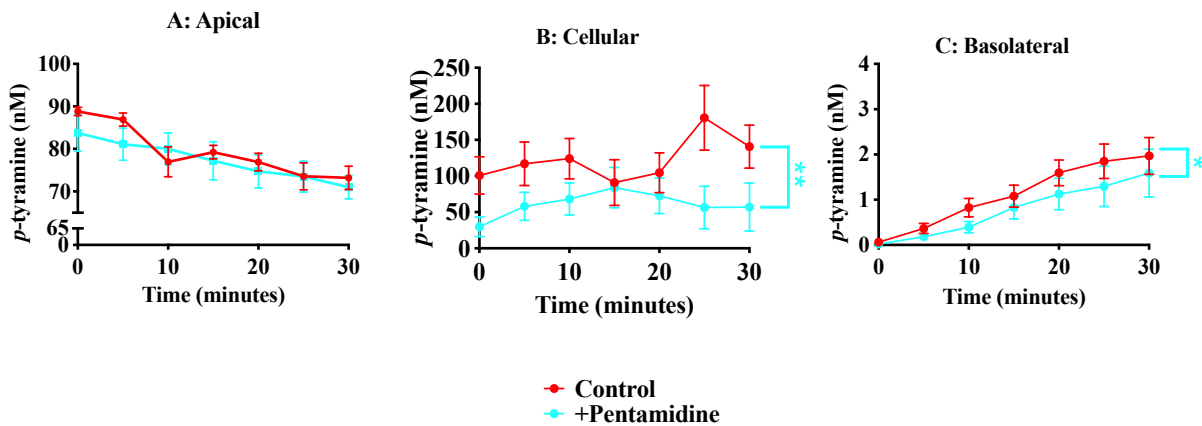


**Figure 3.9: Total transcellular transport of TYR across Caco-2 cells following apical compartment loading in the presence and absence of pentamidine.** [ $^3\text{H}$ ]TYR was added at 100 nM in the apical compartment and the transport was monitored for varying time points. After transport, the radioactivity was counted and the concentration of TYR was obtained from standard curves. The “zero” time point represents 100 nM of TYR added to the apical compartment and removed at 10 seconds, which was the shortest time frame at which the experiment could be reliably performed. The data is represented as mean  $\pm$  SEM,  $n = 9-10$  cultures from 10 independent experiments for control, and  $n = 5$  from 5 independent experiments for pentamidine. Comparisons were made between different compartments using GraphPad Prism version 6 by two-way ANOVA,  $**P = 0.001$ ,  $*P = 0.05$ . This figure was adapted from Sarkar et al., 2020.

### 3.4.3 Effect of inhibition of OCT1 on apical TYR transport

To distinguish between OCT1 and OCT2, the effect of 10  $\mu\text{M}$  ATR, a selective OCT1 inhibitor (Müller et al., 2005), was tested. There was no effect of ATR on TYR accumulation in any compartment following apical TYR loading: apical (two way ANOVA;  $P = 0.054$ , treatment;

$P < 0.0001$ , time;  $P = 0.5246$ , time x treatment; Figure 3.10A); cellular (two way ANOVA;  $P = 0.277$ , treatment;  $P = 0.614$ , time;  $P = 0.506$ , time x treatment; Figure 3.10B); basolateral (two way ANOVA;  $P = 0.614$ , treatment;  $P < 0.0001$ , time;  $P = 0.940$ , time x treatment; Figure 3.10C).

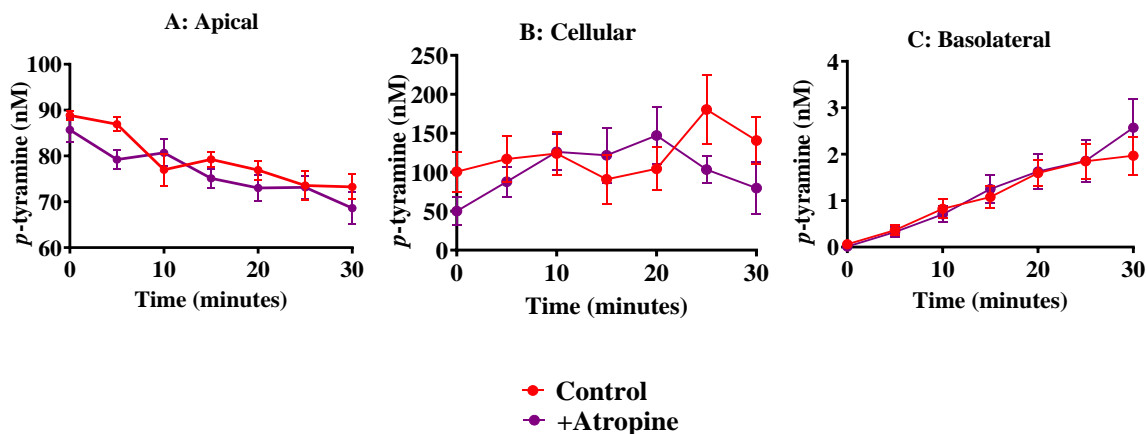


**Figure 3.10: Total transcellular transport of TYR across Caco-2 cells following apical compartment loading in the presence and absence of ATR.** [<sup>3</sup>H]TYR was added at 100 nM in the apical compartment and the transport was monitored for varying time points. After transport, the radioactivity was counted and concentration of TYR obtained from standard curves. The “zero” time point represents 100 nM of TYR added to the apical compartment and removed at 10 seconds, which was the shortest time frame at which the experiment could be reliably performed. The data is represented as mean ± SEM, n = 9-10 cultures from 10 independent experiments for control, and n = 5 from 5 independent experiments for ATR. Comparisons were made between different compartments using GraphPad Prism version 6 by two-way ANOVA. This figure was adapted from Sarkar et al., 2020.

#### 3.4.4 Investigation of the presence of OCT2 in Caco-2 cells

The above studies suggested TYR was transported across apical membranes by OCT2. The presence of OCT2 in Caco-2 cells was attempted to be confirmed by western blot with rat kidney, rat striatum, rat frontal cortex synaptosome and rat intestine used as positive controls and comparators. Using the anti-SLC22A2 polyclonal primary Elabscience<sup>®</sup> antibody, I identified the same predominant molar mass band (~70 kDa) in rat kidney (an abundant source for OCT2) and

Caco-2 cells, but a different sized predominant band was present in rat striatum, rat frontal cortex synaptosome and rat intestine preparations (~49 kDa; Figure 3.11A). Since inconsistencies were observed in the protein bands across different tissues, the membrane was stripped (Figure 3.11B) and re-probed with a different antibody anti-SLC22A2 primary antibody (Picoband™ Boster Biological Technology). On reprobing, I only identified a band at ~62 kDa in rat kidney (Figure 3.11C). For rat striatum and rat frontal cortex synaptosome, the only bands observed were at ~28 kDa (Figure 3.11C), different than the predominant bands observed in Figure 3.11A. For rat intestine one band was consistent between the two antibodies (~42 kDa) although each also identified other, unique, bands. For Caco-2 cells, the second antibody, identified a predominant band at ~42 kDa, different than that observed with the Elabscience® primary antibody (Figure 3.11A).

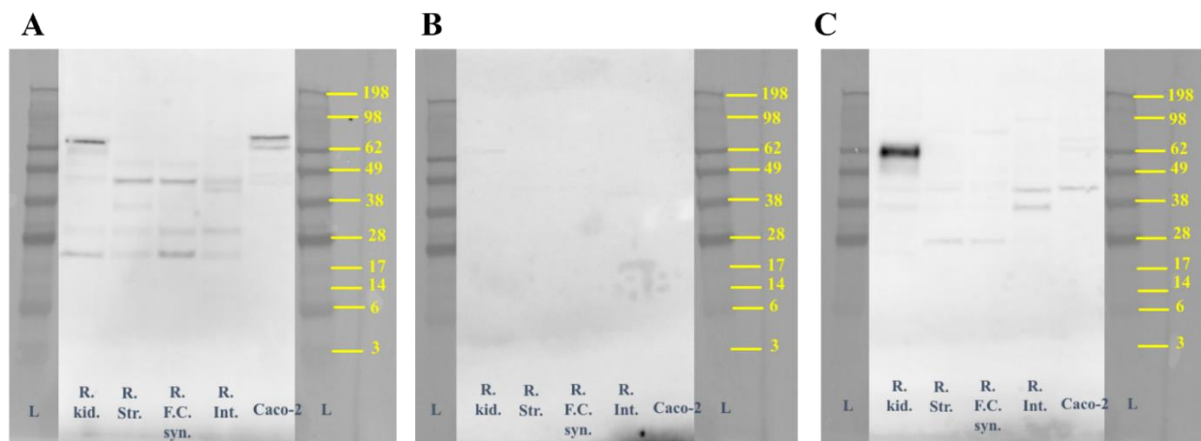


**Figure 3.11: Western blot to look for the presence of OCT2 in Caco-2 cells.** A- Western blot of 20 µg each of rat kidney (R.kid.), rat striatum (R. Str.), rat frontal cortex synaptosome (R. F.C. syn.), rat intestine (R. Int.) and Caco-2 cells with SLC22A2 polyclonal primary antibody (Elabscience®; 1:200); L represents prestained ladder; markings represent molar mass in kDa; B- The same membrane (as A) after mild stripping; C- The same membrane (as A and B) after reprobing with anti-SLC22A2 Picoband™ primary antibody (Boster Biological Technology; 1:400).

To further examine the inconsistencies observed between the banding patterns with the two primary antibodies, the order of their use was reversed. The anti-SLC22A2 Picoband™ primary antibody (Boster Biological Technology) generally identified the same bands as before (Figure 3.11C) in all tissues (Figure 3.12A) although extra bands were seen at 80 kDa in rat striatum and rat frontal cortex synaptosome (Figure 3.12A cf Figures 3.11A and 3.11C). Harsh stripping was required to remove all bands from membranes (Figures 3.12B and C). On reprobing the membrane with the Elabscience® primary antibody, it showed generally the same banding pattern for rat striatum and rat frontal cortex synaptosome as in Figure 3.11A. An additional band was seen at approximately 49 kDa (Figure 3.12D) in Caco-2 cells, however, with the previously observed band at 62 kDa no longer seen. Further additional bands were observed between 13-15 kDa in intestine (Figure 3.12D) when compared to Figure 3.11A.

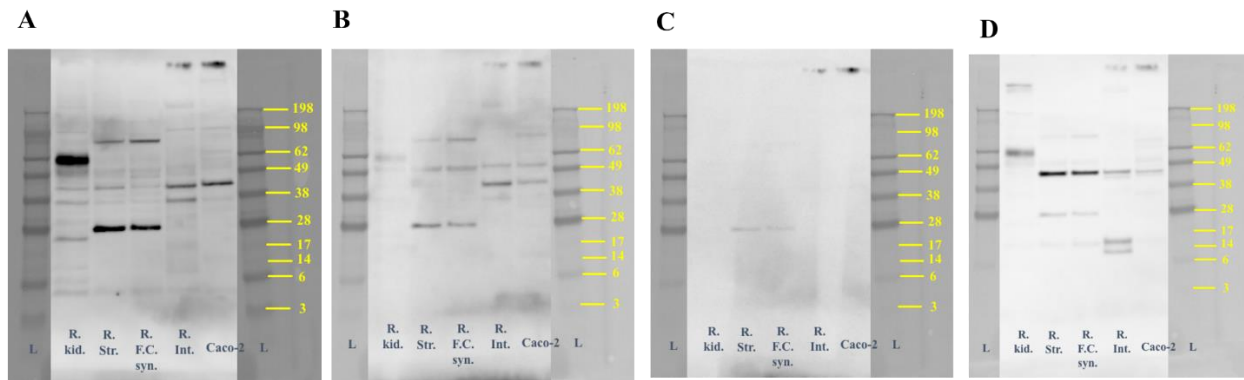


**Figure 3.12 Western blot to look for the presence of OCT2 in Caco-2 cells with reversal of order of the use of primary antibodies** A- Western blot of 20 µg each of rat kidney (R.kid.), rat striatum (R. Str.), rat frontal cortex synaptosome (R. F.C. syn.), rat intestine (R. Int.) and Caco-2 cells with anti-SLC22A2 Picoband™ primary antibody (Boster Biological Technology; 1:400); L represents prestained ladder; markings represent molar mass in kDa; B- The same membrane (as A) after mild stripping; C- The same membrane (as B) after harsh stripping; and D -The same membrane (as A and C) after reprobing with Elabscience polyclonal primary antibody (1:200).

### 3.5 Pharmacological characterization of the basolateral membrane transporter

#### 3.5.1 Effect of inhibition of all OCT isoforms on basolateral TYR transport

Decynium-22 treatment resulted in decreased cellular accumulation of TYR (two-way ANOVA;  $P = 0.03$ , treatment;  $P = 0.2902$ , time;  $P = 0.9922$ , treatment x time; Figure 3.13B) following basolateral addition, although there was no effect on apical accumulation (two-way ANOVA;  $P = 0.6257$ , treatment;  $P < 0.0001$ , time;  $P = 0.9351$ , treatment x time; Figure 3.13C). There was, however, increased TYR concentration seen in the basolateral compartment (two-way ANOVA;  $P = 0.0211$ , treatment;  $P = 0.6847$ , time;  $P = 0.7038$ , treatment x time; Figure 3.13A).

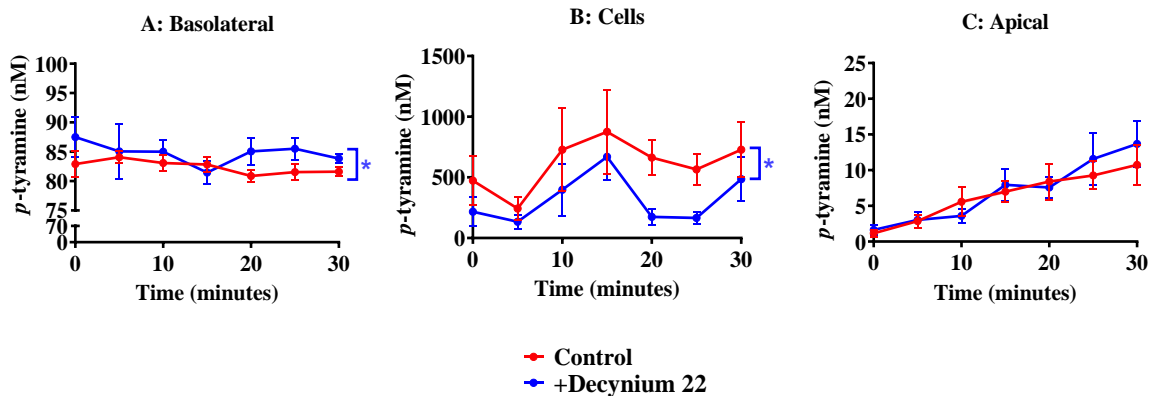


**Figure 3.13: Total transcellular transport of TYR across Caco-2 cells following basolateral compartment loading in the presence and absence of decynium 22.** [ $^3\text{H}$ ]TYR was added at 100 nM in the basolateral compartment and the transport was monitored for varying time points. After transport, the radioactivity was counted, and the concentration of TYR was obtained from standard curves. The “zero” time point represents 100 nM of TYR added to the basolateral compartment and removed at 10 seconds, which was the shortest time frame at which the experiment could be reliably performed. The data represents mean  $\pm$  SEM,  $n = 9-10$  decynium-22. Comparisons were made between different compartments using GraphPad Prism version 6 by two-way ANOVA,  $*P = 0.03$  (for cellular compartment);  $*P = 0.0211$  (for basolateral compartment).

### 3.5.2 Effect of inhibition of OCT1 and OCT2 isoforms on basolateral TYR transport

In contrast, there was no effect of pentamidine on TYR transport to either the cellular (two-way ANOVA;  $P = 0.3102$ , treatment;  $P = 0.8335$ , time;  $P = 0.5587$ , treatment x time; Figure 3.14B) or the apical (two-way ANOVA;  $P = 0.3867$ , treatment;  $P = 0.0007$ , time;  $P = 0.9776$ , treatment x time; Figure 3.14C) compartments following basolateral addition. For the basolateral compartment however, decreased TYR concentration was observed (two-way ANOVA;  $P < 0.0001$ , treatment;  $P = 0.4486$ , time;  $P = 0.9994$ , treatment x time; Figure 3.14A).

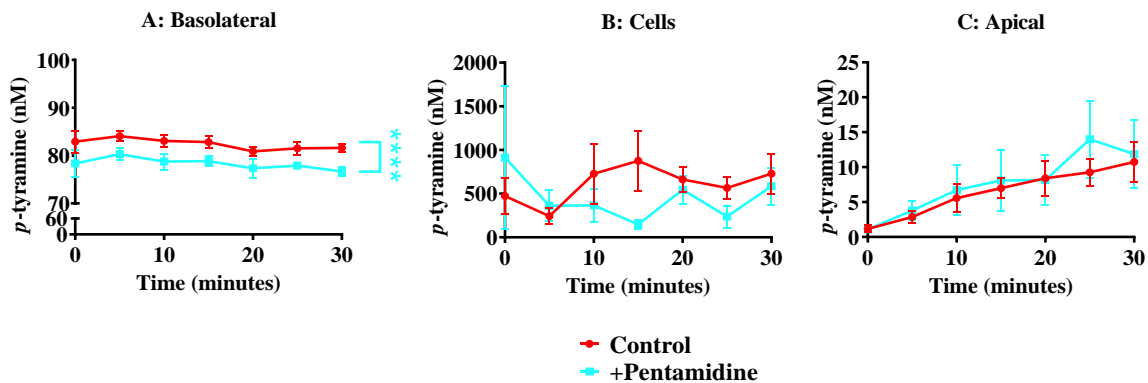


**Figure 3.14: Total transcellular transport of TYR across Caco-2 cells following basolateral compartment loading in the presence and absence of pentamidine.** [ $^3\text{H}$ ]TYR was added at 100 nM in the basolateral compartment and the transport was monitored for varying time points. After transport, the radioactivity was counted, and the concentration of TYR was obtained from standard curves. The “zero” time point represents 100 nM of TYR added to the basolateral compartment and removed at 10 seconds, which was the shortest time frame at which the experiment could be reliably performed. The data represents mean  $\pm$  SEM,  $n = 9-10$  cultures from 10 independent experiments for control, and  $n = 4-5$  from 5 independent experiments for pentamidine. Comparisons were made between different compartments using GraphPad Prism version 6 by two-way ANOVA, \*\*\*\* $P < 0.0001$ .

### 3.5.3 Effect of inhibition of OCT1 on basolateral TYR transport

Surprisingly, the active TYR accumulation in the cellular compartment was significantly decreased with ATR treatment (two-way ANOVA;  $P = 0.020$ , treatment;  $P = 0.8932$ , time;  $P = 0.7783$ , treatment x time; Figure 3.15B) following basolateral addition, suggesting that the active transporter is ATR sensitive.

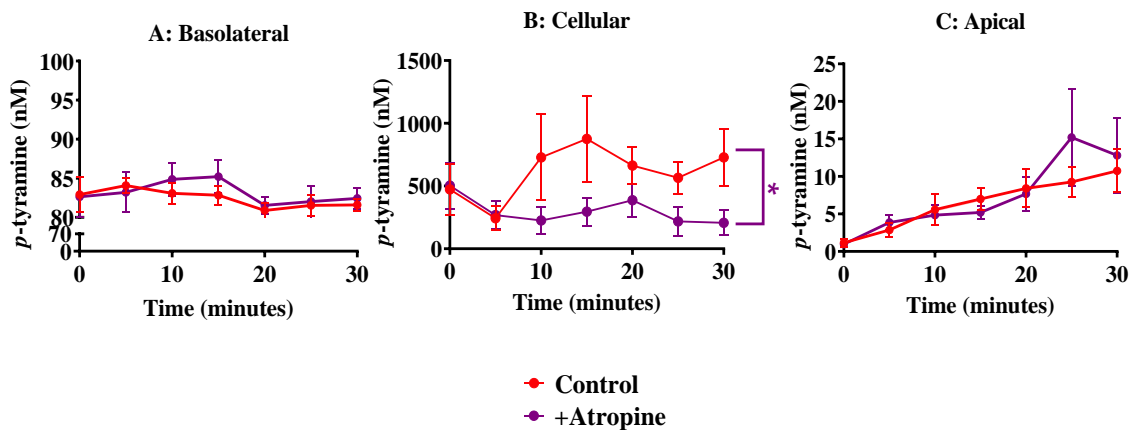


**Figure 3.15: Total transcellular transport of TYR across Caco-2 cells following basolateral compartment loading in the presence and absence of ATR.** [ $^3\text{H}$ ]TYR was added at 100 nM in the basolateral compartment and the transport was monitored for varying time points. After transport, the radioactivity was counted, and the concentration of TYR was obtained from standard curves. The “zero” time point represents 100 nM of TYR added to the basolateral compartment and removed at 10 seconds, which was the shortest time frame at which the experiment could be reliably performed. The data represents mean  $\pm$  SEM,  $n = 9-10$  cultures from 10 independent experiments for control, and  $n = 5$  from 5 independent experiments for ATR. Comparisons were made between different compartments using GraphPad Prism version 6 by two-way ANOVA,  $*P = 0.020$ . This figure was adapted from Sarkar et al., 2020.

### 3.5.4 Effect of the replacing sodium on TYR transport

When sodium chloride was replaced with choline chloride in the assay buffer, decreased cellular (two-way ANOVA;  $P = 0.0174$ , treatment;  $P = 0.6205$ , time;  $P = 0.9378$ , treatment x time; Figure 3.16B) and apical (two way ANOVA;  $P = 0.0016$ , treatment;  $P = 0.0063$ , time;  $P =$

0.8352, treatment x time; Figure 3.16C) compartment accumulation of TYR following basolateral addition was observed.

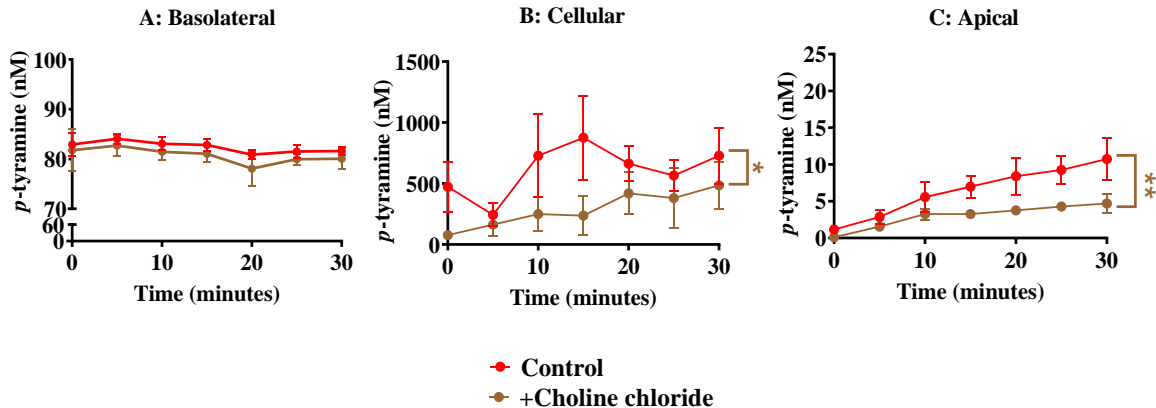


**Figure 3.16: Total transcellular transport of TYR across Caco-2 cells following basolateral compartment loading in the presence and absence of choline chloride.** [<sup>3</sup>H]TYR was added at 100 nM in the basolateral compartment and the transport was monitored for varying time points. After transport, the radioactivity was counted, and the concentration of TYR was obtained from standard curves. The “zero” time point represents 100 nM of TYR added to the basolateral compartment and removed at 10 seconds, which was the shortest time frame at which the experiment could be reliably performed. The data represents mean  $\pm$  SEM, n = 9-10 cultures from 10 independent experiments for control, and n = 5 from 5 independent experiments for choline chloride. Comparisons were made between different compartments using GraphPad Prism version 6 by two-way ANOVA, \* $P = 0.0174$ , \*\* $P = 0.0016$ . This figure was adapted from Sarkar et al., 2020.

With apical addition, TYR concentration was increased in the cellular compartment (two-way ANOVA;  $P = 0.0002$ , treatment;  $P = 0.3389$ , time;  $P = 0.09$ , treatment x time; Figure 3.17B) but was decreased in the basolateral compartment (two way ANOVA;  $P = 0.0017$ , treatment;  $P < 0.0001$ , time;  $P = 0.5021$ , treatment x time; Figure 3.17C) when sodium chloride was replaced with choline chloride in the assay buffer.

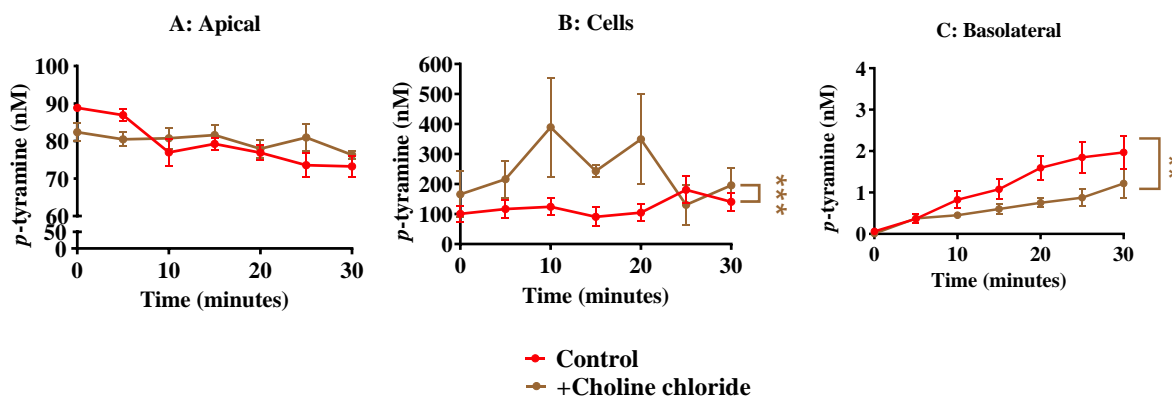


**Figure 3.17: Total transcellular transport of TYR across Caco-2 cells following apical compartment loading in the presence and absence of choline chloride.** [<sup>3</sup>H]TYR was added at 100 nM in the apical compartment and the transport was monitored for varying time points. After transport, the radioactivity was counted, and the concentration of TYR was obtained from standard curves. The “zero” time point represents 100 nM of TYR added to the apical compartment and removed at 10 seconds, which was the shortest time frame at which the experiment could be reliably performed. The data represents mean  $\pm$  SEM,  $n = 9-10$  cultures from 10 independent experiments for control, and  $n = 5$  from 5 independent experiments for choline chloride. Comparisons were made between different compartments using GraphPad Prism version 6 by two-way ANOVA,  $**P = 0.0017$ ,  $***P = 0.0002$ .

### 3.5.5 Kinetic characterization of the Na<sup>+</sup>-dependent, active transporter of TYR in Caco-2 basolateral membranes

The kinetic parameters of the Na<sup>+</sup>-dependent, active transporter of TYR in Caco-2 basolateral membranes were characterized by Michaelis-Menten analysis giving  $V_{\max} = 43.0 \pm 19.1$  nM/second and  $K_t = 33.1 \pm 47.4$  nM (Figure 3.18).

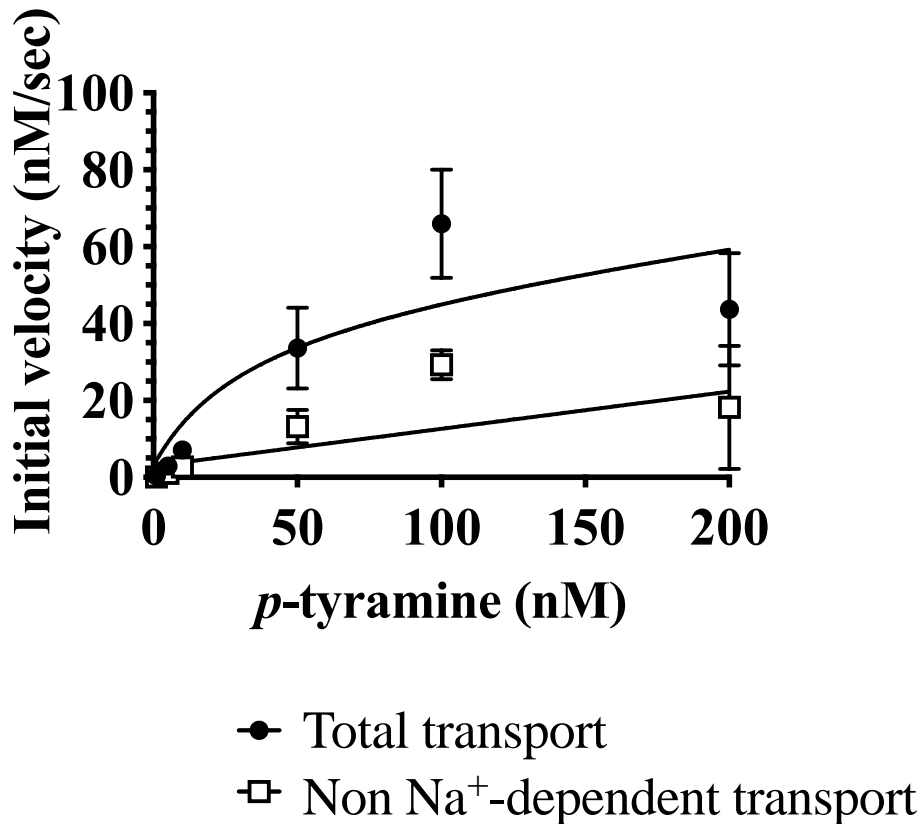


**Figure 3.18: Kinetics of basolateral Caco-2 Na<sup>+</sup>-dependent active TYR transporter.** [<sup>3</sup>H]TYR was added at varying concentrations to the basolateral compartment and the transport was monitored for varying time points. The initial linear phase of a plot of cellular TYR versus time was used to determine the initial velocity of transport at each concentration. Total transport characterized all TYR transport processes across Caco-2 membranes. Non active transporter dependent TYR transport was characterized by replacing sodium chloride with choline chloride. The difference between total and non-specific transport was used to determine the Michaelis Menten kinetics for the Na<sup>+</sup>-dependent active TYR transporter, using the receptor binding tool of GraphPad version 6. The data is represented as mean  $\pm$  SEM, n = 3 independent experiments. Reprinted from Sarkar et al., 2020.

### 3.6 Identification of the basolateral membrane active transporter

#### 3.6.1 SDS PAGE isolation of proteins from TYR affinity columns

Optimization studies revealed that by the third elution fraction with 50x concentration of TYR, no protein remained bound to the column (Figure 3.19). For 10x concentration of ATR elution, considerable protein was eluted in the first two fractions (Figure 3.19). Common protein

bands in TYR and ATR elution fractions were observed at 198 kDa, 62 kDa, 55 kDa, 49 kDa, 43 kDa, 42 kDa, 41 kDa, 16 kDa, 15 kDa and 14 kDa (Figure 3.20).

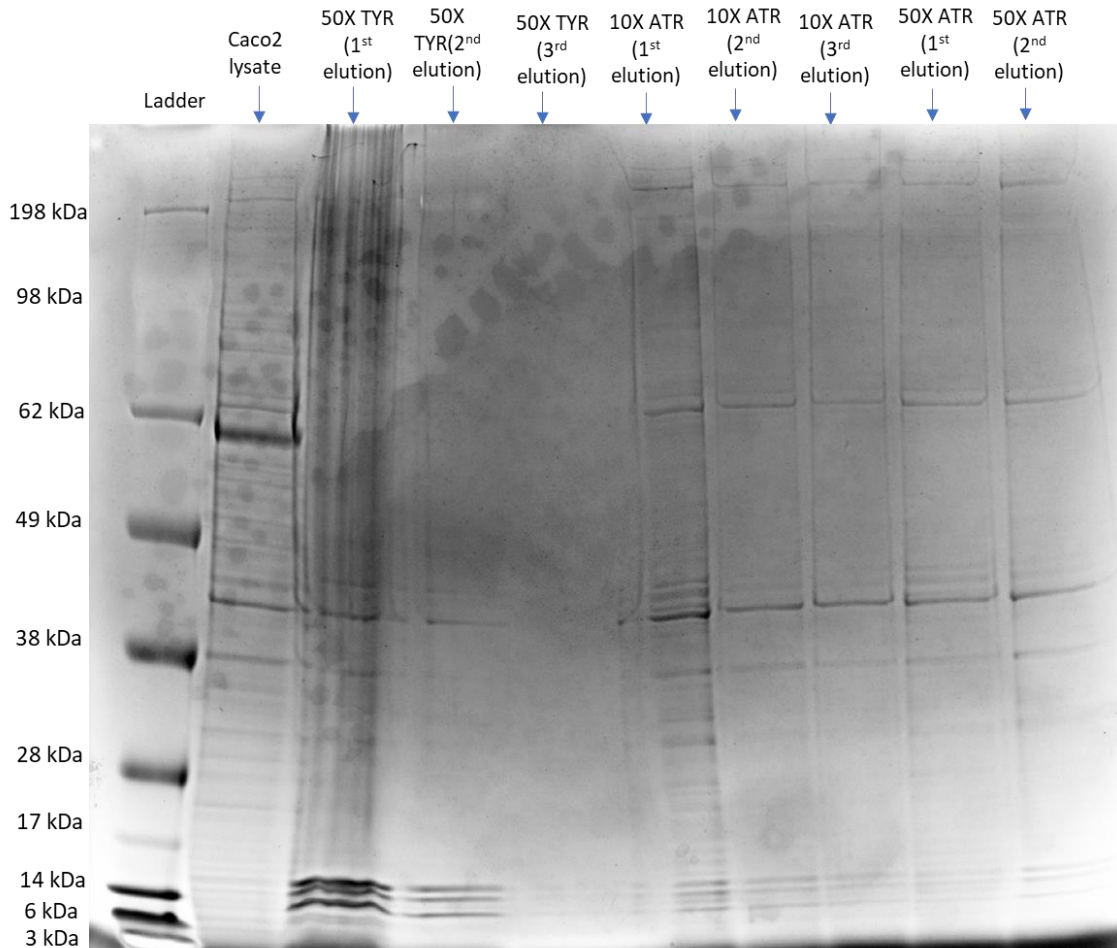


**Figure 3.19: Representative SDS PAGE image of the elution profile from TYR affinity columns.** SDS PAGE was performed on the collected protein fractions from three elution steps from the TYR affinity columns using 50x TYR or 10x ATR concentrations as the eluents. The gel was stained with staining solution containing 0.25% (w/v) Coomassie Brilliant Blue R-250, 50% (v/v) 95% ethanol and 10% (v/v) glacial acetic acid, destained with a deionized water:95% ethanol:glacial acetic acid (8:1:1) solution, and digitally recorded using a Biorad Chemidoc system.

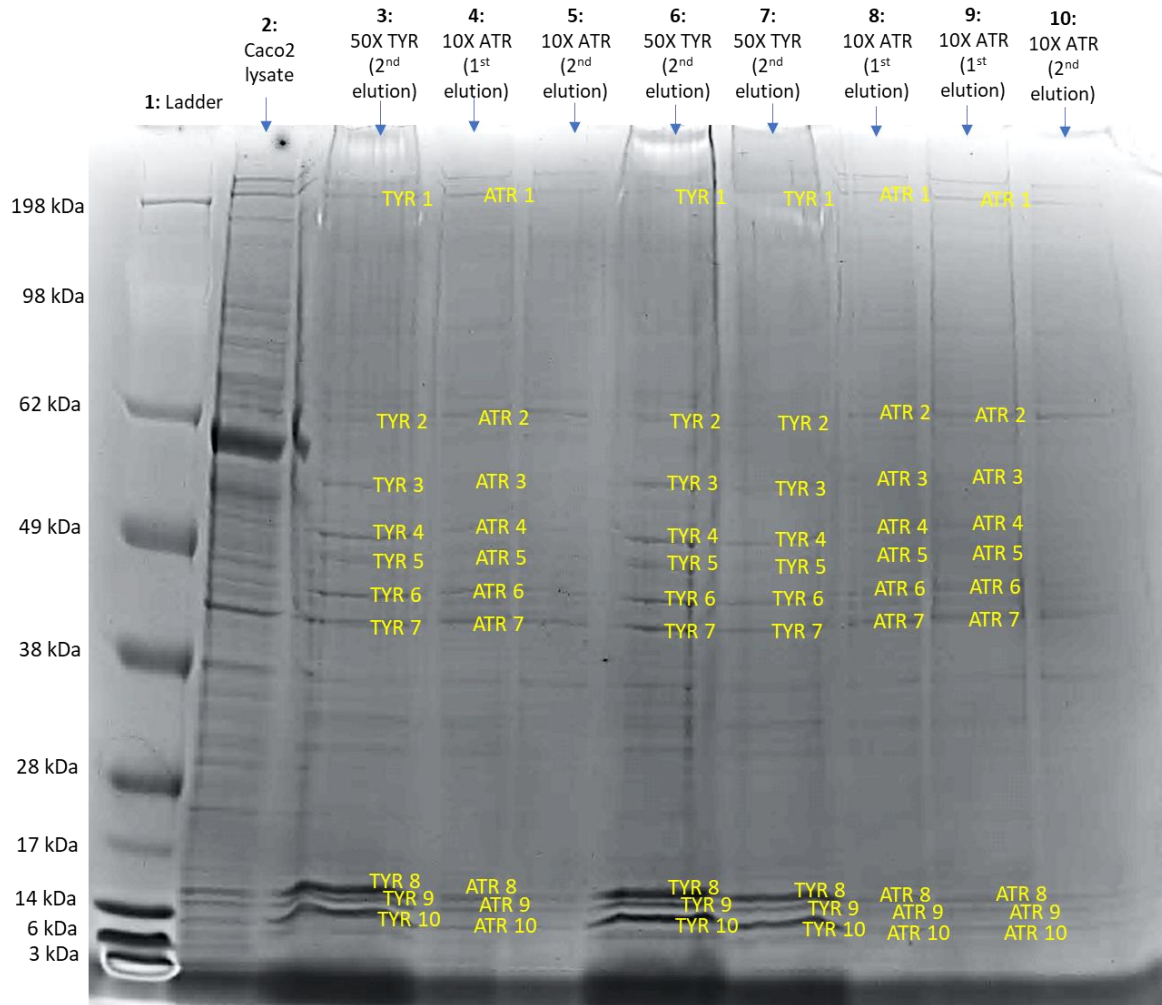


**Figure 3.20: Representative SDS-PAGE of Caco-2 proteins eluted from TYR affinity columns.** SDS PAGE was performed on the collected protein fractions from three elution steps from the TYR affinity columns using 50x TYR or 10x ATR concentrations as the eluents. The gel was stained with a 0.25% (w/v) Coomassie Brilliant Blue R-250, 50% (v/v) 95% ethanol and 10% (v/v) glacial acetic acid mixture, destained with a deionized water:95% ethanol:glacial acetic acid (8:1:1) solution, and digitally recorded using a Biorad Chemidoc system. This was replicated three times with similar banding pattern observed each time.

### 3.6.2 Protein identification

The selected common binding proteins between TYR and ATR were identified by the Biological Mass Spectrometry Core Facility (Dalhousie University, Halifax, NS). A total of 124 unique proteins were identified (see appendix A), twenty of which were membrane proteins, and two of which were known transporter proteins (Table 3.1). These transporter proteins were

identified as cadherin-17 and solute carrier family-2 - facilitated glucose membrane transporter 14. Although cadherin-17 is an active transporter, it is not a Na<sup>+</sup>-dependent transporter nor is it known to include TYR in its substrate profile.

**Table 3.1: Classification of common TYR and ATR binding proteins.**

<b>Criteria</b>	<b>Number of proteins identified</b>
Total common proteins	124
Membrane proteins	20
Transporters	2
Active transporter	1
Na <sup>+</sup> -dependent transporter	0
TYR = known substrate	0

The gel bands from SDS-PAGE were collected, dried, and identified by mass spectrometry at the Biological Mass Spectrometry Core Facility at Dalhousie University.

### **3.7 Modelling of TYR transport kinetics across human intestinal epithelial cells**

#### **3.7.1 Comparison of baseline simulation with experimental**

Using known kinetic parameters for simple diffusion, apical membrane OCT2, and the basolateral membrane active transporter (Berry et al., 2013, 2016) (Figure 2.9, Table 3.2), the model produced TYR concentration curves that did not recapitulate experimental observations for either basolateral (Figure 3.21) or apical (Figure 3.22) compartment loading.

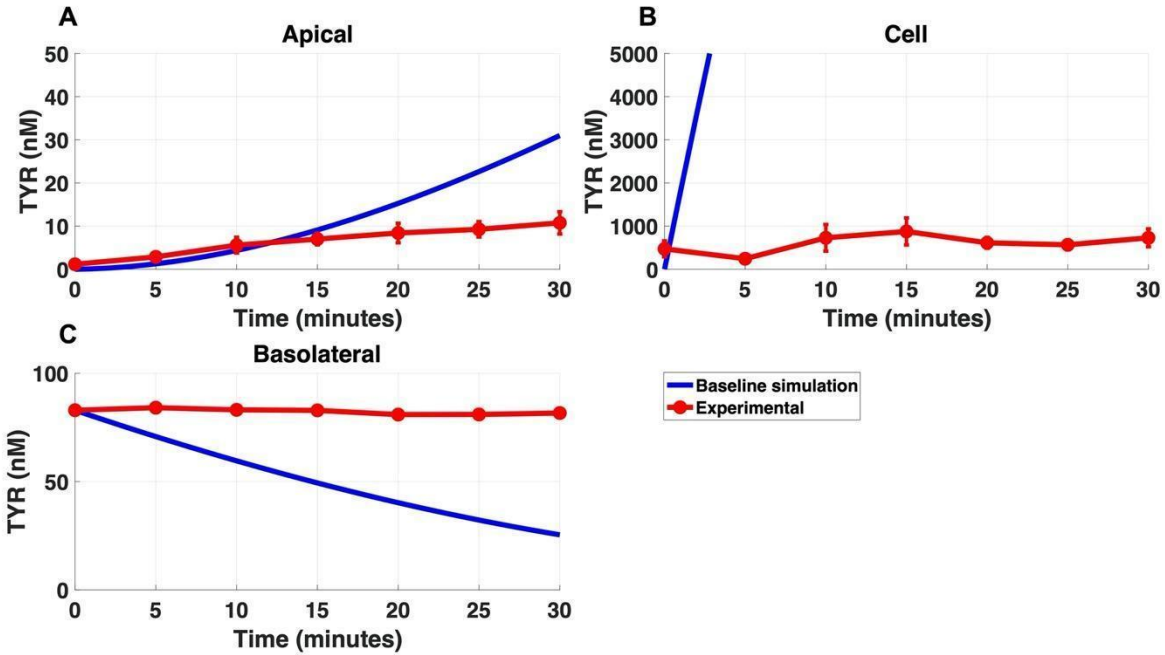


**Figure 3.21: Comparison of the baseline model for TYR transport following basolateral loading to experimental findings.** The transport of 100 nM TYR across Caco-2 cells was modeled for basolateral loading using MATLAB vR2021a. Comparisons were made between the baseline model (representing known TYR transporters that have been characterized; blue curve) for the apical (A), cellular (B) and basolateral (C) compartments, versus experimental observations (red curves). Kinetic parameters used for this modelling were:  $V_{\max\_OCT2} = 0.1$  nM/second,  $K_{t\_OCT2\_apicalto\text{cell}} = 101.5$  nM,  $V_{\max\_baso\_active} = 43.0$  nM/second and  $K_{t\_baso\_active} = 33.1$  nM. Reprinted from Sarkar et al., 2022.

**Table 3.2: Kinetic parameters used for each model scenario.**

Parameter	Experimentally determined kinetics	Parameters used for Figures 3.21, 3.22	Parameters used for Figures 3.23, 3.24	Parameters used for Figures 3.25, 3.26	Parameters used for Figures 3.27, 3.28	Parameters used for Figures 3.29, 3.30
$V_{\max\_OCT2}$	0.1 nM/s	0.1 nM/s	0.1 nM/s	0.1 nM/s	2.3 nM/s	2.3 nM/s
$K_t\_OCT2\_apicalto cell$	101.5 nM	101.5 nM	101.5 nM	101.5 nM	110.4 nM	110.4 nM
$K_t\_OCT2\_cellto apical$	n/a	n/a	n/a	n/a	1227.9 nM	110.4 nM
$V_{\max\_baso\_active}$	43.0 nM/s	43.0 nM/s	43.0 nM/s	43.0 nM/s	3.3 nM/s	3.3 nM/s
$K_t\_baso\_active$	33.1 nM	33.1 nM	33.1 nM	33.1 nM	29.0 nM	29.0 nM
$V_{\max\_baso\_new\_FD}$	n/a	n/a	0.01-2 nM/s	50 nM/s	6.0 nM/s	6.0 nM/s
$K_t\_baso\_new\_FD\_baso to cell$	n/a	n/a	101.5 nM	101.5-1015 nM	584.1 nM	628.3nM*
$K_t\_baso\_new\_FD\_cell to baso$			n/a	n/a	672.4nM	628.3 nM*

Kinetic parameter used for OCT2 and the added basolateral membrane transporter for different model scenarios. \* $K_t\_baso\_new\_FD\_baso to cell$  and  $K_t\_baso\_new\_FD\_cell to baso$  from Figures 3.27 and 3.28 did not show a meaningful directional preference, and so for studies shown in Figures 3.29 and 3.30 the average value of 628.3 nM was used as the  $K_t$  in each direction for the basolateral bidirectional facilitated diffusion transporter. This table was adapted from Sarkar et al., 2022.

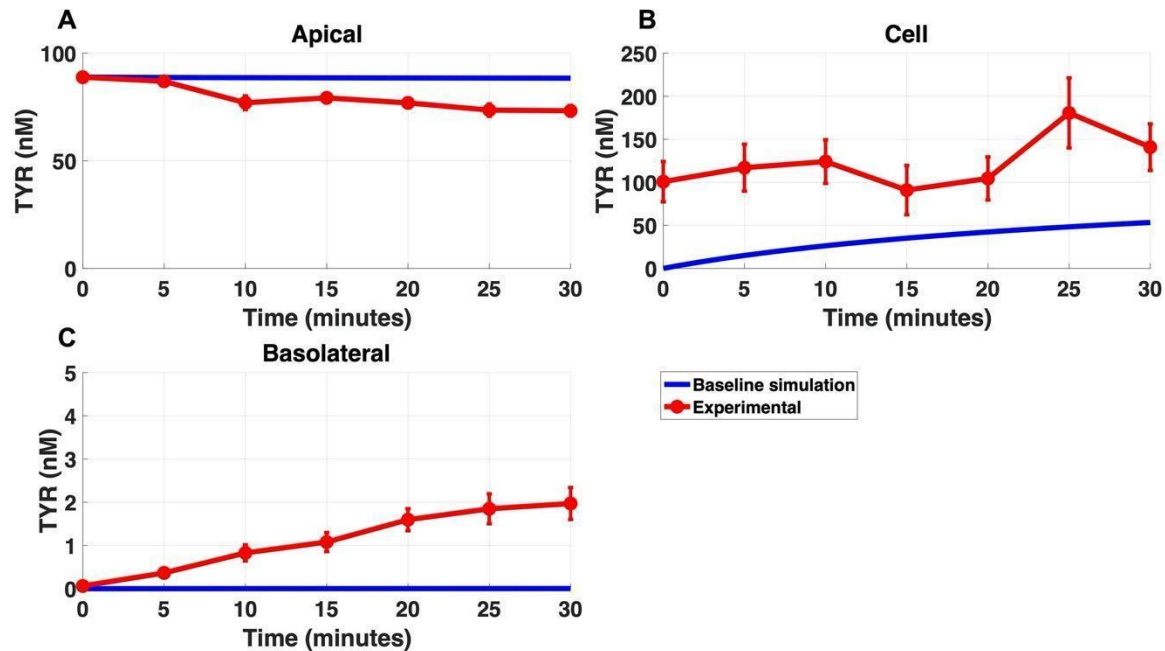


**Figure 3.22: Comparison of the baseline model for TYR transport following apical loading to experimental findings.** The transport of 100 nM TYR across Caco-2 cells was modeled for apical loading using MATLAB vR2021a. Comparisons were made between the baseline model (representing known TYR transporters; blue curve) for the apical (A), cellular (B) and basolateral compartments (C), versus experimental observations (red curves). Kinetic parameters used for this modelling were:  $V_{\max\_OCT2} = 0.1$  nM/second,  $K_t\_OCT2\_apicalto\ cell = 101.5$  nM,  $V_{\max\_baso\_active} = 43.0$  nM/second and  $K_t\_baso\_active = 33.1$  nM (Table 3.2). Reprinted from Sarkar et al., 2022.

### 3.7.2 Introduction of OCT2 in the basolateral membrane.

OCT2 was introduced to the Caco-2 basolateral membrane at different densities (0–1 - 20X  $V_{\max}$  of OCT2, Table 3.2) but all failed to improve model accuracy following basolateral addition of TYR (Figure 3.23) and worsened model accuracy for apical loading (Figure 3.24).

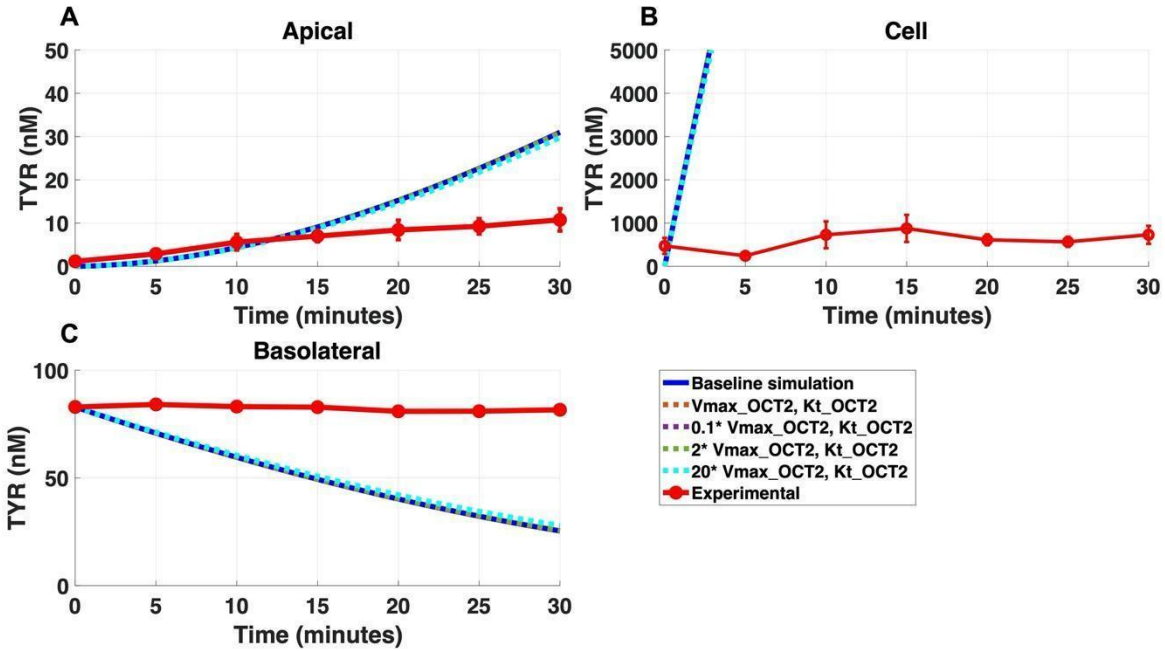


**Figure 3.23: Comparison of TYR transport with the introduction of OCT2 to the Caco-2 basolateral membrane, following basolateral TYR loading, to experimental findings.** The transport of 100 nM of TYR across Caco-2 cells was modeled following basolateral loading using MATLAB vR2021a. Comparisons were made between the models (baseline = blue curve; modified = dotted curves) for the apical (A), cellular (B) and basolateral compartments (C), versus experimental observations (red curves). Kinetic parameters used for this modelling were:  $V_{\max\_OCT2} = 0.1$  nM/second,  $K_{t\_OCT2\_apicalto cell} = 101.5$  nM,  $V_{\max\_baso\_active} = 43.0$  nM/second,  $K_{t\_baso\_active} = 33.1$  nM,  $V_{\max\_baso\_new\_FD} = 0.01-2$  nM/second and  $K_{t\_baso\_new\_FD\_basotocell} = 101.5$  nM (Table 3.2). Note that the predicted curves overlapped with each other. Reprinted from Sarkar et al., 2022.

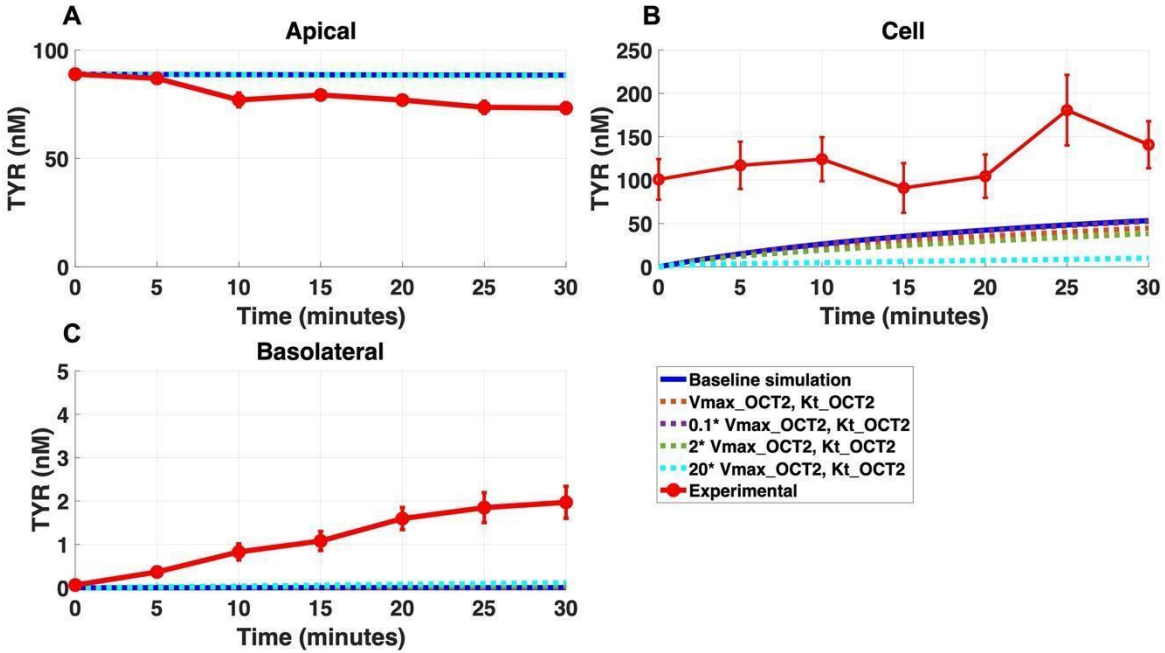


**Figure 3.24: Comparison of TYR transport with the introduction of OCT2 to the Caco-2 basolateral membrane, following apical TYR loading, to experimental findings.** The transport of 100 nM TYR across Caco-2 cells was modeled following apical loading by using MATLAB vR2021a. Comparisons were made between the models (baseline = blue curve; modified = dotted curves) for the apical (A), cellular (B) and basolateral compartments (C), versus experimental observations (red curves). Kinetic parameters used for this modelling were:  $V_{\max\_OCT2} = 0.1$  nM/second,  $K_t\_OCT2\_apicalto cell = 101.5$  nM,  $V_{\max\_baso\_active} = 43.0$  nM/second,  $K_t\_baso\_active = 33.1$  nM,  $V_{\max\_baso\_new\_FD} = 0.01-2$  nM/second and  $K_t\_baso\_new\_FD\_basotocell = 101.5$  nM (Table 3.2). Note that the predicted curves overlapped with each other for apical and basolateral compartments. Reprinted from Sarkar et al., 2022.

### 3.7.3 Introduction of a non-OCT2 facilitated diffusion transporter in the basolateral membrane

Introduction of a facilitated diffusion transporter not confined to OCT2  $K_t$ , provided a closer match to experimental results following basolateral loading (Figure 3.25A-C) with kinetic parameters of  $V_{\max} = 50$  nM/s and  $K_t = 203-507.5$  nM giving the best matches. In contrast, such a transporter worsened modelling following apical loading (Figure 3.26) when using the same kinetic parameters.

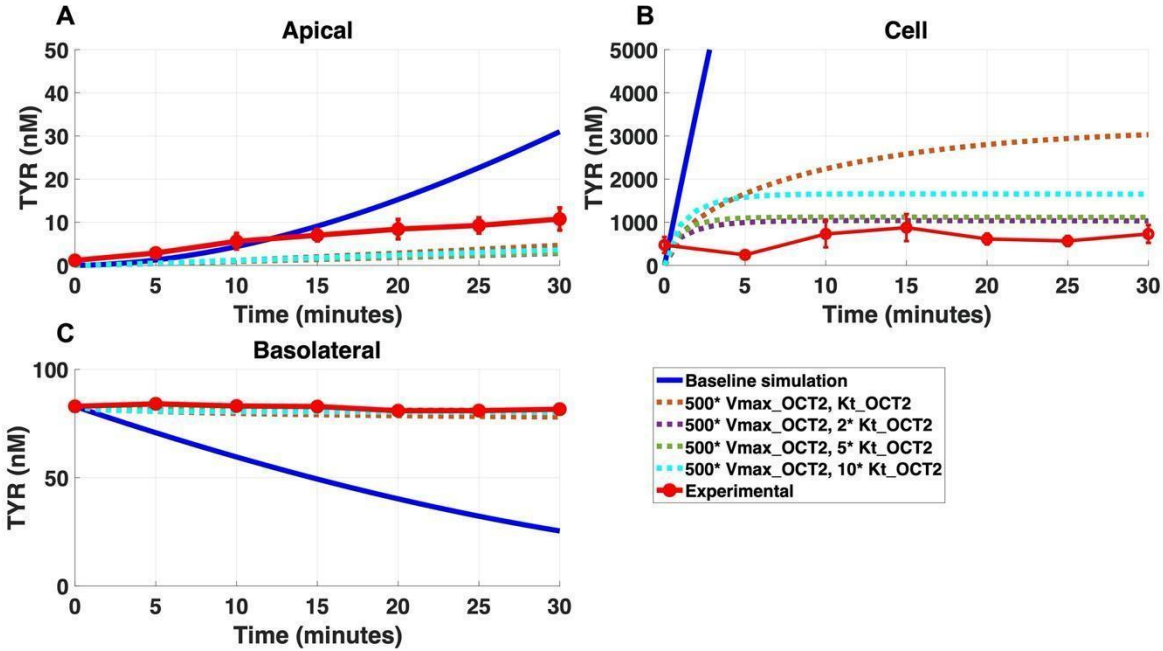


**Figure 3.25: Comparison of TYR transport with the introduction of a non-OCT2 facilitated diffusion transporter to the Caco-2 basolateral membrane, following basolateral TYR loading, to experimental findings.** The transport of 100 nM TYR across Caco-2 cells was modeled following basolateral loading using MATLAB vR2021a. Comparisons were made between the models (baseline = blue curve; modified = dotted curves) and experimental observations (red curves) for the apical (A), cellular (B) and basolateral compartments (C). Kinetic parameters used for this modelling were:  $V_{\max\_OCT2} = 0.1$  nM/second,  $K_{t\_OCT2\_apicalto cell} = 101.5$  nM,  $V_{\max\_baso\_active} = 43.0$  nM/second,  $K_{t\_baso\_active} = 33.1$  nM,  $V_{\max\_baso\_new\_FD} = 50$  nM/second and  $K_{t\_baso\_new\_FD\_basotocell} = 101.5-1015$  nM (Table 3.2). Note that the predicted curves overlapped with each other for basolateral compartment. Reprinted from Sarkar et al., 2022.

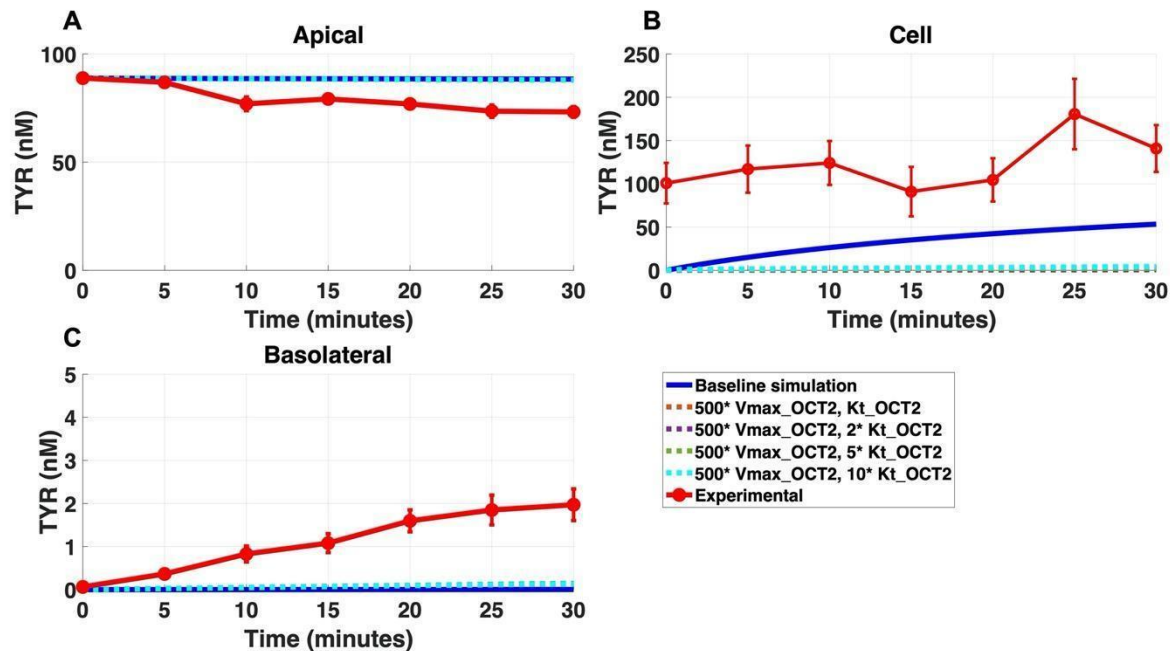


**Figure 3.26: Comparison of TYR transport with the introduction of a non-OCT2 facilitated diffusion transporter to the Caco-2 basolateral membrane, following apical TYR loading, to experimental findings.** The transport of 100 nM of TYR across Caco-2 cells was modeled for apical loading using MATLAB vR2021a. Comparisons were made between the models (baseline = blue curve; modified = dotted curves) and experimental observations (red curves) for the apical (A), cellular (B) and basolateral compartments (C). Kinetic parameters used for this modelling were:  $V_{\max\_OCT2} = 0.1$  nM/second,  $K_{t\_OCT2\_apicalto cell} = 101.5$  nM,  $V_{\max\_baso\_active} = 43.0$  nM/second,  $K_{t\_baso\_active} = 33.1$  nM,  $V_{\max\_baso\_new\_FD} = 50$  nM/second and  $K_{t\_baso\_new\_FD\_basotocell} = 101.5-1015$  nM (Table 3.2). Note that the predicted curves overlapped with each other. Reprinted from Sarkar et al., 2022.

### 3.7.4 Introduction of asymmetry in facilitated diffusion transporters

With improvement seen in modelling accuracy for basolateral loading but worsening for apical loading, I hypothesized that one or more of the facilitated diffusion transporters needed to show asymmetric transport characteristics. When an approximate 10-fold asymmetry in OCT2 (values for which were solved for by MATLAB; Table 3.2) was present in combination with approximately symmetric transport by the added basolateral membrane facilitated diffusion transporter, recapitulation of experimental observations was possible for TYR transcellular transport following both basolateral (Figure 3.27) and apical (Figure 3.28) loading.

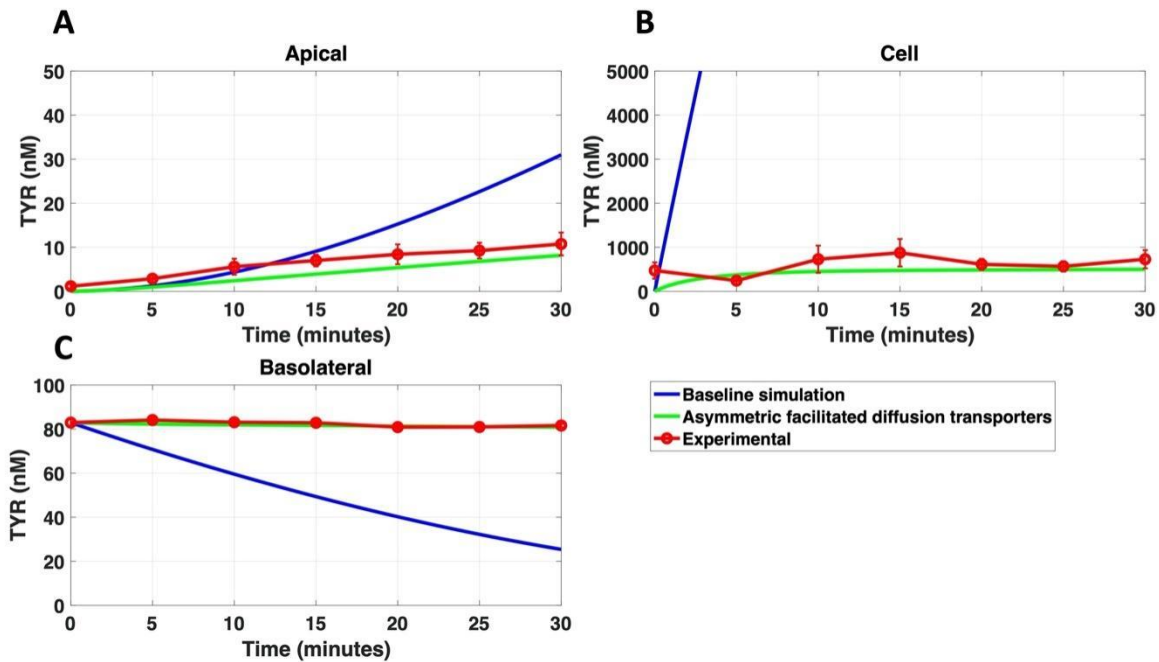


**Figure 3.27: Comparison of TYR transport with the introduction of asymmetry in OCT2 and the facilitated diffusion transporter in the Caco-2 basolateral membrane, following basolateral TYR loading, to experimental findings.** The transport of 100 nM TYR across Caco-2 cells was modeled following basolateral loading using MATLAB vR2021a. Comparisons were made between the models (baseline = blue curve; modified = green curves) and experimental observations (red curves) for the apical (A), cellular (B) and basolateral compartments (C). Solved kinetic parameters from this modelling were:  $V_{\max\_OCT2} = 2.3$  nM/s,  $K_{t\_OCT2\_apicalto\text{cell}} = 110.4$  nM,  $K_{t\_OCT2\_\text{cell}to\text{apical}} = 1227.9$  nM,  $V_{\max\_baso\_active} = 3.3$  nM/s,  $K_{t\_baso\_active} = 29.0$  nM,  $V_{\max\_baso\_new\_FD} = 6.0$  nM/s,  $K_{t\_baso\_new\_FD\_baso\text{to}\text{cell}} = 584.1$  nM and  $K_{t\_baso\_new\_FD\_cell\text{to}\text{baso}} = 672.4$  nM (Table 3.2). Reprinted from Sarkar et al., 2022.

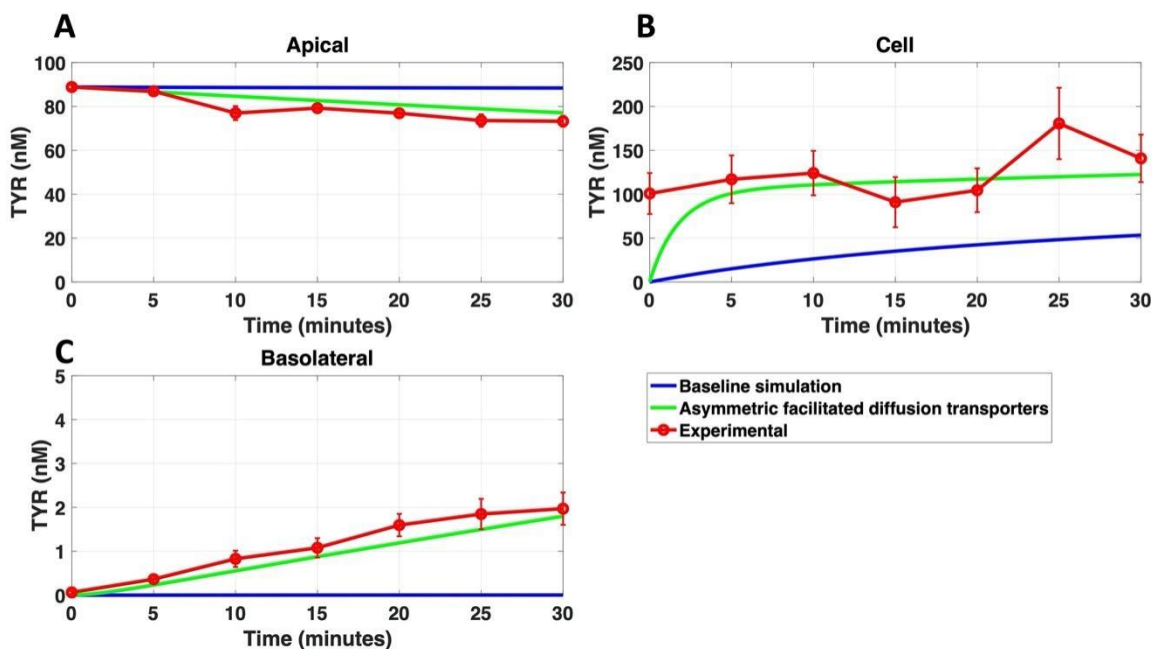


**Figure 3.28: Comparison of TYR transport with the introduction of asymmetry in OCT2 and the facilitated diffusion transporter in the Caco-2 basolateral membrane, following apical TYR loading, to experimental findings.** The transport of 100 nM of TYR across Caco-2 cells was modeled following apical loading using MATLAB vR2021a. Comparisons were made between the models (baseline = blue curve; modified = green curves) and experimental observations (red curves) for the apical (A), cellular (B) and basolateral compartments (C). Solved kinetic parameters from this modelling were:  $V_{\max\_OCT2} = 2.3$  nM/s,  $K_t\_OCT2\_apicalto\text{cell} = 110.4$  nM,  $K_t\_OCT2\_cel\text{to}apical = 1227.9$  nM,  $V_{\max\_baso\_active} = 3.3$  nM/s,  $K_t\_baso\_active = 29.0$  nM,  $V_{\max\_baso\_new\_FD} = 6.0$  nM/s,  $K_t\_baso\_new\_FD\_baso\text{to}cell = 584.1$  nM and  $K_t\_baso\_new\_FD\_cell\text{to}baso = 672.4$  nM (Table 3.2). Reprinted from Sarkar et al., 2022.

### 3.7.5 Introduction of intracellular compartmentalization

To examine for a possible alternative to asymmetry of TYR transport by OCT2, I tested whether the introduction of intracellular compartmentalization allowed experimental results to be modelled. While a compartmentalization factor of 0.36 (64% of intracellular TYR is sequestered into one or more intracellular compartments) allowed good matching to experimental observations following basolateral compartment loading (Figures 3.29A-C), it was visibly not as effective as asymmetric OCT2 transport (c.f. Figure 3.27). This was verified by generally lower RMSD values for asymmetric OCT2 transport (2.75, 289.76 and 0.9868 for apical, cellular and basolateral

compartments respectively) than for compartmentalization (4.23, 228.39 and 1.88, respectively) model fits.

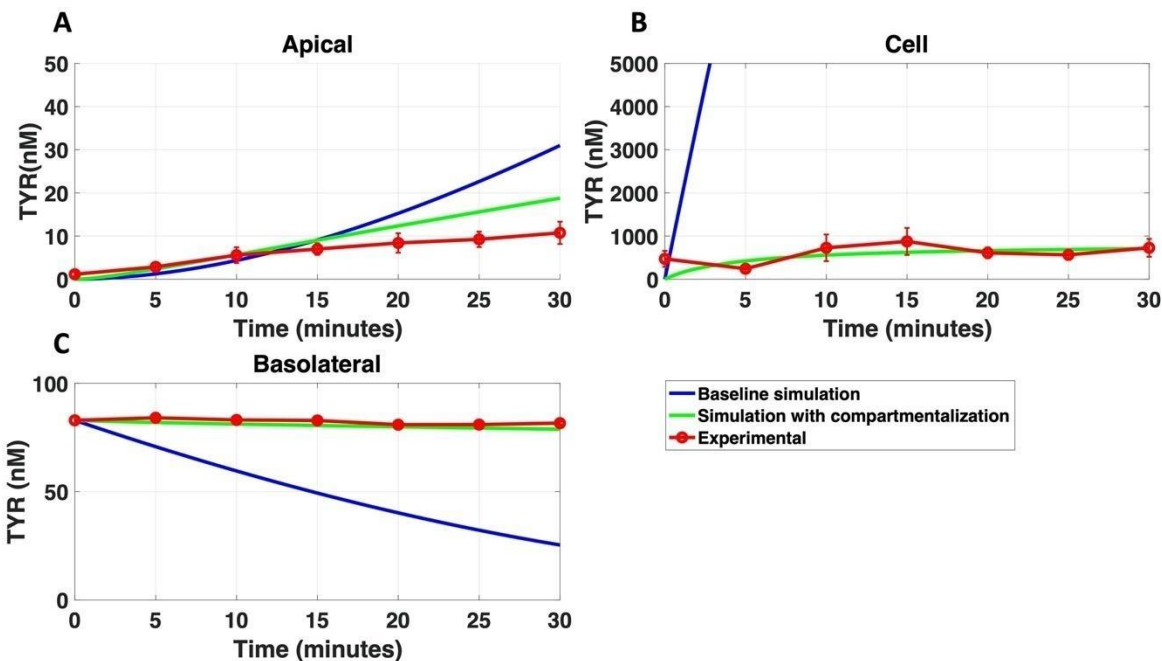


**Figure 3.29: Comparison of TYR transport with the introduction of compartmentalization and symmetry in the facilitated diffusion transporter in the Caco-2 basolateral membrane, following basolateral TYR loading, to experimental findings.** The transport of 100 nM TYR across Caco-2 cells was modeled following basolateral loading using MATLAB vR2021a. Comparisons were made between the models (baseline = blue curve; modified = green curves) and experimental observations (red curves) for the apical (A), cellular (B) and basolateral compartments (C). Kinetic parameters producing this modelling were:  $V_{\max\_OCT2} = 2.3$  nM/s,  $K_{t\_OCT2\_apicalto\text{cell}} = 110.4$  nM,  $K_{t\_OCT2\_cellto\text{apical}} = 110.4$  nM,  $V_{\max\_baso\_active} = 3.3$  nM/s,  $K_{t\_baso\_active} = 29.0$  nM,  $V_{\max\_baso\_new\_FD} = 6.0$  nM/s,  $K_{t\_baso\_new\_FD\_baso\text{cell}} = 628.3$  nM\* and  $K_{t\_baso\_new\_FD\_cell\text{baso}} = 628.3$  nM\*. \* $K_{t\_baso\_new\_FD\_baso\text{cell}}$  and  $K_{t\_baso\_new\_FD\_cell\text{baso}}$  from Figures 3.27 and 3.28 did not show a physiologically meaningful directional preference, and so the average value of 628.3 nM was used in each direction for the basolateral bidirectional facilitated diffusion transporter (Table 3.2). Reprinted from Sarkar et al., 2022.

Similarly following apical loading, while marked improvements compared to the baseline model were possible with compartmentalization (Figures 3.30A-C), these were not as robust (RMSD = 7.52, 46.22 and 0.84 for apical, cellular and basolateral compartments) as with asymmetric OCT2 transport (c.f. Figures 3.28 A-C; RMSD = 4.34, 48.86 and 0.26). Furthermore,

the solved kinetics for the required intracellular compartment transporter ( $V_{\max} = 5.2 \times 10^{-21}$  nM/second;  $K_t = 154.5$  nM; when using Equations 18-21) were physiologically inconsequential.

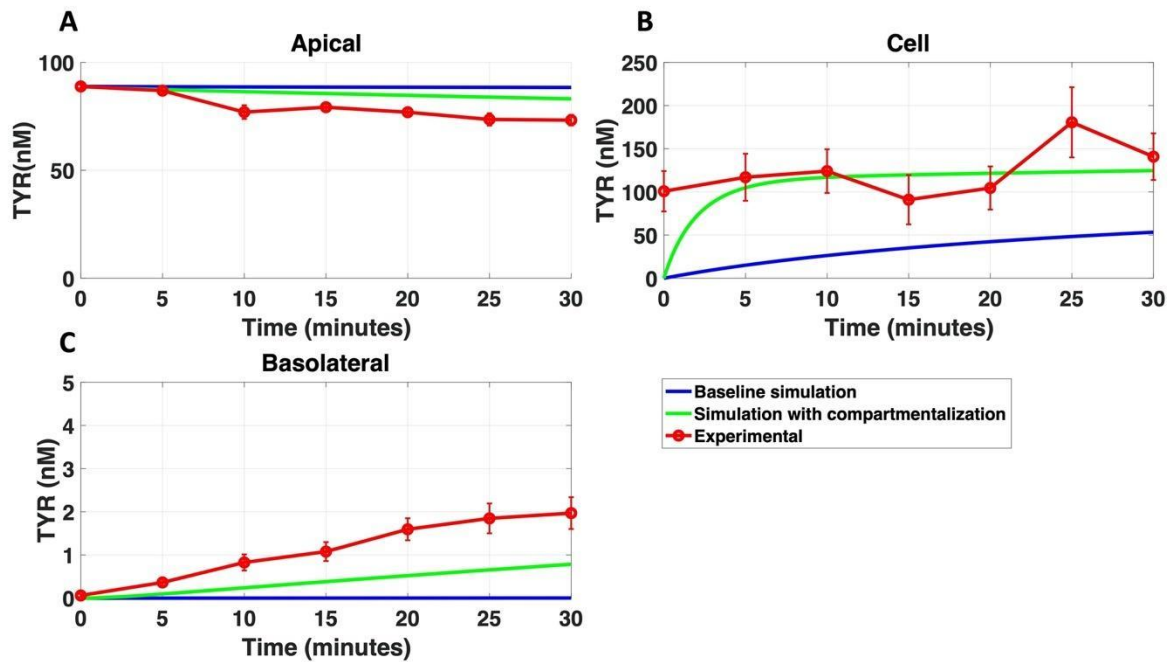


**Figure 3.30: Comparison of TYR transport with the introduction of compartmentalization and symmetry in the facilitated diffusion transporter in the Caco-2 basolateral membrane, following apical TYR loading, to experimental findings.** The transport of 100 nM TYR across Caco-2 cells was modeled following apical loading using MATLAB vR2021a. Comparisons were made between the models (baseline = blue curve; modified = green curves) and experimental observations (red curves) for the apical (A), cellular (B) and basolateral compartments (C). Optimized kinetic parameters for this modelling were:  $V_{\max\_OCT2} = 2.3$  nM/s,  $K_{t\_OCT2\_apicalto cell} = 110.4$  nM,  $K_{t\_OCT2\_cellto apical} = 110.4$  nM,  $V_{\max\_baso\_active} = 3.3$  nM/s,  $K_{t\_baso\_active} = 29.0$  nM,  $V_{\max\_baso\_new\_FD} = 6.0$  nM/s,  $K_{t\_baso\_new\_FD\_basotocell} = 628.3$  nM\* and  $K_{t\_baso\_new\_FD\_celltobaso} = 628.3$  nM\*. \* $K_{t\_baso\_new\_FD\_basotocell}$  and  $K_{t\_baso\_new\_FD\_celltobaso}$  from Figures 3.27 and 3.28 did not show a meaningful directional preference, and so the average value of 628.3 nM was used as the  $K_t$  in each direction for the basolateral bidirectional facilitated diffusion transporter (Table 3.2). Reprinted from Sarkar et al., 2022.

## 4 DISCUSSION

### 4.1 Caco-2 cells offer a suitable polarized model system for TA transport

The discovery of TAAR1, has led to an increase in interest in the therapeutic potential of endogenous TA systems. This interest primarily reflects the demonstrated role of TAAR1 in different diseases including a spectrum of psychiatric, metabolic and immune-related disorders (Borowsky et al., 2001; Bunzow et al., 2001; Revel et al., 2011; Berry et al., 2017; Christian and Berry, 2018; Gainetdinov et al., 2018; Nair et al., 2022). TA are not only endogenously synthesized, but they are present in common foodstuffs (Coutts et al., 1986; Finberg and Gillman, 2011; An et al., 2015; Biji et al., 2016; Martin and Vij, 2016; Nalazek-Rudnicka and Wasik, 2017; Ohta et al., 2017; Liu et al., 2018; Park et al., 2019; Zhang et al., 2019; Chen et al., 2022) and also synthesized by the commensal intestinal microbiota (Lauweryns and Van Ranst, 1988; Bover-Cid et al., 2001; Gardini et al., 2001; Moreno-Arribas and Lonvaud-Funel, 2001; Connil et al., 2002; Lucas et al., 2003; Coton et al., 2004; Fernández et al., 2004; Marcobal et al., 2006; Bugda Gwilt et al., 2020). Due to the unique intracellular locale of TAAR1 (Barak et al., 2008; Raab et al., 2016; Pitts et al., 2019), because of the absence of one or more *N*-terminal glycosylation sites (Barak et al., 2008), it is interesting to identify the ways by which TA access to TAAR1 is controlled. I selected the Caco-2 cell line as a physiologically relevant cell line for my study. On differentiation Caco-2 cells express enzymes, receptors and transporter proteins that are characteristic of those present in the human intestinal epithelia (Lea, 2015), and it has been well established that Caco-2 cells offer a reliable correlation of drug permeation/transport to that seen after oral intake in humans (Artursson and Karlsson, 1991; Cheng et al., 2008; Sun et al., 2008; Lea, 2015). In addition, there have been well-documented reports applying Caco-2 cells to study the effects of microbiota and diet on the intestinal epithelia (Shimizu, 2010; Lea, 2015).

Before characterizing the transport of TA across a Caco-2 barrier, I first established culture conditions to generate a tight, polarized Caco-2 monolayer on Transwell® inserts to mimic the *in vivo* situation. The tightness of the monolayer was determined by studying the paracellular transport of LY and by measuring TEER. LY is a fluorescent dilithium salt that only undergoes paracellular diffusion transport (Rozehnal et al., 2012; Zhang et al., 2014; Strugari et al., 2018; Thomson et al., 2019). A LY exclusion of greater than 97% indicates tight junctional contacts and a fully established monolayer (Debebe et al., 2012; Rastogi et al., 2013). On average, 23 days in culture consistently gave a permeability measurement of < 3% (Figure 2.2). The resistance across the Transwell® insert was also measured. The TEER measurement was used as the prime method to determine of Caco-2 monolayer integrity since Caco-2 cells could not be used post LY exclusion measurement. On reaching the 23<sup>rd</sup> day, TEER measurement was observed to be > 45  $\Omega\text{cm}^2$  (Figure 2.3). Although the TEER value that I obtained is lower than other literature reports of values around 100-400  $\Omega\text{cm}^2$  (Hidalgo et al., 1989; Mukherjee et al., 2004; Srinivasan et al., 2015; Lopez-Escalera and Wellejus, 2022), it has been shown that TEER results are highly variable between users. As such, the standard TEER criteria for a polarized Caco-2 monolayer for my system was set to be a resistance of 45  $\Omega\text{cm}^2$  or greater.

In order to verify that TYR had in fact been transported across the membrane and not simply bound to the outer leaflet as has previously been suggested (Tejwani and Anderson, 2008), I performed subcellular fractionation of Caco-2 cells to identify the TYR subcellular distribution. I confirmed that TYR does not interact with the plasma membrane (Figure 3.1). The majority (> 97%) of the added radiolabelled TYR was associated with the ribosome+cytosolic compartment, with only very minor levels associated with the plasma membrane and/or mitochondrial fractions (Figure 3.1).

## **4.2 There are distinct TA transport processes across apical and basolateral Caco-2 membranes**

Both transporter and non-transporter mediated mechanisms for TA membrane passage have been suggested. Blakeley et al. (Blakeley and Nicol, 1978) reported that TYR (7.3  $\mu\text{M}$ ) was transported across rabbit erythrocyte membranes by simple diffusion. Similarly, Tcherkansky et al. showed that TYR (at 0.1 – 1 mM) was transported across isolated rat intestinal sacs and rat intestinal segments by simple diffusion (Tcherkansky et al., 1994). Such studies are generally consistent with more recent work showing that TYR and 2-PE can readily diffuse across synthetic lipid bilayers (Berry et al., 2013). Other studies, however, have reported facilitated transport of TA. 2-PE membrane passage at 0–15 - 200  $\mu\text{M}$  has been suggested to be via an uptake 2 transporter mediated process in rat isolated lung (Ben-Harari and Bakhle, 1980), at 10 nM via a  $\text{Na}^+$ -dependent facilitated transport system in rabbit erythrocyte preparations (Mason et al., 1983), and via a  $\text{H}^+$ -dependent active transport process at 1.1  $\mu\text{M}$  in Caco-2 cells (Fischer et al., 2010). In addition, neuronal release at 100 nM of TYR also has characteristics consistent with a non-exocytotic process mediated by OCT2 (Berry et al., 2016). Further, TYR was suggested to cross the blood-brain barrier in a  $\text{H}^+$  gradient dependent manner that was suggested to be one or more cationic drug-sensitive transport systems other than OCT (Akanuma et al., 2018). Together, the above studies suggest the involvement of simple diffusion, energy-dependent active transporters, and facilitated diffusion transporters in various cell preparations. Systematic examination of TA transport across human intestinal cells at physiological levels has not previously been reported. In my studies, I have identified distinct transport processes that control physiological levels of TYR and 2-PE passage across the Caco-2 apical and basolateral membranes, corresponding to transport from the intestinal lumen (apical) and circulatory system (basolateral) *in vivo*.

#### 4.2.1 TYR and 2-PE are transported by a diffusion-mediated process across the Caco-2 apical membrane

TYR can be converted via MAO-A/B to give *p*-hydroxyphenylacetic acid and by dopamine- $\beta$ -hydroxylase to give OA. Hence, TYR metabolic pathways were inhibited in all studies, thus ensuring that radioactivity levels were indeed a true reflection of TYR (or 2-PE), and not a metabolic by-product. When looking into the apical membrane transport, no difference was observed between the TYR concentration in the apical and cellular compartments with equimolar accumulations seen in both the compartments (Figure 3.2), suggesting a transporter-mediated diffusion TYR transport process across the Caco-2 apical membrane. Similarly, when looking at 2-PE transport, no difference was seen between 2-PE concentrations in apical and cellular compartments following apical addition of 2-PE with equimolar 2-PE concentrations seen in the two compartments (Figure 3.5). This similar characteristic of TYR and 2-PE transport pattern at the apical membrane, with the involvement of a similar transporter protein, can be expected since they are both endogenous agonists for the same receptor protein (TAAR1) and have strong structural similarity.

#### 4.2.2 The apical TYR transporter is OCT2 in Caco-2 cells

Previous work has reported that a transporter with the pharmacological characteristics of OCT2 acts as a high affinity ( $K_t = 101.5$  nM) TYR transporter in rat brain synaptosomes (Berry et al., 2016). OCT2 belongs to the solute carrier family of transporters and is generally regarded as a polyspecific, high capacity, low-selectivity, bi-directional, facilitated diffusion transporter (Nies et al., 2014). In addition to neurons, OCT2 is also highly expressed in the small intestine (Gorboulev et al., 1997; Bleasby et al., 2000; Martel et al., 2001; Hayer-Zillgen et al., 2002; Slitt et al., 2002; Nigam, 2018; Koepsell, 2020b). Since TA can be locally synthesized by cells of the gastrointestinal tract (Lauweryns and Van Ranst, 1988; Vieira-Coelho and Soares-da-Silva, 1993),

are abundant in commonly consumed foods (Coutts et al., 1986; Finberg and Gillman, 2011a; An et al., 2015a; Biji et al., 2016; Martin and Vij, 2016; Nalazek-Rudnicka and Wasik, 2017; Ohta et al., 2017; Liu et al., 2018b; Park et al., 2019; Zhang et al., 2019; Chen et al., 2022), and are readily produced from dietary amino acids by the constitutive intestinal microbiota (Bover-Cid et al., 2001; Gardini et al., 2001; Moreno-Arribas and Lonvaud-Funel, 2001; Connil et al., 2002; Lucas et al., 2003; Coton et al., 2004; Fernández et al., 2004; Marcobal et al., 2006; Williams et al., 2014; Bugda Gwilt et al., 2020), I sought to confirm if intestinal transport of TYR also involve OCT2. Unfortunately, validated, highly selective inhibitors of OCT2 have not been described. I therefore utilized the same combinatorial pharmacological approach to infer the involvement of OCT2 as described previously (Berry et al., 2016).

Decynium-22, an inhibitor of all hOCTs and PMAT (Engel et al., 2004; Engel and Wang, 2005; Gasser et al., 2006; Schömig et al., 2006; Xia et al., 2009; Duan and Wang, 2010; Hagan et al., 2011), decreased the concentration of TYR in the cellular compartment following apical addition (Figure 3.8B), confirming that either the hOCTs or PMAT are involved in transport of TYR into the cells from the apical compartment. Additionally, pentamidine, a dual inhibitor of both OCT1 and OCT2 (Jung et al., 2008), also decreased cellular accumulation of TYR (Figure 3.9 B and C), indicating the involvement of one of these facilitated diffusion transporters. Although both OCT1 (Zhang et al., 1997; Bleasby et al., 2000; Martel et al., 2001; Hayer-Zillgen et al., 2002) and OCT2 have previously been reported to be present in human gastrointestinal cells (Gorboulev et al., 1997; Bleasby et al., 2000; Martel et al., 2001; Hayer-Zillgen et al., 2002; Slitt et al., 2002; Koepsell, 2020b), on the basis of previous work which reported OCT2-mediated TYR transport in rat brain synaptosomes (Berry et al., 2016), I reasoned that OCT2 was the most likely candidate. To confirm this, I investigated the effects of ATR, a muscarinic antagonist which also

selectively inhibits the OCT1 isoform (Müller et al., 2005). In contrast to pentamidine, ATR did not affect TYR cellular accumulation following apical addition (Figure 3.10), suggesting that the apical TYR transporter in the Caco-2 membrane is OCT2. Differences were mostly observed in the cellular compartments in the presence and absence of inhibitors, and not in the apical and basolateral compartments due to the huge difference in volumes of the compartments.

I then sought to confirm the presence of OCT2 in Caco-2 cells through western blot studies. The calculated molar mass of OCT2 has been reported to be 66 kDa (Okuda et al., 1996). I observed an apparent OCT2 band present in Caco-2 cells at 62 kDa when the Elabscience<sup>®</sup> anti-SLC22A2 polyclonal primary antibody was used (Figure 3.11A). This was consistent with the positive control in rat kidney which also showed a prominent band at 62 kDa (Figure 3.11A). A 62 kDa band was not visible for rat intestine preparations, however, with bands observed at ~46 kDa, ~42 kDa, ~31 kDa and ~25 kDa. This may be indicative of tissue dependent expression of different isoforms of OCT2. I therefore tested a different primary antibody: Picoband<sup>™</sup> anti-SLC22A2 (Boster Biological Technology), to check if this antibody also showed similar a staining pattern as that of Elabscience<sup>®</sup> antibody. Following stripping and re-staining the same membrane as Figure 3.11A with the Boster antibody, a band at 62 kDa was only observed in rat kidney (Figure 3.11C) with a different predominant band identified at ~42 kDa for Caco-2 cells, while rat striatum and rat frontal cortex synaptosome showed predominant bands at ~28 kDa (Figure 3.11C). These banding patterns suggest that either there are tissue specific isoforms of OCT2 with large differences in apparent molar mass which has never been reported, or that there are major issues with the selectivity of commercial OCT2 antibodies.

To further investigate the specificities of the antibodies I repeated the above experiment but reversed the order of use of the two primary antibodies (Figure 3.12A). Generally, the same bands

were observed (c.f. Figures 3.11C and 3.12 A) in all tissues with the exception of rat striatum and rat frontal cortex synaptosome, where an extra band was seen at 80 kDa (Figure 3.12 A). Following stripping and reprobing with the Elabscience<sup>®</sup> antibody similar banding patterns was observed for rat striatum and frontal cortex synaptosome (Figure 3.12D) to those previously observed with the Elabscience antibody (Figure 3.11A), and no band was observed at 62 kDa in Caco-2 cells. In addition, additional bands were observed at ~49 kDa in Caco-2 cells, ~20 kDa in kidney and ~13-15 kDa in intestine (Figure 3.12 D). As such, my ability to conclusively confirm OCT2 presence was limited by the commercially available antibodies, and future knock-down studies would be required to further address this question.

Although I could not conclusively verify the presence of OCT2 in Caco-2 cells, the effects of pentamidine and ATR are strongly indicative that OCT2 transports TYR across Caco-2 apical membranes at nanomolar levels. This is consistent with previous observations in rat native neuronal membranes (Berry et al., 2016), although I cannot exclude the possibility that an unidentified facilitated diffusion transporter with the same pharmacological profile as OCT2 could be mediating the transport observed here. This is in contrast to the previous report of Fischer et al. (2010), who indicated no involvement of any of the OCT family in 2-PE (1.1  $\mu$ M) uptake, even though 2-PE transport was studied at supraphysiological levels.

#### 4.2.3 TYR and 2-PE are transported via an active transport process across the basolateral membrane

In marked contrast to apical addition, with basolateral TYR addition, there was clear evidence of active accumulation observed, with 5-10 fold higher TYR concentrations obtained in the cellular compartment than that added to the basolateral compartment (Figure 3.3). Furthermore, there was a greater than 5-fold larger trans-cellular passage of TYR following

basolateral addition than after apical addition (Figure 3.4). Active transport of TYR across gastrointestinal cell barriers has not been previously reported. With 2-PE transport, there was a trend towards significance observed between cellular and basolateral concentrations with basolateral addition (Figure 3.6). Additionally, significantly higher cellular 2-PE accumulation was observed in the basolateral to apical direction (Figure 3.7), suggesting similar active transport of 2-PE across the basolateral membrane was occurring. In this respect, it is worth noting that the 2-PE transport pattern was only monitored for five minutes and these initial time-points are associated with large error bars in the cellular concentration of 2-PE. In addition, there was no significant difference in TYR concentration observed in the first five minutes. It can therefore be suggested that 2-PE likely follows a similar pattern as TYR with respect to transport across the basolateral membrane of Caco-2 cells, being largely an active transporter-mediated event. Future work should confirm this by monitoring 2-PE transport for longer time-points as was performed for TYR transport.

#### 4.2.4 TYR active transport is Na<sup>+</sup>-dependent

Transmembrane Na<sup>+</sup> gradients are often used as an energy source for active transport of cellular metabolites (Alberts et al., 2002). On replacing Na<sup>+</sup> in the assay buffer with choline, there was a significant decrease in TYR accumulation in the cells following basolateral addition (Figure 3.16), indicating that the unknown active transporter is dependent on cellular Na<sup>+</sup> gradients. Interestingly, a similar Na<sup>+</sup>-dependent active transport of nanomolar TA levels (corresponding to physiological levels) has previously been reported in other membrane preparations. Mason et al. (1983) reported Na<sup>+</sup>-dependent uptake of 10 nM 2-PE in rabbit erythrocytes, while Ben-Harari and Bakhle (1980), identified Na<sup>+</sup>-dependent uptake of 2-PE (0.15–200 μM) in isolated rat lung. Surprisingly, ATR, being an OCT1 inhibitor, also decreased cellular TYR concentrations

following basolateral addition (Figure 3.15) suggesting that the Na<sup>+</sup>-dependent active TYR transporter is also ATR-sensitive. Kinetic characterization of the active transporter, assuming Michaelis Menten kinetics, indicated a K<sub>t</sub> value of 33.1 ± 47.4 nM and a V<sub>max</sub> of 43.0 ± 19.1 nM/second (Figure 3.18). On replacing Na<sup>+</sup> with choline for apical TYR loading, there was an increase in cellular TYR observed (Figure 3.17B) with a corresponding decrease in basolateral TYR (Figure 3.17C), suggesting that TYR passage from the cellular to basolateral compartment is Na<sup>+</sup>-dependent.

The physiological basis for a basolateral active TYR transporter is unknown. Although TAAR1 is present in neuroendocrine and enterochromaffin cells of the intestine in humans and rodents (Kidd et al., 2008; Ito et al., 2009; Revel et al., 2013; Raab et al., 2015), where it regulates secretion of hormones in response to nutrient sensing, this is unlikely to be the basis for a basolateral active transporter. Were the basis of an active transporter to be to provide nutrient-derived signals to TAAR1, one would expect the transporter to be located on the apical (luminal) side of the cell. Rather, I propose that the basolateral active TYR transporter may be indicative of a need to protect against excess TYR in the blood. Intestinal epithelial cells are known to contain abundant MAO (Vieira-Coelho et al., 1998), and as such active uptake of TYR from the blood into gastrointestinal epithelial cells may be for the purpose of metabolism. This may relate to the well-known ‘cheese effect’ seen in patients prescribed MAO inhibitors (Price and Smith, 1971; Stratton et al., 1991; Anderson et al., 1993; Shalaby, 1996; Finberg and Gillman, 2011), where excess TYR levels can lead to indirect sympathomimetic amplification of norepinephrine signals, which can in turn give rise to severe migraine, hypertensive crisis, and even death (Price and Smith, 1971; Stratton et al., 1991; Anderson et al., 1993; Shalaby, 1996; Finberg and Gillman, 2011b).

In addition, recent reports indicate TAAR1-mediated signalling in leukocytes suggesting the role of TAAR1 in the immune system (D'Andrea et al., 2003; Nelson et al., 2007; Wasik et al., 2012; Babusyte et al., 2013; Sriram et al., 2016; Christian and Berry, 2018; Fleischer et al., 2018; Barnes et al., 2021). Furthermore, TYR acts as a positive chemotactic agent for leukocytes (Babusyte et al., 2013) due to the presence of TAAR1 (Nelson et al., 2007; Wasik et al., 2012). TAAR1 activation has been suggested to promote T<sub>H</sub>-cell differentiation (Babusyte et al., 2013), resulting in decreased secretion of phosphoprotein 1 and increased interleukin 4 secretion. This suggests that TAAR1 promotes differentiation to the anti-inflammatory T<sub>H</sub>2 phenotype, which could also subsequently result in B cell activation. In addition, TYR has been shown to directly increase immunoglobulin E secretion from B cells (Babusyte et al., 2013). Furthermore, it has been reported recently that high levels of TYR, in addition to inducing prostaglandin E2 hypersecretion, can also disrupt the tight-junction protein distribution in gastrointestinal cells (Pretorius and Smith, 2022, 2023). Together, the available evidence suggests that TYR-induced activation of leukocyte TAAR1 can promote immune system activation. In such a situation, active uptake of TYR to limit local plasma concentrations would safeguard against inappropriate immune system activation that could be manifest as inflammatory disorders of the gastrointestinal tract. In this respect, TA and TAAR links to inflammatory bowel disease (Wilson et al., 2015; Nagao-Kitamoto et al., 2016; Kolho et al., 2017; Santoru et al., 2017; Christian and Berry, 2018; Yuan et al., 2018; Paley, 2019; Bugda Gwilt et al., 2020), Crohn's disease (ayur et al., 2016; Santoru et al., 2017; Christian and Berry, 2018; Bugda Gwilt et al., 2020), ulcerative colitis (Santoru et al., 2017; Christian and Berry, 2018; Gwilt et al., 2019), celiac disease (Di Cagno et al., 2011; De Angelis et al., 2016; Bugda Gwilt et al., 2020), and colorectal cancer (Goedert et al., 2014; Sinha et al., 2016; Bugda Gwilt et al., 2020) have all been reported. Furthermore, metabolomic studies have

further strengthened these suggested links (Jacobs et al., 2016; Kolho et al., 2017; Santoru et al., 2017; Yuan et al., 2018; Paley, 2019).

#### 4.3 TYR affinity column isolated proteins do not fit transporter selection criteria

To attempt to identify the Na<sup>+</sup>-dependent active transporter, I made use of the observation from my initial experiments that the transporter binds to both TYR and ATR (Figure 3.15 and 3.16) and designed TYR affinity columns by crosslinking TYR to an NHS-activated Sepharose stationary phase. After the crosslinking, the efficiency of the coupling was verified to make sure that adequate levels of TYR were bound to the NHS-activated Sepharose stationary column (Figure 2.8). As can be seen in Figure 4.1, TYR couples via nucleophilic attack at the ester linkage to form a stable amide linkage, via the amine group of TYR. Overlap of the NHS absorbance peak with TYR at 235 nm (Figure 2.6) would cause nonspecific absorbance measurements while measuring the absorbance for TYR to monitor the efficiency of the generated TYR affinity column.

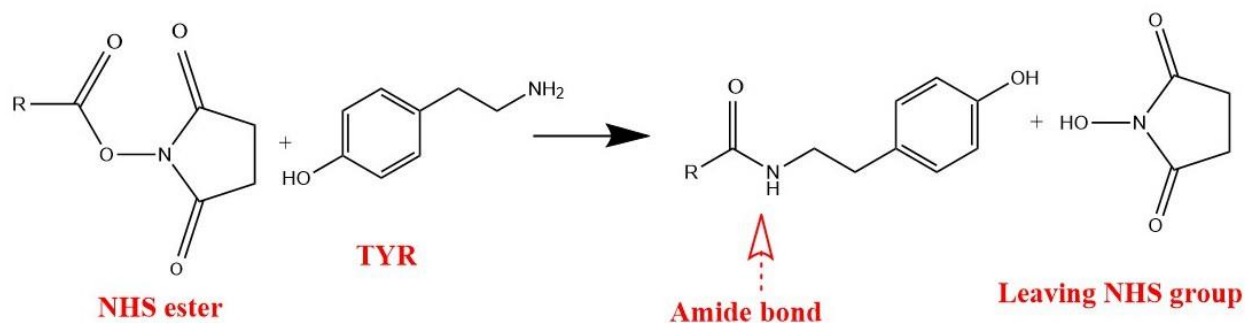


**Figure 4.1: Binding of TYR to NHS-activated Sepharose column.** TYR couples via nucleophilic attack at the NHS ester linkage to form a stable amide linkage with elimination of NHS from the NHS ester Sepharose column. The figure was generated in ChemDraw 22.0.0.

Addition of NaOH allowed TYR and NHS to be distinguished due to the auto-oxidation of TYR at basic pH, shifting its absorption maximum to 300 nm (Figure 2.7). A consistent 40% decrease

in absorption was seen compared to the input solution following the coupling reaction (Figure 2.8), which confirms that TYR was coupled to the column.

TYR binding proteins from Caco-2 cells were then isolated using the prepared affinity columns (Figure 3.20). From all the proteins identified, the target protein had to meet the selection criteria of being a membrane bound, active transporter protein, which was Na<sup>+</sup>-dependent, and ideally would be known to include TYR as a substrate. As shown in Table 3.1 and in appendix A, a total of 124 proteins were identified out of which twenty were membrane proteins, but only two were known transporters. The two transporter proteins identified were solute carrier family 2-facilitated glucose membrane transporter 14 (*Slc2A14*), and cadherin-17 (Table 3.1). *Slc2A14* is a hexose transporter that is involved in transporting glucose and dehydroascorbate across membranes, and is known to be expressed in the small intestine, colon, lung, brain, liver, heart, skeletal muscle, blood, placenta, kidney and testis (Wu and Freeze, 2002; Shaghaghi et al., 2017; Alexander et al., 2021; Liu, 2022). This transporter is not, however, an active transporter, and is not dependent on the Na<sup>+</sup> gradient (Wu and Freeze, 2002; Shaghaghi et al., 2017; Alexander et al., 2021; Liu, 2022). Cadherin 17 is a calcium-dependent cell adhesion protein also known as Human Peptide Transporter-1. It is expressed throughout the intestine and pancreatic ducts and is involved in intestinal peptide transport (Dantzig et al., 1994; Yang et al., 1999; Landowski et al., 2003). This transporter is an active transporter, but it is dependent on an inwardly-coupled proton gradient and not on the Na<sup>+</sup> gradient. As such, neither transporter fit the selection criteria, and were therefore not considered further.

The lack of identified transporters meeting selection criteria likely relates to the TYR coupling taking place by linkage via the amine group of TYR, with the amine moiety of TYR likely necessary for binding to target proteins such as the active transporter. In this respect, other

known TYR binding proteins such as OCT1 (Iseki et al., 1993; Breidert et al., 1998a; Gebauer et al., 2021), OCT2 (Breidert et al., 1998; Schömig et al., 2006; Gozal et al., 2014; Berry et al., 2016; Gebauer et al., 2021), OCT3 (Gozal et al., 2014; Berry et al., 2016; Gebauer et al., 2021) and MAO-A/B (Vieira-Coelho et al., 1998) that have been shown to be present in Caco-2 cells (Bleasby et al., 2000; Martel et al., 2001; Maubon et al., 2007; Horie et al., 2011) were also not among the proteins isolated from TYR-affinity columns. Future work should design alternate TYR affinity columns where linkage is via a different part of the structure of TYR, such as the phenolic group, or by attaching a linker arm to the  $\beta$ -carbon of TYR. In this respect, possible  $\text{Na}^+$ -dependent active transporters that can be investigated include uptake 1 transporters that are typified by DAT, NET and SERT, which include TYR in their substrate profile (Raiteri et al., 1977; Danek Burgess and Justice, 1999; Liang et al., 2009).

#### **4.4 Modelling of TYR transport predicts the presence of additional TYR transporters**

In intestinal cells, other TYR transport processes could exist but be masked by the active accumulation of TYR across the basolateral Caco-2 membrane. To study this, I developed a computational model based on the known kinetics of identified TYR transport processes. On modelling TYR transport across Caco-2 cells with identified transporter kinetics, experimental concentration-time relationships could not be replicated for either basolateral or apical TYR loading (Figures 3.21 and 3.22). This suggested that the presence of one or more additional TYR transporters was required. Even though the baseline model did not recapitulate experimental observations, basolateral loading was modelled considerably more poorly than the apical addition hence the additional transporter was proposed to be present in the basolateral membrane. Further, such an additional transporter is most likely a facilitated diffusion transporter since there was already an active transporter in place for TYR in the basolateral membrane, and it would be

irrational to have a second active transporter with the identical molecule in the same membrane. Since OCT2 was already known to be expressed in Caco-2 cells (Horie et al., 2011) and from my pharmacological characterization (Figure 3.9 and 3.10) and western blot results (Figure 3.11 and 3.12), I first investigated whether also adding OCT2 to the basolateral membrane would improve the model (Figure 2.10). Even when the density of the added basolateral membrane OCT2 was allowed to vary experimental TYR concentration-time relationships could not be recreated (Figures 3.23 and 3.24), suggesting that the needed additional, basolateral facilitated diffusion transporter is not OCT2.

I therefore systematically varied both the  $V_{\max}$  and  $K_t$  values for the added basolateral membrane transporter to model a facilitated diffusion transporter with non-OCT2 kinetics. Marked improvement in modelling accuracy was observed for TYR basolateral addition when  $V_{\max} = 55$  nM/second and  $K_t = 203-507.5$  nM (Figure 3.25). In contrast, modelling of apical loading worsened (Figure 3.26) under these same conditions. Since improvement of transcellular passage modelling in one direction came at the expense of worsening of model accuracy in the other direction, I hypothesized that either asymmetry (directional preference of transport) was needed in one or more of the facilitated diffusion transporters, or that compartmentalization of TYR within the cell was occurring at the high cellular concentrations seen following basolateral loading.

Asymmetry was introduced by allowing the  $K_t$  to vary in each direction of transport for both of the facilitated diffusion transporters, OCT2 in the apical membrane and the added unidentified basolateral membrane facilitated diffusion transporter, while keeping the  $V_{\max}$  constant, and allowing the kinetic parameters to be solved for by the model (Table 3.2). Introduction of asymmetry allowed for recapitulation of experimental results in all compartments for both basolateral-to-apical and apical-to-basolateral TYR transport when an approximate 10-fold

preference of OCT2 for transporting TYR into the cell from the apical compartment was present (Figures 3.27 and 3.28). Under these conditions no physiologically meaningful directional preference was required for the basolateral membrane facilitated diffusion transporter. In particular, this also successfully modelled the marginally higher  $X_{\text{cell}}$  compared to  $X_{\text{apical}}$  that was seen experimentally following apical loading (Figure 3.28). Interestingly, asymmetric bidirectional facilitated diffusion transporters have previously been described with respect to amino acid transport across the blood brain barrier (Zaragozá, 2020), although I am unaware of any previous reports of directionality exhibited by OCT2. Such directionality may reflect known differences in pH between the intestinal lumen and cytosolic compartments *in vivo*, with typical luminal (apical) pH ranging from 6.0 - 6.5 while the cytosolic space has a pH of 7.4 (Abrahamse et al., 1992; Thwaites et al., 1999; Neuhoff et al., 2005). As shown below (Equations 38 – 41), under such conditions, assuming a pKa for TYR of 10.9 (Holland et al., 2015), using the Hendersen-Hasselbach equation predicts a close to 10-fold difference in the TYR ionization state.

In the luminal space:

$$6.5 = 10.9 + \log \left\{ \frac{A^-}{[HA]} \right\} \quad \text{(Equation 38)}$$

$$\frac{A^-}{[HA]} = 0.000039 \quad \text{(Equation 39)}$$

While in the cytosolic compartment with a pH of 7.4:

$$7.4 = 10.9 + \log \left\{ \frac{A^-}{[HA]} \right\} \quad \text{(Equation 40)}$$

$$\frac{A^-}{[HA]} = 0.00032 \quad \text{(Equation 41)}$$

This matches nicely with the 10-fold directional preference and would be seen as a 10-fold increase in protonated TYR in the luminal space compared to the cytosol, suggesting that OCT2 preferentially binds, and therefore transports, the protonated (positively charged) form of TYR.

As a possible alternative to asymmetry of TYR transport by OCT2, I also examined whether the introduction of intracellular compartmentalization of TYR could recapitulate experimental concentration-time relationships. Intracellular localization of TAAR1 has already been established in various cell types and tissues (Bunzow et al., 2001; Lindemann et al., 2005; Miller et al., 2005; Barak et al., 2008; Miller, 2011; Revel et al., 2013; Raab et al., 2015; Pei et al., 2016; Espinoza et al., 2018; Pitts et al., 2019; Barnes et al., 2021; Qatato et al., 2021). In particular, endoplasmic reticulum and golgi apparatus (Barak et al., 2008; Raab et al., 2015; Qatato et al., 2021), secretory vesicle (Espinoza et al., 2018), nuclear (Pitts et al., 2019; Barnes et al., 2021) and unspecified intracellular membrane (Miller et al., 2005; Miller, 2011) TAAR1 localizations have been suggested. Thus, physiologically, accumulation of TYR in one or more of these compartments could be a requirement for TAAR1 binding to occur. As can be seen from my subcellular fractionation study (Figure 3.1), 97.7% of TYR was associated to the ribosomal and cytosolic fractions, making these fractions the potential compartments for TYR sequestration. Initially, a compartmentalization factor, 'z', where 'z' represents the fraction of intracellular TYR available for crossing basolateral and apical membranes, was introduced. A value of  $z = 0.36$ , indicating 64% of TYR was sequestered into one or more subcellular compartment(s), gave the best match to experimental results (Figure 3.29 and 3.30). With 64% of TYR sequestered into a compartment comprising 10% of the cellular volume, this further suggested such a compartment would require an active transporter to accumulate the TYR. Further, the compartmentalization modelling appeared to provide a better fit for basolateral, compared to apical, loading, suggesting that a

compartment transporter would primarily only be active at the higher intracellular concentrations seen following basolateral loading. Although this modelling closely matched experimental results for some compartments (Figures 3.29 and 3.30), it was less robust than that obtained with asymmetric transport (Figures 3.27 and 3.28). This was consistent with intracellular compartmentalization being associated with 2 - 4 fold higher RMSD values in two of the three compartments, suggesting that asymmetric transport was more likely than compartmentalization. Further, while modelling of the required kinetic parameters for a subcellular compartment(s) indicated a potentially physiologically relevant  $K_t$  value (154.5 nM), consistent with activity primarily at the higher concentrations seen following basolateral transport, the required  $V_{max}$  ( $5.2 \times 10^{-21}$  nM/second) is equivalent to a mere 86 molecules per second per cell transported, indicating an unrealistically low density of transporter to be of physiological relevance. Together, the above studies indicate the need for asymmetry in OCT2-mediated TYR transport, resulting in unequal bidirectional TYR transport across the apical membrane of Caco-2 cells, which may reflect the pH differences between the intestinal lumen and epithelial cell cytosol.

**Table 4.1: Required kinetic parameters to recapitulate experimental TYR transport.**

<b>Parameter</b>	<b>Predicted kinetics from model</b>	<b>Experimentally determined kinetics</b>
$V_{\max\_OCT2}$	2.3 nM/second	0.1 nM/second
$K_t\_OCT2\_apicalto\text{cell}$	110.4 nM	101.5 nM
$K_t\_OCT2\_cellto\text{apical}$	1227.9 nM	n/a
$V_{\max\_baso\_active}$	3.3 nM/second	43.0 nM/second
$K_t\_baso\_active$	29.0 nM	33.1 nM
$V_{\max\_baso\_new\_FD}$	6.0 nM/second	n/a
$K_t\_baso\_new\_FD\_baso\text{cell}$	628.3 nM	n/a
$K_t\_new\_FD\_cellto\text{baso}$	628.3 nM	n/a

This table was adapted from Sarkar et al., 2022. n/a refers to not applicable.

In summary, overall kinetic parameters that recapitulate experimental observations were obtained for OCT2, the Na<sup>+</sup>-dependent basolateral active transporter, and the unknown new basolateral facilitated diffusion transporter (Table 4.1). The  $V_{\max}$  and  $K_t$  values for TYR uptake into the cell via OCT2 are similar to what was reported from previously determined experimental kinetic studies in rat brain synaptosomes (Berry et al., 2016). The  $K_t$  appears to be a closer match than  $V_{\max}$  since TYR uptake is by the same transporter (OCT2) in both tissues, but OCT2 could be present at different densities in both the tissues. Differences between human and rodent OCTs regarding their substrate selectivity have been described (Koepsell et al., 2007; Samodelov et al., 2020) and this should also be considered when comparing the current results to those previously reported in rat brain synaptosomes. Asymmetry in OCT2, however, was not investigated and reported in previous studies for OCT2 (Berry et al., 2016) and has been reported here for the first

time. This suggests that the previously observed TYR transport by neuronal OCT2 should be re-examined with respect to unequal bi-directionality. Further, the possible presence of active transport should also be examined in neuronal preparations. For the Na<sup>+</sup>-dependent active transporter, even though the K<sub>t</sub> obtained through modelling is in good agreement with that experimentally determined (Table 4.1), the modelled V<sub>max</sub> was found to be 10-fold lower than that experimentally determined.

The current modelling also suggests the need for additional, low-affinity, basolateral membrane-facilitated diffusion transporters. Combined with my observation that there is an active accumulation of TYR within the cells following basolateral addition (Figure 3.3), and the observed high K<sub>t</sub> of the basolateral membrane facilitated diffusion transporter (628.3 nM), I propose that this is not a selective TYR transporter but rather a transporter that non-selectively includes TYR in its substrate spectrum at the high intracellular concentrations seen due to active transport. With respect to the identity of such a transporter, modelling provides limited details. TYR is a substrate for OCT3 with a reported K<sub>t</sub> of approximately 280 nM (Chen et al., 2010), not too dissimilar from my modelled K<sub>t</sub> of approximately 600 nM. In the current studies, there is considerable uncertainty in the estimation of the rates of change of intracellular TYR, and consequently in the deduced kinetics, due to the high variability of measured intracellular TYR concentrations because of the very small volume of the cellular compartment. OCT3 has been reported to be expressed in the small intestine (Shirasaka et al., 2016; Dawed et al., 2019), making it a good potential initial candidate for the additional basolateral TYR facilitated diffusion transporter. In addition, the facilitated diffusion transporter *Slc2A14* that was identified through my protein purification study (Table 3.1 and appendix A), with expression reported in the intestine (Shaghghi et al., 2017), can also be considered as a possible candidate for this transporter. More confident identification of

candidate transporters will, however, require further studies to identify the TYR binding proteins present in Caco-2 cell preparations.

Such a transporter could become important pathologically during compromised TYR metabolism, such as following treatment with MAO inhibitors, where it would provide a channel for elevated dietary TYR to enter the bloodstream. Such excess levels of TYR are known to cause indirect sympathomimetic effects leading to severe hypertensive crisis, and in extreme situations, death (Price and Smith, 1971; Stratton et al., 1991; Anderson et al., 1993; Shalaby, 1996; Finberg and Gillman, 2011). Further, elevated blood TYR could lead to pathological immune responses, acting as a positive chemotactic agent for leukocytes, promoting pro-inflammatory differentiation, and increasing immunoglobulin E secretion from B cells (Babusyte et al., 2013). Such a situation may also suggest the TAAR system as a novel therapeutic target for food- induced intestinal inflammation and gastrointestinal disorders in susceptible individuals, and is consistent with recent reports linking TA and TAAR to such conditions (Di Cagno et al., 2011; Goedert et al., 2014; Wilson et al., 2015; De Angelis et al., 2016; Jacobs et al., 2016; Nagao-Kitamoto et al., 2016; Sinha et al., 2016; Kolho et al., 2017; Santoru et al., 2017; Christian and Berry, 2018; Yuan et al., 2018; Gwilt et al., 2019; Paley, 2019; Bugda Gwilt et al., 2020; Pretorius and Smith, 2022, 2023).

The results from the studies reported here are likely to be generally relevant to other cell types beyond Caco-2 cells. The lung epithelia, brain, hepatocytes, kidney, and heart are known to express facilitated diffusion transporters such as OCT2 and 3 (Wu et al., 2000b; Lips et al., 2012) and PMAT (Wang, 2016), and in and at least some of these tissues are also known to express TAAR1 (Borowsky et al., 2001; Lindemann et al., 2005; Revel et al., 2013; Cisneros and Ghorpade, 2014; Fleischer et al., 2018). In particular, cells associated with barrier functions such as the blood-brain-barrier and fetal-placental barrier express a broad range of broad-spectrum

transporters and as such identifying those that regulate endogenous TAAR1 agonist passage across these membranes may be an avenue to novel therapeutic options.

#### **4.5 Conclusions**

I have established for the first time that there are different TYR transport processes present in the apical and basolateral membranes of Caco-2 cells (Figure 4.2). Across the apical membrane, TYR transport takes place by an OCT2-like facilitated diffusion transporter. In contrast, across the basolateral membrane, a Na<sup>+</sup>-dependent active transport process for TYR is present, that is also sensitive to ATR. The same trends were also observed for 2-PE. Through computer simulations, I have been able to establish that experimental TYR transport characteristics can only be modelled with the presence of an additional basolateral membrane TYR facilitated diffusion transporter and asymmetry in OCT2-mediated apical TYR transport. Intracellular TYR compartmentalization was unable to replace the need for asymmetry of TYR transport at the apical membrane. Although TYR-affinity columns allowed identification of 124 putative TYR binding-proteins, two of the proteins were known transporters, with only one of them being an active transporter. This active transporter was, however, not a Na<sup>+</sup>-dependent transporter. More work is needed in order to design alternate TYR affinity columns in order to identify the novel transporters reported here. These transporters may provide targets through which TA function can be regulated therapeutically and provide an additional molecular basis for how the constitutive intestinal microbiota can affect human health through host-diet-microbiota interactions.

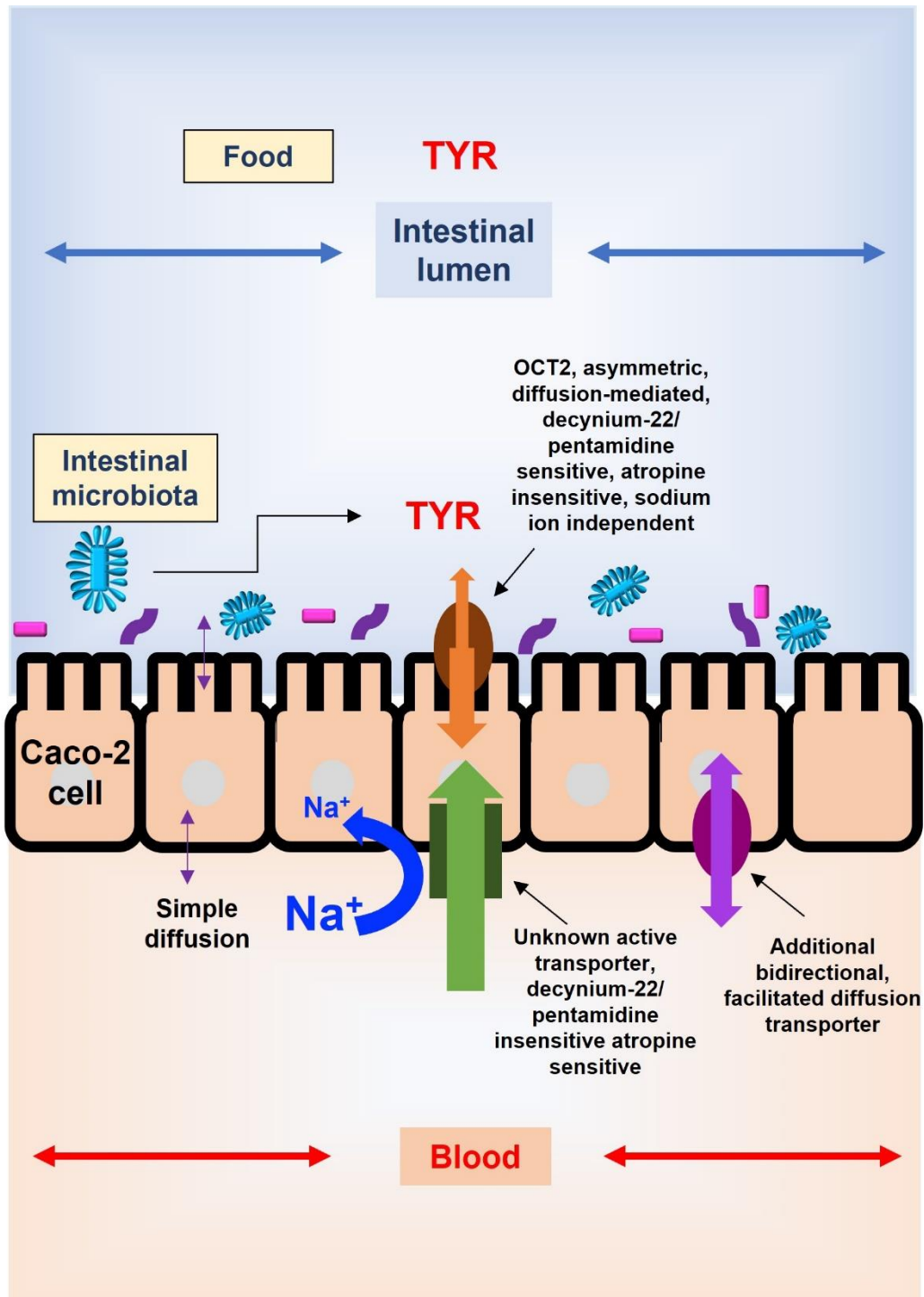


**Figure 4.2: Proposed TYR transport mechanisms across Caco-2 cells.** TYR is transported across the apical membrane of Caco-2 cell by OCT2 and simple diffusion. TYR is transported across the basolateral membrane by a Na<sup>+</sup>-dependent active transporter, an additional, as yet unidentified, bidirectional, facilitated diffusion transporter, and via simple diffusion. This figure was generated in MS PowerPoint.

#### 4.6 Limitations and future directions

1. The Caco-2 cell line is derived from an adenocarcinoma and has been shown to exhibit altered expression of efflux transporters (Darling et al., 2020) compared to the *in vivo* tissues. The presence of other proteins and enzymes *in vivo* may result in differences in the regulation of TA transport across the intestinal membrane than those seen here. In addition, the Caco-2 monolayer system lacks the complex, multicellular environments that are normally seen in *in vivo* tissues. Further, the Caco-2 cell model does not provide a representation of transport of TA across the vascular endothelial layer before reaching the blood, which should be investigated through further *in vivo* studies. Additionally, the Transwell<sup>®</sup> system is also limited to representing transport of TA across Caco-2 epithelial cells and does not represent transport across the endothelium to reach the blood. Future studies can also address this by culturing epithelial and endothelial cell types across the two sides of the Transwell<sup>®</sup>.
2. 2-PE transport properties require systematic examination over extended timeframes to confirm similarity (or difference) to TYR.
3. Commercially available OCT2 antibodies appear to have poor selectivity in western blot studies which makes validation of OCT2-mediated TYR transport difficult. OCT2 knockdown studies are required to validate the role of OCT2 in TYR transport.
4. The current modelling was performed initially with kinetic parameters of OCT2 determined in a different cell and species type. There have been differences reported in human and rodent OCTs regarding their substrate selectivity (Tahara et al., 2005; Koepsell et al., 2007; Samodelov et al., 2020; Kuehne et al., 2022). Verification of the kinetic parameters of TYR transport via OCT2 in Caco-2 cells is warranted.

5. The characterization of complex TYR transport properties with the presence of OCT2 in the Caco-2 apical membrane with asymmetric characteristics, Na<sup>+</sup>-dependent active transporter in the Caco-2 basolateral membrane, and an additional facilitated diffusion transporter in the Caco-2 cell, suggests that previously described transport in synaptosomes should be re-examined.
6. Designing alternate affinity columns to isolate TYR binding proteins by using a different part of the structure of TYR than the amine moiety is required. This can identify potential TYR transporters for future systematic study.
7. The high variability of TYR concentration in cells causes some inherent uncertainty in conclusions.

## 5. REFERENCES

- Adriaenssens, A., Lam, B. Y. H., Billing, L., Skeffington, K., Sewing, S., Reimann, F., et al. (2015). A transcriptome-led exploration of molecular mechanisms regulating somatostatin-producing D-cells in the gastric epithelium. *Endocrinology* 156, 3924–3936. doi: 10.1210/en.2015-1301.
- Aggarwal, S., Mortensen, O. V. (2017). Overview of monoamine transporters. *Curr Protoc Pharmacol* 79, 12.16.1-12.16.17. doi: 10.1002/cpph.32.
- Agista, A. Z., Tanuseputero, S. A., Koseki, T., Ardiansyah, Budijanto, S., Sultana, H., et al. (2022). Tryptamine, a microbial metabolite in fermented rice bran suppressed lipopolysaccharide-induced inflammation in a murine macrophage model. *Int J Mol Sci* 23, 11209. doi: 10.3390/ijms231911209.
- Akanuma, S. I., Yamazaki, Y., Kubo, Y., and Hosoya, K. I. (2018). Role of cationic drug-sensitive transport systems at the blood-cerebrospinal fluid barrier in para-tyramine elimination from rat brain. *Fluids Barriers CNS* 15, 1. doi: 10.1186/S12987-017-0087-9.
- Alberts, B., Johnson, A., Lewis, J., Raff, M., Roberts, K., and Walter, P. (2002). Carrier proteins and active membrane transport. *Mol Biol Cell*, New York.
- Alexander, J. L., Wilson, I. D., Teare, J., Marchesi, J. R., Nicholson, J. K., and Kinross, J. M. (2017). Gut microbiota modulation of chemotherapy efficacy and toxicity. *Nat Rev Gastroenterol Hepatol* 14, 356–365. doi: 10.1038/nrgastro.2017.20.

- Alexander, S. P. H., Kelly, E., Mathie, A., Peters, J. A., Veale, E. L., Armstrong, J. F., et al. (2021). The concise guide to Pharmacology 2021/22: Transporters. *Br J Pharmacol* 178, S412–S513. doi: 10.1111/bph.15543.
- Alnefeesi, Y., Tamura, J. K., Lui, L. M. W., Jawad, M. Y., Ceban, F., Ling, S., et al. (2021). Trace amine-associated receptor 1 (TAAR1): Potential application in mood disorders: A systematic review. *Neurosci Biobehav Rev* 131, 192–210. doi: 10.1016/j.neubiorev.2021.09.020.
- Altay, G., Larrañaga, E., Tosi, S., Barriga, F. M., Batlle, E., Fernández-Majada, V., et al. (2019). Self-organized intestinal epithelial monolayers in crypt and villus-like domains show effective barrier function. *Sci Rep* 9, 1–14. doi: 10.1038/s41598-019-46497-x.
- An, D., Chen, Z., Zheng, J., Chen, S., Wang, L., Huang, Z., et al. (2015). Determination of biogenic amines in oysters by capillary electrophoresis coupled with electrochemiluminescence. *Food Chem* 168, 1–6. doi: 10.1016/j.foodchem.2014.07.019.
- Anderson, M. C., Hasan, F., McCrodden, J. M., and Tipton, K. F. (1993). Monoamine oxidase inhibitors and the cheese effect. *Neurochem Res* 18, 1145–1149. doi: 10.1007/bf00978365/metrics.
- Ando-yamamoto, M., Hayashi, H., Sugiyama, T., Fukui, H., Watanabe, T., and Wada, H. (1987). Purification of L-dopa decarboxylase from rat liver and production of polyclonal and monoclonal antibodies against it. *J Biochem* 101, 405–414. doi: 10.1093/oxfordjournals.jbchem.a121925.

- Anton, S., Dufour, M. C., and Gadenne, C. (2007). Plasticity of olfactory-guided behaviour and its neurobiological basis: lessons from moths and locusts. *Entomol Exp Appl* 123, 1–11. doi: 10.1111/j.1570-7458.2007.00516.x.
- Aperia, A., Hokfelt, T., Meister, B., Bertorello, A., Fryckstedt, J., Holtback, U., et al. (1990). The significance of L-amino acid decarboxylase and DARPP-32 in the kidney. *Am J Hypertens* 3, 11S-13S. doi: 10.1093/ajh/3.6.11s.
- Artursson, P., and Karlsson, J. (1991). Correlation between oral drug absorption in humans and apparent drug permeability coefficients in human intestinal epithelial (Caco-2) cells. *Biochem Biophys Res Commun* 175, 880–885. doi: 10.1016/0006-291x(91)91647-u.
- Babusyte, A., Kotthoff, M., Fiedler, J., and Krautwurst, D. (2013). Biogenic amines activate blood leukocytes via trace amine-associated receptors TAAR1 and TAAR2. *J Leukoc Biol* 93, 387–394. doi: 10.1189/jlb.0912433.
- Bacq, A., Balasse, L., Biala, G., Guiard, B., Gardier, A. M., Schinkel, A., et al. (2012). Organic cation transporter 2 controls brain norepinephrine and serotonin clearance and antidepressant response. *Mol Psychiatry* 17, 926–939. doi: 10.1038/mp.2011.87.
- Baker, G. B., Bornstein, R. A., Rouget, A. C., Ashton, S. E., van Muyden, J. C., and Coutts, R. T. (1991). Phenylethylaminergic mechanisms in attention-deficit disorder. *Biol Psychiatry* 29, 15–22. doi: 10.1016/0006-3223(91)90207-3.
- Baker, G. B., Raiteri, M., Bertollini, A., Carmine, R. del, Keane, P. E., and Martin, I. L. (2011). Interaction of  $\beta$ -phenethylamine with dopamine and noradrenaline in the central nervous system of the rat. *J Pharm Pharmacol* 28, 456–457. doi: 10.1111/j.2042-7158.1976.tb04658.x.

- Barak, L. S., Salahpour, A., Zhang, X., Masri, B., Sotnikova, T. D., Ramsey, A. J., et al. (2008). Pharmacological characterization of membrane-expressed human trace amine-associated receptor 1 (TAAR1) by a bioluminescence resonance energy transfer cAMP biosensor. *Mol Pharmacol* 74, 585–594. doi: 10.1124/mol.108.048884.
- Barbieri, F., Montanari, C., Gardini, F., and Tabanelli, G. (2019). Biogenic amine production by lactic acid bacteria: a review. *Foods* 8, 17. doi: 10.3390/foods8010017.
- Barnes, D. A., Galloway, D. A., Hoener, M. C., Berry, M. D., and Moore, C. S. (2021). TAAR1 expression in human macrophages and brain tissue: A potential novel facet of MS neuroinflammation. *Int J Mol Sci* 22, 11576. doi: 10.3390/ijms222111576/s1.
- Barnes, D. A., Hoener, M. C., Moore, C. S., and Berry, M. D. (2022). TAAR1 regulates purinergic-induced TNF secretion from peripheral, but not CNS-resident, macrophages. *J Neuroimmune Pharmacol*, 1–12. doi: 10.1007/s11481-022-10053-8/metrics.
- Batista-Lima, F. J., Rodrigues, F. M. dos S., Gadelha, K. K. L., Oliveira, D. M. N. de, Carvalho, E. F., Oliveira, T. L., et al. (2019). Dual excitatory and smooth muscle-relaxant effect of  $\beta$ -phenylethylamine on gastric fundus strips in rats. *Clin Exp Pharmacol Physiol* 46, 40–47. doi: 10.1111/1440-1681.13033.
- Beaulieu, J. M., Gainetdinov, R. R., and Caron, M. G. (2009). Akt/GSK3 signaling in the action of psychotropic drugs. *Annu Rev Pharmacol Toxicol* 49, 327–347. doi: 10.1146/annurev.pharmtox.011008.145634.
- Begni, V., Sanson, A., Luoni, A., Sensini, F., Grayson, B., Munni, S., et al. (2021). Towards novel treatments for schizophrenia: molecular and behavioural signatures of the psychotropic agent SEP-363856. *Int J Mol Sci* 22, 4119. doi: 10.3390/ijms22084119.

- Ben-Harari, R. R., and Bakhle, Y. S. (1980). Uptake of beta-phenylethylamine in rat isolated lung. *Biochem Pharmacol* 29, 489–494. doi: 10.1016/0006-2952(80)90367-6.
- Berry, M. D. (2004). Mammalian central nervous system trace amines. Pharmacologic amphetamines, physiologic neuromodulators. *J Neurochem* 90, 257–271. doi: 10.1111/j.1471-4159.2004.02501.x.
- Berry, M. D., Gainetdinov, R. R., Hoener, M. C., and Shahid, M. (2017). Pharmacology of human trace amine-associated receptors: Therapeutic opportunities and challenges. *Pharmacol Ther* 180, 161–180. doi: 10.1016/j.pharmthera.2017.07.002.
- Berry, M. D., Hart, S., Pryor, A. R., Hunter, S., and Gardiner, D. (2016). Pharmacological characterization of a high-affinity *p*-tyramine transporter in rat brain synaptosomes. *Sci Rep* 6, 38006. doi: 10.1038/srep38006.
- Berry, M. D., Shitut, M. R., Almousa, A., Alcorn, J., and Tomberli, B. (2013). Membrane permeability of trace amines: Evidence for a regulated, activity-dependent, nonexocytotic, synaptic release. *Synapse* 67, 656–667. doi: 10.1002/syn.21670.
- Biji, K. B., Ravishankar, C. N., Venkateswarlu, R., Mohan, C. O., and Gopal, T. K. S. (2016). Biogenic amines in seafood: a review. *J Food Sci Technol* 53, 2210–2218. doi: 10.1007/s13197-016-2224-x.
- Black, S. W., Schwartz, M. D., Chen, T. M., Hoener, M. C., and Kilduff, T. S. (2017). TAAR1 Agonists as Narcolepsy Therapeutics. *Biol Psychiatry* 82, 623. doi: 10.1016/j.biopsych.2016.10.012.

- Blakeley, A. G., and Nicol, C. J. (1978). Accumulation of amines by rabbit erythrocytes in vitro. *J Physiol* 277, 77. doi: 10.1113/jphysiol.1978.sp012261.
- Bleasby, K., Chauhan, S., and Brown, C. D. A. (2000). Characterization of MPP<sup>+</sup> secretion across human intestinal Caco-2 cell monolayers: role of P-glycoprotein and a novel Na<sup>+</sup>-dependent organic cation transport mechanism. *Br J Pharmacol* 129, 619. doi: 10.1038/sj.bjp.0703078.
- Bly, M. (2005). Examination of the trace amine-associated receptor 2 (TAAR2). *Schizophr Res* 80, 367–368. doi: 10.1016/j.schres.2005.06.003.
- Boenisch, H. (1980). Extraneuronal Transport of Catecholamines. *Pharmacology* 21, 93–108. doi: 10.1159/000137422.
- Bönisch, H., Bryan, L. J., Henseling, M., O'Donnell, S. R., Stockmann, P., and Trendelenburg, U. (1985). The effect of various ions on uptake<sub>2</sub> of catecholamines. *Naunyn Schmiedebergs Arch Pharmacol* 328, 407–416. doi: 10.1007/BF00692909/metrics.
- Bonner, T. I., Davenport, A. P., Foord, S. M., Maguire, J. J., and Parker, W. A. E. (2019). Trace amine receptor. *IUPHAR/BPS Guide to Pharmacology*, 2019, 4. doi: 10.2218/gtopdb/f64/2019.4.
- Borison, R. L., Mosnaim, A. D., and Sabelli, H. C. (1975). Brain 2-phenylethylamine as a major mediator for the central actions of amphetamine and methylphenidate. *Life Sci* 17, 1331–1343. doi: 10.1016/0024-3205(75)90147-2.

- Borowsky, B., Adham, N., Jones, K. A., Raddatz, R., Artymyshyn, R., Ogozalek, K. L., et al. (2001). Trace amines: Identification of a family of mammalian G protein-coupled receptors. *Proc Natl Acad Sci U S A* 98, 8966–8971. doi: 10.1073/pnas.151105198.
- Bottalico, B., Larsson, I., Brodzski, J., Hernandez-Andrade, E., Casslén, B., Marsál, K., et al. (2004). Norepinephrine Transporter (NET), Serotonin Transporter (SERT), Vesicular Monoamine Transporter (VMAT2) and Organic Cation Transporters (OCT1, 2 and EMT) in human placenta from pre-eclamptic and normotensive pregnancies. *Placenta* 25, 518–529. doi: 10.1016/j.placenta.2003.10.017.
- Bouchard, S., and Roberge, A. G. (1979). Biochemical properties and kinetic parameters of dihydroxyphenylalanine--5-hydroxytryptophan decarboxylase in brain, liver, and adrenals of cat. *Can J Biochem* 57, 1014–1018. doi: 10.1139/O79-126.
- Boulton, A. A. (1976). Identification, distribution, metabolism, and function of *meta* and *para* tyramine, phenylethylamine and tryptamine in brain. *Adv Biochem Psychopharmacol* 15, 57–67. PMID: 799463.
- Boulton, A. A., and Wu, P. H. (1972). Biosynthesis of cerebral phenolic amines. I. *In vivo* formation of *p*-tyramine, octopamine, and synephrine. *Can J Biochem* 50, 261–267. doi: 10.1139/o72-037.
- Boulton, A. A., and Wu, P. H. (1973). Biosynthesis of cerebral phenolic amines. II. *In vivo* regional formation of *p*-tyramine and octopamine from tyrosine and dopamine. *Can J Biochem* 51, 428–435. doi: 10.1139/o73-050.

- Bover-Cid, S., Izquierdo-Pulido, M., and Carmen Vidal-Carou, M. (2001). Changes in biogenic amine and polyamine contents in slightly fermented sausages manufactured with and without sugar. *Meat Sci* 57, 215–221. doi: 10.1016/s0309-1740(00)00096-6.
- Bradaia, A., Trube, G., Stalder, H., Norcross, R. D., Ozmen, L., Wettstein, J. G., et al. (2009). The selective antagonist EPPTB reveals TAAR1-mediated regulatory mechanisms in dopaminergic neurons of the mesolimbic system. *Proc Natl Acad Sci USA* 106, 20081–20086. doi: 10.1073/pnas.0906522106.
- Brahmachary, R. L., and Dutta, J. (1979). Phenylethylamine as a biochemical marker of tiger. *Z Naturforsch C Biosci* 34, 632–633. doi: 10.1515/znc-1979-7-824.
- Braulke, L. J., Klingenspor, M., DeBarber, A., Tobias, S. C., Grandy, D. K., Scanlan, T. S., et al. (2008). 3-Iodothyronamine: A novel hormone controlling the balance between glucose and lipid utilisation. *J. Comp. Physiol. B, Biochem* 178, 167–177. doi: 10.1007/s00360-007-0208-x.
- Breidert, T., Spitzenberger, F., Gründemann, D., and Schömig, E. (1998). Catecholamine transport by the organic cation transporter type 1 (OCT1). *Br J Pharmacol* 125, 218–224. doi: 10.1038/sj.bjp.0702065.
- Brial, F., Le Lay, A., Hedjazi, L., Tsang, T., Fearnside, J. F., Otto, G. W., et al. (2019). Systems genetics of hepatic metabolome reveals octopamine as a target for non-alcoholic fatty liver disease treatment. *Scientific Reports* 9, 1–10. doi: 10.1038/s41598-019-40153-0.
- Broadley, K. J. (2010). The vascular effects of trace amines and amphetamines. *Pharmacol Ther* 125, 363–375. doi: 10.1016/j.pharmthera.2009.11.005.

- Brown, C. M., McGrath, J. C., Midgley, J. M., Muir, A. G. B., O'Brien, J. W., Thonoor, C. M., et al. (1988). Activities of octopamine and synephrine stereoisomers on  $\alpha$ -adrenoceptors. *Br J Pharmacol* 93, 417–429. doi: 10.1111/j.1476-5381.1988.tb11449.x.
- Brunkwall, L., and Orho-Melander, M. (2017). The gut microbiome as a target for prevention and treatment of hyperglycaemia in type 2 diabetes: from current human evidence to future possibilities. *Diabetologia* 60, 943. doi: 10.1007/s00125-017-4278-3.
- Budiman, T., Bamberg, E., Koepsell, H., and Nagel, G. (2000). Mechanism of electrogenic cation transport by the cloned organic cation transporter 2 from rat. *J Biol Chem* 275, 29413–29420. doi: 10.1074/jbc.m004645200.
- Bugda Gwilt, K., González, D. P., Olliffe, N., Oller, H., Hoffing, R., Puzan, M., et al. (2020). Actions of trace Amines in the brain-gut-microbiome axis via Trace Amine-Associated Receptor-1 (TAAR1). *Cell Mol Neurobiol* 40, 191–201. doi: 10.1007/s10571-019-00772-7.
- Bunzow, J. R., Sonders, M. S., Arttamangkul, S., Harrison, L. M., Zhang, G., Quigley, D. I., et al. (2001). Amphetamine, 3,4-Methylenedioxymethamphetamine, lysergic acid diethylamide, and metabolites of the catecholamine neurotransmitters are agonists of a rat Trace Amine Receptor. *Mol Pharmacol* 60, 1181–1188. doi: 10.1124/mol.60.6.1181.
- Burczynski, M. E., Peterson, R. L., Twine, N. C., Zuberek, K. A., Brodeur, B. J., Casciotti, L., et al. (2006). Molecular classification of Crohn's disease and ulcerative colitis patients using transcriptional profiles in peripheral blood mononuclear cells. *J Mol Diagn* 8, 51–61. doi: 10.2353/jmoldx.2006.050079.

- Durden, D. A., and Philips, S. R. (1980). Kinetic Measurements of the Turnover Rates of Phenylethylamine and Tryptamine *In Vivo* in the Rat Brain. *J Neurochem* 34, 1725–1732. doi: 10.1111/j.1471-4159.1980.tb11267.x.
- Burns, C., and Kidron, A. (2022). Biochemistry, Tyramine. *StatPearls*.
- Busch, A. E., Karbach, U., Miska, D., Gorboulev, V., Akhoundova, A., Volk, C., et al. (1998). Human neurons express the Polyspecific Cation Transporter hOCT2, which translocates monoamine neurotransmitters, amantadine, and memantine. *Mol Pharmacol* 54, 342–352. doi: 10.1124/mol.54.2.342.
- Carbonaro, T. M., and Gatch, M. B. (2016). Neuropharmacology of *N,N*-dimethyltryptamine. *Brain Res Bull* 126, 74–88. doi: 10.1016/j.brainresbull.2016.04.016.
- Carpéné, C., Galitzky, J., Belles, C., and Zakaroff-Girard, A. (2018). Mechanisms of the antilipolytic response of human adipocytes to tyramine, a trace amine present in food. *J Physiol Biochem* 74, 623–633. doi: 10.1007/S13105-018-0643-Z/metrics.
- Carpéné, C., Les, F., Mercader-Barceló, J., Boulet, N., Briot, A., and Grolleau, J. L. (2022). High doses of tyramine stimulate glucose transport in human fat cells. *J Physiol Biochem* 78, 543–556. doi: 10.1007/S13105-021-00864-3/metrics.
- Chen, L., Hong, C., Chen, E. C., Yee, S. W., Xu, L., Almof, E. U., et al. (2013). Genetic and epigenetic regulation of the Organic Cation Transporter 3, SLC22A3. *Pharmacogenomics J* 13, 110. doi: 10.1038/tpj.2011.60.
- Chen, L., Pawlikowski, B., Schlessinger, A., More, S. S., Stryke, D., Johns, S. J., et al. (2010). Role of Organic Cation Transporter 3 (SLC22A3) and its missense variants in the

- pharmacologic action of metformin. *Pharmacogenet Genomics* 20, 687. doi: 10.1097/fpc.0b013e32833fe789.
- Chen, Y., Wu, C., Xu, W., Lu, Z., Fu, R., He, X., et al. (2022). Evaluation of degradation capability of nitrite and biogenic amines of lactic acid bacteria isolated from pickles and potential in sausage fermentation. *J Food Process Preserv* 46. doi: 10.1111/jfpp.16141.
- Cheng, K. C., Li, C., and Uss, A. S. (2008). Prediction of oral drug absorption in humans--from cultured cell lines and experimental animals. *Expert Opin Drug Metab Toxicol* 4, 581–590. doi: 10.1517/17425255.4.5.581.
- Cheng, M. H., and Bahar, I. (2019). Monoamine transporters: structure, intrinsic dynamics and allosteric regulation. *Nat Struct Mol Biol* 26, 545. doi: 10.1038/s41594-019-0253-7.
- Chiellini, G., Erba, P., Carnicelli, V., Manfredi, C., Frascarelli, S., Ghelardoni, S., et al. (2012). Distribution of exogenous [125I]-3-iodothyronamine in mouse *in vivo*: relationship with trace amine-associated receptors. *J Endocrinol* 213, 223–230. doi: 10.1530/joe-12-0055.
- Chiellini, G., Frascarelli, S., Ghelardoni, S., Carnicelli, V., Tobias, S. C., DeBarber, A., et al. (2007). Cardiac effects of 3-iodothyronamine: a new aminergic system modulating cardiac function. *The FASEB J* 21, 1597–1608. doi: 10.1096/FJ.06-7474com.
- Chiu, C. F., Park, J. M., Chen, H. H., Mau, C. Z., Chen, P. S., Su, Y. H., et al. (2022). Organic cation transporter 2 activation enhances sensitivity to oxaliplatin in human pancreatic ductal adenocarcinoma. *Biomed Pharmacother* 153, 113520. doi: 10.1016/j.biopha.2022.113520.

- Christensen, H. N. (1990). Role of amino acid transport and counter transport in nutrition and metabolism. *Physiol Rev* 70, 43–77. doi: 10.1152/physrev.1990.70.1.43.
- Christenson, J. G., Dairman, W., and Udenfriend, S. (1970). Preparation and properties of a homogeneous aromatic L-amino acid decarboxylase from hog kidney. *Arch Biochem Biophys* 141, 356–367. doi: 10.1016/0003-9861(70)90144-x.
- Christian, S. L., and Berry, M. D. (2018). Trace amine-associated receptors as novel therapeutic targets for immunomodulatory disorders. *Front Pharmacol* 9, 680. doi: 10.3389/fphar.2018.00680/bibtex.
- Cisneros, I. E., and Ghorpade, A. (2014). Methamphetamine and HIV-1-induced neurotoxicity: Role of trace amine associated receptor 1 cAMP signaling in astrocytes. *Neuropharmacology* 85, 499–507. doi: 10.1016/j.neuropharm.2014.06.011.
- Connil, N., Le Breton, Y., Dousset, X., Auffray, Y., Rincé, A., and Prévost, H. (2002). Identification of the *Enterococcus faecalis* tyrosine decarboxylase operon involved in tyramine production. *Appl Environ Microbiol* 68, 3537–3544. doi: 10.1128/aem.68.7.3537-3544.2002.
- Coradduzza, D., Solinas, T., Azara, E., Culeddu, N., Cruciani, S., Zinellu, A., et al. (2022). Plasma polyamine biomarker panels: Agmatine in support of prostate cancer diagnosis. *Biomolecules* 12. doi: 10.3390/biom12040514/S1.
- Correll, C. U., Koblán, K. S., Hopkins, S. C., Li, Y., Heather Dworak, Goldman, R., et al. (2021). Safety and effectiveness of ulotaront (SEP-363856) in schizophrenia: results of a 6-month, open-label extension study. *NPJ Schizophr* 7. doi: 10.1038/s41537-021-00190-z.

- Costa, C., Huneau, J. F., and Tomé, D. (2000). Characteristics of L-glutamine transport during Caco-2 cell differentiation. *Biochimica et Biophysica Acta (BBA) - Biomembranes* 1509, 95–102. doi: 10.1016/s0005-2736(00)00281-9.
- Coton, M., Coton, E., Lucas, P., and Lonvaud, A. (2004). Identification of the gene encoding a putative tyrosine decarboxylase of *Carnobacterium divergens* 508. Development of molecular tools for the detection of tyramine-producing bacteria. *Food Microbiol* 21, 125–130. doi: 10.1016/j.fm.2003.10.004.
- Couroussé, T., and Gautron, S. (2015). Role of organic cation transporters (OCTs) in the brain. *Pharmacol Ther* 146, 94–103. doi: 10.1016/j.pharmthera.2014.09.008.
- Coutts, R. T., Baker, G. B., and Pasutto, F. M. (1986). Foodstuffs as sources of psychoactive amines and their precursors: content, significance and identification. *Adv Drug Res* 15, 169–232.
- Cripps, M. J., Bagnati, M., Jones, T. A., Ogunkolade, B. W., Sayers, S. R., Caton, P. W., et al. (2020). Identification of a subset of trace amine-associated receptors and ligands as potential modulators of insulin secretion. *Biochem Pharmacol* 171, 113685. doi: 10.1016/j.bcp.2019.113685.
- D’Andrea, G., D’Arrigo, A., Facchinetti, F., Del Giudice, E., Colavito, D., Bernardini, D., et al. (2012). Octopamine, unlike other trace amines, inhibits responses of astroglia-enriched cultures to lipopolysaccharide via a  $\beta$ -adrenoreceptor-mediated mechanism. *Neurosci Lett* 517, 36–40. doi: 10.1016/j.neulet.2012.04.013.
- D’Andrea, G., Terrazzino, S., Fortin, D., Farruggio, A., Rinaldi, L., and Leon, A. (2003). HPLC electrochemical detection of trace amines in human plasma and platelets and

- expression of mRNA transcripts of trace amine receptors in circulating leukocytes. *Neurosci Lett* 346, 89–92. doi: 10.1016/s0304-3940(03)00573-1.
- Danek Burgess, K. S., and Justice, J. B. (1999). Effects of serine mutations in transmembrane domain 7 of the human norepinephrine transporter on substrate binding and transport. *J Neurochem* 73, 656–664. doi: 10.1046/j.1471-4159.1999.0730656.x.
- Danielson, T. J., Boulton, A. A., and Robertson, H. A. (1977). m-Octopamine, p-octopamine and phenylethanolamine in rat brain: A sensitive, specific assay and the effects of some drugs. *J Neurochem* 29, 1131–1135. doi: 10.1111/j.1471-4159.1977.tb06519.x.
- Dantzig, A. H., Hoskins, J., Tabas, L. B., Bright, S., Shepard, R. L., Jenkins, I. L., et al. (1994). Association of intestinal peptide transport with a protein related to the cadherin superfamily. *Science* 264, 430–433. doi: 10.1126/science.8153632.
- Darling, N. J., Mobbs, C. L., González-Hau, A. L., Freer, M., and Przyborski, S. (2020). Bioengineering novel in vitro co-culture models that represent the human intestinal mucosa with improved caco-2 structure and barrier function. *Front Bioeng Biotechnol* 8, 992. doi: 10.3389/fbioe.2020.00992/bibtex.
- Davis, B. A. (1989). Biogenic amines and their metabolites in body fluids of normal, psychiatric and neurological subjects. *J Chromatogr A* 466, 89–218. doi: 10.1016/S0021-9673(01)84617-3.
- Dawed, A. Y., Zhou, K., van Leeuwen, N., Mahajan, A., Robertson, N., Koivula, R., et al. (2019). Variation in the Plasma Membrane Monoamine Transporter (PMAT) (encoded by SLC29A4) and Organic Cation Transporter 1 (OCT1) (Encoded by SLC22A1) and

- gastrointestinal intolerance to metformin in Type 2 Diabetes: An IMI DIRECT Study. *Diabetes Care* 42, 1027–1033. doi: 10.2337/DC18-2182.
- De Angelis, M., Vannini, L., Di Cagno, R., Cavallo, N., Minervini, F., Francavilla, R., et al. (2016). Salivary and fecal microbiota and metabolome of celiac children under gluten-free diet. *Int J Food Microbiol* 239, 125–132. doi: 10.1016/j.ijfoodmicro.2016.07.025.
- Debebe, Z., Nekhai, S., Ashenafi, M., Lovejoy, D. B., Kalinowski, D. S., Gordeuk, V. R., et al. (2012). Development of a sensitive HPLC method to measure *in vitro* permeability of E- and Z-isomeric forms of thiosemicarbazones in Caco-2 monolayers. *J Chromatogr B* 906, 25–32. doi: 10.1016/j.jchromb.2012.08.011.
- Dedic, N., Jones, P. G., Hopkins, S. C., Lew, R., Shao, L., Campbell, J. E., et al. (2019). SEP-363856, a novel psychotropic agent with a unique, Non-D2 receptor mechanism of action. *J Pharmacol Exp Ther* 371, 1–14. doi: 10.1124/jpet.119.260281.
- Dewan, A., Pacifico, R., Zhan, R., Rinberg, D., and Bozza, T. (2013). Non-redundant coding of aversive odours in the main olfactory pathway. *Nature* 497, 486–489. doi: 10.1038/nature12114.
- Di Cagno, R., De Angelis, M., De Pasquale, I., Ndagijimana, M., Vernocchi, P., Ricciuti, P., et al. (2011). Duodenal and faecal microbiota of celiac children: Molecular, phenotype and metabolome characterization. *BMC Microbiol* 11, 1–21. doi: 10.1186/1471-2180-11-219/tables/5.
- Dial, E. J., Cooper, L. C., and Lichtenberger, L. M. (1991). Amino acid- and amine-induced gastrin release from isolated rat endocrine granules. *Am J Physiol* 260, G175-G181. doi: 10.1152/ajpgi.1991.260.2.g175.

- Dinan, T. G., and Cryan, J. F. (2015). The impact of gut microbiota on brain and behaviour: Implications for psychiatry. *Curr Opin Clin Nutr Metab Care* 18, 552–558. doi: 10.1097/mco.0000000000000221.
- Ding, S., Wang, X., Zhuge, W., Yang, J., and Zhuge, Q. (2017). Dopamine induces glutamate accumulation in astrocytes to disrupt neuronal function leading to pathogenesis of minimal hepatic encephalopathy. *Neuroscience* 365, 94–113. doi: 10.1016/j.neuroscience.2017.09.040.
- Dinter, J., Mühlhaus, J., Wienchol, C. L., Yi, C. X., Nürnberg, D., Morin, S., et al. (2015). Inverse agonistic action of 3-Iodothyronamine at the human trace amine-associated receptor 5. *PLoS One* 10, 2. doi: 10.1371/journal.pone.0117774.
- Dominici, P., Tancini, B., Barra, D., and Voltattorni, C. B. (1987). Purification and characterization of rat-liver 3,4-dihydroxyphenylalanine decarboxylase. *Eur J Biochem* 169, 209–213. doi: 10.1111/j.1432-1033.1987.tb13599.x.
- Dourish, C. T. (1982). An observational analysis of the behavioural effects of  $\beta$ -Phenylethylamine in isolated and grouped mice. *Prog Neuropsychopharmacol Biol Psychiatry* 6, 143–158. doi: 10.1016/s0278-5846(82)80190-5.
- Downer, R. G. H., Hiripi, L., and Juhos, S. (1993). Characterization of the tyraminerpic system in the central nervous system of the locust, *Locusta migratoria migratoides*. *Neurochem Res* 18, 1245–1248. doi: 10.1007/bf00975042.
- Doyle, K. P., Suchland, K. L., Ciesielski, T. M. P., Lessov, N. S., Grandy, D. K., Scanlan, T. S., et al. (2007). Novel Thyroxine Derivatives, Thyronamine and 3-iodothyronamine,

- induce transient hypothermia and marked neuroprotection against stroke injury. *Stroke* 38, 2569–2576. doi: 10.1161/strokeaha.106.480277.
- Drake, K. A., Torgerson, D. G., Gignoux, C. R., Galanter, J. M., Roth, L. A., Huntsman, S., et al. (2014). A genome-wide association study of bronchodilator response in Latinos implicates rare variants. *J Allergy Clin Immunol* 133, 370. doi: 10.1016/j.jaci.2013.06.043.
- Duan, H., and Wang, J. (2010). Selective transport of monoamine neurotransmitters by human plasma membrane monoamine transporter and organic cation transporter 3. *J Pharmacol Exp Ther* 335, 743–753. doi: 10.1124/jpet.110.170142.
- Duan, J., Martinez, M., Sanders, A. R., Hou, C., Saitou, N., Kitano, T., et al. (2004). Polymorphisms in the trace amine receptor 4 (TRAR4) gene on chromosome 6q23.2 are associated with susceptibility to schizophrenia. *Am J Hum Genet* 75, 624–638. doi: 10.1086/424887.
- Dyck, L. E. (1989). Release of some endogenous trace amines from rat striatal slices in the presence and absence of a monoamine oxidase inhibitor. *Life Sci* 44, 1149–1156. doi: 10.1016/0024-3205(89)90309-3.
- Dyck, L. E., Yang, C. R., and Boulton, A. A. (1983). The biosynthesis of *p*-tyramine, *m*-tyramine, and *beta*-phenylethylamine by rat striatal slices. *J Neurosci Res* 10, 211–220. doi: 10.1002/JNR.490100209.
- Efimova, E. V., Kuvarzin, S. R., Mor, M. S., Katolikova, N. V., Shemiakova, T. S., Razenkova, V., et al. (2022). Trace amine-associated receptor 2 is expressed in the limbic brain areas

- and is involved in dopamine regulation and adult neurogenesis. *Front Behav Neurosci* 16, 93. doi: 10.3389/fnbeh.2022.847410/bibtex.
- Eisenhofer, G. (2001). The role of neuronal and extraneuronal plasma membrane transporters in the inactivation of peripheral catecholamines. *Pharmacol Ther* 91, 35–62. doi: 10.1016/S0163-7258(01)00144-9.
- Elliott, J., Callingham, B. A., and Sharman, D. F. (1989). Semicarbazide-Sensitive Amine Oxidase (SSAO) of the rat aorta: Interactions with some naturally occurring amines and their structural analogues. *Biochem Pharmacol* 38, 1507–1515. doi: 10.1016/0006-2952(89)90191-3.
- Engel, K., and Wang, J. (2005). Interaction of organic cations with a newly identified plasma membrane monoamine transporter. *Mol Pharmacol* 68, 1397–1407. doi: 10.1124/mol.105.016832.
- Engel, K., Zhou, M., and Wang, J. (2004). Identification and characterization of a novel monoamine transporter in the human brain. *J Biol Chem* 279, 50042–50049. doi: 10.1074/jbc.m407913200.
- Eraly, S. A., and Nigam, S. K. (2002). Novel human cDNAs homologous to Drosophila Orct and mammalian carnitine transporters. *Biochem Biophys Res Commun* 297, 1159–1166. doi: 10.1016/S0006-291X(02)02343-4.
- Espinoza, S., Ghisi, V., Emanuele, M., Leo, D., Sukhanov, I., Sotnikova, T. D., et al. (2015). Postsynaptic D2 dopamine receptor supersensitivity in the striatum of mice lacking TAAR1. *Neuropharmacology* 93, 308–313. doi: 10.1016/j.neuropharm.2015.02.010.

- Espinoza, S., Pittaluga, A. M., Di Genova, U., Salahpour, A., Zucchi, R., Rutigliano, G., et al. (2018). The Case for TAAR1 as a modulator of central nervous system function. *Front Pharmacol* 8, 987. doi: 10.3389/fphar.2017.00987.
- Espinoza, S., Salahpour, A., Masri, B., Sotnikova, T. D., Messa, M., Barak, L. S., et al. (2011). Functional interaction between Trace Amine-Associated Receptor 1 and Dopamine D2 receptor. *Mol Pharmacol* 80, 416–425. doi: 10.1124/mol.111.073304.
- Eyun, S. Il, Moriyama, H., Hoffmann, F. G., and Moriyama, E. N. (2016). Molecular Evolution and functional divergence of trace amine-associated receptors. *PLoS One* 11, e0151023. doi: 10.1371/journal.pone.0151023.
- Faraj, B. A., Olkowski, Z. L., and Jackson, R. T. (1994). Expression of a high-affinity serotonin transporter in human lymphocytes. *Int J Immunopharmacol* 16, 561–567. doi: 10.1016/0192-0561(94)90107-4.
- Farooqui, T. (2007). Octopamine-mediated neuromodulation of insect senses. *Neurochem Res* 32, 1511–1529. doi: 10.1007/S11064-007-9344-7.
- Farooqui, T., and Farooqui, A. A. (2016). Trace Amines and their relevance to neurological disorders: A commentary. *Trace Amines and Neurological Disorders: Potential Mechanisms and Risk Factors*, 257–268. doi: 10.1016/b978-0-12-803603-7.00017-3.
- Fehler, M., Broadley, K. J., Ford, W. R., and Kidd, E. J. (2010). Identification of trace-amine-associated receptors (TAAR) in the rat aorta and their role in vasoconstriction by  $\beta$ -phenylethylamine. *Naunyn Schmiedebergs Arch Pharmacol* 382, 385–398. doi: 10.1007/S00210-010-0554-1.

- Fernández, M., Linares, D. M., and Alvarez, M. A. (2004). Sequencing of the tyrosine decarboxylase cluster of *Lactococcus lactis* IPLA 655 and the development of a PCR method for detecting tyrosine decarboxylating lactic acid bacteria. *J Food Prot* 67, 2521–2529. doi: 10.4315/0362-028X-67.11.2521.
- Ferragud, A., Howell, A. D., Moore, C. F., Ta, T. L., Hoener, M. C., Sabino, V., et al. (2016). The trace amine-associated receptor 1 agonist RO5256390 blocks compulsive, binge-like eating in rats. *Neuropsychopharmacology* 42, 1458–1470. doi: 10.1038/npp.2016.233.
- Ferrer-Martinez, A., Felipe, A., Nicholson, B., Casado, J., Pastor-Anglada, M., and Mcgivannt, J. (1995). Induction of the high-affinity Na<sup>+</sup>-dependent glutamate transport system XAG-by hypertonic stress in the renal epithelial cell line NBL-1. *Biochem. J* 310, 689–692. doi: 10.1042/bj3100689
- Ferrero, D. M., Wacker, D., Roque, M. A., Baldwin, M. W., Stevens, R. C., and Liberles, S. D. (2012). Agonists for 13 trace amine-associated receptors provide insight into the molecular basis of odor selectivity. *ACS Chem Biol* 7, 1184–1189. doi: 10.1021/cb300111e
- Fetissov, S. O., Bensing, S., Mulder, J., Le Maitre, E., Hulting, A. L., Harkany, T., et al. (2009). Autoantibodies in autoimmune polyglandular syndrome type I patients react with major brain neurotransmitter systems. *J Comp Neurol* 513, 1–20. doi: 10.1002/cne.21913.

- Finberg, J. P. M., and Gillman, K. (2011). Selective inhibitors of monoamine oxidase type B and the “cheese effect.” *Int Rev Neurobiol* 100, 169–190. doi: 10.1016/b978-0-12-386467-3.00009-1.
- Fischer, W., Neubert, R. H. H., and Brandsch, M. (2010). Transport of phenylethylamine at intestinal epithelial (Caco-2) cells: mechanism and substrate specificity. *Eur J Pharm Biopharm* 74, 281–289. doi: 10.1016/j.ejpb.2009.11.014.
- Fleischer, J., Schwarzenbacher, K., and Breer, H. (2007). Expression of trace amine–associated receptors in the Grueneberg Ganglion. *Chem Senses* 32, 623–631. doi: 10.1093/chemse/bjm032.
- Fleischer, L. M., Somaiya, R. D., and Miller, G. M. (2018). Review and Meta-Analyses of TAAR1 expression in the immune system and cancers. *Front Pharmacol* 9, 683. doi: 10.3389/fphar.2018.00683.
- Fogh, J., Wright, W. C., and Loveless, J. D. (1977). Absence of HeLa cell contamination in 169 cell lines derived from human tumors. *JNCI: J Nat Can Inst* 58, 209–214. doi: 10.1093/jnci/58.2.209.
- Friedman, M. H. (2008). Principles and models of biological transport. *Principles and Models of Biological Transport*. doi: 10.1007/978-0-387-79240-8.
- Fung, T. C., Olson, C. A., and Hsiao, E. Y. (2017). Interactions between the microbiota, immune and nervous systems in health and disease. *Nat Neurosci* 20, 145. doi: 10.1038/nn.4476.

- Furuzawa, Y., Ohmori, Y., and Watanabe, T. (1994). Immunohistochemical colocalization of serotonin, aromatic L-amino acid decarboxylase and polypeptide hormones in islet A- and PP-cells of the cat pancreas. *J Vet Med Sci* 56, 911–916. doi: 10.1292/jvms.56.911.
- Fuxe, K., Grobecker, H., and Jonsson, J. (1967). The effect of  $\beta$ -phenylethylamine on central and peripheral monoamine-containing neurons. *Eur J Pharmacol* 2, 202–207. doi: 10.1016/0014-2999(67)90088-x.
- Gainetdinov, R. R., Hoener, M. C., and Berry, M. D. (2018). Trace amines and their Receptors. *Pharmacol Rev* 70, 549–620. doi: 10.1124/pr.117.015305.
- Gao, S., Liu, S., Yao, J., Li, N., Yuan, Z., Zhou, T., et al. (2017). Genomic organization and evolution of olfactory receptors and trace amine-associated receptors in channel catfish, *Ictalurus punctatus*. *Biochimica et Biophysica Acta (BBA) - General Subjects* 1861, 644–651. doi: 10.1016/j.bbagen.2016.10.017.
- Gardini, F., Martuscelli, M., Caruso, M. C., Galgano, F., Crudele, M. A., Favati, F., et al. (2001). Effects of pH, temperature and NaCl concentration on the growth kinetics, proteolytic activity and biogenic amine production of *Enterococcus faecalis*. *Int J Food Microbiol* 64, 105–117. doi: 10.1016/s0168-1605(00)00445-1.
- Gasser, P. J., Hurley, M. M., Chan, J., and Pickel, V. M. (2017). Organic cation transporter 3 (OCT3) is localized to intracellular and surface membranes in select glial and neuronal cells within the basolateral amygdaloid complex of both rats and mice. *Brain Struct Funct* 222, 1913. doi: 10.1007/s00429-016-1315-9.
- Gasser, P. J., Lowry, C. A., and Orchinik, M. (2006). Corticosterone-sensitive monoamine transport in the rat dorsomedial hypothalamus: potential role for organic cation

- transporter 3 in stress-induced modulation of monoaminergic neurotransmission. *J Neurosci* 26, 8758–8766. doi: 10.1523/jneurosci.0570-06.2006.
- Gebauer, L., Jensen, O., Neif, M., Brockmöller, J., and Dücker, C. (2021). Overlap and specificity in the substrate spectra of human monoamine transporters and organic cation transporters 1, 2 and 3. *Int J Mol Sci* 22, 12816. doi: 10.3390/ijms222312816/s1.
- Gerasimenko, T. N., Senyavina, N. V., Anisimov, N. U., and Tonevitskaya, S. A. (2016). A model of cadmium uptake and transport in caco-2 cells. *Bull Exp Biol Med* 161, 187–192. doi: 10.1007/s10517-016-3373-7/metrics.
- Giacomini, K. M., Huang, S. M., Tweedie, D. J., Benet, L. Z., Brouwer, K. L. R., Chu, X., et al. (2010). Membrane transporters in drug development. *Nat Rev Drug Discov* 9, 215. doi: 10.1038/nrd3028.
- Glahn, R. P., Wien, E. M., Van Campen, D. R., and Miller, D. D. (1996). Caco-2 cell iron uptake from meat and casein digests parallels *in vivo* studies: use of a novel *in vitro* method for rapid estimation of iron bioavailability. *J Nutr* 126, 332–339. doi: 10.1093/jn/126.1.332.
- Gliem, S., Schild, D., and Manzini, I. (2009). Highly specific responses to amine odorants of individual olfactory receptor neurons *in situ*. *Eur J Neurosci* 29, 2315–2326. doi: 10.1111/j.1460-9568.2009.06778.x.
- Gloriam, D. E. I., Bjarnadóttir, T. K., Schiöth, H. B., and Fredriksson, R. (2005). High species variation within the repertoire of trace amine receptors. *Ann N Y Acad Sci* 1040, 323–327. doi: 10.1196/annals.1327.052.

- Goedert, J. J., Sampson, J. N., Moore, S. C., Xiao, Q., Xiong, X., Hayes, R. B., et al. (2014). Fecal metabolomics: assay performance and association with colorectal cancer. *Carcinogenesis* 35, 2089–2096. doi: 10.1093/carcin/bgu131.
- Gorboulev, V., Ulzheimer, J. C., Akhoundova, A., Ulzheimer-Teuber, I., Karbach, U., Quester, S., et al. (1997). Cloning and characterization of two human polyspecific organic cation transporters. *DNA Cell Biol* 16, 871–881. doi: 10.1089/dna.1997.16.871.
- Gordon, J., and Barnes, N. M. (2003). Lymphocytes transport serotonin and dopamine: Agony or ecstasy? *Trends Immunol* 24, 438–443. doi: 10.1016/s1471-4906(03)00176-5.
- Goto, M., Masuda, S., Saito, H., and Inui, K. I. (2003). Decreased expression of P-glycoprotein during differentiation in the human intestinal cell line Caco-2. *Biochem Pharmacol* 66, 163–170. doi: 10.1016/s0006-2952(03)00242-9.
- Gouyon, F., Onesto, C., Dalet, V., Pages, G., Leturque, A., and Brot-Laroche, E. (2003). Fructose modulates GLUT5 mRNA stability in differentiated caco-2 cells: role of cAMP-signalling pathway and PABP (polyadenylated-binding protein)-interacting protein (Paip) 2. *Biochem J* 375, 167–174. doi: 10.1042/bj20030661.
- Gozal, E. A., O'Neill, B. E., Sawchuk, M. A., Zhu, H., Halder, M., Chou, C. C., et al. (2014). Anatomical and functional evidence for trace amines as unique modulators of locomotor function in the mammalian spinal cord. *Front Neural Circuits* 8. doi: 10.3389/fncir.2014.00134.
- Greenshaw, A. J. (1984).  $\beta$ -Phenylethylamine and reinforcement. *Prog Neuropsychopharmacol Biol Psychiatry* 8, 615–620. doi: 10.1016/0278-5846(84)90023-x.

- Grimsby, J., Toth, M., Chen, K., Kumazawa, T., Klaidman, L., Adams, J. D., et al. (1997). Increased stress response and  $\beta$ -phenylethylamine in MAOB-deficient mice. *Nature Genetics* 17, 206–210. doi: 10.1038/ng1097-206.
- Gründemann, D., Schechinger, B., Rappold, G. A., and Schömig, E. (1998). Molecular identification of the corticosterone-sensitive extraneuronal catecholamine transporter. *Nature Neuroscience* 1, 349–351. doi: 10.1038/1557.
- Gunshin, H., Mackenzie, B., Berger, U. V., Gunshin, Y., Romero, M. F., Boron, W. F., et al. (1997). Cloning and characterization of a mammalian proton-coupled metal-ion transporter. *Nature* 388, 482–488. doi: 10.1038/41343.
- Guo, L., Dai, W., Xu, Z., Liang, Q., Miller, E. T., Li, S., et al. (2022). Evolution of brain-expressed biogenic amine receptors into olfactory trace amine-associated receptors. *Mol Biol Evol* 39. doi: 10.1093/molbev/msac006.
- Gwilt, K. B., Olliffe, N., Hoffing, R. A., and Miller, G. M. (2019). Trace amine associated receptor 1 (TAAR1) expression and modulation of inflammatory cytokine production in mouse bone marrow-derived macrophages: a novel mechanism for inflammation in ulcerative colitis. *Immunopharmacol Immunotoxicol* 577–585. doi: 10.1080/08923973.2019.1672178.
- Hagan, C. E., Schenk, J. O., and Neumaier, J. F. (2011). The contribution of low-affinity transport mechanisms to serotonin clearance in synaptosomes. *Synapse* 65, 1015–1023. doi: 10.1002/syn.20929.
- Han, J., Zeng, A., Hou, Z., Xu, Y., Zhao, H., Wang, B., et al. (2022). Identification of diagnostic markers related to fecal and plasma metabolism in primary Sjögren's

- syndrome. *Am J Transl Res* 14, 7378-7390. Han, J., Zeng, A., Hou, Z., Xu, Y., Zhao, H., Wang, B., et al. (2022). Identification of diagnostic markers related to fecal and plasma metabolism in primary Sjögren's syndrome. *Am J Transl Res* 14, 7378-7390. PMID: 36398264.
- Han, T., Everett, R. S., Proctor, W. R., Ng, C. M., Costales, C. L., Brouwer, K. L. R., et al. (2013). Organic cation transporter 1 (OCT1/mOct1) is localized in the apical membrane of Caco-2 cell monolayers and enterocytes. *Mol Pharmacol* 84, 182–189. doi: 10.1124/mol.112.084517/-/dc1.
- Harmeier, A., Obermueller, S., Meyer, C. A., Revel, F. G., Buchy, D., Chaboz, S., et al. (2015). Trace amine-associated receptor 1 activation silences GSK3 $\beta$  signaling of TAAR1 and D2R heteromers. *Eur Neuropsychopharmacol* 25, 2049–2061. doi: 10.1016/j.euroneuro.2015.08.011.
- Harris, J., Trivedi, S., and Ramakrishna, B. L. (1988). A Contribution to the Neuromodulatory/Neurotransmitter Role of Trace Amines. *Trace Amines*, 213–221. doi: 10.1007/978-1-4612-4602-2\_18.
- Hashiguchi, Y., Futura, Y., and Nishida, M. (2008). Evolutionary patterns and selective pressures of odorant/pheromone receptor gene families in teleost fishes. *PLoS One* 3, e4083. doi: 10.1371/journal.pone.0004083.
- Hashiguchi, Y., and Nishida, M. (2007). Evolution of trace amine associated receptor (TAAR) gene family in vertebrates: lineage-specific expansions and degradations of a second class of vertebrate chemosensory receptors expressed in the olfactory epithelium. *Mol Biol Evol* 24, 2099–2107. doi: 10.1093/molbev/msm140.

- Hayashi, M., Yamaji, Y., Kitajima, W., and Saruta, T. (1990). Aromatic L-amino acid decarboxylase activity along the rat nephron. *Am J Physiol* 258, F28-33. doi: 10.1152/ajprenal.1990.258.1.f28.
- Hayer-Zillgen, M., Brüss, M., and Bönisch, H. (2002). Expression and pharmacological profile of the human organic cation transporters hOCT1, hOCT2 and hOCT3. *Br J Pharmacol* 136, 829. doi: 10.1038/sj.bjp.0704785.
- Henry, D. P., Russell, W. L., Clemens, J. A., and Plebus, L. A. (1988). Phenylethylamine and *p*-Tyramine in the extracellular space of the rat brain: Quantification using a new radioenzymatic assay and in situ microdialysis. *Trace Amines*, 239–250. doi: 10.1007/978-1-4612-4602-2\_20.
- Hibino, T., Yuzurihara, M., Kase, Y., and Takeda, A. (2009). Synephrine, a component of *Evodiae Fructus*, constricts isolated rat aorta via adrenergic and serotonergic receptors. *J Pharmacol Sci* 111, 73–81. doi: 10.1254/jphs.09077fp.
- Hidalgo, I. J., Raub, T. J., and Borchardt, R. T. (1989). Characterization of the human colon carcinoma cell line (caco-2) as a model system for intestinal epithelial permeability. *Gastroenterology* 96, 736–749. doi: 10.1016/0016-5085(89)90897-4.
- Hilgers, A. R., Conradi, R. A., and Burton, P. S. (1990). Caco-2 cell monolayers as a model for drug transport across the intestinal mucosa. *Pharmaceutical Research: An Official Journal of the American Association of Pharmaceutical Scientists* 7, 902–910. doi: 10.1023/a:1015937605100/metrics.

- Holland, B. W., Berry, M. D., Gray, C. G., and Tomberli, B. (2015). A permeability study of O<sub>2</sub> and the trace amine *p*-tyramine through model phosphatidylcholine bilayers. *PLoS One* 10. doi: 10.1371/journal.pone.0122468.
- Homberg, U., Seyfarth, J., Binkle, U., Monastirioti, M., and Alkema, M. J. (2013). Identification of distinct tyraminerpic and octopaminergic neurons innervating the central complex of the desert locust, *Schistocerca gregaria*. *J Comp Neurol* 521, 2025. doi: 10.1002/cne.23269.
- Honda, K., and Littman, D. R. (2016). The microbiota in adaptive immune homeostasis and disease. *Nature* 535, 75–84. doi: 10.1038/nature18848.
- Hopkins, S. C., Dedic N., and Koblan K. S. (2021). Effect of TAAR1/5-HT<sub>1A</sub> agonist SEP-363856 on REM sleep in humans. *Transl. Psychiatry* 11, 228. doi: 10.1038/s41398-021-01331-9.
- Horie, A., Sakata, J., Nishimura, M., Ishida, K., Taguchi, M., and Hashimoto, Y. (2011). Mechanisms for membrane transport of metformin in human intestinal epithelial caco-2 cells. *Biopharm Drug Dispos* 32, 253–260. doi: 10.1002/bdd.755.
- Horowitz, L. F., Saraiva, L. R., Kuang, D., Yoon, K. H., Buck, L. B., Horowitz, L. F., et al. (2014). Olfactory receptor patterning in a higher primate. *J Neurosci* 34, 12241. doi: 10.1523/jneurosci.1779-14.2014.
- Hosoya, K. I., Kim, K. J., and Lee, V. H. L. (1996). Age-dependent expression of P-glycoprotein gp170 in Caco-2 cell monolayers. *Pharm Res* 13, 885–890. doi: 10.1023/a:1016005212640/metrics.

- Hu, L. A., Zhou, T., Ahn, J., Wang, S., Zhou, J., Hu, Y., et al. (2009). Human and mouse trace amine-associated receptor 1 have distinct pharmacology towards endogenous monoamines and imidazoline receptor ligands. *Biochem Journal* 424, 39–45. doi: 10.1042/bj20090998.
- Humbert, J. R., Hammond, K. B., Hathaway, W. E., Marcoux, J. G., and O'Brien, D. (1970). Trimethylaminuria: The fish-odour syndrome. *The Lancet* 296, 770–771. doi: 10.1016/s0140-6736(70)90241-2.
- Hussain, A., Saraiva, L. R., and Korsching, S. I. (2009). Positive Darwinian selection and the birth of an olfactory receptor clade in teleosts. *Proc Natl Acad Sci U S A* 106, 4313–4318. doi: 10.1073/pnas.0803229106.
- Irsfeld, M., Spadafore, M., and Prüß, Dr. B. M. (2013).  $\beta$ -phenylethylamine, a small molecule with a large impact. *Webmedcentral* 4, 4409. PMID: 24482732.
- Iseki, K., Sugawara, M., Saitoh, N., and Miyazaki, K. (1993). The transport mechanisms of organic cations and their zwitterionic derivatives across rat intestinal brush-border membrane. II. Comparison of the membrane potential effect on the uptake by membrane vesicles. *Biochim Biophys Acta Biomembr* 1152, 9–14. doi: 10.1016/0005-2736(93)90225-o.
- Ito, J., Ito, M., Nambu, H., Fujikawa, T., Tanaka, K., Iwaasa, H., et al. (2009). Anatomical and histological profiling of orphan G-protein-coupled receptor expression in gastrointestinal tract of C57BL/6J mice. *Cell Tissue Res* 338, 257–269. doi: 10.1007/s00441-009-0859-x.

- Iversen, L. L. (1965). The uptake of catecholamines at high perfusion concentrations in the rat isolated heart: A novel catecholamine uptake process. *Br J Pharmacol Chemother* 25, 18–33. doi: 10.1111/j.1476-5381.1965.tb01753.x.
- Iversen, L. L. (1971). Role of transmitter uptake mechanisms in synaptic neurotransmission. *Br J Pharmacol* 41, 571–591. doi: 10.1111/j.1476-5381.1971.tb07066.x.
- Iversen, L. L. (1973). Catecholamine uptake processes. *Br Med Bull* 29, 130–135. doi: 10.1093/oxfordjournals.bmb.a070982
- Jacobs, J. P., Goudarzi, M., Singh, N., Tong, M., McHardy, I. H., Ruegger, P., et al. (2016). A disease-associated microbial and metabolomics state in relatives of pediatric inflammatory bowel disease patients. *Cell Mol Gastroenterol Hepatol* 2, 750–766. doi: 10.1016/j.jcmgh.2016.06.004.
- Jaeger, C. B., Ruggiero, D. A., Albert, V. R., Park, D. H., Joh, T. H., and Reis, D. J. (1984). Aromatic L-amino acid decarboxylase in the rat brain: immunocytochemical localization in neurons of the brain stem. *Neuroscience* 11, 691–713. doi: 10.1016/0306-4522(84)90053-8.
- Jaeger, C. B., Teitelman, G., Joh, T. H., Albert, V. R., Park, D. H., and Reis, D. J. (1983). Some neurons of the rat central nervous system contain aromatic-L-amino-acid decarboxylase but not monoamines. *Science* 219, 1233–1235. doi: 10.1126/science.6131537.
- Janssen, P. A. J., Leysen, J. E., Megens, A. A. H. P., and Awouters, F. H. L. (1999). Does phenylethylamine act as an endogenous amphetamine in some patients? *Int J Neuropsychopharmacol* 2, 229–240. doi: 10.1017/s1461145799001522.

- Jansson, J., Willing, B., Lucio, M., Fekete, A., Dicksved, J., Halfvarson, J., et al. (2009). Metabolomics reveals metabolic biomarkers of Crohn's Disease. *PLoS One* 4, e6386. doi: 10.1371/journal.pone.0006386.
- Jayanthi, L. D., Vargas, G., and DeFelice, L. J. (2002). Characterization of cocaine and antidepressant-sensitive norepinephrine transporters in rat placental trophoblasts. *Br J Pharmacol* 135, 1927–1934. doi: 10.1038/sj.bjp.0704658.
- Jochems, P. G. M., Garssen, J., Van Keulen, A. M., Masereeuw, R., and Jeurink, P. V. (2018). Evaluating human intestinal cell lines for studying dietary protein absorption. *Nutrients* 10, 322. doi: 10.3390/nu10030322.
- Johnson, M. A., Tsai, L., Roy, D. S., Valenzuela, D. H., Mosley, C., Magklara, A., et al. (2012). Neurons expressing trace amine-associated receptors project to discrete glomeruli and constitute an olfactory subsystem. *Proc Natl Acad Sci U S A* 109, 13410–13415. doi: 10.1073/pnas.1206724109.
- Jones, R. S. G. (1982). Tryptamine modifies cortical neurone responses evoked by stimulation of nucleus raphe medianus. *Brain Res Bull* 8, 435–437. doi: 10.1016/0361-9230(82)90079-x.
- Jones, R. S. G. (1983). Trace biogenic amines: a possible functional role in the CNS. *Trends Pharmacol Sci* 4, 426–429. doi: 10.1016/0165-6147(83)90476-5.
- Jones, R. S. G., and Boulton, A. A. (1980). Interactions between *p*-tyramine, *m*-tyramine, or  $\beta$ -phenylethylamine and dopamine on single neurones in the cortex and caudate nucleus of the rat. *Can J Physiol Pharmacol* 58, 222–227. doi: 10.1139/y80-038.

- Jonker, J. W., Wagenaar, E., Eijl, S. van, and Schinkel, A. H. (2003). Deficiency in the organic cation transporters 1 and 2 (Oct1/Oct2 [Slc22a1/Slc22a2]) in mice abolishes renal secretion of organic cations. *Mol Cell Biol* 23, 7902–7908. doi: 10.1128/mcb.23.21.7902-7908.2003.
- Jordan, R., Midgley, J. M., Thonoor, C. M., and Williams, C. M. (2011).  $\beta$ -Adrenergic activities of octopamine and synephrine stereoisomers on guinea-pig atria and trachea. *J Pharm Pharmacol* 39, 752–754. doi: 10.1111/j.2042-7158.1987.tb06986.x.
- Jung, N., Lehmann, C., Rubbert, A., Knispel, M., Hartmann, P., Van Lunzen, J., Stellbrink H., Faetkenheuer G., and Taubert D. (2008). Relevance of the organic cation transporters 1 and 2 for antiretroviral drug therapy in human immunodeficiency virus infection. *Drug Metab Dispos* 36, 1616–1623. doi: 10.1124/dmd.108.020826.
- Juorio, A. V., Greenshaw, A. J., and Wishart, T. B. (1988). Reciprocal changes in striatal dopamine and  $\beta$ -phenylethylamine induced by reserpine in the presence of monoamine oxidase inhibitors. *Naunyn Schmiedebergs Arch Pharmacol* 338, 644–648. doi: 10.1007/bf00165628/metrics.
- Juorio, A. V., Li, X. M., Walz, W., and Paterson, I. A. (1993). Decarboxylation of L-dopa by cultured mouse astrocytes. *Brain Res* 626, 306–309. doi: 10.1016/0006-8993(93)90592-b.
- Kalinina, D. S., Ptukha, M. A., Goriainova, A. V., Merkulyeva, N. S., Kozlova, A. A., Murtazina, R. Z., et al. (2021). Role of the trace amine associated receptor 5 (TAAR5) in the sensorimotor functions. *Sci Rep* 11, 1–11. doi: 10.1038/s41598-021-02289-w.

- Karbach, U., Kricke, J., Meyer-Wentrup, F., Gorboulev, V., Volk, C., Loffing-Cueni, D., et al. (2000). Localization of organic cation transporters OCT1 and OCT2 in rat kidney. *Am J Physiol Renal Physiol* 279. doi: 10.1152/ajprenal.2000.279.4.f679.
- Karoum, F., Linnoila, M., Potter, W. Z., Chuang, L. W., Goodwin, F. K., and Wyatt, R. J. (1982). Fluctuating high urinary phenylethylamine excretion rates in some bipolar affective disorder patients. *Psychiatry Res* 6, 215–222. doi: 10.1016/0165-1781(82)90009-9.
- Kekuda, R., Prasad, P. D., Wu, X., Wang, H., Fei, Y. J., Leibach, F. H., et al. (1998). Cloning and functional characterization of a potential-sensitive, polyspecific Organic Cation Transporter (OCT3) most abundantly expressed in placenta. *J Biol Chem* 273, 15971–15979. doi: 10.1074/jbc.273.26.15971.
- Kidd, M., Modlin, I. M., Gustafsson, B. I., Drozdov, I., Hauso, O., and Pfragner, R. (2008). Luminal regulation of normal and neoplastic human EC cell serotonin release is mediated by bile salts, amines, tastants, and olfactants. *Am J Physiol Gastrointest Liver Physiol* 295, 260–272. doi: 10.1152/ajpgi.00056.2008
- Kim, H. I., Raffler, J., Lu, W., Lee, J. J., Abbey, D., Saleheen, D., et al. (2017). Fine mapping and functional analysis reveal a role of SLC22A1 in acylcarnitine transport. *Am J Hum Genet* 101, 489. doi: 10.1016/j.ajhg.2017.08.008.
- Kipp, H., Khoursandi, S., Scharlau, D., and Kinne, R. K. H. (2003). More than apical: Distribution of SGLT1 in caco-2 cells. *Am J Physiol Cell Physiol* 285. doi: 10.1152/ajpcell.00041.2003.

- Kitahama, K., Ikemoto, K., Jouvet, A., Araneda, S., Nagatsu, I., Raynaud, B., et al. (2009). Aromatic L-amino acid decarboxylase-immunoreactive structures in human midbrain, pons, and medulla. *J Chem Neuroanat* 38, 130–140. doi: 10.1016/j.jchemneu.2009.06.010.
- Kleinau, G., Pratzka, J., Nürnberg, D., Grüters, A., Führer-Sakel, D., Krude, H., et al. (2011). Differential modulation of beta-adrenergic receptor signaling by trace amine-associated receptor 1 agonists. *PLoS One* 6, e27073. doi: 10.1371/journal.pone.0027073.
- Klykov, O., and Weller, M. G. (2015). Quantification of N-hydroxysuccinimide and N-hydroxysulfosuccinimide by hydrophilic interaction chromatography (HILIC). *Analytical Methods* 7, 6443–6448. doi: 10.1039/c5ay00042d.
- Koblan, K. S., Kent, J., Hopkins, S. C., Krystal, J. H., Cheng, H., Goldman, R., et al. (2020). A non-D2-receptor-binding drug for the treatment of schizophrenia. *N Engl J Med* 382, 1497–1506. doi: 10.1056/nejmoa1911772.
- Koehler, M. R., Wissinger, B., Gorboulev, V., Koepsell, H., and Schmid, M. (1997). The two human organic cation transporter genes SLC22A1 and SLC22A2 are located on chromosome 6q26. *Cytogenet Cell Genet* 79, 198–200. doi: 10.1159/000134720.
- Koepsell, H. (2013). The SLC22 family with transporters of organic cations, anions and zwitterions. *Mol Aspects Med* 34, 413–435. doi: 10.1016/j.mam.2012.10.010.
- Koepsell, H. (2020a). Glucose transporters in the small intestine in health and disease. *Pflugers Archiv* 472, 1207. doi: 10.1007/s00424-020-02439-5.

- Koepsell, H. (2020b). Organic cation transporters in health and disease. *Pharmacol Rev* 72, 253–319. doi: 10.1124/pr.118.015578.
- Koepsell, H., Lips, K., and Volk, C. (2007). Polyspecific Organic cation transporters: Structure, function, physiological roles, and biopharmaceutical implications. *Pharm Res* 24, 1227–1251. doi: 10.1007/s11095-007-9254-z.
- Koh, A. H. W., Chess-Williams, R., and Lohning, A. E. (2019). Differential mechanisms of action of the trace amines octopamine, synephrine and tyramine on the porcine coronary and mesenteric artery. *Sci Rep* 9, 1–9. doi: 10.1038/s41598-019-46627-5.
- Kolho, K. L., Pessia, A., Jaakkola, T., de Vos, W. M., and Velagapudi, V. (2017). Faecal and serum metabolomics in paediatric inflammatory bowel disease. *J Crohns Colitis* 11, 321–334. doi: 10.1093/ecco-jcc/jjw158.
- Könczöl, Rendes, K., Dékány, M., Müller, J., Riethmüller, E., and Balogh, G. T. (2016). Blood-brain barrier specific permeability assay reveals *N*-methylated tyramine derivatives in standardised leaf extracts and herbal products of Ginkgo biloba. *J Pharm Biomed Anal* 131, 167–174. doi: 10.1016/j.jpba.2016.08.032.
- Kononenko, N. L., Wolfenberger, H., and Pflüger, H. J. (2009). Tyramine as an independent transmitter and a precursor of octopamine in the locust central nervous system: an immunocytochemical study. *J Comp Neurol* 512, 433–452. doi: 10.1002/cne.21911.
- Kovács, T., Mikó, E., Vida, A., Sebő, É., Toth, J., Csonka, T., et al. (2019). Cadaverine, a metabolite of the microbiome, reduces breast cancer aggressiveness through trace amino acid receptors. *Sci Rep* 9, 1–14. doi: 10.1038/s41598-018-37664-7.

- Kuehne, A., Floerl, S., and Hagos, Y. (2022). Investigations with drugs and pesticides revealed new species- and substrate-dependent inhibition by Elacridar and Imazalil in human and mouse organic cation transporter OCT2. *Int J Mol Sci* 23, 15795. doi: 10.3390/ijms232415795.
- Lancaster, G. A., and Sourkes, T. L. (1972). Purification and properties of Hog-kidney 3,4-dihydroxyphenylalanine decarboxylase. *Can J Biochem* 50, 791-797. doi: 10.1139/O72-110.
- Landowski, C. P., Sun, D., Foster, D. R., Menon, S. S., Barnett, J. L., Welage, L. S., et al. (2003). Gene expression in the human intestine and correlation with oral valacyclovir pharmacokinetic parameters. *J Pharmacol Exp Ther* 306, 778-786. doi: 10.1124/jpet.103.051011.
- Lauweryns, J. M., and Van Ranst, L. (1988). Immunocytochemical localization of aromatic L-amino acid decarboxylase in human, rat, and mouse bronchopulmonary and gastrointestinal endocrine cells. *J Histochem Cytochem* 36, 1181-1186. doi: 10.1177/36.9.2900264.
- Lea, T. (2015). Caco-2 Cell Line. *The Impact of Food Bioactives on Health: In Vitro and Ex Vivo Models*, 103-111. doi: 10.1007/978-3-319-16104-4\_10.
- Lee, D., Lee, J. H., Kim, B. H., Lee, S., Kim, D. W., and Kang, K. S. (2022). Phytochemical combination (*p*-Synephrine, *p*-Octopamine hydrochloride, and hispidulin) for improving obesity in obese mice induced by high-fat diet. *Nutrients* 14, 2164. doi: 10.3390/nu14102164.

- Lenders, J. W. M., Eisenhofer, G., Abeling, N. G. G. M., Berger, W., Murphy, D. L., Konings, C. H., et al. (1996). Specific genetic deficiencies of the A and B isoenzymes of monoamine oxidase are characterized by distinct neurochemical and clinical phenotypes. *J Clin Invest* 97, 1010. doi: 10.1172/jci118492.
- Leonti, M., and Casu, L. (2014). Soma, food of the immortals according to the Bower Manuscript (Kashmir, 6th century A.D.). *J Ethnopharmacol* 155, 373–386. doi: 10.1016/j.jep.2014.05.029.
- Li, Q., Korzan, W. J., Ferrero, D. M., Chang, R. B., Roy, D. S., Buchi, M., et al. (2013). Synchronous evolution of an odor biosynthesis pathway and behavioral response. *Current Biology* 23, 11–20. doi: 10.1016/j.cub.2012.10.047.
- Li, Q., Tachie-Baffour, Y., Liu, Z., Baldwin, M. W., Kruse, A. C., and Liberles, S. D. (2015). Non-classical amine recognition evolved in a large clade of olfactory receptors. *Elife* 4. doi: 10.7554/elife.10441.
- Li, X. -M, Juorio, A. V., Paterson, I. A., Walz, W., Zhu, M. -Y, and Boulton, A. A. (1992). Gene expression of aromatic L-amino acid decarboxylase in cultured rat glial cells. *J Neurochem* 59, 1172–1175. doi: 10.1111/j.1471-4159.1992.tb08363.x.
- Li, Y., Li, L., Stephens, M. J., Zenner, D., Murray, K. C., Winship, I. R., et al. (2014). Synthesis, transport, and metabolism of serotonin formed from exogenously applied 5-HTP after spinal cord injury in rats. *J Neurophysiol* 111, 145–163. doi: 10.1152/jn.00508.2013.
- Liang, C. S., and Sprecher, D. (1979). Cardiovascular actions of *beta*-phenylethylamine. *Am J Physiol* 236, 592–595. doi: 10.1152/ajpheart.1979.236.4.h592.

- Liang, X., Yee, S. W., Chien, H. C., Chen, E. C., Luo, Q., Zou, L., et al. (2018). Organic cation transporter 1 (OCT1) modulates multiple cardiometabolic traits through effects on hepatic thiamine content. *PLoS Biol* 16, e2002907. doi: 10.1371/journal.pbio.2002907.
- Liang, Y. J., Zhen, J., Chen, N., and Reith, M. E. A. (2009). Interaction of catechol and non-catechol substrates with externally or internally facing dopamine transporters. *J Neurochem* 109, 981. doi: 10.1111/j.1471-4159.2009.06034.x.
- Libants, S., Carr, K., Wu, H., Teeter, J. H., Chung-Davidson, Y. W., Zhang, Z., et al. (2009). The sea lamprey *Petromyzon marinus* genome reveals the early origin of several chemosensory receptor families in the vertebrate lineage. *BMC Evol Biol* 9, 180. doi: 10.1186/1471-2148-9-180.
- Liberles, S. D. (2014). Mammalian pheromones. *Annu Rev Physiol* 76, 151–175. doi: 10.1146/annurev-physiol-021113-170334.
- Liberles, S. D. (2015). Trace amine-associated receptors: ligands, neural circuits, and behaviors. *Curr Opin Neurobiol* 34, 1. doi: 10.1016/j.conb.2015.01.001.
- Liberles, S. D., and Buck, L. B. (2006). A second class of chemosensory receptors in the olfactory epithelium. *Nature* 442, 645–650. doi: 10.1038/nature05066.
- Lichtenberger, L. M., Delansorne, R., and Graziani, L. A. (1982). Importance of amino acid uptake and decarboxylation in gastrin release from isolated G cells. *Nature* 295, 698–700. doi: 10.1038/295698a0.

- Lin, Z., Canales, J. J., Björgvinsson, T., Thomsen, M., Qu, H., Liu, Q. R., et al. (2011). Monoamine transporters: vulnerable and vital doorkeepers. *Prog Mol Biol Transl Sci* 98, 1–46. doi: 10.1016/b978-0-12-385506-0.00001-6.
- Lindemann, L., Ebeling, M., Kratochwil, N. A., Bunzow, J. R., Grandy, D. K., and Hoener, M. C. (2005). Trace amine-associated receptors form structurally and functionally distinct subfamilies of novel G protein-coupled receptors. *Genomics* 85, 372–385. doi: 10.1016/j.ygeno.2004.11.010.
- Lindemann, L., and Hoener, M. C. (2005). A renaissance in trace amines inspired by a novel GPCR family. *Trends Pharmacol Sci* 26, 274–281. doi: 10.1016/j.tips.2005.03.007.
- Lindemann, L., Meyer, C. A., Jeanneau, K., Bradaia, A., Ozmen, L., Bluethmann, H., et al. (2008). Trace amine-associated receptor 1 modulates dopaminergic activity. *J Pharmacol Exp Ther* 324, 948–956. doi: 10.1124/jpet.107.132647.
- Lindstrom, P., and Sehlin, J. (1983). Mechanisms underlying the effects of 5-hydroxytryptamine and 5-hydroxytryptophan in pancreatic islets. A proposed role for L-aromatic amino acid decarboxylase. *Endocrinology* 112, 1524–1529. doi: 10.1210/endo-112-4-1524.
- Linnoila, R. I., Gazdar, A. F., Funa, K., and Becker, K. L. (1993). Long-term selective culture of hamster pulmonary endocrine cells. *Anat Rec* 236, 231–240. doi: 10.1002/ar.1092360128.
- Lips, K. S., Volk, C., Schmitt, B. M., Pfeil, U., Arndt, P., Miska, D., et al. (2005). Polyspecific cation transporters mediate luminal release of acetylcholine from bronchial epithelium. *Am J Respir Cell Mol Biol* 33, 79–88. doi: 10.1165/rcmb.2004-0363oc.

- Liu, J. F., Seaman, R., Siemian, J. N., Bhimani, R., Johnson, B., Zhang, Y., et al. (2018a). Role of trace amine-associated receptor 1 in nicotine's behavioral and neurochemical effects. *Neuropsychopharmacology* 43, 2435–2444. doi: 10.1038/s41386-018-0017-9.
- Liu, J. F., Thorn, D. A., Zhang, Y., and Li, J. X. (2016). Effects of trace amine-associated receptor 1 agonists on the expression, reconsolidation, and extinction of cocaine reward memory. *Int J Neuropsychopharmacol* 19, 1–9. doi: 10.1093/ijnp/pyw009.
- Liu, R. (2022). Functional characterization of glucose transporter SLC2A14/GLUT14 and Vitamin C transporter SLC23A1/SVCT1 : SLC2A14 isoforms substrates and redundancy of the SLC23A1 N-terminus. *Master's thesis*.
- Liu, S. J., Xu, J. J., Ma, C. L., and Guo, C. F. (2018b). A comparative analysis of derivatization strategies for the determination of biogenic amines in sausage and cheese by HPLC. *Food Chem* 266, 275–283. doi: 10.1016/j.foodchem.2018.06.001.
- Liu, X., Grandy, D. K., and Janowsky, A. (2014). Ractopamine, a livestock feed additive, is a full agonist at trace amine-associated receptor 1. *J Pharmacol Exp Ther* 350, 124. doi: 10.1124/jpet.114.213116.
- Lopez-Escalera, S., and Wellejus, A. (2022). Evaluation of Caco-2 and human intestinal epithelial cells as in vitro models of colonic and small intestinal integrity. *Biochem Biophys Rep* 31, 101314. doi: 10.1016/j.bbrep.2022.101314.
- Lovenberg, W., Weissbach, H., and Udenfriend, S. (1962). Aromatic L-amino acid decarboxylase. *J Biol Chem* 237, 89-93. PMID: 14466899.

- Lucas, L. H., Ersoy, B. A., Kuelzto, L. A., Joshi, S. B., Brandau, D. T., Thyagarajapuram, N., et al. (2006). Probing protein structure and dynamics by second-derivative ultraviolet absorption analysis of cation- $\pi$  interactions. *Protein Sci* 15, 2228. doi: 10.1110/ps.062133706.
- Lucas, P., Landete, J., Coton, M., Coton, E., and Lonvaud-Funel, A. (2003). The tyrosine decarboxylase operon of *Lactobacillus brevis* IOEB 9809: characterization and conservation in tyramine-producing bacteria. *FEMS Microbiol Lett* 229, 65–71. doi: 10.1016/s0378-1097(03)00787-0.
- Luo, A., Leach, S. T., Barres, R., Hesson, L. B., Grimm, M. C., and Simar, D. (2017). The microbiota and epigenetic regulation of T Helper 17/Regulatory T Cells: In search of a balanced immune system. *Front Immunol* 8. doi: 10.3389/fimmu.2017.00417.
- Mahraoui, L., Rodolosse, A., Barbat, A., Dussaulx, E., Zweibaum, A., Rousset, M., et al. (1994a). Presence and differential expression of SGLT1, GLUT1, GLUT2, GLUT3 and GLUT5 hexose-transporter mRNAs in Caco-2 cell clones in relation to cell growth and glucose consumption. *Biochem Journal* 298, 629. doi: 10.1042/bj2980629.
- Mahraoui, L., Takeda, J., Mesonero, J., Chantret, I., Dussaulx, E., Bell, G. I., et al. (1994b). Regulation of expression of the human fructose transporter (GLUT5) by cyclic AMP. *Biochem J* 301 ( Pt 1), 169–175. doi: 10.1042/bj3010169.
- Mahrooz, A., Alizadeh, A., Hashemi-Soteh, M. B., Ghaffari-Cherati, M., and Hosseyni-Talei, S. R. (2017). The Polymorphic Variants rs3088442 and rs2292334 in the organic cation transporter 3 (OCT3) gene and susceptibility against Type 2 Diabetes: Role of their interaction. *Arch Med Res* 48, 162–168. doi: 10.1016/j.arcmed.2017.03.010.

- Maier, J., Niello, M., Rudin, D., Daws, L. C., and Sitte, H. H. (2021). The interaction of organic cation transporters 1-3 and PMAT with psychoactive substances. *Handb Exp Pharmacol* 266, 199–214. doi: 10.1007/164\_2021\_469.
- Mailleau, C., Capeau, J., and Brahm-Horn, C. (1998). Interrelationship between the Na<sup>+</sup>/glucose cotransporter and CFTR in Caco-2 cells: Relevance to cystic fibrosis. *J Cell Physiol*, 472–481. doi: 10.1002/(SICI)1097-4652(199809)176:3<472::AID-JCP4>3.0.CO;2-L..
- Malki, A., Fiedler, J., Fricke, K., Ballweg, I., Pfaffl, M. W., and Krautwurst, D. (2015). Class I odorant receptors, TAS1R and TAS2R taste receptors, are markers for subpopulations of circulating leukocytes. *J Leukoc Biol* 97, 533–545. doi: 10.1189/jlb.2a0714-331rr/-/dc1.
- Marcobal, A., De Las Rivas, B., and Muñoz, R. (2006). First genetic characterization of a bacterial beta-phenylethylamine biosynthetic enzyme in *Enterococcus faecium* RM58. *FEMS Microbiol Lett* 258, 144–149. doi: 10.1111/j.1574-6968.2006.00206.x.
- Mariotti, V., Melissari, E., Iofrida, C., Righi, M., Di Russo, M., Donzelli, R., et al. (2014). Modulation of gene expression by 3-Iodothyronamine: Genetic evidence for a lipolytic pattern. *PLoS One* 9, e106923. doi: 10.1371/journal.pone.0106923.
- Martel, F., Gründemann, D., Calhau, C., and Schömig, E. (2001). Apical uptake of organic cations by human intestinal Caco-2 cells: putative involvement of ASF transporters. *Naunyn Schmiedebergs Arch Pharmacol* 363, 40–49. doi: 10.1007/s002100000335.
- Martel, F., Monteiro, R., Lemos, C. (2003). Uptake of serotonin at the apical and basolateral membranes of human intestinal epithelial (Caco-2) cells occurs through the neuronal

- serotonin transporter (SERT). *J Pharmacol Exp Ther* 306, 355-362. doi: 10.1124/jpet.103.049668.
- Martin, V. T., and Vij, B. (2016). Diet and headache: Part 1. *Headache: The Journal of Head and Face Pain* 56, 1543–1552. doi: 10.1111/head.12953.
- Mason, M., Wolf, M. E., and Mosnaim, A. D. (1983). Studies in the mechanism of phenylethylamine uptake by rabbit erythrocytes. *Comp Biochem Physiol C Comp Pharmacol Toxicol* 76, 215–219. doi: 10.1016/0742-8413(83)90066-x.
- Maubon, N., Le Vee, M., Fossati, L., Audry, M., Le Ferrec, E., Bolze, S., et al. (2007). Analysis of drug transporter expression in human intestinal caco-2 cells by real-time PCR. *Fundam Clin Pharmacol* 21, 659–663. doi: 10.1111/j.1472-8206.2007.00550.x.
- Maulén, N. P., Henríquez, E. A., Kempe, S., Cárcamo, J. G., Schmid-Kotsas, A., Bachem, M., et al. (2003). Up-regulation and polarized expression of the sodium-ascorbic acid transporter SVCT1 in post-confluent differentiated CaCo-2 cells. *J Biol Chem* 278, 9035–9041. doi: 10.1074/jbc.m205119200.
- McGuire, P. S., and Seiden, L. S. (1980). Differential effects of imipramine in rats as a function of DRL schedule value. *Pharmacol Biochem Behav* 13, 691–694. doi: 10.1016/0091-3057(80)90013-1.
- Michael, E. S., Covic, L., and Kuliopulos, A. (2019). Trace amine-associated receptor 1 (TAAR1) promotes anti-diabetic signaling in insulin-secreting cells. *J Biol Chem* 294, 4401. doi: 10.1074/jbc.ra118.005464.

- Miller, G. M. (2011). The emerging role of trace amine associated receptor 1 in the functional regulation of monoamine transporters and dopaminergic activity. *J Neurochem* 116, 164. doi: 10.1111/j.1471-4159.2010.07109.x.
- Miller, G. M., Verrico, C. D., Jassen, A., Konar, M., Yang, H., Panas, H., et al. (2005). Primate trace amine receptor 1 modulation by the dopamine transporter. *J Pharmacol Exp Ther* 313, 983–994. doi: 10.1124/jpet.105.084459.
- Miller-Fleming, L., Olin-Sandoval, V., Campbell, K., and Ralser, M. (2015). Remaining mysteries of molecular biology: The role of polyamines in the cell. *J Mol Biol* 427, 3389–3406. doi: 10.1016/j.jmb.2015.06.020.
- Moreno-Arribas, V., and Lonvaud-Funel, A. (2001). Purification and characterization of tyrosine decarboxylase of *Lactobacillus brevis* IOEB 9809 isolated from wine. *FEMS Microbiol Lett* 195, 103–107. doi: 10.1111/j.1574-6968.2001.tb10505.x.
- Moreno-Navarrete, J. M., Ortega, F. J., Rodríguez-Hermosa, J. I., Sabater, M., Pardo, G., Ricart, W., et al. (2011). OCT1 expression in adipocytes could contribute to increased metformin action in obese subjects. *Diabetes* 60, 168. doi: 10.2337/db10-0805.
- Mosnaim, A. D., Callaghan, O. H., Hudzik, T., and Wolf, M. E. (2013). Rat brain-uptake index for phenylethylamine and various monomethylated derivatives. *Neurochem Res* 38, 842–846. doi: 10.1007/s11064-013-0988-1.
- Mühlhaus, J., Dinter, J., Nürnberg, D., Rehders, M., Depke, M., Golchert, J., et al. (2014). Analysis of Human TAAR8 and Murine Taar8b mediated signaling pathways and expression profile. *Int J Mol Sci* 15, 20638. doi: 10.3390/ijms151120638.

- Mukherjee, T., Squillante, E., Gillespie, M., and Shao, J. (2004). Transepithelial electrical resistance is not a reliable measurement of the caco-2 monolayer integrity in transwell. *Drug Deliv* 11, 11–18. doi: 10.1080/10717540490280345.
- Müller, J., Lips, K. S., Metzner, L., Neubert, R. H. H., Koepsell, H., and Brandsch, M. (2005). Drug specificity and intestinal membrane localization of human organic cation transporters (OCT). *Biochem Pharmacol* 70, 1851–1860. doi: 10.1016/j.bcp.2005.09.011.
- Murtazina, R. Z., Zhukov, I. S., Korenkova, O. M., Popova, E. A., Kuvarzin, S. R., Efimova, E. V., et al. (2021). Genetic deletion of Trace-Amine Associated Receptor 9 (TAAR9) in rats leads to decreased blood cholesterol levels. *Int J Mol Sci* 22, 1–15. doi: 10.3390/ijms22062942.
- Nagao-Kitamoto, H., Shreiner, A. B., Gilliland, M. G., Kitamoto, S., Ishii, C., Hirayama, A., et al. (2016). Functional characterization of inflammatory bowel disease-associated gut dysbiosis in gnotobiotic mice. *CMGH* 2, 468–481. doi: 10.1016/j.jcmgh.2016.02.003.
- Nagel, G., Volk, C., Friedrich, T., Ulzheimer, J. C., Bamberg, E., and Koepsell, H. (1997). A reevaluation of substrate specificity of the rat cation transporter rOCT1. *J Biol Chem* 272, 31953–31956. doi: 10.1074/jbc.272.51.31953.
- Nair, P. C., Chalker, J. M., Mckinnon, R. A., Langmead, C. J., Gregory, K. J., and Bastiampillai, T. (2022). Trace Amine-Associated Receptor 1 (TAAR1): molecular and clinical insights for the treatment of schizophrenia and related comorbidities. *ACS Pharmacol Transl Sci* 5, 183–188. doi: 10.1021/acspsci.2c00016.

- Nalazek-Rudnicka, K., and Wasik, A. (2017). Development and validation of an LC–MS/MS method for the determination of biogenic amines in wines and beers. *Monatsh Chem* 148, 1685. doi: 10.1007/s00706-017-1992-y.
- Nazimek J et al. (2017). A phase 1 functional neuroimaging study of a new compound in healthy volunteers with high or low schizotypy. *Brain and Neurosci Adv* 1, 222-223. Doi: <https://doi.org/10.1177/2398212817705279>.
- NCT03669640 (2018). A study to assess the effects of RO6889450 (Ralmitaront) in participants with schizophrenia or schizoaffective disorder and negative symptoms.
- NCT04512066 (2020). A trial of the efficacy and the safety of RO6889450 (Ralmitaront) vs placebo in patients with an acute exacerbation of schizophrenia or schizoaffective disorder.
- Nelson, D. A., Tolbert, M. D., Singh, S. J., and Bost, K. L. (2007). Expression of neuronal trace amine-associated receptor (Taar) mRNAs in leukocytes. *J Neuroimmunol* 192, 21–30. doi: 10.1016/j.jneuroim.2007.08.006.
- Nelson, T. M., Borgogna, J. L. C., Brotman, R. M., Ravel, J., Walk, S. T., and Yeoman, C. J. (2015). Vaginal biogenic amines: biomarkers of bacterial vaginosis or precursors to vaginal dysbiosis? *Front Physiol* 6, 253. doi: 10.3389/fphys.2015.00253.
- Neuhoff, S., Ungell, A. L., Zamora, I., and Artursson, P. (2005). pH-Dependent passive and active transport of acidic drugs across caco-2 cell monolayers. *Eur J Pharm Sci* 25, 211–220. doi: 10.1016/j.ejps.2005.02.009.

- Nies, A. T., Koepsell, H., Damme, K., and Schwab, M. (2011). Organic cation transporters (OCTs, MATEs), in vitro and *in vivo* evidence for the importance in drug therapy. *Handb exp pharmacol* 201, 105–167. doi: 10.1007/978-3-642-14541-4\_3.
- Nies, A. T., Koepsell, H., Winter, S., Burk, O., Klein, K., Kerb, R., et al. (2009). Expression of organic cation transporters OCT1 (SLC22A1) and OCT3 (SLC22A3) is affected by genetic factors and cholestasis in human liver. *Hepatology* 50, 1227–1240. doi: 10.1002/hep.23103.
- Nies, A. T., Schaeffeler, E., Van Der Kuip, H., Cascorbi, I., Bruhn, O., Kneba, M., et al. (2014). Cellular uptake of imatinib into leukemic cells is independent of human organic cation transporter 1 (OCT1). *Clin Cancer Res* 20, 985–994. doi: 10.1158/1078-0432.ccr-13-1999.
- Nigam, S. K. (2018). The SLC22 Transporter Family: A paradigm for the impact of drug transporters on metabolic pathways, signaling, and disease. *Annu Rev Pharmacol Toxicol* 58, 663–687. doi: 10.1146/annurev-pharmtox-010617-052713.
- Nishimura, K., Utsumi, K., Yuhara, M., Fujitani, Y., and Iritani, A. (1989). Identification of puberty-accelerating pheromones in male mouse urine. *J Exp Zool* 251, 300–305. doi: 10.1002/jez.1402510306.
- Niwa, T., Murayama, N., Umeyama, H., Shimizu, M., and Yamazaki, H. (2011). Human liver enzymes responsible for metabolic elimination of tyramine, a vasopressor agent from daily food. *Drug Metab Lett* 5, 216–219. doi: 10.2174/187231211796905026.

- O'Donnell, J. M., and Seiden, L. S. (1983). Differential-reinforcement-of-low-rate 72-second schedule: selective effects of antidepressant drugs. *J Pharmacol Exp Ther* 224, 80-88. PMID: 6848751.
- Ohta, H., Takebe, Y., Murakami, Y., Takahama, Y., and Morimura, S. (2017). Tyramine and  $\beta$ -phenylethylamine, from fermented food products, as agonists for the human trace amine-associated receptor 1 (hTAAR1) in the stomach. *OUP* 81, 1002–1006. doi: 10.1080/09168451.2016.1274640.
- Okada, R., Koshizuka, K., Yamada, Y., Moriya, S., Kikkawa, N., Kinoshita, T., et al. (2019). Regulation of oncogenic targets by miR-99a-3p (Passenger Strand of miR-99a-Duplex) in head and neck squamous cell carcinoma. *Cells* 8. doi: 10.3390/cells8121535.
- Okuda, M., Saito, H., Urakami, Y., Takano, M., and Inui, K. (1996). cDNA cloning and functional expression of a novel rat kidney Organic Cation Transporter, OCT2. *Biochem Biophys Res Commun* 224, 500–507. doi: 10.1006/bbrc.1996.1056.
- Paczkowski, N. J., Vuocolo, H. E., and Bryan-Lluka, L. J. (1996). Conclusive evidence for distinct transporters for 5-hydroxytryptamine and noradrenaline in pulmonary endothelial cells of the rat. *Naunyn Schmiedebergs Arch Pharmacol* 353, 423–430. doi: 10.1007/bf00261439.
- Paetsch, P. R., Baker, G. B., and Greenshaw, A. J. (1993). Induction of functional down-regulation of  $\beta$ -adrenoceptors in rats by 2-phenylethylamine. *J Pharm Sci* 82, 22–24. doi: 10.1002/jps.2600820105.

- Paetsch, P. R., and Greenshaw, A. J. (1993). Down-regulation of beta-adrenergic and dopaminergic receptors induced by 2-phenylethylamine. *Cell Mol Neurobiol* 13, 203–215. doi: 10.1007/bf00733750.
- Paley, E. L. (2019). Diet-related metabolic perturbations of gut microbial shikimate pathway-tryptamine-tRNA aminoacylation-protein synthesis in human health and disease. *Int J Tryptophan Re.* 12: 1178646919834550. doi: 10.1177/1178646919834550.
- Panas, M. W., Xie, Z., Panas, H. N., Hoener, M. C., Vallender, E. J., and Miller, G. M. (2012). Trace amine associated receptor 1 signaling in activated lymphocytes. *J Neuroimmune Pharmacol* 7, 866–876. doi: 10.1007/s11481-011-9321-4.
- Park, Y. K., Lee, J. H., and Mah, J. H. (2019). Occurrence and reduction of biogenic amines in traditional Asian fermented soybean foods: A review. *Food Chem* 278, 1–9. doi: 10.1016/j.foodchem.2018.11.045.
- Parker, E. M., and Cubeddu, L. X. (1988). Comparative effects of amphetamine, phenylethylamine and related drugs on dopamine efflux, dopamine uptake and mazindol binding. *J Pharmacol Exp Ther* 245, 199-210. PMID: 3129549.
- Paterson, I. A. (1988). The potentiation of cortical neurone responses to noradrenaline by  $\beta$ -phenylethylamine: Effects of lesions of the locus coeruleus. *Neurosci Lett* 87, 139–144. doi: 10.1016/0304-3940(88)90159-0.
- Paterson, I. A. (1993). The potentiation of cortical neuron responses to noradrenaline by 2-phenylethylamine is independent of endogenous noradrenaline. *Neurochem Res* 18, 1329–1336. doi: 10.1007/bf00975055.

- Paterson, I. A., and Boulton, A. A. (1988).  $\beta$ -phenylethylamine enhances single cortical neurone responses to noradrenaline in the rat. *Brain Res Bull* 20, 173–177. doi: 10.1016/0361-9230(88)90175-x.
- Paulos, M. A., and Tessel, R. E. (1982). Excretion of  $\beta$ -phenethylamine is elevated in humans after profound stress. *Science* 215, 1127–1129. doi: 10.1126/science.7063846.
- Pegg, A. E. (2016). Functions of polyamines in mammals. *J Biol Chem* 291, 14904–14912. doi: 10.1074/jbc.r116.731661.
- Pei, Y., Asif-Malik, A., and Canales, J. J. (2016). Trace amines and the trace amine-associated receptor 1: Pharmacology, neurochemistry, and clinical implications. *Front Neurosci* 10, 148. doi: 10.3389/fnins.2016.00148/bibtex.
- Pei, Y., Mortas, P., Hoener, M. C., and Canales, J. J. (2015). Selective activation of the trace amine-associated receptor 1 decreases cocaine's reinforcing efficacy and prevents cocaine-induced changes in brain reward thresholds. *Prog Neuropsychopharmacol Biol Psychiatry* 63, 70–75. doi: 10.1016/j.pnpbp.2015.05.014.
- Perdikis, D. A., Davies, R., Zhuravkov, A., Brenner, B., Etter, L., and Basson, M. D. (1998). Differential effects of mucosal pH on human (Caco-2) intestinal epithelial cell motility, proliferation, and differentiation. *Dig Dis Sci* 43, 1537–1546. doi: 10.1023/a:1018871016691/metrics.
- Philips, S. R., and Boulton, A. A. (1979). The effect of monoamine oxidase inhibitors on some arylalkylamines in rat striatum. *J Neurochem* 33, 159–167. doi: 10.1111/j.1471-4159.1979.tb11718.x.

- Piletz, J. E., Aricioglu, F., Cheng, J. T., Fairbanks, C. A., Gilad, V. H., Haenisch, B., et al. (2013). Agmatine: clinical applications after 100 years in translation. *Drug Discov Today* 18, 880–893. doi: 10.1016/j.drudis.2013.05.017.
- Pitts, M. S., McShane, J. N., Hoener, M. C., Christian, S. L., and Berry, M. D. (2019). TAAR1 levels and sub-cellular distribution are cell line but not breast cancer subtype specific. *Histochem Cell Biol* 152, 155–166. doi: 10.1007/s00418-019-01791-7.
- Pretorius, L., and Smith, C. (2020). The trace aminergic system: a gender-sensitive therapeutic target for IBS? *J Biomed Sci* 27, 1–19. doi: 10.1186/s12929-020-00688-1.
- Pretorius, L., and Smith, C. (2022). *Aspalathus linearis* (Rooibos) and agmatine may act synergistically to beneficially modulate intestinal tight junction integrity and inflammatory profile. *Pharmaceuticals* 15, 1097. doi: 10.3390/ph15091097.
- Pretorius, L., and Smith, C. (2023). Tyramine-induced gastrointestinal dysregulation is attenuated via estradiol associated mechanisms in a zebrafish larval model. *Toxicol Appl Pharmacol* 461. doi: 10.1016/j.taap.2023.116399.
- Price, K., and Smith, S. E. (1971). Cheese reaction and tyramine. *The Lancet* 297, 130–131. doi: 10.1016/s0140-6736(71)90858-0.
- Qatato, M., Venugopalan, V., Al-Hashimi, A., Rehders, M., Valentine, A. D., Hein, Z., et al. (2021). Trace amine-associated receptor 1 trafficking to cilia of thyroid epithelial cells. *Cells* 10, 1518. doi: 10.3390/cells10061518.

- Raab, S., Wang, H., Uhles, S., Cole, N., Alvarez-Sanchez, R., Künnecke, B., et al. (2015). Incretin-like effects of small molecule trace amine-associated receptor 1 agonists. *Mol Metab* 5, 47–56. doi: 10.1016/j.molmet.2015.09.015.
- Raab, S., Wang, H., Uhles, S., Cole, N., Alvarez-Sanchez, R., Künnecke, B., et al. (2016). Incretin-like effects of small molecule trace amine-associated receptor 1 agonists. *Mol Metab* 5, 47–56. doi: 10.1016/j.molmet.2015.09.015.
- Raiteri, M., Del Carmine, R., Bertollini, A., and Levi, G. (1977). Effect of sympathomimetic amines on the synaptosomal transport of noradrenaline, dopamine and 5-hydroxytryptamine. *Eur J Pharmacol* 41, 133–143. doi: 10.1016/0014-2999(77)90202-3.
- Ramessur, R., Corbett, M., Marshall, D., Acencio, M. L., Barbosa, I. A., Dand, N., et al. (2022). Biomarkers of disease progression in people with psoriasis: a scoping review. *Br J Dermatol* 187, 481. doi: 10.1111/bjd.21627.
- Rangel, R., Dobroff, A. S., Guzman-Rojas, L., Salmeron, C. C., Gelovani, J. G., Sidman, R. L., et al. (2013). Targeting mammalian organelles with internalizing phage (iPhage) libraries. *Nat Protoc* 8, 1916. doi: 10.1038/nprot.2013.119.
- Rastogi, H., Pinjari, J., Honrao, P., Praband, S., and Somani, R. (2013). The impact of permeability enhancers on assessment for monolayer of colon adenocarcinoma cell line (caco-2) used in in vitro permeability assay. *J Drug Deliv Ther* 3, 20–29. doi: 10.22270/jddt.v3i3.506.
- Reese, E. A., Bunzow, J. R., Arttamangkul, S., Sonders, M. S., and Grandy, D. K. (2007). Trace amine-associated receptor 1 displays species-dependent stereoselectivity for

- isomers of methamphetamine, amphetamine, and para-hydroxyamphetamine. *J Pharmacol Exp Ther* 321, 178–186. doi: 10.1124/jpet.106.115402.
- Regard, J. B., Kataoka, H., Cano, D. A., Camerer, E., Yin, L., Zheng, Y. W., et al. (2007). Probing cell type-specific functions of Gi *in vivo* identifies GPCR regulators of insulin secretion. *J Clin Invest* 117, 4034–4043. doi: 10.1172/jci32994.
- Regard, J. B., Sato, I. T., and Coughlin, S. R. (2008). Anatomical profiling of G protein-coupled receptor expression. *Cell* 135, 561. doi: 10.1016/j.cell.2008.08.040.
- Revel, F. G., Moreau, J. L., Gainetdinov, R. R., Bradaia, A., Sotnikova, T. D., Mory, R., et al. (2011). TAAR1 activation modulates monoaminergic neurotransmission, preventing hyperdopaminergic and hypoglutamatergic activity. *Proc Natl Acad Sci U S A* 108, 8485–8490. doi: 10.1073/pnas.1103029108.
- Revel, F. G., Moreau, J. L., Pouzet, B., Mory, R., Bradaia, A., Buchy, D., et al. (2013). A new perspective for schizophrenia: TAAR1 agonists reveal antipsychotic- and antidepressant-like activity, improve cognition and control body weight. *Mol Psychiatry* 18, 543–556. doi: 10.1038/mp.2012.57.
- Reynolds, G. P., and Gray, D. O. (1978). Gas chromatographic detection of N-methyl-2-phenylethylamine: a new component of human urine. *J Chromatogr B Biomed Sci Appl* 145, 137–140. doi: 10.1016/s0378-4347(00)81676-x.
- Roeder, T. (2005). Tyramine and octopamine: ruling behavior and metabolism. *Annu Rev Entomol* 50, 447–477. doi: 10.1146/annurev.ento.50.071803.130404.

- Rorsman, F., Husebye, E. S., Winqvist, O., Björk, E., Karlsson, F. A., and Kämpe, O. (1995). Aromatic-L-amino-acid decarboxylase, a pyridoxal phosphate-dependent enzyme, is a beta-cell autoantigen. *Proc Natl Acad Sci USA* 92, 8626. doi: 10.1073/pnas.92.19.8626.
- Roy, S., and Trinchieri, G. (2017). Microbiota: a key orchestrator of cancer therapy. *Nature Reviews Cancer* 17, 271–285. doi: 10.1038/nrc.2017.13.
- Rozehnal, V., Nakai, D., Hoepner, U., Fischer, T., Kamiyama, E., Takahashi, M., et al. (2012). Human small intestinal and colonic tissue mounted in the Ussing chamber as a tool for characterizing the intestinal absorption of drugs. *Eur J Pharm Scis* 46, 367–373. doi: 10.1016/j.ejps.2012.02.025.
- Ruiz-Hernández, A., Cabrera-Becerra, S., Vera-Juárez, G., Hong, E., Fengyang, H., Arauz, J., Villafana S. (2020). Diabetic nephropathy produces alterations in the tissue expression profile of the orphan receptors GPR149, GPR153, GPR176, TAAR3, TAAR5 and TAAR9 in Wistar rats. *Nucleosides Nucleotides Nucleic Acids*, 1150–1161. doi: 10.1080/15257770.2020.1780437.
- Rutigliano, G., Accorroni, A., and Zucchi, R. (2018). The case for TAAR1 as a modulator of central nervous system function. *Front Pharmacol* 8. doi: 10.3389/fphar.2017.00987.
- Saavedra, J. M. (1974). Enzymatic isotopic assay for and presence of beta-phenylethylamine in brain. *J Neurochem* 22, 211–216. doi: 10.1111/j.1471-4159.1974.tb11581.x.
- Saavedra, J. M., and Axelrod, J. (1972). Psychotomimetic *N*-methylated tryptamines: formation in brain *in vivo* and *in vitro*. *Science* 175, 1365–1366. doi: 10.1126/science.175.4028.1365.

- Saavedra, J. M., and Axelrod, J. (1973). Effect of drugs on the tryptamine content of rat tissues. *J Pharmacol Exp Ther* 185. PMID: 4268231.
- Sabelli, H. C., and Javaid, J. I. (1995). Phenylethylamine modulation of affect: therapeutic and diagnostic implications. *J Neuropsychiatry Clin Neurosci* 7, 6–14. doi: 10.1176/jnp.7.1.6.
- Sala-Rabanal, M., Li, D. C., Dake, G. R., Kurata, H. T., Inyushin, M., Skatchkov, S. N., et al. (2013). Polyamine transport by the polyspecific organic cation transporters OCT1, OCT2, and OCT3. *Mol Pharm* 10, 1450–1458. doi: 10.1021/mp400024d.
- Sambuy, Y., De Angelis, I., Ranaldi, G., Scarino, M. L., Stammati, A., and Zucco, F. (2005). The Caco-2 cell line as a model of the intestinal barrier: Influence of cell and culture-related factors on caco-2 cell functional characteristics. *Cell Biol Toxicol* 21, 1–26. doi: 10.1007/s10565-005-0085-6/metrics.
- Samodelov, S. L., Kullak-Ublick, G. A., Gai, Z., and Visentin, M. (2020). Organic cation transporters in human physiology, pharmacology, and toxicology. *Int J Mol Sci* 21, 1–21. doi: 10.3390/ijms21217890.
- Sánchez, M., Suárez, L., Andrés, M. T., Flórez, B. H., Bordallo, J., Riestra, S., et al. (2017). Modulatory effect of intestinal polyamines and trace amines on the spontaneous phasic contractions of the isolated ileum and colon rings of mice. *Food Nutr Res.* 61, 1321948. doi: 10.1080/16546628.2017.1321948.

- Santorù, M. L., Piras, C., Murgia, A., Palmas, V., Camboni, T., Liggi, S., et al. (2017). Cross sectional evaluation of the gut-microbiome metabolome axis in an Italian cohort of IBD patients. *Sci Rep* 7, 9523. doi: 10.1038/s41598-017-10034-5.
- Santos, P. S. C., Courtiol, A., Heidel, A. J., Höner, O. P., Heckmann, I., Nagy, M., et al. (2016). MHC-dependent mate choice is linked to a trace-amine-associated receptor gene in a mammal. *Sci Rep* 16, 1–9. doi: 10.1038/srep38490.
- Sata, R., Ohtani, H., Tsujimoto, M., Murakami, H., Koyabu, N., Nakamura, T., et al. (2005). Functional analysis of organic cation transporter 3 expressed in human placenta. *J Pharmacol Exp Ther* 315, 888–895. doi: 10.1124/jpet.105.086827.
- Scanlan, T. S., Suchland, K. L., Hart, M. E., Chiellini, G., Huang, Y., Kruzich, P. J., et al. (2004). 3-Iodothyronamine is an endogenous and rapid-acting derivative of thyroid hormone. *Nature Medicine* 2004 10:6 10, 638–642. doi: 10.1038/nm1051.
- Schmitt, B. M., Gorbunov, D., Schlachtbauer, P., Egenberger, B., Gorboulev, V., Wischmeyer, E., et al. (2009). Charge-to-substrate ratio during organic cation uptake by rat OCT2 is voltage dependent and altered by exchange of glutamate 448 with glutamine. *Am J Physiol Renal Physiol* 296, 709–722. doi: 10.1152/ajprenal.90323.2008.
- Schömig, E., Lazar, A., and Gründemann, D. (2006). Extraneuronal monoamine transporter and organic cation transporters 1 and 2: a review of transport efficiency. *Handb Exp Pharmacol* 175, 151–180. doi: 10.1007/3-540-29784-7\_8.
- Schorn, S., Dicke, A. K., Neugebauer, U., Schröter, R., Friedrich, M., Reuter, S., et al. (2021). Expression and function of organic cation transporter 2 in pancreas. *Front Cell Dev Biol* 9, 1328. doi: 10.3389/fcell.2021.688885/bibtex.

- Schroeter, S., Apparsundaram, S., Wiley, R. G., Miner, L. H., Susan R. Sesack, and Blakely, R. D. (2000). Immunolocalization of the cocaine- and antidepressant-sensitive 1-norepinephrine transporter. *J Comp Neurol*, 211–232. doi: 10.1002/(sici)1096-9861(20000501)420:2<211::aid-cne5>3.0.co;2-3.
- Schroeter, S., Levey, A. I., and Blakely, R. D. (1997). Polarized expression of the antidepressant-sensitive serotonin transporter in epinephrine-synthesizing chromaffin cells of the rat adrenal gland. *Mol Cell Neurosci* 9, 170–184. doi: 10.1006/mcne.1997.0619.
- Schwartz, M. D., Black, S. W., Fisher, S. P., Palmerston, J. B., Morairty, S. R., Hoener, M. C., et al. (2016). Trace amine-associated receptor 1 regulates wakefulness and EEG spectral composition. *Neuropsychopharmacology* 42, 1305–1314. doi: 10.1038/npp.2016.216.
- Shaghghi, M. A., Zhouyao, H., Tu, H., El-Gabalawy, H., Crow, G. H., Levine, M., et al. (2017). The SLC2A14 gene, encoding the novel glucose/dehydroascorbate transporter GLUT14, is associated with inflammatory bowel disease. *Am J Clin Nutr* 106, 1508. doi: 10.3945/ajcn.116.147603.
- Shalaby, A. R. (1996). Significance of biogenic amines to food safety and human health. *Food Research International* 29, 675–690. doi: 10.1016/s0963-9969(96)00066-x.
- Shannon, H. E., and Thompson, W. A. (1984). Behavior maintained under fixed-interval and second-order schedules by intravenous injections of endogenous noncatecholic phenylethylamines in dogs. *J Pharmacol Exp Ther* 228, 691-695. PMID: 6707918.

- Shimizu, M. (2010). Interaction between food substances and the intestinal epithelium. *Biosci Biotechnol Biochem* 74, 232–241. doi: 10.1271/bbb.90730.
- Shirasaka, Y., Lee, N., Zha, W., Wagner, D., and Wang, J. (2016). Involvement of organic cation transporter 3 (Oct3/Slc22a3) in the bioavailability and pharmacokinetics of antidiabetic metformin in mice. *Drug Metab Pharmacokinet* 31, 385. doi: 10.1016/j.dmpk.2016.04.005.
- Sikkema, J. M., Franx, A., Fijnheer, R., Nikkels, P. G. J., Bruinse, H. W., and Boomsma, F. (2002). Semicarbazide-sensitive amine oxidase in pre-eclampsia: no relation with markers of endothelial cell activation. *Clinica Chimica Acta* 324, 31–38. doi: 10.1016/s0009-8981(02)00215-2.
- Silkaitis, R. P., and Mosnaim, A. D. (1976). Pathways linking L-phenylalanine and 2-phenylethylamine with *p*-tyramine in rabbit brain. *Brain Res* 114, 105–115. doi: 10.1016/0006-8993(76)91010-6.
- Simmler, L. D., Buchy, D., Chaboz, S., Hoener, M. C., and Liechti, M. E. (2016). In Vitro Characterization of psychoactive substances at rat, mouse, and human trace amine-associated receptor 1. *J Pharmacol Exp Ther* 357, 134–144. doi: 10.1124/jpet.115.229765.
- Sinha, R., Ahn, J., Sampson, J. N., Shi, J., Yu, G., Xiong, X., et al. (2016). Fecal microbiota, fecal metabolome, and colorectal cancer interrelations. *PLoS One* 11, e0152126. doi: 10.1371/journal.pone.0152126.

- Slitt, A. L., Cherrington, N. J., Hartley, D. P., Leazer, T. M., and Klaassen, C. D. (2002). Tissue distribution and renal developmental changes in rat organic cation transporter mRNA levels. *Drug Metab Dispos* 30, 212–219. doi: 10.1124/dmd.30.2.212.
- Snoddy, A. M., Heckathorn, D., and Tessel, R. E. (1985). Cold-restraint stress and urinary endogenous  $\beta$ -phenylethylamine excretion in rats. *Pharmacol Biochem Behav* 22, 497–500. doi: 10.1016/0091-3057(85)90054-1.
- Snodgrass, E., and Iversen, L. (1974). Formation and release of 3H-tryptamine from 3H-tryptophan in rat spinal cord slices. *Adv Biochem Psychopharmacol* 10, 141–150. PMID: 4211048.
- Solmaz, İ., Kaplan, O., Çelebier, M., Lay, İ., and Anlar, B. (2022). A combination of Q-TOF LC/MS and LC-MS/MS based metabolomics in pediatric-onset multiple sclerosis demonstrates potential biomarkers for unclassified patients. *Turk J Med Sci* 52, 1299–1310. doi: 10.55730/1300-0144.5436.
- Song, W., Luo, Q., Zhang, Y., Zhou, L., Liu, Y., Ma, Z., et al. (2019). Organic cation transporter 3 (Oct3) is a distinct catecholamines clearance route in adipocytes mediating the beiging of white adipose tissue. *PLoS Biol* 17, e2006571. doi: 10.1371/journal.pbio.2006571.
- Sood, R., Bear, C., Auerbach, W., Reyes, E., Jensen, T., Kartner, N., et al. (1992). Regulation of CFTR expression and function during differentiation of intestinal epithelial cells. *EMBO J* 11, 2487–2494. doi: 10.1002/j.1460-2075.1992.tb05313.x.

- Sotnikova, T. D., Beaulieu, J. M., Espinoza, S., Masri, B., Zhang, X., Salahpour, A., et al. (2010). The dopamine metabolite 3-methoxytyramine is a neuromodulator. *PLoS One* 5, e13452. doi: 10.1371/journal.pone.0013452.
- Spasojevic, D., Prokopijevic, M., Prodanovic, O., Zelenovic, N., Polovic, N., Radotic, K., et al. (2019). Peroxidase-sensitive tyramine carboxymethyl xylan hydrogels for enzyme encapsulation. *Macromol Res* 27, 764–771. doi: 10.1007/s13233-019-7111-7/metrics.
- Srinivasan, B., Kolli, A. R., Esch, M. B., Abaci, H. E., Shuler, M. L., and Hickman, J. J. (2015). TEER measurement techniques for *in vitro* barrier model systems. *J Lab Autom* 20, 107. doi: 10.1177/2211068214561025.
- Sriram, U., Cenna, J. M., Haldar, B., Fernandes, N. C., Razmpour, R., Fan, S., et al. (2016). Methamphetamine induces trace amine-associated receptor 1 (TAAR1) expression in human T lymphocytes: role in immunomodulation. *J Leukoc Biol* 99, 213–223. doi: 10.1189/jlb.4a0814-395rr.
- Stavrou, S., Gratz, M., Tremmel, E., Kuhn, C., Hofmann, S., Heidegger, H., et al. (2018). TAAR1 induces a disturbed GSK3 $\beta$  phosphorylation in recurrent miscarriages through the ODC. *Endocr Connect* 7, 372. doi: 10.1530/ec-17-0272.
- Stierum, R., Gaspari, M., Dommels, Y., Ouatas, T., Pluk, H., Jespersen, S., et al. (2003). Proteome analysis reveals novel proteins associated with proliferation and differentiation of the colorectal cancer cell line Caco-2. *Biochim Biophys Acta (BBA) - Proteins and Proteomics* 1650, 73–91. doi: 10.1016/s1570-9639(03)00204-8.

- Stoff, D. M., Jeste, D. V., Gillin, J. C., Moja, E. A., Cohen, L., Stauderman, K. A., et al. (1984). Behavioral supersensitivity to  $\beta$ -phenylethylamine after chronic administration of haloperidol. *Biol psychiatry (1969)* 19, 101–106. PMID: 6538440.
- Stratton, J. E., Hutkins, R. W., and Taylor, S. L. (1991). Biogenic Amines in Cheese and other Fermented Foods: A Review. *J Food Prot* 54, 460–470. doi: 10.4315/0362-028x-54.6.460.
- Strugari, A. F. G., Stan, M. S., Gharbia, S., Hermenean, A., and Dinischiotu, A. (2018). Characterization of nanoparticle intestinal transport using an in vitro co-culture model. *Nanomaterials 2019, Vol. 9, Page 5 9*, 5. doi: 10.3390/nano9010005.
- Suhre, K., Shin, S. Y., Petersen, A. K., Mohny, R. P., Meredith, D., Wägele, B., et al. (2011). Human metabolic individuality in biomedical and pharmaceutical research. *Nature 2011 477:7362* 477, 54–60. doi: 10.1038/nature10354.
- Sukhanov, I., Caffino, L., Efimova, E. V., Espinoza, S., Sotnikova, T. D., Cervo, L., et al. (2016). Increased context-dependent conditioning to amphetamine in mice lacking TAAR1. *Pharmacol Res* 103, 206–214. doi: 10.1016/j.phrs.2015.11.002.
- Sukhanov, I., Dorofeikova, M., Dolgorukova, A., Dorotenko, A., and Gainetdinov, R. R. (2018). Trace amine-associated receptor 1 modulates the locomotor and sensitization effects of nicotine. *Front Pharmacol* 9, 329. doi: 10.3389/fphar.2018.00329/bibtex.
- Sumi-Ichinose, C., Hasegawa, S., Ichinose, H., Sawada, H., Kobayashi, K., Sakai, M., et al. (1995). Analysis of the alternative promoters that regulate tissue-specific expression of human aromatic L-amino acid decarboxylase. *J Neurochem* 64, 514–524. doi: 10.1046/j.1471-4159.1995.64020514.x.

- Sun, H., Chow, E. C. Y., Liu, S., Du, Y., and Pang, K. S. (2008). The Caco-2 cell monolayer: usefulness and limitations. *Expert Opin Drug Metab Toxicol* 4, 395–411. doi: 10.1517/17425255.4.4.395.
- Sun, H., and Pang, K. S. (2008). Permeability, Transport, and Metabolism of Solutes in Caco-2 Cell Monolayers: A Theoretical Study. *Drug Metab Dispos* 36, 102–123. doi: 10.1124/dmd.107.015321.
- Sung, U., Apparsundaram, S., Galli, A., Kahlig, K. M., Savchenko, V., Schroeter, S., et al. (2003). A regulated interaction of syntaxin 1A with the antidepressant-sensitive norepinephrine transporter establishes catecholamine clearance capacity. *J Neurosci* 23, 1697–1709. doi: 10.1523/jneurosci.23-05-01697.2003.
- Syed, A. S., Sansone, A., Röner, S., Bozorg Nia, S., Manzini, I., and Korsching, S. I. (2015). Different expression domains for two closely related amphibian TAARs generate a bimodal distribution similar to neuronal responses to amine odors. *Sci Rep* 5, 13935. doi: 10.1038/srep13935.
- Szabo, A. (2015). Psychedelics and immunomodulation: Novel approaches and therapeutic opportunities. *Front Immunol* 6, 358. doi: 10.3389/fimmu.2015.00358/bibtex.
- Szabo, A., Kovacs, A., Frecska, E., and Rajnavolgyi, E. (2014). Psychedelic *N,N*-dimethyltryptamine and 5-methoxy-*N,N*-dimethyltryptamine modulate innate and adaptive inflammatory responses through the sigma-1 receptor of human monocyte-derived dendritic cells. *PLoS One* 9, e106533. doi: 10.1371/journal.pone.0106533.
- Szumska, J., Qatato, M., Rehders, M., Führer, D., Biebermann, H., Grandy, D. K., et al. (2015). Trace amine-associated receptor 1 localization at the apical plasma membrane

- domain of fisher rat thyroid epithelial cells is confined to cilia. *Eur Thyroid J* 4, 30–41. doi: 10.1159/000434717.
- Tahara, H., Kusuhara, H., Endou, H., Koepsell, H., Imaoka, T., Fuse, E., et al. (2005). A species difference in the transport activities of H<sub>2</sub> receptor antagonists by rat and human renal organic anion and cation transporters. *J Pharmacol Exp Ther* 315, 337–345. doi: 10.1124/jpet.105.088104.
- Tai, W., Chen, Z., and Cheng, K. (2013). Expression profile and functional activity of peptide transporters in prostate cancer cells. *Mol Pharm* 10, 477. doi: 10.1021/mp300364k.
- Taksande, B. G., Kotagale, N. R., Tripathi, S. J., Ugale, R. R., and Chopde, C. T. (2009). Antidepressant like effect of selective serotonin reuptake inhibitors involve modulation of imidazoline receptors by agmatine. *Neuropharmacology* 57, 415–424. doi: 10.1016/j.neuropharm.2009.06.035.
- Tchercansky, D. M., Acevedo, C., and Rubio, M. C. (1994). Studies of tyramine transfer and metabolism using an in vitro intestinal preparation. *J Pharm Sci* 83, 549–552. doi: 10.1002/jps.2600830421.
- Tejwani, R. W., and Anderson, B. D. (2008). Influence of intravesicular pH drift and membrane binding on the liposomal release of a model amine-containing permeant. *J Pharm Sci* 97, 381–399. doi: 10.1002/jps.21108.
- Tessarolo, J. A., Tabesh, M. J., Nesbitt, M., and Davidson, W. S. (2014). Genomic organization and evolution of the trace amine-associated receptor (TAAR) repertoire in atlantic salmon (*Salmo salar*). *G3: Genes, Genomes, Genetics* 4, 1135–1141. doi: 10.1534/G3.114.010660.

- Thaiss, C. A., Zmora, N., Levy, M., and Elinav, E. (2016). The microbiome and innate immunity. *Nature* 535, 65–74. doi: 10.1038/nature18847.
- Thomson, A., Smart, K., Somerville, M. S., Lauder, S. N., Appanna, G., Horwood, J., et al. (2019). The Ussing chamber system for measuring intestinal permeability in health and disease. *BMC Gastroenterol* 19, 1–14. doi: 10.1186/s12876-019-1002-4.
- Thorn, D. A., Jing, L., Qiu, Y., Gancarz-Kausch, A. M., Galuska, C. M., Dietz, D. M., et al. (2014). Effects of the trace amine-associated receptor 1 agonist RO5263397 on abuse-related effects of cocaine in rats. *Neuropsychopharmacology* 39, 2309. doi: 10.1038/npp.2014.91.
- Thwaites, D. T., Kennedy, D. J., Raldua, D., Anderson, C. M. H., Mendoza, M. E., Bladen, C. L., et al. (2002). H<sup>+</sup>/dipeptide absorption across the human intestinal epithelium is controlled indirectly via a functional Na<sup>+</sup>/H<sup>+</sup> exchanger. *Gastroenterology* 122, 1322-1333. doi: 10.1053/gast.2002.32992.
- Trupin, S. (2017). A perspective on the editorial by Ken Gillman: “‘Much ado about nothing’: monoamine oxidase inhibitors, drug interactions, and dietary tyramine’.” *CNS Spectr* 22, 390. doi: 10.1017/s1092852917000372.
- Vaganova, A. N., Katolikova, N. V., Murtazina, R. Z., Kuvarzin, S. R., and Gainetdinov, R. R. (2022). Public transcriptomic data meta-analysis demonstrates TAAR6 expression in the mental disorder-related brain areas in human and mouse brain. *Biomolecules* 12, 1259. doi: 10.3390/biom12091259/s1.

- Vallender, E. J., Xie, Z., Westmoreland, S. V., and Miller, G. M. (2010). Functional evolution of the trace amine associated receptors in mammals and the loss of TAAR1 in dogs. *BMC Evol Biol* 10, 51. doi: 10.1186/1471-2148-10-51.
- Vanti, W. B., Muglia, P., Nguyen, T., Cheng, R., Kennedy, J. L., George, S. R., et al. (2003). Discovery of a null mutation in a human trace amine receptor gene. *Genomics* 82, 531–536. doi: 10.1016/s0888-7543(03)00173-3.
- Varma, D. R., Deng, X. F., Chemtob, S., Nantel, F., and Bouvier, M. (2011). Characterization of the vasorelaxant activity of tyramine and other phenylethylamines in rat aorta. *Can J Physiol Pharmacol* 73, 742–746. doi: 10.1139/Y95-097.
- Varounis, C., Katsi, V., Nihoyannopoulos, P., Lekakis, J., and Tousoulis, D. (2017). Cardiovascular hypertensive crisis: Recent evidence and review of the literature. *Front Cardiovasc Med* 3, 51. doi: 10.3389/fcvm.2016.00051/bibtex.
- Vattai, A., Akyol, E., Kuhn, C., Hofmann, S., Heidegger, H., von Koch, F., et al. (2017). Increased trace amine-associated receptor 1 (TAAR1) expression is associated with a positive survival rate in patients with breast cancer. *J Cancer Res Clin Oncol* 143, 1637–1647. doi: 10.1007/s00432-017-2420-8.
- Vialou, V., Amphoux, A., Zwart, R., Giros, B., and Gautron, S. (2004). Organic Cation Transporter 3 (Slc22a3) is implicated in salt-intake regulation. *J Neurosci* 24, 2846. doi: 10.1523/jneurosci.5147-03.2004.
- Vieira-Coelho, M. A., Lucas Teixeira, V., Guimarães, J. T., Serrão, M. P., and Soares-Da-Silva, P. (1998). Caco-2 cells in culture synthesize and degrade dopamine and 5-

- hydroxytryptamine: A comparison with rat jejunal epithelial cells. *Life Sci* 64, 69–81. doi: 10.1016/s0024-3205(98)00535-9.
- Vieira-Coelho, M., and Soares-da-Silva, P. (1993). Dopamine formation, from its immediate precursor 3,4-dihydroxyphenylalanine, along the rat digestive tract. *Fundam Clin Pharmacol* 7, 235–243. doi: 10.1111/j.1472-8206.1993.tb00237.x.
- Vollmar, J., Kim, Y. O., Marquardt, J. U., Becker, D., Galle, P. R., Schuppan, D., et al. (2019). Deletion of organic cation transporter OCT3 promotes hepatic fibrosis via upregulation of  $\text{tgf}\beta$ . *Am J Physiol Gastrointest Liver Physiol* 317, G195–G202. doi: 10.1152/ajpgi.00088.2019.
- Vollmar, J., Lautem, A., Closs, E., Schuppan, D., Kim, Y. O., Grimm, D., et al. (2017). Loss of organic cation transporter 3 (OCT3) leads to enhanced proliferation and hepatocarcinogenesis. *Oncotarget* 8, 115667. doi: 10.18632/oncotarget.23372.
- Wainscott, D. B., Little, S. P., Yin, T., Tu, Y., Rocco, V. P., He, J. X., et al. (2007). Pharmacologic characterization of the cloned human Trace Amine-Associated Receptor1 (TAAR1) and evidence for species differences with the rat TAAR1. *J Pharmacol Exp Ther* 320, 475–485. doi: 10.1124/jpet.106.112532.
- Wallrabenstein, I., Kuklan, J., Weber, L., Zborala, S., Werner, M., Altmüller, J., et al. (2013). Human Trace Amine-Associated Receptor TAAR5 can be activated by trimethylamine. *PLoS One* 8, e54950. doi: 10.1371/journal.pone.0054950.
- Wang, J. (2016). The plasma membrane monoamine transporter (PMAT): Structure, function, and role in organic cation disposition. *Clin Pharmacol Ther* 100, 489–499. doi: 10.1002/cpt.442.

- Wasik, A. M., Millan, M. J., Scanlan, T., Barnes, N. M., and Gordon, J. (2012). Evidence for functional trace amine associated receptor-1 in normal and malignant B cells. *Leuk Res* 36, 245–249. doi: 10.1016/j.leukres.2011.10.002.
- Whisenant, T. C., and Nigam, S. K. (2022). Organic Anion Transporters (OAT) and other SLC22 transporters in progression of renal cell carcinoma. *Cancers (Basel)* 14, 4772. doi: 10.3390/cancers14194772/s1.
- Williams, B. B., Van Benschoten, A. H., Cimermancic, P., Donia, M. S., Zimmermann, M., Taketani, M., et al. (2014). Discovery and characterization of gut microbiota decarboxylases that can produce the neurotransmitter tryptamine. *Cell Host Microbe* 16, 495–503. doi: 10.1016/j.chom.2014.09.001.
- Wilson, A., Teft, W. A., Morse, B. L., Choi, Y. H., Woolsey, S., DeGorter, M. K., et al. (2015). Trimethylamine-N-oxide: A novel biomarker for the identification of inflammatory bowel disease. *Dig Dis Sci* 60, 3620–3630. doi: 10.1007/s10620-015-3797-3.
- Wilson, G., Hassan, I. F., Dix, C. J., Williamson, I., Shah, R., Mackay, M., et al. (1990). Transport and permeability properties of human Caco-2 cells: An in vitro model of the intestinal epithelial cell barrier. *J Control Release* 11, 25–40. doi: 10.1016/0168-3659(90)90118-d.
- Wiśniewska, A., Stachowicz, A., Kuś, K., Ulatowska-biała, M., Totoń-Żurańska, J., Kiepusa, A., et al. (2021). Inhibition of atherosclerosis and liver steatosis by agmatine in western diet-fed apoE-knockout mice is associated with decrease in hepatic de novo lipogenesis and reduction in plasma triglyceride/high-density lipoprotein cholesterol ratio. *Int J Mol Sci* 22, 10688. doi: 10.3390/ijms221910688.

- Wolf, E. P. (1921). Experimental studies on inflammation: I. The influence of chemicals upon the chemotaxis of leucocytes in vitro. *J Exp Med* 34, 375–396. doi: 10.1084/jem.34.4.375.
- Wolf, E. P. (1923). Experimental studies on inflammation: II. Experimental chemical inflammation *in vivo*. *J Exp Med* 37, 511–524. doi: 10.1084/jem.37.4.511.
- Wolf, M. E., and Mosnaim, A. D. (1983). Phenylethylamine in neuropsychiatric disorders. *Gen Pharmacol: The Vascular System* 14, 385–390. doi: 10.1016/0306-3623(83)90020-4.
- Wu, X., and Freeze, H. H. (2002). GLUT14, a duplicon of GLUT3, is specifically expressed in testis as alternative splice forms. *Genomics* 80, 553–557. doi: 10.1006/geno.2002.7010.
- Wu, X., Kekuda, R., Huang, W., Fei, Y. J., Leibach, F. H., Chen, J., et al. (1998). Identity of the organic cation transporter OCT3 as the extraneuronal monoamine transporter (uptake2) and evidence for the expression of the transporter in the brain. *J Biol Chem* 273, 32776–32786. doi: 10.1074/jbc.273.49.32776.
- Wu, X., Wei, H., Ganapathy, M. E., Wang, H., Kekuda, R., Conway, S. J., et al. (2000a). Structure, function, and regional distribution of the organic cation transporter OCT3 in the kidney. *Am J Physiol Renal Physiol* 279. doi: 10.1152/ajprenal.2000.279.3.f449.
- Wu, X., Wei, H., Ganapathy, M. E., Wang, H., Kekuda, R., Conway, S. J., et al. (2000b). Structure, function, and regional distribution of the organic cation transporter OCT3 in the kidney. *Am J Physiol Renal Physiol* 279. doi: 10.1152/ajprenal.2000.279.3.f449.

- Xia, L., Zhou, M., Kalthorn, T. F., Ho, H. T. B., and Wang, J. (2009). Podocyte-specific expression of organic cation transporter PMAT: implication in puromycin aminonucleoside nephrotoxicity. *Am J Physiol Renal Physiol* 296. doi: 10.1152/ajprenal.00046.2009.
- Xie, Z., and Miller, G. M. (2008).  $\beta$ -Phenylethylamine alters monoamine transporter function via trace amine-associated receptor 1: Implication for Modulatory Roles of Trace Amines in Brain. *J Pharmacol Exp Ther* 325, 617–628. doi: 10.1124/jpet.107.134247.
- Xie, Z., Westmoreland, S. V., and Miller, G. M. (2008). Modulation of monoamine transporters by common biogenic amines via trace amine-associated receptor 1 and monoamine autoreceptors in human embryonic kidney 293 cells and brain synaptosomes. *J Pharmacol Exp Ther* 325, 629–640. doi: 10.1124/jpet.107.135079.
- Yang, C. Y., Dantzig, A. H., and Pidgeon, C. (1999). Intestinal peptide transport systems and oral drug availability. *Pharm Res* 16, 1331–1343. doi: 10.1023/a:1018982505021/metrics.
- Yang, H.-Y. T., and Neff, N. H. (1973).  $\beta$ -Phenylethylamine: A specific substrate for type B monoamine oxidase of brain. *J Pharmacol Exp Ther* 187, 365-371.
- Yang, X. C., and Reis, D. (1999). Agmatine selectively blocks the N-methyl-D-aspartate subclass of glutamate receptor channels in rat hippocampal neurons. *J Pharmacol Exp Ther* 288, 544-549. PMID: 9918557.
- Yang, Y. X., Mu, C. L., Luo, Z., and Zhu, W. Y. (2015). Bromochloromethane, a methane analogue, affects the microbiota and metabolic profiles of the rat gastrointestinal tract. *Appl Environ Microbiol* 82, 778–787. doi: 10.1128/aem.03174-15.

- Yee, S. (1997). In vitro permeability across Caco-2 cells (colonic) can predict *in vivo* (small intestinal) absorption in man - Fact or myth. *Pharm Res* 14, 763–766. doi: 10.1023/a:1012102522787/metrics.
- Yokoo, S., Masuda, S., Yonezawa, A., Terada, T., Katsura, T., and Inui, K. I. (2008). Significance of Organic Cation Transporter 3 (SLC22A3) Expression for the cytotoxic effect of oxaliplatin in colorectal cancer. *Drug Metab and Dispos* 36, 2299–2306. doi: 10.1124/dmd.108.023168.
- Yoon, K. H., Ragozy, T., Lu, Z., Kondoh, K., Kuang, D., Groudine, M., et al. (2015). Olfactory receptor genes expressed in distinct lineages are sequestered in different nuclear compartments. *Proc Natl Acad Sci U S A* 112, E2403–E2409. doi: 10.1073/pnas.1506058112.
- Yu, A. M., Granvil, C. P., Haining, R. L., Krausz, K. W., Corchero, J., Küpfer, A., et al. (2003). The relative contribution of monoamine oxidase and cytochrome P450 Isozymes to the metabolic deamination of the trace amine tryptamine. *J Pharmacol Exp Ther* 304, 539–546. doi: 10.1124/jpet.102.043786.
- Yuan, B. F., Zhu, Q. F., Guo, N., Zheng, S. J., Wang, Y. L., Wang, J., et al. (2018). Comprehensive profiling of fecal metabolome of mice by integrated chemical isotope labeling-mass spectrometry analysis. *Anal Chem* 90, 3512–3520. doi: 10.1021/acs.analchem.7b05355.
- Zaragoza, R. (2020). Transport of amino acids across the blood-brain barrier. *Front Physiol* 11, 973. doi: 10.3389/fphys.2020.00973.

- Zhang, A., Liu, Q., Zhao, H., Zhou, X., Sun, H., Nan, Y., et al. (2016). Phenotypic characterization of nanshi oral liquid alters metabolic signatures during disease prevention. *Sci Rep* 6, 1–10. doi: 10.1038/srep19333.
- Zhang, J., Pacifico, R., Cawley, D., Feinstein, P., and Bozza, T. (2013). Ultrasensitive detection of amines by a trace amine-associated receptor. *J Neurosci* 33, 3228–3239. doi: 10.1523/jneurosci.4299-12.2013.
- Zhang, L., Dresser, M. J., Gray, A. T., Yost, S. C., Terashita, S., and Giacomini, K. M. (1997). Cloning and functional expression of a human liver organic cation transporter. *Mol Pharmacol* 51, 913–921. doi: 10.1124/mol.51.6.913.
- Zhang, L. S., and Davies, S. S. (2016). Microbial metabolism of dietary components to bioactive metabolites: opportunities for new therapeutic interventions. *Genome Med* 8. doi: 10.1186/s13073-016-0296-x.
- Zhang, Y. G., Wu, S., Xia, Y., and Sun, J. (2014). Salmonella-infected crypt-derived intestinal organoid culture system for host–bacterial interactions. *Physiol Rep* 2. doi: 10.14814/phy2.12147.
- Zhang, Y. jia, Zhang, Y., Zhou, Y., Li, G. hui, Yang, W. zhen, and Feng, X. song (2019). A review of pretreatment and analytical methods of biogenic amines in food and biological samples since 2010. *J Chromatogr A* 1605, 360361. doi: 10.1016/j.chroma.2019.07.015.
- Zhu, G., Qian, M., Lu, L., Chen, Y., Zhang, X., Wu, Q., et al. (2019). O-GlcNAcylation of YY1 stimulates tumorigenesis in colorectal cancer cells by targeting SLC22A15 and AANAT. *Carcinogenesis* 40, 1121–1131. doi: 10.1093/carcin/bgz010.

- Zhang, H., Miao, J., Li, F., Xue, W., Tang, K., Zhao, X., et al. (2020). Norepinephrine transporter promotes the invasion of human colon cancer cells. *Oncol Lett* 19, 824-832. doi: 10.3892/ol.2019.11146.
- Zhu, Y., Jameson, E., Crosatti, M., Schäfer, H., Rajakumar, K., Bugg, T. D. H., et al. (2014). Carnitine metabolism to trimethylamine by an unusual Rieske-type oxygenase from human microbiota. *Proc Natl Acad Sci U S A* 111, 4268–4273. doi: 10.1073/pnas.1316569111.
- Zucchi, R., Chiellini, G., Scanlan, T. S., and Grandy, D. K. (2006). Trace amine-associated receptors and their ligands. *Br J Pharmacol* 149, 967–978. doi: 10.1038/sj.bjp.0706948.

## 6. APPENDIX

### A. All common TYR and ATR binding proteins identified from Caco-2 cell

1. Myosin-9 OS=Homo sapiens OX=9606 GN=MYH9 PE=1 SV=4
2. Keratin, type II cytoskeletal 1 OS=Homo sapiens GN=KRT1 PE=1 SV=6 (membrane)
3. Keratin, type II cytoskeletal 2 epidermal OS=Homo sapiens GN=KRT2 PE=1 SV=2
4. Keratin, type I cytoskeletal 10 OS=Homo sapiens GN=KRT10 PE=1 SV=6
5. Histone H4 OS=Homo sapiens OX=9606 GN=H4C1 PE=1 SV=2
6. Myosin-14 OS=Homo sapiens OX=9606 GN=MYH14 PE=1 SV=2 (membrane)
7. Trypsin OS =Sus scrofa PE=1 SV=1
8. Histone H2B OS=Homo sapiens OX=9606 GN=H2BC15 PE=1 SV=1
9. Keratin, type I cytoskeletal 9 OS=Homo sapiens GN=KRT9 PE=1 SV=3
10. Histone H2A OS=Homo sapiens OX=9606 PE=3 SV=1
11. Stress-70 protein, mitochondrial OS=Homo sapiens OX=9606 GN=HSPA9 PE=1 SV=2
12. Prelamin-A/C OS=Homo sapiens OX=9606 GN=LMNA PE=1 SV=1
13. Heat shock cognate 71 kDa protein OS=Homo sapiens OX=9606 GN=HSPA8 PE=1 SV=1
14. X-ray repair cross-complementing protein 6 OS=Homo sapiens OX=9606 GN=XRCC6  
PE=1 SV=2
15. Annexin A6 OS=Homo sapiens OX=9606 GN=ANXA6 PE=1 SV=3
16. Heat shock 70 kDa protein 1B OS=Homo sapiens OX=9606 GN=HSPA1B PE=1 SV=1
17. 60 kDa heat shock protein, mitochondrial OS=Homo sapiens OX=9606 GN=HSPD1 PE=1  
SV=2
18. Keratin, type II cytoskeletal 8 OS=Homo sapiens OX=9606 GN=KRT8 PE=1 SV=7
19. Keratin, type II cytoskeletal 5 OS=Homo sapiens OX=9606 GN=KRT5 PE=1 SV=3
20. Nucleolar protein 58 OS=Homo sapiens OX=9606 GN=NOP58 PE=1 SV=1

21. Pyruvate kinase PKM OS=Homo sapiens OX=9606 GN=PKM PE=1 SV=4
22. Splicing factor 3A subunit 3 OS=Homo sapiens OX=9606 GN=SF3A3 PE=1 SV=1
23. Dolichyl-diphosphooligosaccharide--protein glycosyltransferase subunit 2 OS=Homo sapiens OX=9606 GN=RPN2 PE=1 SV=3
24. Copine-1 OS=Homo sapiens OX=9606 GN=CPNE1 PE=1 SV=1
25. T-complex protein 1 subunit gamma OS=Homo sapiens OX=9606 GN=CCT3 PE=1 SV=4
26. Beta-galactosidase OS=Homo sapiens OX=9606 GN=GLB1 PE=1 SV=2
27. Heterogeneous nuclear ribonucleoprotein L OS=Homo sapiens OX=9606 GN=HNRNPL PE=1 SV=2
28. Histone H3.3 (Fragment) OS=Homo sapiens OX=9606 GN=H3-3B PE=1 SV=1
29. Protein Shroom3 OS=Homo sapiens OX=9606 GN=SHROOM3 PE=1 SV=2
30. T-complex protein 1 subunit alpha OS=Homo sapiens OX=9606 GN=TCP1 PE=1 SV=1
31. ATP synthase subunit alpha, mitochondrial OS=Homo sapiens OX=9606 GN=ATP5F1A PE=1 SV=1
32. Serine hydroxymethyltransferase, mitochondrial OS=Homo sapiens OX=9606 GN=SHMT2 PE=1 SV=3
33. Aldehyde dehydrogenase, mitochondrial OS=Homo sapiens OX=9606 GN=ALDH2 PE=1 SV=2
34. Annexin A11 OS=Homo sapiens OX=9606 GN=ANXA11 PE=1 SV=1
35. Dihydrolipoyl dehydrogenase, mitochondrial OS=Homo sapiens OX=9606 GN=DLD PE=1 SV=2
36. Keratin, type I cytoskeletal 18 OS=Homo sapiens OX=9606 GN=KRT18 PE=1 SV=2

37. Methylmalonate-semialdehyde dehydrogenase [acylating], mitochondrial OS=Homo sapiens OX=9606 GN=ALDH6A1 PE=1 SV=2
38. ATP synthase subunit beta, mitochondrial OS=Homo sapiens OX=9606 GN=ATP5F1B PE=1 SV=3
39. Histone-binding protein RBBP4 OS=Homo sapiens OX=9606 GN=RBBP4 PE=1 SV=3
40. Tubulin beta chain OS=Homo sapiens OX=9606 GN=TUBB PE=1 SV=2
41. Coronin-1C OS=Homo sapiens OX=9606 GN=CORO1C PE=1 SV=1
42. Tubulin alpha chain OS=Homo sapiens OX=9606 GN=TUBA1C PE=1 SV=1
43. Tubulin beta-4B chain OS=Homo sapiens OX=9606 GN=TUBB4B PE=1 SV=1
44. Keratin, type I cytoskeletal 19 OS=Homo sapiens OX=9606 GN=KRT19 PE=1 SV=4
45. Solute carrier family 2, facilitated glucose transporter member 14 OS=Homo sapiens OX=9606 GN=SLC2A14 PE=1 SV=1
46. Protein disulfide-isomerase A6 OS=Homo sapiens OX=9606 GN=PDIA6 PE=1 SV=1
47. Lupus La protein OS=Homo sapiens OX=9606 GN=SSB PE=1 SV=2
48. RuvB-like 2 OS=Homo sapiens OX=9606 GN=RUVBL2 PE=1 SV=3
49. Elongation factor Tu, mitochondrial OS=Homo sapiens OX=9606 GN=TUFM PE=1 SV=2
50. Actin, cytoplasmic 1 OS=Homo sapiens OX=9606 GN=ACTB PE=1 SV=1
51. Serpin H1 OS=Homo sapiens OX=9606 GN=SERPINH1 PE=1 SV=2
52. Annexin A7 OS=Homo sapiens OX=9606 GN=ANXA7 PE=1 SV=3
53. Eukaryotic initiation factor 4A-II OS=Homo sapiens OX=9606 GN=EIF4A2 PE=1 SV=2
54. Eukaryotic initiation factor 4A-III OS=Homo sapiens OX=9606 GN=EIF4A3 PE=1 SV=4
55. Actin-related protein 3 OS=Homo sapiens OX=9606 GN=ACTR3 PE=1 SV=3

56. Citrate synthase, mitochondrial OS=Homo sapiens OX=9606 GN=CS PE=1 SV=2
57. 26S proteasome non-ATPase regulatory subunit 11 OS=Homo sapiens OX=9606  
GN=PSMD11 PE=1 SV=3
58. Reticulon-4 OS=Homo sapiens OX=9606 GN=RTN4 PE=1 SV=2
59. Acetyl-CoA acetyltransferase, mitochondrial OS=Homo sapiens OX=9606 GN=ACAT1  
PE=1 SV=1
60. Creatine kinase B-type OS=Homo sapiens OX=9606 GN=CKB PE=1 SV=1
61. Actin, alpha cardiac muscle 1 OS=Homo sapiens OX=9606 GN=ACTC1 PE=1 SV=1
62. Interleukin enhancer-binding factor 2 OS=Homo sapiens OX=9606 GN=ILF2 PE=1 SV=2
63. 3-ketoacyl-CoA thiolase, mitochondrial OS=Homo sapiens OX=9606 GN=ACAA2 PE=1  
SV=2
64. Cullin-4B OS=Homo sapiens OX=9606 GN=CUL4B PE=1 SV=4
65. Translocon-associated protein subunit delta OS=Homo sapiens OX=9606 GN=SSR4 PE=1  
SV=1
66. Peptidyl-prolyl cis-trans isomerase A OS=Homo sapiens GN=PPIA PE=1 SV=2
67. Histone H2B type 1-J OS=Homo sapiens OX=9606 GN=H2BC11 PE=1 SV=3
68. Nucleophosmin OS=Homo sapiens OX=9606 GN=NPM1 PE=1 SV=2
69. Microsomal glutathione S-transferase 3 OS=Homo sapiens OX=9606 GN=MGST3 PE=1  
SV=1
70. Activated RNA polymerase II transcriptional coactivator p15 OS=Homo sapiens OX=9606  
GN=SUB1 PE=1 SV=3
71. Ragulator complex protein LAMTOR1 OS=Homo sapiens OX=9606 GN=LAMTOR1  
PE=1 SV=2

72. Actin-related protein 2/3 complex subunit 5 OS=Homo sapiens OX=9606 GN=ARPC5  
PE=1 SV=3
73. 60S ribosomal protein L34 OS=Homo sapiens OX=9606 GN=RPL34 PE=1 SV=3
74. 40S ribosomal protein S16 OS=Homo sapiens OX=9606 GN=RPS16 PE=1 SV=1
75. 40S ribosomal protein S19 OS=Homo sapiens OX=9606 GN=RPS19 PE=1 SV=2
76. Peroxiredoxin-5, mitochondrial OS=Homo sapiens OX=9606 GN=PRDX5 PE=1 SV=4
77. 40S ribosomal protein S15a OS=Homo sapiens OX=9606 GN=RPS15A PE=1 SV=2
78. 40S ribosomal protein S20 OS=Homo sapiens OX=9606 GN=RPS20 PE=1 SV=1
79. 60S ribosomal protein L36 OS=Homo sapiens OX=9606 GN=RPL36 PE=1 SV=3
80. 40S ribosomal protein S14 OS=Homo sapiens OX=9606 GN=RPS14 PE=1 SV=3
81. Cytochrome c oxidase subunit 4 isoform 1, mitochondrial OS=Homo sapiens OX=9606  
GN=COX4I1 PE=1 SV=1
82. 40S ribosomal protein S26 OS=Homo sapiens OX=9606 GN=RPS26 PE=1 SV=3
83. 60S ribosomal protein L23 OS=Homo sapiens OX=9606 GN=RPL23 PE=1 SV=1
84. ATP synthase subunit delta, mitochondrial OS=Homo sapiens OX=9606 GN=ATP5F1D  
PE=1 SV=2
85. 60S ribosomal protein L22 OS=Homo sapiens OX=9606 GN=RPL22 PE=1 SV=2
86. Protein mago nashi homolog 2 OS=Homo sapiens OX=9606 GN=MAGOHB PE=1 SV=1
87. Histone H2A type 2-B OS=Homo sapiens OX=9606 GN=H2AC21 PE=1 SV=3
88. Histone H2A.Z OS=Homo sapiens OX=9606 GN=H2AZ1 PE=1 SV=2
89. 60S ribosomal protein L31 OS=Homo sapiens OX=9606 GN=RPL31 PE=1 SV=1
90. Small nuclear ribonucleoprotein Sm D2 OS=Homo sapiens OX=9606 GN=SNRPD2 PE=1  
SV=1

91. Nuclear cap-binding protein subunit 2 OS=Homo sapiens OX=9606 GN=NCBP2 PE=1 SV=1
92. Myosin light polypeptide 6 OS=Homo sapiens OX=9606 GN=MYL6 PE=1 SV=1
93. Oligosaccharyltransferase complex subunit OSTC OS=Homo sapiens OX=9606 GN=OSTC PE=1 SV=1
94. Cysteine-rich and transmembrane domain-containing protein 1 OS=Homo sapiens OX=9606 GN=CYSTM1 PE=1 SV=1
95. 39S ribosomal protein L49, mitochondrial OS=Homo sapiens OX=9606 GN=MRPL49 PE=1 SV=1
96. 60S acidic ribosomal protein P1 OS=Homo sapiens OX=9606 GN=RPLP1 PE=1 SV=1
97. Ergosterol biosynthetic protein 28 homolog OS=Homo sapiens OX=9606 GN=ERG28 PE=1 SV=1
98. 40S ribosomal protein S12 OS=Homo sapiens OX=9606 GN=RPS12 PE=1 SV=3
99. 60S acidic ribosomal protein P2 OS=Homo sapiens OX=9606 GN=RPLP2 PE=1 SV=1
100. SRA stem-loop-interacting RNA-binding protein, mitochondrial OS=Homo sapiens OX=9606 GN=SLIRP PE=1 SV=1
101. 60S ribosomal protein L30 OS=Homo sapiens OX=9606 GN=RPL30 PE=1 SV=2
102. 60S ribosomal protein L35a OS=Homo sapiens OX=9606 GN=RPL35A PE=1 SV=2
103. Cytochrome c oxidase subunit 5B, mitochondrial OS=Homo sapiens OX=9606 GN=COX5B PE=1 SV=2
104. Small nuclear ribonucleoprotein Sm D1 OS=Homo sapiens OX=9606 GN=SNRPD1 PE=1 SV=1
105. Profilin-1 OS=Homo sapiens OX=9606 GN=PFN1 PE=1 SV=2

106. Small nuclear ribonucleoprotein Sm D3 OS=Homo sapiens OX=9606 GN=SNRPD3  
PE=1 SV=1
107. Heterogeneous nuclear ribonucleoproteins C1/C2 OS=Homo sapiens OX=9606  
GN=HNRNPC PE=1 SV=4
108. Fatty acid-binding protein 5 OS=Homo sapiens OX=9606 GN=FABP5 PE=1 SV=3
109. Protein transport protein Sec61 subunit beta OS=Homo sapiens OX=9606 GN=SEC61B  
PE=1 SV=2
110. Acyl-coenzyme A thioesterase 13 OS=Homo sapiens OX=9606 GN=ACOT13 PE=1  
SV=1
111. Dermcidin OS=Homo sapiens OX=9606 GN=DCD PE=1 SV=2
112. 60S ribosomal protein L23a OS=Homo sapiens OX=9606 GN=RPL23A PE=1 SV=1
113. Vesicle-associated membrane protein 8 OS=Homo sapiens OX=9606 GN=VAMP8 PE=1  
SV=1
114. General transcription factor IIF subunit 2 OS=Homo sapiens OX=9606 GN=GTF2F2  
PE=1 SV=2
115. Multifunctional methyltransferase subunit TRM112-like protein OS=Homo sapiens  
OX=9606 GN=TRMT112 PE=1 SV=1
116. Cadherin-17 OS=Homo sapiens OX=9606 GN=CDH17 PE=1 SV=3
117. Thioredoxin OS=Homo sapiens GN=TXN PE=1 SV=3
118. RPS10-NUDT3 readthrough OS=Homo sapiens OX=9606 GN=RPS10-NUDT3 PE=3  
SV=1
119. U6 snRNA-associated Sm-like protein LSm3 OS=Homo sapiens OX=9606 GN=LSM3  
PE=1 SV=2

120. Single-stranded DNA-binding protein, mitochondrial OS=Homo sapiens OX=9606  
GN=SSBP1 PE=1 SV=1
121. Cytochrome c oxidase polypeptide Va OS=Homo sapiens OX=9606 GN=COX5A PE=1  
SV=1
122. COX assembly mitochondrial protein homolog OS=Homo sapiens OX=9606 GN=CMC1  
PE=1 SV=1
123. Histone H3 OS=Homo sapiens OX=9606 GN=H3-2 PE=1 SV=1
124. Cytochrome c OS=Homo sapiens GN=CYCS PE=1 SV=2

## **B. Codes used for MATLAB to investigate the presence of additional TYR transporters in Caco-2 cell**

### **B.i Solving baseline and plotting**

```
%This Matlab function shows all the baseline scenarios with Simple
%diffusion, Facilitated diffisuion and Active transport
function combined_vol_output = Baseline()

%Prompting the user to input the values

prompt = 'Enter the concentration of the apical compartment (in nmol): ';
X_apical = input(prompt);
prompt = 'Enter the concentration of the cellular compartment (in nmol): ';
X_cell = input(prompt);
prompt = 'Enter the concentration of the basolateral compartment (in nmol): ';
X_baso = input(prompt);

global X_initial %Define the initial concentrations for the layers (nM)

X_initial = [X_apical, X_cell, X_baso]; %Initial concentrations for three layers

%%%Define the volume for each of the compartments (defined in cubic meters)

global vol_apical %Volume of apical compartment
global vol_cell %Volume of cellular compartment
```

global vol\_baso % Volume of basolateral compartment

vol\_apical = 100e-6\*1e-3;

vol\_cell = 0.82e-6\*1e-3;

vol\_baso = 600e-6\*1e-3;

min\_conv = 60; %Used for converting seconds to mins

%%%Defining alpha for simple diffusion

global alpha %Half-life constant for membrane (min-1)

p = 22.6e-10 \* min\_conv; %Permeability (1/min)

A = 3.3e-5; %Surface area (m2)

alpha = p\*A; %Half-life of Caco-2 cell

%%%Defining constant values for Facilitated diffusion

global Kapical\_FD %Substrate concentration (nM) (Apical compartment)

global Vm\_apical\_FD %Maximum rate achieved (nM/min) (Apical compartment)

Kapical\_FD = 101.5; %Substrate concentration for apical compartment for Facilitated transporter

Vm\_apical\_FD = 0.11 \* min\_conv; %Maximum rate achieved between apical and cell for Facilitated transporter

```
% Vm_apical_FD = 2.57369 * min_conv; %Maximum rate achieved between apical and
cell for Facilitated transporter
```

```
% Vm_apical_FD = 2.57369 * min_conv; %Maximum rate achieved between apical and
cell for Facilitated transporter
```

```
%%%Defining constant values for Active Transport
```

```
global Kbaso_AT %Substrate concentration (nM)
```

```
global Vm_baso_AT %Maximum rate achieved (nM/min)
```

```
Kbaso_AT = 33.1; %Substrate concetration for basolateral-cell compartment for
Active transporter
```

```
% Kbaso_AT = 29.2678; %Substrate concetration for basolateral-cell compartment
for Active transporter
```

```
Vm_baso_AT = 43.0 * min_conv; %Maximum rate achieved between basolateral and
```

```
%%%Time span for output
```

```
global T
```

```
T = 30;
```

```
tspan = 0:1:T;
```

```
ODE_X_baseline = @ODE_Combined_Diffusion_Active_Trasport_Baseline;
```

```
[t,X_CD_AT] = ode45(ODE_X_baseline, tspan, X_initial); %MATLAB ODE solver
```

```
combined_vol_output = X_CD_AT; %All the output values
```

```
apical_baseline_output = X_CD_AT(:,1);
```

```
cell_baseline_output = X_CD_AT(:,2);
```

```
baso_baseline_output = X_CD_AT(:,3);
```

```
if gt(X_apical,X_baso)
```

```
    Title = 'Apical addition';
```

```
else
```

```
    Title = 'Basolateral addition';
```

```
end
```

```
%Importing values for experimental data from matlab
```

```
if gt(X_apical , X_baso)
```

```
    apical_exp_values = xlsread('Apical_addition','Apical');
```

```
    apical_exp_mean = apical_exp_values(:,end-2);
```

```
    apical_exp_std = apical_exp_values(:,end-1);
```

```
%Importing the Cellular experimental values
```

```
cell_exp_values = xlsread('Apical_addition','Cell');
```

```
cell_exp_mean = cell_exp_values(:,end-2);
```

```
cell_exp_std = cell_exp_values(:,end-1);
```

```

%Importing the Basolateral experimental values
baso_exp_values = xlsread('Apical_addition','Baso');
baso_exp_mean   = baso_exp_values(:,end-2);
baso_exp_std    = baso_exp_values(:,end-1);

time_span_exp   = apical_exp_values(1:end,1); % Time span for the experimental values

elseif It(X_apical, X_baso) %Basolateral addition to the Apical compartment

%Importing the Apical experimental values
apical_exp_values = xlsread('Baso_addition','Apical');
apical_exp_mean   = apical_exp_values(:,end-2);
apical_exp_std    = apical_exp_values(:,end-1);

%Importing the Cellular experimental values
cell_exp_values   = xlsread('Baso_addition','Cell');
cell_exp_mean     = cell_exp_values(:,end-2);
cell_exp_std      = cell_exp_values(:,end-1);

%Importing the Basolateral experimental values
baso_exp_values   = xlsread('Baso_addition','Baso');
baso_exp_mean     = baso_exp_values(:,end-2);
baso_exp_std      = baso_exp_values(:,end-1);

time_span_exp     = apical_exp_values(1:end,1);

end

```

```

%Plot of Concentration vs Time with the Experimental values superimposed

%Plotting the Apical compartment results

Figure(1)

nexttile

% subplot(3,1,1)

hold on

plot(t, apical_baseline_output,'b', 'Linewidth', 6)

grid on

set(gca,'FontSize',25,'fontweight','bold')

set(gcf,'color','w');

title('Apical','fontweight','bold');

xlabel('Time (minutes)','fontweight','bold');

ylabel('TYR (nM)','fontweight','bold');

hold on

plot(time_span_exp, apical_exp_mean,'r','Marker','o','MarkerSize',10,'Linewidth', 6)

hold on

errorbar(time_span_exp,apical_exp_mean,apical_exp_std,'r', 'Linewidth', 4)

if gt(X_apical, X_baso) %Graph limits for apical addition

    ylim([0 50])

else

    ylim([0 50]);

end

legend({'Baseline simulation', 'Experimental'},'FontSize',20)

```

```

%Plotting the Cellular compartment results

% Figure(2)

% subplot(3,1,2)

nexttile

hold on

plot(t, cell_baseline_output, 'b', 'Linewidth', 6)

grid on

set(gca,'FontSize',25,'fontweight','bold')

set(gcf,'color','w');

title('Cell','fontweight','bold')

xlabel('Time (minutes)','fontweight','bold')

ylabel('TYR (nM)','fontweight','bold')

hold on

plot(time_span_exp, cell_exp_mean,'r','Marker','o','MarkerSize',10,'Linewidth', 6)

hold on

errorbar(time_span_exp,cell_exp_mean,cell_exp_std,'r', 'Linewidth', 4)

ylim([0 5000]);

% legend({'Theoretical', 'Experimental'},'FontSize',42)

%Plotting the Basolateral compartment results

% Figure(3)

% subplot(3,1,3)

nexttile

```

```

hold on
plot(t, baso_baseline_output, 'b', 'Linewidth', 6)
grid on
set(gca, 'FontSize', 25, 'fontweight', 'bold')
set(gcf, 'color', 'w');
title('Basolateral', 'fontweight', 'bold')
xlabel('Time (minutes)', 'fontweight', 'bold')
ylabel('TYR (nM)', 'fontweight', 'bold')
hold on
plot(time_span_exp, baso_exp_mean, 'r', 'Marker', 'o', 'MarkerSize', 10, 'Linewidth', 6)
hold on
errorbar(time_span_exp, baso_exp_mean, baso_exp_std, 'r', 'Linewidth', 4)
if gt(X_apical, X_baso) %Graph limits for apical addition
    ylim([0 100])
else
    ylim([0 100]);
end
% legend({'Baseline', 'Experimental'}, 'FontSize', 42)
end

% Combined Diffusion and Active transport function for baseline scenario
function dXdT = ODE_Combined_Diffusion_Active_Trasport_Baseline(~, X)
global alpha
global Kapical_FD
global Kbaso_AT

```

```

global Vm_apical_FD
global Vm_baso_AT
global vol_apical
global vol_cell
global vol_baso

% Apical compartment: Simple diffusion and Facilitated diffusion
diff_X1 = (-1 * (alpha / vol_apical) * ((X(1) - X(2)))) +...
    ((vol_cell/vol_apical) * ((-1) * (Vm_apical_FD*X(1) / (Kapical_FD + X(1))) +
(Vm_apical_FD*X(2) / (Kapical_FD + X(2)))));

% Cellular compartment: Simple diffusion, Active transport and Facilitated
% diffusion from the apical compartment only
diff_X2 = (-1 * (alpha / vol_cell) * (X(2) - X(1))) + (-1 * (alpha / vol_cell) * (X(2) - X(3)))...
    + ((Vm_apical_FD * X(1)) / (Kapical_FD + X(1))) + (-1) * (Vm_apical_FD * X(2) /
(Kapical_FD + X(2)))...
    + (Vm_baso_AT * X(3) / (Kbaso_AT + X(3)));

% Basolateral compartment: Simple diffusion, Active transport and Facilitated diffusion
diff_X3 = (-1 * (alpha / vol_baso) * ((X(3) - X(2))))...
    + (-1 * (vol_cell / vol_baso) * (Vm_baso_AT*X(3) / (Kbaso_AT + X(3))));

dXdt = [diff_X1; diff_X2; diff_X3];

end

```

B.ii Introducing OCT2 in the basolateral membrane at varying densities and plotting

```
function combined_vol_output = OCT2_in_basolateral_membrane_scenario_1()

prompt = 'Enter the concentration of the apical compartment (in nM): ';

X_apical = input(prompt);

prompt = 'Enter the concentration of the cellular compartment (in nM): ';

X_cell = input(prompt);

prompt = 'Enter the concentration of the basolateral compartment (in nM): ';

X_baso = input(prompt);

global X_initial %Define the initial concentrations for the layers (nM)

X_initial = [X_apical, X_cell, X_baso]; %Initial concentrations for three layers

global vol_apical %Volume of apical compartment

global vol_cell %Volume of cellular compartment

global vol_baso %Volume of basolateral compartment

vol_apical = 100e-6*1e-3;

vol_cell = 0.82e-6*1e-3;

vol_baso = 600e-6*1e-3;

min_conv = 60; %Used for converting seconds to mins

%%%Defining alpha for simple diffusion

global alpha %Half-life constant for membrane (min-1)
```

p = 22.6e-10 \* min\_conv; %Permeability (1/min)

A = 3.3e-5; %Surface area (m2)

alpha = p\*A; %Half-life of Caco-2 cell

%%%Defining constant values for Faciliated diffusion

global Kapical\_FD %Substrate concentration (nM) (Apical compartment)

global Vm\_apical\_FD %Maximum rate achieved (nM/min) (Apical compartment)

Kapical\_FD = 101.5; %Substrate concentration for apical compartment for Facilitated  
transporter

Vm\_apical\_FD = 0.11 \* min\_conv; %Maximum rate achieved between apical and cell for  
Facilitated transporter

%%%Defining constant values for Active Transport

global Kbaso\_AT %Substrate concentration (nM)

global Vm\_baso\_AT %Maximum rate achieved (nM/min)

Kbaso\_AT = 33.1; %Substrate concetration for basolateral-cell compartment for Active  
transporter

Vm\_baso\_AT = 43.0 \* min\_conv; %Maximum rate achieved between basolateral and cell  
for Active transporter

```

%%%Time span for output

global T

T = 30;

tspan = 0:1:T;

%Combined diffusion and active transport (Baseline)
ODE_X_baseline = @ODE_Combined_Diffusion_Active_Trasport_Baseline;

[t,X_CD_AT] = ode45(ODE_X_baseline, tspan, X_initial); %MATLAB ODE solver

combined_vol_output = X_CD_AT;      %All the output values
apical_baseline_output = X_CD_AT(:,1); %Apical values
cell_baseline_output = X_CD_AT(:,2); %Cellular values
baso_baseline_output = X_CD_AT(:,3); %Basolateral values

%%%Introducing different scenarios of Facilitated diffusion in the basolateral compartment

%Scenario 1a, Basolateral Vm_baso_FD_new = Vm_apical_FD and
%Kbaso_FD_new = Kapical

```

```
global Vm_baso_FD_new
```

```
global Kbaso_FD_new
```

```
Vm_baso_FD_new = Vm_apical_FD; %Define Vmax for FD in basolateral compartment
```

```
Kbaso_FD_new = Kapical_FD; %Define Kbaso for FD in basolateral compartment
```

```
ODE_X_scenario1a = @ODE_Combined_Diffusion_Active_Trasport_Scenario;
```

```
[t,X_SC_1a] = ode45(ODE_X_scenario1a, tspan, X_initial);
```

```
apical_sc1a_output = X_SC_1a(:,1); %Scenario 1a apical concetration values
```

```
cell_sc1a_output = X_SC_1a(:,2); %Scenario 1a cellular concentration values
```

```
baso_sc1a_output = X_SC_1a(:,3); %Scenario 1a basolateral concentration values
```

```
%Scenario 1b, Basolateral Vm_baso_FD_new = 0.1 * Vm_apical_FD and
```

```
%Kbaso_FD_new = Kapical
```

```
Vm_baso_FD_new = 0.1*Vm_apical_FD; %Define Vmax for FD in basolateral  
compartment
```

```
Kbaso_FD_new = Kapical_FD; %Define Kbaso for FD in basolateral compartment
```

```
ODE_X_scenario1b = @ODE_Combined_Diffusion_Active_Trasport_Scenario;
```

```

[t,X_SC_1b] = ode45(ODE_X_scenario1b, tspan, X_initial);

apical_sc1b_output = X_SC_1b(:,1); %Scenario 1b apical concentration values
cell_sc1b_output   = X_SC_1b(:,2); %Scenario 1b cellular concentration values
baso_sc1b_output   = X_SC_1b(:,3); %Scenario 1b basolateral concentration values

%Scenario 1c, Basolateral Vm_baso_FD_new = 2 * Vm_apical_FD and
%Kbaso_FD_new = Kapical

Vm_baso_FD_new = 2*Vm_apical_FD; %Define Vmax for FD in baseolateral compartment
Kbaso_FD_new   = Kapical_FD;     %Define Kbaso for FD in baseolateral compartment

ODE_X_scenario1c = @ODE_Combined_Diffusion_Active_Trasport_Scenario;

[t,X_SC_1c] = ode45(ODE_X_scenario1c, tspan, X_initial);

apical_sc1c_output = X_SC_1c(:,1); %Scenario 1c apical concentration values
cell_sc1c_output   = X_SC_1c(:,2); %Scenario 1c cellular concentration values
baso_sc1c_output   = X_SC_1c(:,3); %Scenario 1c basolateral concentration values

%Scenario 1d, Basolateral Vm_baso_FD_new = 20 * Vm_apical_FD and
%Kbaso_FD_new = Kapical

```

```

Vm_baso_FD_new      = 20*Vm_apical_FD; %Define Vmax for FD in basolateral
                    compartment
Kbaso_FD_new       = Kapical_FD;      %Define Kbaso for FD in basolateral compartment

ODE_X_scenario1d = @ODE_Combined_Diffusion_Active_Trasport_Scenario;

[t,X_SC_1d]      = ode45(ODE_X_scenario1d, tspan, X_initial);

apical_sc1d_output = X_SC_1d(:,1); %Scenario 1d apical concentration values
cell_sc1d_output   = X_SC_1d(:,2); %Scenario 1d cellular concentration values
baso_sc1d_output   = X_SC_1d(:,3); %Scenario 1d basolateral concentration values

%Importing values for experimental data from matlab
if gt(X_apical , X_baso) %Apical addition to Basolateral compartment
    %Importing the Apical experimental values
    apical_exp_values = xlsread('Apical_addition','Apical');
    apical_exp_mean   = apical_exp_values(:,end-2); %Mean experimental values
    apical_exp_std    = apical_exp_values(:,end-1); %Std err experimental values

    %Importing the Cellular experimental values
    cell_exp_values   = xlsread('Apical_addition','Cell');
    cell_exp_mean     = cell_exp_values(:,end-2); %Mean experimental values
    cell_exp_std      = cell_exp_values(:,end-1); %Std err experimental values

```

```

%Importing the Basolateral experimental values

baso_exp_values = xlsread('Apical_addition','Baso');

baso_exp_mean = baso_exp_values(:,end-2); %Mean experimental values
baso_exp_std = baso_exp_values(:,end-1); %Std err experimental values

time_span_exp = apical_exp_values(1:end,1); %Time span for the experimental values

elseif It(X_apical, X_baso) %Basolateral addition to the Apical compartment

%Importing the Apical experimental values

apical_exp_values = xlsread('Baso_addition','Apical');

apical_exp_mean = apical_exp_values(:,end-2); %Mean experimental values
apical_exp_std = apical_exp_values(:,end-1); %Std err experimental values

%Importing the Cellular experimental values

cell_exp_values = xlsread('Baso_addition','Cell');

cell_exp_mean = cell_exp_values(:,end-2); %Mean experimental values
cell_exp_std = cell_exp_values(:,end-1); %Std err experimental values

%Importing the Basolateral experimental values

baso_exp_values = xlsread('Baso_addition','Baso');

baso_exp_mean = baso_exp_values(:,end-2); %Mean experimental values
baso_exp_std = baso_exp_values(:,end-1); %Std err experimental values

```

```

    time_span_exp    = apical_exp_values(1:end,1); %Time span for the experimental values
end

if gt(X_apical,X_baso)
    Title = 'Apical addition';
else
    Title = 'Basolateral addition';
end

%Plot of Concentration vs Time with the Experimental values superimposed
%Scenario color codes
a_color_code = [0.8500 0.3250 0.0980];
b_color_code = [0.4940 0.1840 0.5560];
c_color_code = [0.4660 0.6740 0.1880];
d_color_code = [0, 1, 1];

%Plotting the Apical compartment results
Figure(1)
nexttile
hold on
plot(t, apical_baseline_output,'b', 'Linewidth', 6)
grid on

```

```

hold on
plot(t, apical_sc1a_output, ':', 'Color', a_color_code, 'MarkerSize', 12, 'Linewidth', 6)
hold on
plot(t, apical_sc1b_output, ':', 'Color', b_color_code, 'MarkerSize', 12, 'Linewidth', 6)
hold on
plot(t, apical_sc1c_output, ':', 'Color', c_color_code, 'MarkerSize', 12, 'Linewidth', 6)
hold on
plot(t, apical_sc1d_output, ':', 'Color', d_color_code, 'MarkerSize', 12, 'Linewidth', 6)
set(gca, 'FontSize', 25, 'fontweight', 'bold')
set(gcf, 'color', 'w');
title('Apical')
xlabel('Time (minutes)')
ylabel('TYR (nM)')
hold on
plot(tim8 e_span_exp, apical_exp_mean, 'r', 'Marker', 'o', 'MarkerSize', 10, 'Linewidth', 6)
hold on
errorbar(time_span_exp, apical_exp_mean, apical_exp_std, 'r', 'Linewidth', 4)
if gt(X_apical, X_baso) %Graph limits for apical addition
    ylim([0 100])
else
    ylim([0 100]);
end
% legend({'Theoretical', 'Scenario 1a, Vmax\_apical\_FD, Kapical\_FD', ...

```

```

%      'Scenario 1b, 0.1x Vmax\_apical\_FD, Kapical\_FD','Scenario 1c, 2x Vmax\_apical,
      Kapical\_FD', 'Scenario 1d, 20x Vmax\_apical, Kapical\_FD'
%      'Experimental'},...
%      'FontSize', 30)
legend({'Baseline simulation', Vmax\_OCT2, Kt\_OCT2',...
      '0.1* Vmax\_OCT2, Kt\_OCT2',' 2* Vmax\_OCT2, Kt\_OCT2', '20* Vmax\_OCT2,
      Kt\_OCT2',...
      'Experimental'},...
      'FontSize', 20)

%Plotting the Cellular compartment results

% Figure(2)

nexttile

hold on

plot(t, cell_baseline_output, 'b', 'Linewidth', 6)

grid on

hold on

plot(t, cell_sc1a_output, ':','Color',a_color_code,'MarkerSize',12,'Linewidth',6)

hold on

plot(t, cell_sc1b_output, ':','Color',b_color_code,'MarkerSize',12,'Linewidth',6)

hold on

plot(t, cell_sc1c_output, ':','Color',c_color_code,'MarkerSize',12,'Linewidth',6)

hold on

plot(t, cell_sc1d_output, ':','Color',d_color_code,'MarkerSize',12,'Linewidth',6)

```

```

set(gca,'FontSize',25,'fontweight','bold')

set(gcf,'color','w');

title('Cell')

xlabel('Time (minutes)')

ylabel('TYR (nM)')

hold on

plot(time_span_exp, cell_exp_mean,'r','Marker','o','MarkerSize',10,'Linewidth', 4)

hold on

errorbar(time_span_exp,cell_exp_mean,cell_exp_std,'r', 'Linewidth', 3)

ylim([0 250]);

% legend({'Theoretical','Scenario 1a, Vmax\apical\FD, Kapical\FD',...
%       'Scenario 1b, 0.1x Vmax\apical\FD, Kapical\FD','Scenario 1c, 2x Vmax\apical,
%       Kapical\FD', 'Scenario 1d, 20x Vmax\apical, Kapical\FD'
%       'Experimental'}),...
%       'FontSize', 42)

%Plotting the Basolateral compartment results

% Figure(3)

nexttile

hold on

plot(t, baso_baseline_output, 'b', 'Linewidth',6)

grid on

```

```

hold on
plot(t, baso_sc1a_output, ':', 'Color', a_color_code, 'MarkerSize', 12, 'Linewidth', 6)
hold on
plot(t, baso_sc1b_output, ':', 'Color', b_color_code, 'MarkerSize', 12, 'Linewidth', 6)
hold on
plot(t, baso_sc1c_output, ':', 'Color', c_color_code, 'MarkerSize', 12, 'Linewidth', 6)
hold on
plot(t, baso_sc1d_output, ':', 'Color', d_color_code, 'MarkerSize', 12, 'Linewidth', 6)
set(gca, 'FontSize', 25, 'fontweight', 'bold')
set(gcf, 'color', 'w');
title('Basolateral')
xlabel('Time (minutes)')
ylabel('TYR (nM)')
hold on
plot(time_span_exp, baso_exp_mean, 'r', 'Marker', 'o', 'MarkerSize', 10, 'Linewidth', 6)
hold on
errorbar(time_span_exp, baso_exp_mean, baso_exp_std, 'r', 'Linewidth', 4)
if gt(X_apical, X_baso) %Graph limits for apical addition
    ylim([0 5])
else
    ylim([0 5]);
end
% % legend({'Theoretical', 'Scenario 1a, Vmax\_apical\_FD, Kapical\_FD', ...

```

```

%      'Scenario 1b, 0.1x Vmax\_apical\_FD, Kapical\_FD','Scenario 1c, 2x Vmax\_apical,
      Kapical\_FD', 'Scenario 1d, 20x Vmax\_apical, Kapical\_FD'
%      'Experimental'},...
%      'FontSize', 30)
end

```

```

%Combined Diffusion and Active transport function for baseline scenario

```

```

function dXdt = ODE_Combined_Diffusion_Active_Trasport_Baseline(~,X)

```

```

global alpha

```

```

global Kapical_FD

```

```

global Kbaso_AT

```

```

global Vm_apical_FD

```

```

global Vm_baso_AT

```

```

global vol_apical

```

```

global vol_cell

```

```

global vol_baso

```

```

%Apical compartment: Simple diffusion and Facilitated diffusion

```

```

diff_X1 = (-1 * (alpha / vol_apical) * ((X(1) - X(2)))) +...

```

```

    ((vol_cell/vol_apical) * ((-1) * (Vm_apical_FD*X(1) / (Kapical_FD + X(1))) +
    (Vm_apical_FD*X(2) / (Kapical_FD + X(2))));

```

```

%Cellular compartment: Simple diffusion, Active transport and Facilitated

```

```
%diffusion from the apical compartment only
```

```
diff_X2 = (-1 * (alpha / vol_cell) * (X(2) - X(1))) + (-1 * (alpha / vol_cell) * (X(2) - X(3)))...
```

```
  + ((Vm_apical_FD * X(1)) / (Kapical_FD + X(1))) + (-1) * (Vm_apical_FD * X(2) /  
    (Kapical_FD + X(2)))...
```

```
  + (Vm_baso_AT * X(3) / (Kbaso_AT + X(3)));
```

```
%Basolateral compartment: Simple diffusion, Active transport and Faciliated diffusion
```

```
diff_X3 = (-1 * (alpha / vol_baso) * ((X(3) - X(2))))...
```

```
  + (-1 * (vol_cell / vol_baso) * (Vm_baso_AT*X(3) / (Kbaso_AT + X(3))));
```

```
dXdt = [diff_X1; diff_X2; diff_X3];
```

```
end
```

```
%Combined Diffusion and Active transport function for scenarios
```

```
function dXdt = ODE_Combined_Diffusion_Active_Trasport_Scenario(~,X)
```

```
global alpha
```

```
global Kapical_FD
```

```
global Kbaso_AT
```

```
global Vm_apical_FD
```

```
global Vm_baso_AT
```

```
global vol_apical
```

global vol\_cell

global vol\_baso

global Vm\_baso\_FD\_new

global Kbaso\_FD\_new

%Apical compartment: Simple diffusion and Facilitated diffusion

diff\_X1 = (-1 \* (alpha / vol\_apical) \* ((X(1) - X(2)))) +...

((vol\_cell/vol\_apical) \* ((-1) \* (Vm\_apical\_FD\*X(1) / (Kapical\_FD + X(1))) +  
(Vm\_apical\_FD\*X(2) / (Kapical\_FD + X(2)))));

%Cellular compartment: Simple diffusion, Active transport and Facilitated diffusion from the  
apical and basolateral compartments

diff\_X2 = (-1 \* (alpha / vol\_cell) \* (X(2) - X(1))) + (-1 \* (alpha / vol\_cell) \* (X(2) - X(3)))...

+ (((Vm\_apical\_FD \* X(1)) / (Kapical\_FD + X(1))) - (Vm\_apical\_FD \* X(2) / (Kapical\_FD  
+ X(2))))...

+ (Vm\_baso\_AT \* X(3) / (Kbaso\_AT + X(3)))...

+ ((Vm\_baso\_FD\_new \* X(3) / (Kbaso\_FD\_new + X(3))) - ((Vm\_baso\_FD\_new \* X(2)) /  
(Kbaso\_FD\_new + X(2))));

%Basolateral compartment: Simple diffusion, Active transport and Facilitated

%diffusion (OCT 2 parameters)

diff\_X3 = (-1 \* (alpha / vol\_baso) \* ((X(3) - X(2))))...

+ (-1 \* (vol\_cell / vol\_baso) \* (Vm\_baso\_AT\*X(3) / (Kbaso\_AT + X(3))))...

```

+ (-1 * (vol_cell / vol_baso) * (((Vm_baso_FD_new * X(3)) / (Kbaso_FD_new + X(3))) -
(Vm_baso_FD_new * X(2) / (Kbaso_FD_new + X(2)))));

```

```

dXdt = [diff_X1; diff_X2; diff_X3];

```

```

end

```

B.iii Introducing a transporter with non-OCT2 kinetics in the basolateral membrane and plotting

```

function combined_vol_output = OCT2_in_basolateral_membrane_scenario_1()

```

```

prompt = 'Enter the concentration of the apical compartment (in nM): ';

```

```

X_apical = input(prompt);

```

```

prompt = 'Enter the concentration of the cellular compartment (in nM): ';

```

```

X_cell = input(prompt);

```

```

prompt = 'Enter the concentration of the basolateral compartment (in nM): ';

```

```

X_baso = input(prompt);

```

```

global X_initial %Define the initial concentrations for the layers (nM)

```

```

X_initial = [X_apical, X_cell, X_baso]; %Initial concentrations for three layers

```

```

global vol_apical %Volume of apical compartment

```

```

global vol_cell %Volume of cellular compartment

```

```

global vol_baso %Volume of basolateral compartment

```

```

vol_apical = 100e-6*1e-3;

```

```

vol_cell = 0.82e-6*1e-3;

```

```
vol_baso = 600e-6*1e-3;
```

```
min_conv = 60; %Used for converting seconds to mins
```

```
%%%Defining alpha for simple diffusion
```

```
global alpha %Half-life constant for membrane (min-1)
```

```
p = 22.6e-10 * min_conv; %Permeability (1/min)
```

```
A = 3.3e-5; %Surface area (m2)
```

```
alpha = p*A; %Half-life of Caco-2 cell
```

```
%%%Defining constant values for Faciliated diffusion
```

```
global Kapical_FD %Substrate concentration (nM) (Apical compartment)
```

```
global Vm_apical_FD %Maximum rate achieved (nM/min) (Apical compartment)
```

```
Kapical_FD = 101.5; %Substrate concentration for apical compartment for Facilitated  
transporter
```

```
Vm_apical_FD = 0.11 * min_conv; %Maximum rate achieved between apical and cell for  
Facilitated transporter
```

```
%%%Defining constant values for Active Transport
```

```

global Kbaso_AT    %Substrate concentration (nM)

global Vm_baso_AT  %Maximum rate achieved (nM/min)

Kbaso_AT    = 33.1; %Substrate concentration for basolateral-cell compartment for Active
              transporter

Vm_baso_AT  = 43.0 * min_conv; %Maximum rate achieved between basolateral and cell
              for Active transporter

%%%Time span for output

global T

T = 30;

tspan = 0:1:T;

%Combined diffusion and active transport (Baseline)

ODE_X_baseline = @ODE_Combined_Diffusion_Active_Trasport_Baseline;

[t,X_CD_AT] = ode45(ODE_X_baseline, tspan, X_initial); %MATLAB ODE solver

combined_vol_output = X_CD_AT;    %All the output values

apical_baseline_output = X_CD_AT(:,1); %Apical values

cell_baseline_output = X_CD_AT(:,2); %Cellular values

```

```

baso_baseline_output = X_CD_AT(:,3); %Basolateral values

%%%Introducing different scenarios of Facilitated diffusion in the basolateral compartment

%Scenario 1a, Basolateral  $500 \cdot Vm\_baso\_FD\_new = Vm\_apical\_FD$  and
%Kbaso_FD_new = Kapical

global Vm_baso_FD_new
global Kbaso_FD_new

Vm_baso_FD_new = Vm_apical_FD; %Define Vmax for FD in basolateral compartment
Kbaso_FD_new = Kapical_FD; %Define Kbaso for FD in basolateral compartment

ODE_X_scenario1a = @ODE_Combined_Diffusion_Active_Trasport_Scenario;

[t,X_SC_1a] = ode45(ODE_X_scenario1a, tspan, X_initial);

apical_sc1a_output = X_SC_1a(:,1); %Scenario 1a apical concentration values
cell_sc1a_output = X_SC_1a(:,2); %Scenario 1a cellular concentration values
baso_sc1a_output = X_SC_1a(:,3); %Scenario 1a basolateral concentration values

%Scenario 1b, Basolateral  $Vm\_baso\_FD\_new = 500 \cdot Vm\_apical\_FD$  and
%Kbaso_FD_new = 2* Kapical

```

```

Vm_baso_FD_new      = 500*Vm_apical_FD; %Define Vmax for FD in basolateral
                    compartment

Kbaso_FD_new      = 2*Kapical_FD;    %Define Kbaso for FD in basolateral compartment

ODE_X_scenario1b = @ODE_Combined_Diffusion_Active_Trasport_Scenario;

[t,X_SC_1b]      = ode45(ODE_X_scenario1b, tspan, X_initial);

apical_sc1b_output = X_SC_1b(:,1); %Scenario 1b apical concentration values
cell_sc1b_output   = X_SC_1b(:,2); %Scenario 1b cellular concentration values
baso_sc1b_output   = X_SC_1b(:,3); %Scenario 1b basolateral concentration values

%Scenario 1c, Basolateral Vm_baso_FD_new = 500 * Vm_apical_FD and
%Kbaso_FD_new =25* Kapical

Vm_baso_FD_new      = 500*Vm_apical_FD; %Define Vmax for FD in basolateral
                    compartment

Kbaso_FD_new      = 5* Kapical_FD;    %Define Kbaso for FD in basolateral compartment

ODE_X_scenario1c = @ODE_Combined_Diffusion_Active_Trasport_Scenario;

[t,X_SC_1c]      = ode45(ODE_X_scenario1c, tspan, X_initial);

```

```

apical_sc1c_output = X_SC_1c(:,1); %Scenario 1c apical concentration values
cell_sc1c_output   = X_SC_1c(:,2); %Scenario 1c cellular concentration values
baso_sc1c_output   = X_SC_1c(:,3); %Scenario 1c basolateral concentration values

%Scenario 1d, Basolateral Vm_baso_FD_new = 500* Vm_apical_FD and
%Kbaso_FD_new = 10* Kapical

Vm_baso_FD_new      = 500*Vm_apical_FD; %Define Vmax for FD in baseolateral
    compartment
Kbaso_FD_new        = 10* Kapical_FD;    %Define Kbaso for FD in baseolateral compartment

ODE_X_scenario1d = @ODE_Combined_Diffusion_Active_Trasport_Scenario;

[t,X_SC_1d]      = ode45(ODE_X_scenario1d, tspan, X_initial);

apical_sc1d_output = X_SC_1d(:,1); %Scenario 1d apical concentration values
cell_sc1d_output   = X_SC_1d(:,2); %Scenario 1d cellular concentration values
baso_sc1d_output   = X_SC_1d(:,3); %Scenario 1d basolateral concentration values

%Importing values for experimental data from matlab
if gt(X_apical , X_baso) %Apical addition to Basolateral compartment
    %Importing the Apical experimental values

```

```

apical_exp_values = xlsread('Apical_addition','Apical');
apical_exp_mean   = apical_exp_values(:,end-2); %Mean experimental values
apical_exp_std    = apical_exp_values(:,end-1); %Std err experimental values

%Importing the Cellular experimental values
cell_exp_values   = xlsread('Apical_addition','Cell');
cell_exp_mean     = cell_exp_values(:,end-2); %Mean experimental values
cell_exp_std      = cell_exp_values(:,end-1); %Std err experimental values

%Importing the Basolateral experimental values
baso_exp_values   = xlsread('Apical_addition','Baso');
baso_exp_mean     = baso_exp_values(:,end-2); %Mean experimental values
baso_exp_std      = baso_exp_values(:,end-1); %Std err experimental values

time_span_exp     = apical_exp_values(1:end,1); %Time span for the experimental values

elseif It(X_apical, X_baso) %Basolateral addition to the Apical compartment
%Importing the Apical experimental values
apical_exp_values = xlsread('Baso_addition','Apical');
apical_exp_mean   = apical_exp_values(:,end-2); %Mean experimental values
apical_exp_std    = apical_exp_values(:,end-1); %Std err experimental values

%Importing the Cellular experimental values

```

```

cell_exp_values = xlsread('Baso_addition','Cell');
cell_exp_mean   = cell_exp_values(:,end-2); %Mean experimental values
cell_exp_std    = cell_exp_values(:,end-1); %Std err experimental values

%Importing the Basolateral experimental values
baso_exp_values = xlsread('Baso_addition','Baso');
baso_exp_mean   = baso_exp_values(:,end-2); %Mean experimental values
baso_exp_std    = baso_exp_values(:,end-1); %Std err experimental values

time_span_exp   = apical_exp_values(1:end,1); %Time span for the experimental values
end

if gt(X_apical,X_baso)
    Title = 'Apical addition';
else
    Title = 'Basolateral addition';
end

%Plot of Concentration vs Time with the Experimental values superimposed
%Scenario color codes
a_color_code = [0.8500 0.3250 0.0980];
b_color_code = [0.4940 0.1840 0.5560];
c_color_code = [0.4660 0.6740 0.1880];

```

```

d_color_code = [0, 1, 1];

%Plotting the Apical compartment results

Figure(1)

nexttile

hold on

plot(t, apical_baseline_output,'b', 'Linewidth', 6)

grid on

hold on

plot(t, apical_sc1a_output,':','Color',a_color_code,'MarkerSize',12,'Linewidth',6)

hold on

plot(t, apical_sc1b_output,':','Color',b_color_code,'MarkerSize',12,'Linewidth',6)

hold on

plot(t, apical_sc1c_output,':','Color',c_color_code,'MarkerSize',12,'Linewidth',6)

hold on

plot(t, apical_sc1d_output,':','Color',d_color_code,'MarkerSize',12,'Linewidth',6)

set(gca,'FontSize',25,'fontweight','bold')

set(gcf,'color','w');

title('Apical')

xlabel('Time (minutes)')

ylabel('TYR (nM)')

hold on

plot(tim8 e_span_exp, apical_exp_mean,'r','Marker','o','MarkerSize',10,'Linewidth', 6)

```

```

hold on

errorbar(time_span_exp,apical_exp_mean,apical_exp_std,'r', 'Linewidth', 4)

if gt(X_apical, X_baso) %Graph limits for apical addition

    ylim([0 100])

else

    ylim([0 100]);

end

% legend({'Theoretical','Scenario 1a, 500* Vmax\_apical\_FD, Kapical\_FD',...
%         'Scenario 1b, 500x Vmax\_apical\_FD, 2* Kapical\_FD','Scenario 1c, 500x
%         Vmax\_apical, Kapical\_FD', 'Scenario 1d, 500x Vmax\_apical, 10* Kapical\_FD',...
%         'Experimental'},...
%         'FontSize', 30)

legend({'Baseline simulation', Vmax\_OCT2, Kt\_OCT2',...
        '0.1* Vmax\_OCT2, Kt\_OCT2',' 2* Vmax\_OCT2, Kt\_OCT2', '20* Vmax\_OCT2,
        Kt\_OCT2',...
        'Experimental'},...
        'FontSize', 20)

%Plotting the Cellular compartment results

% Figure(2)

nexttile

hold on

plot(t, cell_baseline_output, 'b', 'Linewidth', 6)

grid on

```

```

hold on
plot(t, cell_sc1a_output,':','Color',a_color_code,'MarkerSize',12,'Linewidth',6)
hold on
plot(t, cell_sc1b_output,':','Color',b_color_code,'MarkerSize',12,'Linewidth',6)
hold on
plot(t, cell_sc1c_output,':','Color',c_color_code,'MarkerSize',12,'Linewidth',6)
hold on
plot(t, cell_sc1d_output,':','Color',d_color_code,'MarkerSize',12,'Linewidth',6)
set(gca,'FontSize',25,'fontweight','bold')
set(gcf,'color','w');
title('Cell')
xlabel('Time (minutes)')
ylabel('TYR (nM)')
hold on
plot(time_span_exp, cell_exp_mean,'r','Marker','o','MarkerSize',10,'Linewidth', 4)
hold on
errorbar(time_span_exp,cell_exp_mean,cell_exp_std,'r', 'Linewidth', 3)
ylim([0 250]);

% legend({'Theoretical','Scenario 1a, 500* Vmax\_apical\_FD, Kapical\_FD',...
        'Scenario 1b, 500x Vmax\_apical\_FD, 2* Kapical\_FD','Scenario 1c, 500x
        Vmax\_apical, Kapical\_FD', 'Scenario 1d, 500x Vmax\_apical, 10* Kapical\_FD',...
        %      'Experimental'},...

```

```

%      'Experimental'},...
%      'FontSize', 42)

%Plotting the Basolateral compartment results
% Figure(3)
nexttile
hold on
plot(t, baso_baseline_output, 'b', 'Linewidth',6)
grid on
hold on
plot(t, baso_sc1a_output, ':', 'Color', a_color_code, 'MarkerSize', 12, 'Linewidth', 6)
hold on
plot(t, baso_sc1b_output, ':', 'Color', b_color_code, 'MarkerSize', 12, 'Linewidth', 6)
hold on
plot(t, baso_sc1c_output, ':', 'Color', c_color_code, 'MarkerSize', 12, 'Linewidth', 6)
hold on
plot(t, baso_sc1d_output, ':', 'Color', d_color_code, 'MarkerSize', 12, 'Linewidth', 6)
set(gca, 'FontSize', 25, 'fontweight', 'bold')
set(gcf, 'color', 'w');

```

```

title('Basolateral')
xlabel('Time (minutes)')
ylabel('TYR (nM)')
hold on
plot(time_span_exp, baso_exp_mean,'r','Marker','o','MarkerSize',10,'Linewidth', 6)
hold on
errorbar(time_span_exp,baso_exp_mean,baso_exp_std,'r', 'Linewidth', 4)
if gt(X_apical, X_baso) %Graph limits for apical addition
    ylim([0 5])
else
    ylim([0 5]);
end
% % legend({'Theoretical','Scenario 1a, 500* Vmax\_apical\_FD, Kapical\_FD',...
    'Scenario 1b, 500x Vmax\_apical\_FD, 2* Kapical\_FD','Scenario 1c, 500x Vmax\_apical,
    Kapical\_FD', 'Scenario 1d, 500x Vmax\_apical, 10* Kapical\_FD',...
%     'Experimental'},...
%     'Experimental'},...
%     'FontSize', 30)
end

%Combined Diffusion and Active transport function for baseline scenario
function dXdt = ODE_Combined_Diffusion_Active_Trasport_Baseline(~,X)
global alpha

```

global Kapical\_FD

global Kbaso\_AT

global Vm\_apical\_FD

global Vm\_baso\_AT

global vol\_apical

global vol\_cell

global vol\_baso

%Apical compartment: Simple diffusion and Facilitated diffusion

diff\_X1 = (-1 \* (alpha / vol\_apical) \* ((X(1) - X(2)))) +...

((vol\_cell/vol\_apical) \* ((-1) \* (Vm\_apical\_FD\*X(1) / (Kapical\_FD + X(1))) +  
(Vm\_apical\_FD\*X(2) / (Kapical\_FD + X(2)))));

%Cellular compartment: Simple diffusion, Active transport and Facilitated

%diffusion from the apical compartment only

diff\_X2 = (-1 \* (alpha / vol\_cell) \* (X(2) - X(1))) + (-1 \* (alpha / vol\_cell) \* (X(2) - X(3)))...

+ ((Vm\_apical\_FD \* X(1)) / (Kapical\_FD + X(1))) + (-1) \* (Vm\_apical\_FD \* X(2) /  
(Kapical\_FD + X(2)))...

+ (Vm\_baso\_AT \* X(3) / (Kbaso\_AT + X(3)));

%Basolateral compartment: Simple diffusion, Active transport and Facilitated diffusion

diff\_X3 = (-1 \* (alpha / vol\_baso) \* ((X(3) - X(2))))...

+ (-1 \* (vol\_cell / vol\_baso) \* (Vm\_baso\_AT\*X(3) / (Kbaso\_AT + X(3))));

```
dXdt = [diff_X1; diff_X2; diff_X3];
```

```
end
```

```
%Combined Diffusion and Active transport function for scenarios
```

```
function dXdt = ODE_Combined_Diffusion_Active_Trasport_Scenario(~,X)
```

```
global alpha
```

```
global Kapical_FD
```

```
global Kbaso_AT
```

```
global Vm_apical_FD
```

```
global Vm_baso_AT
```

```
global vol_apical
```

```
global vol_cell
```

```
global vol_baso
```

```
global Vm_baso_FD_new
```

```
global Kbaso_FD_new
```

```
%Apical compartment: Simple diffusion and Facilitated diffusion
```

```
diff_X1 = (-1 * (alpha / vol_apical) * ((X(1) - X(2)))) +...
```

```
((vol_cell/vol_apical) * ((-1) * (Vm_apical_FD*X(1) / (Kapical_FD + X(1))) +  
(Vm_apical_FD*X(2) / (Kapical_FD + X(2)))));
```

%Cellular compartment: Simple diffusion, Active transport and Facilitated diffusion from the apical and basolateral compartments

```
diff_X2 = (-1 * (alpha / vol_cell) * (X(2) - X(1))) + (-1 * (alpha / vol_cell) * (X(2) - X(3)))...
+ (((Vm_apical_FD * X(1)) / (Kapical_FD + X(1))) - (Vm_apical_FD * X(2) / (Kapical_FD
+ X(2))))...
+ (Vm_baso_AT * X(3) / (Kbaso_AT + X(3)))...
+ ((Vm_baso_FD_new * X(3) / (Kbaso_FD_new + X(3))) - ((Vm_baso_FD_new * X(2)) /
(Kbaso_FD_new + X(2))));
```

%Basolateral compartment: Simple diffusion, Active transport and Facilitated

%diffusion (OCT 2 parameters)

```
diff_X3 = (-1 * (alpha / vol_baso) * ((X(3) - X(2))))...
+ (-1 * (vol_cell / vol_baso) * (Vm_baso_AT*X(3) / (Kbaso_AT + X(3))))...
+ (-1 * (vol_cell / vol_baso) * (((Vm_baso_FD_new * X(3)) / (Kbaso_FD_new + X(3))) -
(Vm_baso_FD_new * X(2) / (Kbaso_FD_new + X(2)))));
```

```
dXdt = [diff_X1; diff_X2; diff_X3];
```

```
end
```

B.iv. Solving for asymmetry and plotting

Objective functions

```
function parameter_fit = all_unknowns_objective_function_I_value(input, z, Vm_apical_FD,
Kapical_FD_apical, Kapical_FD_cell, Vm_baso_AT, Kbaso_AT, Vm_baso_FD_new,
Kbaso_FD_new_cell, Kbaso_FD_new_baso)
```

```
variable_list = readTable('variables.xlsx'); %Import the variables
```

```
%%%Define the global parameters (constant)
```

```
%Define the volume for each of the compartments (defined in cubic meters)
```

```
vol_apical = variable_list.Value(1);
```

```
vol_cell = variable_list.Value(2);
```

```
vol_baso = variable_list.Value(3);
```

```
min_conv = variable_list.Value(4); %Used for converting seconds to mins
```

```
%Defining alpha for simple diffusion
```

```
alpha = variable_list.Value(7); %Half-life of Caco-2 cell
```

```
%Time span for output
```

```
T = variable_list.Value(8); %in mins
```

```
dt = 1/30; %Sampling interval in mins
```

```
tspan = 0:dt:T;
```

```
%Ratio of volumes
```

```
y1 = (vol_cell/vol_apical);
```

```
y2 = (vol_cell/vol_baso);
```

```
%Checking for apical or basolateral addition
```

```
if eq(input,1)
```

```
    apical_addition = 1;
```

```
else
```

```
    apical_addition = 0;
```

```
end
```

```
%%%Linear fit parameters for the Cellular and Basolateral compartments only (taken from
```

```
%GraphPad Prism)
```

```
%%%Apical addition
```

```
if eq(apical_addition,1)
```

```
    %Apical compartment
```

```
    slope_apical = -0.5258;
```

```
    delta_apical = 87.27;
```

```
    X_apical_linear = slope_apical.*tspan + delta_apical;
```

```
    %Basolateral compartment
```

```
    slope_baso = 0.06756;
```

```
    delta_baso = 0.09246;
```

```
    X_baso_linear = slope_baso.*tspan + delta_baso;
```

```

%Cellular compartment

slope_cell = 1.627.*ones(size(tspan));

delta_cell = 98.27;

X_cell_linear = slope_cell.*tspan + delta_cell;

else

%%%Basolateral addition

%Apical compartment

slope_apical = 0.3168;

delta_apical = 1.670;

X_apical_linear = slope_apical.*tspan + delta_apical;

%Basolateral compartment

slope_baso = -0.08764;

delta_baso = 83.65;

X_baso_linear = slope_baso.*tspan + delta_baso;

%Cellular compartment

slope_cell = 9.268.*ones(size(tspan));

delta_cell = 464.8;

X_cell_linear = slope_cell.*tspan + delta_cell;

end

```

%The experimentally derived value set (delta values)

f\_apical = slope\_apical;

f\_cell = slope\_cell;

f\_baso = slope\_baso;

%F-values includes Simple Diffusion, Facilitated Diffusion and Active

%Transport

F\_apical = (alpha / vol\_apical) .\* ((z.\*X\_cell\_linear) - X\_apical\_linear) +...

y1 .\* ( (( Vm\_apical\_FD .\* (z.\* X\_cell\_linear) )./( Kapical\_FD\_cell + (z.\* X\_cell\_linear) ))...  
- (( Vm\_apical\_FD .\* X\_apical\_linear )./( Kapical\_FD\_apical + X\_apical\_linear )) );

F\_cell = -1.\*(alpha / vol\_apical) .\* ((z.\* X\_cell\_linear) - X\_apical\_linear) +...

-1.\*(alpha / vol\_baso) .\* ((z.\* X\_cell\_linear) - X\_baso\_linear) + ...

( (Vm\_apical\_FD .\* X\_apical\_linear)./(Kapical\_FD\_apical + X\_apical\_linear)...

- (Vm\_apical\_FD .\* (z.\* X\_cell\_linear))./(Kapical\_FD\_cell + (z.\* X\_cell\_linear)) )...

+ (Vm\_baso\_AT \* X\_baso\_linear) ./ (Kbaso\_AT + X\_baso\_linear)...

+ ( (Vm\_baso\_FD\_new .\* X\_baso\_linear)./(Kbaso\_FD\_new\_baso + X\_baso\_linear)...

- (Vm\_baso\_FD\_new .\* (z.\* X\_cell\_linear))./(Kbaso\_FD\_new\_cell + (z.\* X\_cell\_linear)) );

F\_baso = (alpha / vol\_baso) .\* ((z.\* X\_cell\_linear) - X\_baso\_linear) +...

y2 .\* ( (Vm\_baso\_FD\_new.\* (z.\* X\_cell\_linear))./(Kbaso\_FD\_new\_cell + (z.\*  
X\_cell\_linear))...

```
- (Vm_baso_FD_new.*X_baso_linear)./(Kbaso_FD_new_baso + X_baso_linear)...  
- (Vm_baso_AT*X_baso_linear ./ (Kbaso_AT + X_baso_linear)) );
```

```
obj_apical = sum((F_apical(1:end) - f_apical).^2);
```

```
obj_cell = sum((F_cell(1:end) - f_cell).^2);
```

```
obj_baso = sum((F_baso(1:end) - f_baso).^2);
```

```
%Cumulative objective functions
```

```
obj = (obj_apical + obj_cell + obj_baso);
```

```
parameter_fit = obj;
```

```
end
```

```
Kinetic parameters solver
```

```
%This model only requires the plot and the input file
```

```
%Set the fixed parameters
```

```
variable_list = readTable('variables.xlsx');
```

```
min_conv = variable_list.Value(4); %Conversion from seconds to minutes
```

```
%Set the fixed variables
```

```
z = 1;
```

```

Vm_apical_FD      = 2.25 * min_conv;
Kapical_FD_apical = 110.36;
% Kapical_FD_cell = 1227.86; %Adjust symmetric parameters
Kapical_FD_cell   = 1227.86;

Vm_baso_AT        = 3.32 * min_conv;
Kbaso_AT          = 29.04;

Vm_baso_FD_new    = 5.98 * min_conv;
Kbaso_FD_new_cell = 628.255;
Kbaso_FD_new_baso = 584.1;

% %Solving apical and basolateral additions simultaneously
% obj_apical      = all_unknowns_objective_function_I_value(1, z, Vm_apical_FD,
Kapical_FD_apical, Kapical_FD_cell, Vm_baso_AT, Kbaso_AT, Vm_baso_FD_new,
Kbaso_FD_new_cell, Kbaso_FD_new_baso); %Apical addition
% obj_baso        = all_unknowns_objective_function_I_value(2, z, Vm_apical_FD,
Kapical_FD_apical, Kapical_FD_cell, Vm_baso_AT, Kbaso_AT, Vm_baso_FD_new,
Kbaso_FD_new_cell, Kbaso_FD_new_baso); %Basolateral addition
%
% %Solve simltaenously
% objective = sum(obj_apical,obj_baso);

```

```

% Solve for apical addition objective functions only
% objective = obj_apical;

% Solve for basolateral addition objective functions only
% objective = obj_baso;

% % Change the algorithm properties using the variables below

% evals    = 1e12;
% max_iter = 1e12;
% opt_tol  = 1e-10;
% func_tol = 1e-15;
% step_tol = 1e-12;

%
%
%                               options                               =
optimoptions(@lsqnonlin,'MaxFunctionEvaluations',evals,'MaxIterations',max_iter,...
% 'StepTolerance',step_tol,...
% 'OptimalityTolerance',opt_tol,'FunctionTolerance',func_tol,'Algorithm', 'levenberg-
marquardt');

%
% % The least squares problem
%
% lsqproblem = optimproblem("Objective",objective);
%

```

```

% %Optimization problem

% [sol,~] = solve(lsqproblem,x0,'Options',options);

% show(lsqproblem)

disp('The z-factor value')

disp(z)

disp('The value of Vm_apical_FD (nM/min)')

disp(Vm_apical_FD)

disp('The value of Kapical_FD_apical (nM)')

disp(Kapical_FD_apical)

disp('The value of Kapical_FD_cell (nM)')

disp(Kapical_FD_cell)

disp('The value of Vm_baso_AT (nM/min)')

disp(Vm_baso_AT)

disp('The value of Kbaso_AT (nM)')

disp(Kbaso_AT)

disp('The value of Vm_baso_FD_new (nM/min)')

disp(Vm_baso_FD_new)

disp('The value of Kbaso_FD_new_baso (nM)')

disp(Kbaso_FD_new_baso)

```

```
disp('The value of Kbaso_FD_new_cell (nM)')
```

```
disp(Kbaso_FD_new_cell)
```

```
%Apical Plots
```

```
X_apical = 88.85;
```

```
X_cell = 0;
```

```
X_baso = 0;
```

```
X_i = 0;
```

```
fig_index = 1;
```

```
all_unkowns_solver_plots_I_value(X_apical, X_cell, X_baso,...
```

```
z,...
```

```
Vm_apical_FD, Kapical_FD_apical, Kapical_FD_cell,...
```

```
Vm_baso_AT, Kbaso_AT,...
```

```
Vm_baso_FD_new, Kbaso_FD_new_cell, Kbaso_FD_new_baso,...
```

```
fig_index)
```

```
%Basolateral Plots
```

```
X_apical = 0;
```

```
X_cell = 0;
```

```
X_baso = 82.9;
```

```
fig_index = 4;
```

```

all_unkowns_solver_plots_I_value(X_apical, X_cell, X_baso,...
    Z,...
    Vm_apical_FD, Kapical_FD_apical, Kapical_FD_cell,...
    Vm_baso_AT, Kbaso_AT,...
    Vm_baso_FD_new, Kbaso_FD_new_cell, Kbaso_FD_new_baso,...
    fig_index)

```

For plotting with asymmetry

```

function combined_vol_output = all_unkowns_solver_plots_I_value(X_apical, X_cell,
    X_baso,...
    Z,...
    Vm_a_fd, Kt_a_1, Kt_a_2,...
    Vm_b_AT, Kt_b_AT,...
    Vm_var_2, Kt_var_c, Kt_var_b,...
    fig_counter)

```

```

global X_initial %Define the initial concentrations for the layers (nM)

```

```

X_initial = [X_apical, X_cell, X_baso]; %Initial concentrations for three layers

```

```

%%%The z-factor

```

```

global z

```

$z = Z;$

variable\_list = readTable('variables.xlsx'); %Import the variables

%%%Defining the transport values for Facilitated diffusion (Apical and Cell)

global Vm\_apical\_FD %Maximum rate achieved (nM/min) (Apical compartment)

global Kapical\_FD\_apical %Substrate concentration (nM) for apical (Apical compartment)

global Kapical\_FD\_cell %Substrate concentration (nM) fo cell (Apical compartment)

Vm\_apical\_FD = Vm\_a\_fd; %Maximum rate achieved between apical and cell for  
Facilitated transporter

Kapical\_FD\_apical = Kt\_a\_1; %Substrate concentration for apical compartment to cell  
compartment for Facilitated transporter

Kapical\_FD\_cell = Kt\_a\_2; %Substrate concentration for cell comarptment to apical  
compartment for Facilitated transporter

%%%Defining the transport values for Active Transport (Cell and Baso)

global Kbaso\_AT %Substrate concentration (nM)

global Vm\_baso\_AT %Maximum rate achieved (nM/min)

```
Vm_baso_AT = Vm_b_AT; %Maximum rate achieved between basolateral and cell for  
Active transporter
```

```
Kbaso_AT = Kt_b_AT; %Substrate concentration for basolateral-cell compartment for  
Active transporter
```

```
%%%Defining the transport values for the asymmetric (Cell and Baso)
```

```
global Vm_baso_FD_new
```

```
global Kbaso_FD_new_cell
```

```
global Kbaso_FD_new_baso
```

```
Vm_baso_FD_new = Vm_var_2; %Define Vmax for FD in basolateral compartment
```

```
Kbaso_FD_new_cell = Kt_var_c; %Define Kbaso for FD wrt cell
```

```
Kbaso_FD_new_baso = Kt_var_b; %Define Kbaso for FD wrt baso
```

```
%%%Time span for output
```

```
T = variable_list.Value(8); %Time period
```

```
dt = 0.1/60;
```

```
tspan = 0:dt:T;
```

```
%%%Combined diffusion and active transport (Baseline)
```

```
ODE_X_baseline = @ODE_Combined_Diffusion_Active_Transport_Baseline;
```

```
[~,X_CD_AT] = ode45(ODE_X_baseline, tspan, X_initial); %MATLAB ODE solver
```

```

combined_vol_output = X_CD_AT;      %All the output values
apical_baseline_output = X_CD_AT(:,1); %Apical values
cell_baseline_output = X_CD_AT(:,2); %Cellular values
baso_baseline_output = X_CD_AT(:,3); %Basolateral values

%Solving for all the scenario that includes all the transport processes
ODE_X_scenario_1 = @ODE_Combined_Diffusion_Active_Trasport_Scenario;

[t,X_SC_1] = ode45(ODE_X_scenario_1, tspan, X_initial);

apical_sc1_output = X_SC_1(:,1); %Scenario apical concetration values
cell_sc1_output = X_SC_1(:,2); %Scenario cellular concentration values
baso_sc1_output = X_SC_1(:,3); %Scenario basolateral concentration values
% i_sc1_output = X_SC_1(:,4); %Scenario inner concentration values

if gt(X_apical,X_baso)
    Title = 'Apical addition';
else
    Title = 'Basolateral addition';
end

%Importing values for experimental data from matlab

```

```

if gt(X_apical , X_baso) %Apical addition to Basolateral compartment

    %Importing the Apical experimental values

    apical_exp_values = xlsread('Apical_addition','Apical');

    apical_exp_mean   = apical_exp_values(:,end-2); %Mean experimental values
    apical_exp_std    = apical_exp_values(:,end-1); %Std err experimental values

    %Importing the Cellular experimental values

    cell_exp_values   = xlsread('Apical_addition','Cell');

    cell_exp_mean     = cell_exp_values(:,end-2); %Mean experimental values
    cell_exp_std      = cell_exp_values(:,end-1); %Std err experimental values

    %Importing the Basolateral experimental values

    baso_exp_values   = xlsread('Apical_addition','Baso');

    baso_exp_mean     = baso_exp_values(:,end-2); %Mean experimental values
    baso_exp_std      = baso_exp_values(:,end-1); %Std err experimental values

    time_span_exp     = apical_exp_values(1:end,1); %Time span for the experimental values

elseif lt(X_apical, X_baso) %Basolateral addition to the Apical compartment

    %Importing the Apical experimental values

    apical_exp_values = xlsread('Baso_addition','Apical');

    apical_exp_mean   = apical_exp_values(:,end-2); %Mean experimental values
    apical_exp_std    = apical_exp_values(:,end-1); %Std err experimental values

```

```

%Importing the Cellular experimental values

cell_exp_values = xlsread('Baso_addition','Cell');

cell_exp_mean = cell_exp_values(:,end-2); %Mean experimental values
cell_exp_std = cell_exp_values(:,end-1); %Std err experimental values

%Importing the Basolateral experimental values

baso_exp_values = xlsread('Baso_addition','Baso');

baso_exp_mean = baso_exp_values(:,end-2); %Mean experimental values
baso_exp_std = baso_exp_values(:,end-1); %Std err experimental values

time_span_exp = apical_exp_values(1:end,1); %Time span for the experimental values

end

%Plot of Concentration vs Time with the Experimental values superimposed

% Plotting the Apical compartment results

Figure(fig_counter)

% plot(t, apical_baseline_output,'b', 'Linewidth', 4)

% hold on

plot(t, apical_sc1_output, 'g', 'Linewidth', 4)

hold on

grid on

set(gca,'FontSize',28,'fontweight','bold')

```

```

set(gcf,'color','w');
title(Title,'fontweight','bold');
xlabel('Time (minutes)','fontweight','bold');
ylabel('Apical Concentration (nM)','fontweight','bold');
hold on
plot(time_span_exp, apical_exp_mean,'r','Marker','o','MarkerSize',10,'Linewidth', 4)
hold on
errorbar(time_span_exp,apical_exp_mean,apical_exp_std,'r', 'Linewidth', 2)
legend({'Additional Transporter','Experimental'},FontSize,20)
% legend({'Simulated with Additional Transporter','Experimental'},FontSize,20)

%Plotting the Cellular compartment results
Figure(fig_counter+1)
% plot(t, cell_baseline_output, 'b', 'Linewidth', 4)
% hold on
plot(t, cell_sc1_output, 'g', 'Linewidth', 4)
grid on
set(gca,'FontSize',28,'fontweight','bold')
set(gcf,'color','w');
title(Title,'fontweight','bold')
xlabel('Time (minutes)','fontweight','bold')
ylabel('Cellular Concentration (nM)','fontweight','bold')
hold on

```

```

plot(time_span_exp, cell_exp_mean, 'r', 'Marker', 'o', 'MarkerSize', 10, 'Linewidth', 4)

hold on

errorbar(time_span_exp, cell_exp_mean, cell_exp_std, 'r', 'Linewidth', 2)

legend({'Additional Transporter', 'Experimental'}, 'FontSize', 20)

% legend({'Simulated with Additional Transporter', 'Experimental'}, 'FontSize', 20)

%Plotting the Basolateral compartment results

Figure(fig_counter+2)

% plot(t, baso_baseline_output, 'b', 'Linewidth', 4)

% hold on

plot(t, baso_sc1_output, 'g', 'Linewidth', 4)

grid on

set(gca, 'FontSize', 28, 'fontweight', 'bold')

set(gcf, 'color', 'w');

title('Title', 'fontweight', 'bold')

xlabel('Time (minutes)', 'fontweight', 'bold')

ylabel('Basolateral Concentration (nM)', 'fontweight', 'bold')

hold on

plot(time_span_exp, baso_exp_mean, 'r', 'Marker', 'o', 'MarkerSize', 10, 'Linewidth', 4)

hold on

errorbar(time_span_exp, baso_exp_mean, baso_exp_std, 'r', 'Linewidth', 2)

legend({'Additional Transporter', 'Experimental'}, 'FontSize', 20)

% legend({'Simulated with Additional Transporter', 'Experimental'}, 'FontSize', 20)

```

```

%
% Figure(fig_counter+3)
% nexttile
% hold on
% plot(t, apical_sc1_output, 'g', 'Linewidth', 4)
% hold on
% grid on
% set(gca,'FontSize',22,'fontweight','bold')
% set(gcf,'color','w');
% title(Title,'fontweight','bold');
% xlabel('Time (minutes)','fontweight','bold');
% ylabel('Apical Concentration (nM)','fontweight','bold');
% hold on
% plot(time_span_exp, apical_exp_mean,'r','Marker','o','MarkerSize',10,'Linewidth', 4)
% hold on
% errorbar(time_span_exp,apical_exp_mean,apical_exp_std,'r', 'Linewidth', 2)
%
% nexttile
% hold on
% plot(t, cell_sc1_output, 'g', 'Linewidth', 4)
% grid on
% set(gca,'FontSize',22,'fontweight','bold')
% set(gcf,'color','w');

```

```

% title(Title,'fontweight','bold')

% xlabel('Time (minutes)','fontweight','bold')

% ylabel('Cellular Concentration (nM)','fontweight','bold')

% hold on

% plot(time_span_exp, cell_exp_mean,'r','Marker','o','MarkerSize',10,'Linewidth', 4)

% hold on

% errorbar(time_span_exp,cell_exp_mean,cell_exp_std,'r', 'Linewidth', 2)

% hold on

% inner compartment plot comparison

% c = 0.9;

% inner_plot = cell_sc1_output + (1 - c).* i_sc1_output; %inner plot values

% plot(t,inner_plot, 'b', 'Linewidth', 2, 'LineStyle', '--')

%

% nexttile

% hold on

% plot(t, baso_sc1_output, 'g', 'Linewidth', 4)

% grid on

% set(gca,'FontSize',22,'fontweight','bold')

% set(gcf,'color','w');

% title(Title,'fontweight','bold')

% xlabel('Time (minutes)','fontweight','bold')

% ylabel('Basolateral Concentration (nM)','fontweight','bold')

% hold on

```

```

% plot(time_span_exp, baso_exp_mean,'r','Marker','o','MarkerSize',10,'Linewidth', 4)

% hold on

% errorbar(time_span_exp,baso_exp_mean,baso_exp_std,'r', 'Linewidth', 2)

%The RMSD values

if gt(X_apical,X_baso)

    disp('Apical addition RMSD values');

else

    disp('Basolateral addition RMSD values');

end

a_rmsd = zeros;

b_rmsd = zeros;

c_rmsd = zeros;

counter = 1;

for i = 1:size(tspan,2)

    if eq(tspan(i),time_span_exp(counter))

        a_rmsd(counter) = apical_sc1_output(i);

        b_rmsd(counter) = baso_sc1_output(i);

        c_rmsd(counter) = cell_sc1_output(i);

        counter= counter + 1;

    end

```

```
end
```

```
RMSD = [rms(a_rmsd-apical_exp_mean');rms(c_rmsd(2:end)-  
cell_exp_mean(2:end));rms(b_rmsd-baso_exp_mean')];
```

```
combined_vol_output = RMSD;
```

```
end
```

```
%Combined Diffusion and Active transport function for baseline scenario
```

```
function dXdt = ODE_Combined_Diffusion_Active_Trasport_Baseline(~,X)
```

```
variable_list = readTable('variables.xlsx'); %Import the variables
```

```
%%%Define the volume for each of the compartments (defined in cubic meters)
```

```
vol_apical = variable_list.Value(1);
```

```
vol_cell = variable_list.Value(2);
```

```
vol_baso = variable_list.Value(3);
```

```
%Half-life of Caco-2 cell
```

```
alpha = variable_list.Value(7);
```

```
global Kapical_FD_apical
```

global Kbaso\_AT

global Vm\_baso\_AT

global Vm\_apical\_FD

%Apical compartment: Simple diffusion and Facilitated diffusion

diff\_X1 = (-1 \* (alpha / vol\_apical) \* ((X(1) - X(2))))...

+ ((vol\_cell/vol\_apical) \* ((-1) \* (Vm\_apical\_FD\*X(1) / (Kapical\_FD\_apical + X(1))) +  
(Vm\_apical\_FD\*X(2) / (Kapical\_FD\_apical + X(2)))));

%Cellular compartment: Simple diffusion, Active transport and Facilitated

%diffusion

diff\_X2 = (-1 \* (alpha / vol\_cell) \* (X(2) - X(1))) + (-1 \* (alpha / vol\_cell) \* (X(2) - X(3)))...

+ ((Vm\_apical\_FD \* X(1)) / (Kapical\_FD\_apical + X(1))) + (-1) \* (Vm\_apical\_FD \* X(2) /  
(Kapical\_FD\_apical + X(2)))...

+ (Vm\_baso\_AT \* X(3) / (Kbaso\_AT + X(3)));

%Basolateral compartment: Simple diffusion and Active transport

diff\_X3 = (-1 \* (alpha / vol\_baso) \* ((X(3) - X(2))))...

+ (-1 \* (vol\_cell / vol\_baso) \* (Vm\_baso\_AT\*X(3) / (Kbaso\_AT + X(3))));

dXdt = [diff\_X1; diff\_X2; diff\_X3];

```

end

%Combined Diffusion and Active transport function for scenarios (with z
%factor)

function dXdt = ODE_Combined_Diffusion_Active_Trasport_Scenario(~,X)

variable_list = readTable('variables.xlsx'); %Import the variables

%%%Define the volume for each of the compartments (defined in cubic meters)

vol_apical = variable_list.Value(1);
vol_cell   = variable_list.Value(2);
vol_baso   = variable_list.Value(3);
vol_i      = variable_list.Value(9);

%Half-life of Caco-2 cell
alpha      = variable_list.Value(7);

global z

global Vm_apical_FD
global Kapical_FD_apical
global Kapical_FD_cell

```

global Kbaso\_AT

global Vm\_baso\_AT

global Vm\_baso\_FD\_new

global Kbaso\_FD\_new\_cell

global Kbaso\_FD\_new\_baso

% Apical compartment: Simple diffusion and Facilitated diffusion

diff\_X1 = (-1 \* (alpha / vol\_apical) \* ((X(1) - (z\*X(2)))) + ...

((vol\_cell/vol\_apical) \* ((-1) \* (Vm\_apical\_FD\*X(1) / (Kapical\_FD\_apical + X(1))))...

+ (Vm\_apical\_FD\*(z\*X(2)) / (Kapical\_FD\_cell + (z\*X(2)))));

% Cellular compartment: Simple diffusion, Active transport and Facilitated

% diffusion from the apical and basolateral compartments and inner

% compartment

diff\_X2 = (-1 \* (alpha / vol\_cell) \* ((z\*X(2)) - X(1))) + (-1 \* (alpha / vol\_cell) \* ((z\*X(2)) - X(3)))...

+ (((Vm\_apical\_FD \* X(1)) / (Kapical\_FD\_apical + X(1))) - (Vm\_apical\_FD \* (z\*X(2)) / (Kapical\_FD\_cell + (z\*X(2)))))...

+ (Vm\_baso\_AT \* X(3) / (Kbaso\_AT + X(3)))...

+ ((Vm\_baso\_FD\_new \* X(3) / (Kbaso\_FD\_new\_baso + X(3))) ...

- ((Vm\_baso\_FD\_new \* (z\*X(2))) / (Kbaso\_FD\_new\_cell + (z\*X(2)))));

%Basolateral compartment: Simple diffusion, Active transport and Faciliated diffusion

```
diff_X3 = (-1 * (alpha / vol_baso) * ((X(3) - (z*X(2)))))...  
+ (-1 * (vol_cell / vol_baso) * (Vm_baso_AT*X(3) / (Kbaso_AT + X(3))))...  
+ (-1 * (vol_cell / vol_baso) * (((Vm_baso_FD_new * X(3)) / (Kbaso_FD_new_baso +  
X(3))))...  
- (Vm_baso_FD_new * (z*X(2)) / (Kbaso_FD_new_cell + (z*X(2)))));
```

```
dXdt = [diff_X1; diff_X2; diff_X3];
```

```
end
```

B.v. Solving for intracellular compartmentalization and plotting

Objective functions

```
function parameter_fit = all_unknowns_objective_function_I_value(input, z, Vm_apical_FD,  
Kapical_FD_apical, Kapical_FD_cell, Vm_baso_AT, Kbaso_AT, Vm_baso_FD_new,  
Kbaso_FD_new_cell, Kbaso_FD_new_baso)
```

```
variable_list = readTable('variables.xlsx'); %Import the variables
```

```
%%%Define the global parameters (constant)
```

%Define the volume for each of the compartments (defined in cubic meters)

vol\_apical = variable\_list.Value(1);

vol\_cell = variable\_list.Value(2);

vol\_baso = variable\_list.Value(3);

min\_conv = variable\_list.Value(4); %Used for converting seconds to mins

%Defining alpha for simple diffusion

alpha = variable\_list.Value(7); %Half-life of TYR

%Time span for output

T = variable\_list.Value(8); %in mins

dt = 1/60; %Sampling interval in mins

tspan = 0:dt:T;

%Ratio of volumes

y1 = (vol\_cell/vol\_apical);

y2 = (vol\_cell/vol\_baso);

```
%Checking for apical or basolateral addition
```

```
if eq(input,1)
```

```
    apical_addition = 1;
```

```
else
```

```
    apical_addition = 0;
```

```
end
```

```
%%%%Linear fit parameters for the Cellular and Basolateral compartments only (taken from
```

```
%GraphPad Prism)
```

```
%%%%Apical addition
```

```
if eq(apical_addition,1)
```

```
    %Apical compartment
```

```
    slope_apical = -0.5258;
```

```
    delta_apical = 87.27;
```

```
    X_apical_linear = slope_apical.*tspan + delta_apical;
```

```
    %Basolateral compartment
```

```
slope_baso = 0.06756;  
  
delta_baso = 0.09246;  
  
X_baso_linear = slope_baso.*tspan + delta_baso;
```

```
%Cellular compartment
```

```
slope_cell = 1.627.*ones(size(tspan));  
  
delta_cell = 98.27;  
  
X_cell_linear = slope_cell.*tspan + delta_cell;
```

```
else
```

```
%%%Basolateral addition
```

```
%Apical compartment
```

```
slope_apical = 0.3168;  
  
delta_apical = 1.670;  
  
X_apical_linear = slope_apical.*tspan + delta_apical;
```

```
%Basolateral compartment
```

```
slope_baso = -0.08764;  
  
delta_baso = 83.65;
```

```

X_baso_linear = slope_baso.*tspan + delta_baso;

%Cellular compartment

slope_cell = 9.268.*ones(size(tspan));

delta_cell = 464.8;

X_cell_linear = slope_cell.*tspan + delta_cell;

end

%The experimentally derived value set (delta values)

f_apical = slope_apical;

f_cell = slope_cell;

f_baso = slope_baso;

%% %The objective functions

% Apical-Cell membrane values

% Vm_apical_FD = optimvar('Vm_apical_FD', 1, "LowerBound", 0);

% Kapical_FD_apical = optimvar('Kapical_FD_apical', 1, "LowerBound", 0);

```

```
% Kapical_FD_cell = optimvar('Kapical_FD_cell', 1, "LowerBound", 0);
```

```
% Basolateral-Cell membrane values
```

```
% Vm_baso_AT = optimvar('Vm_baso_AT', 1, "LowerBound", 0);
```

```
% Kbaso_AT = optimvar('Kbaso_AT', 1, "LowerBound", 0);
```

```
% Vm_baso_FD_new = optimvar('Vm_baso_FD_new', 1, "LowerBound", 0);
```

```
% Kbaso_FD_new_baso = optimvar('Kbaso_FD_new_baso', 1, "LowerBound", 0);
```

```
% Kbaso_FD_new_cell = optimvar('Kbaso_FD_new_cell', 1, "LowerBound", 0);
```

```
% Inner-Cell membrane values
```

```
Vi = optimvar('Vi', 1, "LowerBound", 0);
```

```
Ki = optimvar('Ki', 1, "LowerBound", 0);
```

```
%Z factor
```

```
% z = optimvar('z', 1);
```

```
%F-values includes Simple Diffusion, Facilitated Diffusion and Active
```

```
%Transport
```

$$F_{\text{apical}} = (\alpha / \text{vol}_{\text{apical}}) .* ((z.*X_{\text{cell\_linear}}) - X_{\text{apical\_linear}}) + \dots$$

$$y1 .* ( ((V_{\text{m\_apical\_FD}} .* (z.* X_{\text{cell\_linear}})) ./ (K_{\text{apical\_FD\_cell}} + (z.* X_{\text{cell\_linear}}))) \dots$$

$$- ((V_{\text{m\_apical\_FD}} .* X_{\text{apical\_linear}}) ./ (K_{\text{apical\_FD\_apical}} + X_{\text{apical\_linear}}));$$

$$F_{\text{cell}} = -1.*(\alpha / \text{vol}_{\text{apical}}) .* ((z.* X_{\text{cell\_linear}}) - X_{\text{apical\_linear}}) + \dots$$

$$-1.*(\alpha / \text{vol}_{\text{baso}}) .* ((z.* X_{\text{cell\_linear}}) - X_{\text{baso\_linear}}) + \dots$$

$$( (V_{\text{m\_apical\_FD}} .* X_{\text{apical\_linear}}) ./ (K_{\text{apical\_FD\_apical}} + X_{\text{apical\_linear}})) \dots$$

$$- (V_{\text{m\_apical\_FD}} .* (z.* X_{\text{cell\_linear}})) ./ (K_{\text{apical\_FD\_cell}} + (z.* X_{\text{cell\_linear}})) \dots$$

$$+ (V_{\text{m\_baso\_AT}} * X_{\text{baso\_linear}}) ./ (K_{\text{baso\_AT}} + X_{\text{baso\_linear}}) \dots$$

$$+ ( (V_{\text{m\_baso\_FD\_new}} .* X_{\text{baso\_linear}}) ./ (K_{\text{baso\_FD\_new\_baso}} + X_{\text{baso\_linear}})) \dots$$

$$- (V_{\text{m\_baso\_FD\_new}} .* (z.* X_{\text{cell\_linear}})) ./ (K_{\text{baso\_FD\_new\_cell}} + (z.* X_{\text{cell\_linear}})) \dots$$

$$- ( (V_i .* X_{\text{cell\_linear}}) ./ (K_i + X_{\text{cell\_linear}}));$$

$$F_{\text{baso}} = (\alpha / \text{vol}_{\text{baso}}) .* ((z.* X_{\text{cell\_linear}}) - X_{\text{baso\_linear}}) + \dots$$

$$y2 .* ( (V_{\text{m\_baso\_FD\_new}} .* (z.* X_{\text{cell\_linear}})) ./ (K_{\text{baso\_FD\_new\_cell}} + (z.*$$

$$X_{\text{cell\_linear}})) \dots$$

$$- (V_{\text{m\_baso\_FD\_new}} .* X_{\text{baso\_linear}}) ./ (K_{\text{baso\_FD\_new\_baso}} + X_{\text{baso\_linear}}) \dots$$

$$- (V_{\text{m\_baso\_AT}} * X_{\text{baso\_linear}}) ./ (K_{\text{baso\_AT}} + X_{\text{baso\_linear}}));$$

```
obj_apical = sum((F_apical(1:end) - f_apical).^2);
```

```
obj_cell = sum((F_cell(1:end) - f_cell).^2);
```

```
obj_baso = sum((F_baso(1:end) - f_baso).^2);
```

```
%Cumulative objective functions
```

```
obj = (obj_apical + obj_cell + obj_baso);
```

```
parameter_fit = obj;
```

```
end
```

```
Kinetic parameters solver
```

```
%Set the fixed parameters
```

```
variable_list = readTable('variables.xlsx');
```

```
min_conv = variable_list.Value(4); %Conversion from seconds to minutes
```

```
%Set the fixed variables
```

```
z = 1;
```

```
Vm_apical_FD = 2.25 * min_conv;
```

```
Kapical_FD_apical = 110.36;
```

```
% Kapical_FD_cell = 1227.86; %Adjust symmetric parameters
```

```
Kapical_FD_cell = 110.36;
```

```
Vm_baso_AT = 3.32 * min_conv;
```

```
Kbaso_AT = 29.04;
```

```
Vm_baso_FD_new = 5.98 * min_conv;
```

```
Kbaso_FD_new_cell = 628.255;
```

```
Kbaso_FD_new_baso = 628.255;
```

```
%Solving apical and basolateral additions simultaneously
```

```
obj_apical = all_unknowns_objective_function_I_value(1, z, Vm_apical_FD,
```

```
Kapical_FD_apical, Kapical_FD_cell, Vm_baso_AT, Kbaso_AT, Vm_baso_FD_new,
```

```
Kbaso_FD_new_cell, Kbaso_FD_new_baso); %Apical addition
```

```
obj_baso = all_unknowns_objective_function_I_value(2, z, Vm_apical_FD,  
Kapical_FD_apical, Kapical_FD_cell, Vm_baso_AT, Kbaso_AT, Vm_baso_FD_new,  
Kbaso_FD_new_cell, Kbaso_FD_new_baso); %Basolateral addition
```

```
%Solve simltaenously
```

```
objective = sum(obj_apical,obj_baso);
```

```
%Solve for apical addition objective functions only
```

```
% objective = obj_apical;
```

```
%Solve for basolateral addition objective functions only
```

```
% objective = obj_baso;
```

```
%Change the algorithm properties using the variables below
```

```
evals = 1e12;
```

```
max_iter = 1e12;
```

```
opt_tol = 1e-10;
```

```
func_tol = 1e-15;
```

```
step_tol = 1e-12;
```

```
options = optimoptions(@lsqnonlin,'MaxFunctionEvaluations',evals,'MaxIterations',max_iter,...  
  
    'StepTolerance',step_tol,...  
  
    'OptimalityTolerance',opt_tol,'FunctionTolerance',func_tol,'Algorithm', 'levenberg-marquardt');
```

```
%The least squares problem
```

```
lsqproblem = optimproblem("Objective",objective);
```

```
%Initial parameters (values that are not fixed)
```

```
% x0.z = 1;
```

```
x0.Vi = 10;
```

```
x0.Ki = 10;
```

```
%Optimization problem
```

```
[sol,~] = solve(lsqproblem,x0,'Options',options);
```

```
% show(lsqproblem)
```

disp('The z-factor value')

disp(z)

disp('The value of Vm\_apical\_FD (nM/min)')

disp(Vm\_apical\_FD)

disp('The value of Kapical\_FD\_apical (nM)')

disp(Kapical\_FD\_apical)

disp('The value of Kapical\_FD\_cell (nM)')

disp(Kapical\_FD\_cell)

disp('The value of Vm\_baso\_AT (nM/min)')

disp(Vm\_baso\_AT)

disp('The value of Kbaso\_AT (nM)')

disp(Kbaso\_AT)

disp('The value of Vm\_baso\_FD\_new (nM/min)')

disp(Vm\_baso\_FD\_new)

disp('The value of Kbaso\_FD\_new\_baso (nM)')

```
disp(Kbaso_FD_new_baso)
```

```
disp('The value of Kbaso_FD_new_cell (nM)')
```

```
disp(Kbaso_FD_new_cell)
```

```
disp('The value of inner compartment Vi (nM/min)')
```

```
disp(sol.Vi);
```

```
disp('The value of inner compartment Ki (nM)')
```

```
disp(sol.Ki);
```

```
%Apical Plots
```

```
X_apical = 88.85;
```

```
X_cell = 0;
```

```
X_baso = 0;
```

```
X_i = 0;
```

```
fig_index = 1;
```

```
all_unkowns_solver_plots_I_value(X_apical, X_cell, X_baso, X_i,...
```

```
Z,...
```

Vm\_apical\_FD, Kapical\_FD\_apical, Kapical\_FD\_cell,...

Vm\_baso\_AT, Kbaso\_AT,...

Vm\_baso\_FD\_new, Kbaso\_FD\_new\_cell, Kbaso\_FD\_new\_baso,...

sol.Vi, sol.Ki,...

fig\_index)

%Basolateral Plots

X\_apical = 0;

X\_cell = 0;

X\_baso = 82.9;

X\_i = 0;

fig\_index = 5;

all\_unkowns\_solver\_plots\_I\_value(X\_apical, X\_cell, X\_baso, X\_i,...

z,...

Vm\_apical\_FD, Kapical\_FD\_apical, Kapical\_FD\_cell,...

Vm\_baso\_AT, Kbaso\_AT,...

Vm\_baso\_FD\_new, Kbaso\_FD\_new\_cell, Kbaso\_FD\_new\_baso,...

sol.Vi, sol.Ki,...

fig index)

### Plotting with inner compartment

function combined\_vol\_output = all\_unkowns\_solver\_plots\_I\_value(X\_apical, X\_cell, X\_baso,

X\_i,...

Z,...

Vm\_a\_fd, Kt\_a\_1, Kt\_a\_2,...

Vm\_b\_AT, Kt\_b\_AT,...

Vm\_var\_2, Kt\_var\_c, Kt\_var\_b,...

Vi\_var, Ki\_var,...

fig\_counter)

global X\_initial %Define the initial concentrations for the layers (nM)

X\_initial = [X\_apical, X\_cell, X\_baso, X\_i]; %Initial concentrations for three layers

%%%The z-factor

global z

```
z = Z;
```

```
variable_list = readTable('variables.xlsx'); %Import the variables
```

```
%%%Defining the transport values for Facilitated diffusion (Apical and Cell)
```

```
global Vm_apical_FD %Maximum rate achieved (nM/min) (Apical compartment)
```

```
global Kapical_FD_apical %Substrate concentration (nM) for apical (Apical compartment)
```

```
global Kapical_FD_cell %Substrate concentration (nM) fo cell (Apical compartment)
```

```
Vm_apical_FD = Vm_a_fd; %Maximum rate achieved between apical and cell for  
Facilitated transporter
```

```
Kapical_FD_apical = Kt_a_1; %Substrate concentration for apical compartment to cell  
compartment for Facilitated transporter
```

```
Kapical_FD_cell = Kt_a_2; %Substrate concentration for cell compartment to apical  
compartment for Facilitated transporter
```

```
%%%Defining the transport values for Active Transport (Cell and Baso)
```

```
global Kbaso_AT    %Substrate concentration (nM)
```

```
global Vm_baso_AT %Maximum rate achieved (nM/min)
```

```
Vm_baso_AT = Vm_b_AT; %Maximum rate achieved between basolateral and cell for  
Active transporter
```

```
Kbaso_AT = Kt_b_AT; %Substrate concentration for basolateral-cell compartment for  
Active transporter
```

```
%%%Defining the transport values for inner compartment (Cell and Inner)
```

```
global Vi
```

```
global Ki
```

```
Vi = Vi_var;
```

```
Ki = Ki_var;
```

```
%%%Defining the transport values for the asymmetric (Cell and Baso)
```

```
global Vm_baso_FD_new
```

```

global Kbaso_FD_new_cell

global Kbaso_FD_new_baso

Vm_baso_FD_new    = Vm_var_2; %Define Vmax for FD in basolateral compartment

Kbaso_FD_new_cell = Kt_var_c; %Define Kbaso for FD wrt cell

Kbaso_FD_new_baso = Kt_var_b; %Define Kbaso for FD wrt baso

%%%%Time span for output

T    = variable_list.Value(8); %Time period

dt    = 0.1/60;

tspan = 0:dt:T;

%%%%Combined diffusion and active transport (Baseline)

ODE_X_baseline = @ODE_Combined_Diffusion_Active_Trasport_Baseline;

[~,X_CD_AT] = ode45(ODE_X_baseline, tspan, X_initial); %MATLAB ODE solver

combined_vol_output = X_CD_AT; %All the output values

```

```

apical_baseline_output = X_CD_AT(:,1); %Apical values

cell_baseline_output = X_CD_AT(:,2); %Cellular values

baso_baseline_output = X_CD_AT(:,3); %Basolateral values

%Solving for all the scenario that includes all the transport processes

ODE_X_scenario_1 = @ODE_Combined_Diffusion_Active_Trasport_Scenario;

[t,X_SC_1] = ode45(ODE_X_scenario_1, tspan, X_initial);

apical_sc1_output = X_SC_1(:,1); %Scenario apical concentration values

cell_sc1_output = X_SC_1(:,2); %Scenario cellular concentration values

baso_sc1_output = X_SC_1(:,3); %Scenario basolateral concentration values

i_sc1_output = X_SC_1(:,4); %Scenario inner concentration values

if gt(X_apical,X_baso)

    Title = 'Apical addition';

else

    Title = 'Basolateral addition';

```

end

%Importing values for experimental data from matlab

if gt(X\_apical , X\_baso) %Apical addition to Basolateral compartment

%Importing the Apical experimental values

apical\_exp\_values = xlsread('Apical\_addition','Apical');

apical\_exp\_mean = apical\_exp\_values(:,end-2); %Mean experimental values

apical\_exp\_std = apical\_exp\_values(:,end-1); %Std err experimental values

%Importing the Cellular experimental values

cell\_exp\_values = xlsread('Apical\_addition','Cell');

cell\_exp\_mean = cell\_exp\_values(:,end-2); %Mean experimental values

cell\_exp\_std = cell\_exp\_values(:,end-1); %Std err experimental values

%Importing the Basolateral experimental values

baso\_exp\_values = xlsread('Apical\_addition','Baso');

baso\_exp\_mean = baso\_exp\_values(:,end-2); %Mean experimental values

baso\_exp\_std = baso\_exp\_values(:,end-1); %Std err experimental values

```

time_span_exp    = apical_exp_values(1:end,1); %Time span for the experimental values

elseif lt(X_apical, X_baso)    %Basolateral addition to the Apical compartment

    %Importing the Apical experimental values

    apical_exp_values    = xlsread('Baso_addition','Apical');

    apical_exp_mean     = apical_exp_values(:,end-2); %Mean experimental values

    apical_exp_std      = apical_exp_values(:,end-1); %Std err experimental values

    %Importing the Cellular experimental values

    cell_exp_values     = xlsread('Baso_addition','Cell');

    cell_exp_mean      = cell_exp_values(:,end-2); %Mean experimental values

    cell_exp_std       = cell_exp_values(:,end-1); %Std err experimental values

    %Importing the Basolateral experimental values

    baso_exp_values     = xlsread('Baso_addition','Baso');

    baso_exp_mean      = baso_exp_values(:,end-2); %Mean experimental values

    baso_exp_std       = baso_exp_values(:,end-1); %Std err experimental values

```

```

    time_span_exp    = apical_exp_values(1:end,1); %Time span for the experimental values

end

%Plot of Concentration vs Time with the Experimental values superimposed

% Plotting the Apical compartment results

Figure(fig_counter)

plot(t, apical_baseline_output,'b', 'Linewidth', 4)

hold on

plot(t, apical_sc1_output, 'g', 'Linewidth', 4)

hold on

grid on

set(gca,'FontSize',28,'fontweight','bold')

set(gcf,'color','w');

title('Title','fontweight','bold');

xlabel('Time (minutes)','fontweight','bold');

ylabel('Apical Concentration (nM)','fontweight','bold');

hold on

```

```
plot(time_span_exp, apical_exp_mean,'r','Marker','o','MarkerSize',10,'Linewidth', 4)
```

```
hold on
```

```
errorbar(time_span_exp,apical_exp_mean,apical_exp_std,'r', 'Linewidth', 2)
```

```
legend({'Baseline', 'Additional Transporter','Experimental'},'FontSize',20)
```

```
% legend({'Simulated with Additional Transporter','Experimental'},'FontSize',20)
```

```
%Plotting the Cellular compartment results
```

```
Figure(fig_counter+1)
```

```
plot(t, cell_baseline_output, 'b', 'Linewidth', 4)
```

```
hold on
```

```
plot(t, cell_sc1_output, 'g', 'Linewidth', 4)
```

```
grid on
```

```
set(gca,'FontSize',28,'fontweight','bold')
```

```
set(gcf,'color','w');
```

```
title(Title,'fontweight','bold')
```

```
xlabel('Time (minutes)','fontweight','bold')
```

```
ylabel('Cellular Concentration (nM)','fontweight','bold')
```

```
hold on
```

```
% plot(time_span_exp, cell_exp_mean,'r','Marker','o','MarkerSize',10,'Linewidth', 4)
```

```
hold on
```

```
errorbar(time_span_exp,cell_exp_mean,cell_exp_std,'r', 'Linewidth', 2)
```

```
legend({'Baseline', 'Additional Transporter','Experimental'},'FontSize',20)
```

```
% legend({'Simulated with Additional Transporter','Experimental'},'FontSize',20)
```

```
%Plotting the Basolateral compartment results
```

```
Figure(fig_counter+2)
```

```
plot(t, baso_baseline_output, 'b', 'Linewidth', 4)
```

```
hold on
```

```
plot(t, baso_sc1_output, 'g', 'Linewidth', 4)
```

```
grid on
```

```
set(gca,'FontSize',28,'fontweight','bold')
```

```
set(gcf,'color','w');
```

```
title(Title,'fontweight','bold')
```

```
xlabel('Time (minutes)','fontweight','bold')
```

```
ylabel('Basolateral Concentration (nM)','fontweight','bold')
```

```
hold on
```

```

% plot(time_span_exp, baso_exp_mean,'r','Marker','o','MarkerSize',10,'Linewidth', 4)

hold on

errorbar(time_span_exp,baso_exp_mean,baso_exp_std,'r', 'Linewidth', 2)

legend({'Baseline', 'Additional Transporter','Experimental'},'FontSize',20)

% legend({'Simulated with Additional Transporter','Experimental'},'FontSize',20)

%

% Figure(fig_counter+3)

% nexttile

% hold on

% plot(t, apical_sc1_output, 'g', 'Linewidth', 4)

% hold on

% grid on

% set(gca,'FontSize',22,'fontweight','bold')

% set(gcf,'color','w');

% title(Title,'fontweight','bold');

% xlabel('Time (minutes)','fontweight','bold');

% ylabel('Apical Concentration (nM)','fontweight','bold');

% hold on

```

```

% plot(time_span_exp, apical_exp_mean,'r','Marker','o','MarkerSize',10,'Linewidth', 4)

% hold on

% errorbar(time_span_exp,apical_exp_mean,apical_exp_std,'r', 'Linewidth', 2)

%

% nexttile

% hold on

% plot(t, cell_sc1_output, 'g', 'Linewidth', 4)

% grid on

% set(gca,'FontSize',22,'fontweight','bold')

% set(gcf,'color','w');

% title(Title,'fontweight','bold')

% xlabel('Time (minutes)','fontweight','bold')

% ylabel('Cellular Concentration (nM)','fontweight','bold')

% hold on

% plot(time_span_exp, cell_exp_mean,'r','Marker','o','MarkerSize',10,'Linewidth', 4)

% hold on

% errorbar(time_span_exp,cell_exp_mean,cell_exp_std,'r', 'Linewidth', 2)

% hold on

```

```

% inner compartment plot comparison

% c = 0.9;

% inner_plot = cell_sc1_output + (1 - c).* i_sc1_output; %inner plot values

% plot(t,inner_plot, 'b', 'Linewidth', 2, 'LineStyle', '--')

%

% nexttile

% hold on

% plot(t, baso_sc1_output, 'g', 'Linewidth', 4)

% grid on

% set(gca,'FontSize',22,'fontweight','bold')

% set(gcf,'color','w');

% title(Title,'fontweight','bold')

% xlabel('Time (minutes)','fontweight','bold')

% ylabel('Basolateral Concentration (nM)','fontweight','bold')

% hold on

% plot(time_span_exp, baso_exp_mean, 'r', 'Marker', 'o', 'MarkerSize', 10, 'Linewidth', 4)

% hold on

% errorbar(time_span_exp, baso_exp_mean, baso_exp_std, 'r', 'Linewidth', 2)

```

```
end
```

```
%Combined Diffusion and Active transport function for baseline scenario
```

```
function dXdt = ODE_Combined_Diffusion_Active_Trasport_Baseline(~,X)
```

```
variable_list = readTable('variables.xlsx'); %Import the variables
```

```
%%Define the volume for each of the compartments (defined in cubic meters)
```

```
vol_apical = variable_list.Value(1);
```

```
vol_cell = variable_list.Value(2);
```

```
vol_baso = variable_list.Value(3);
```

```
%Half-life of Caco-2 cell
```

```
alpha = variable_list.Value(7);
```

```
global Kapical_FD_apical
```

global Kbaso\_AT

global Vm\_baso\_AT

global Vm\_apical\_FD

%Apical compartment: Simple diffusion and Facilitated diffusion

diff\_X1 = (-1 \* (alpha / vol\_apical) \* ((X(1) - X(2))))...

+ ((vol\_cell/vol\_apical) \* ((-1) \* (Vm\_apical\_FD\*X(1) / (Kapical\_FD\_apical + X(1))) +  
(Vm\_apical\_FD\*X(2) / (Kapical\_FD\_apical + X(2)))));

%Cellular compartment: Simple diffusion, Active transport and Facilitated

%diffusion

diff\_X2 = (-1 \* (alpha / vol\_cell) \* (X(2) - X(1))) + (-1 \* (alpha / vol\_cell) \* (X(2) - X(3)))...

+ ((Vm\_apical\_FD \* X(1)) / (Kapical\_FD\_apical + X(1))) + (-1) \* (Vm\_apical\_FD \* X(2) /  
(Kapical\_FD\_apical + X(2)))...

+ (Vm\_baso\_AT \* X(3) / (Kbaso\_AT + X(3)));

%Basolateral compartment: Simple diffusion and Active transport

```

diff_X3 = (-1 * (alpha / vol_baso) * ((X(3) - X(2))))...
+ (-1 * (vol_cell / vol_baso) * (Vm_baso_AT*X(3) / (Kbaso_AT + X(3))));

dXdt = [diff_X1; diff_X2; diff_X3];

end

%Combined Diffusion and Active transport function for scenarios (with z
%factor)

function dXdt = ODE_Combined_Diffusion_Active_Trasport_Scenario(~,X)

variable_list = readTable('variables.xlsx'); %Import the variables

%%Define the volume for each of the compartments (defined in cubic meters)

vol_apical = variable_list.Value(1);

vol_cell = variable_list.Value(2);

vol_baso = variable_list.Value(3);

vol_i = variable_list.Value(9);

```

%Half-life of Caco-2 cell

alpha = variable\_list.Value(7);

global z

global Vm\_apical\_FD

global Kapical\_FD\_apical

global Kapical\_FD\_cell

global Kbaso\_AT

global Vm\_baso\_AT

global Vm\_baso\_FD\_new

global Kbaso\_FD\_new\_cell

global Kbaso\_FD\_new\_baso

global Vi

global Ki

%Apical compartment: Simple diffusion and Facilitated diffusion

$$\text{diff\_X1} = (-1 * (\alpha / \text{vol\_apical}) * ((X(1) - (z*X(2)))) + \dots$$

$$((\text{vol\_cell}/\text{vol\_apical}) * ((-1) * (\text{Vm\_apical\_FD}*X(1) / (\text{K\_apical\_FD\_apical} + X(1)))) \dots$$

$$+ (\text{Vm\_apical\_FD}*(z*X(2)) / (\text{K\_apical\_FD\_cell} + (z*X(2)))));$$

%Cellular compartment: Simple diffusion, Active transport and Facilitated

%diffusion from the apical and basolateral compartments and inner

%compartment

$$\text{diff\_X2} = (-1 * (\alpha / \text{vol\_cell}) * ((z*X(2)) - X(1))) + (-1 * (\alpha / \text{vol\_cell}) * ((z*X(2)) - X(3))) \dots$$

$$+ (((\text{Vm\_apical\_FD} * X(1)) / (\text{K\_apical\_FD\_apical} + X(1))) - (\text{Vm\_apical\_FD} * (z*X(2)) / (\text{K\_apical\_FD\_cell} + (z*X(2)))) \dots$$

$$+ (\text{Vm\_baso\_AT} * X(3) / (\text{K\_baso\_AT} + X(3))) \dots$$

$$+ ((\text{Vm\_baso\_FD\_new} * X(3) / (\text{K\_baso\_FD\_new\_baso} + X(3))) \dots$$

$$- ((\text{Vm\_baso\_FD\_new} * (z*X(2))) / (\text{K\_baso\_FD\_new\_cell} + (z*X(2)))) \dots$$

$$- ((\text{Vi} * X(2)) / (\text{Ki} + X(2)));$$

%Basolateral compartment: Simple diffusion, Active transport and Facilitated diffusion

```

diff_X3 = (-1 * (alpha / vol_baso) * ((X(3) - (z*X(2)))))...

+ (-1 * (vol_cell / vol_baso) * (Vm_baso_AT*X(3) / (Kbaso_AT + X(3))))...

+ (-1 * (vol_cell / vol_baso) * (((Vm_baso_FD_new * X(3)) / (Kbaso_FD_new_baso +
X(3))))...

- (Vm_baso_FD_new * (z*X(2)) / (Kbaso_FD_new_cell + (z*X(2)))));

```

```

%Inner compartment

```

```

diff_X4 = (vol_cell / vol_i) * (Vi * X(2) / (Ki + X(2)));

```

```

dXdt = [diff_X1; diff_X2; diff_X3; diff_X4];

```

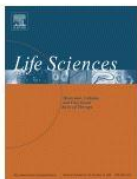
```

end

```

## C. Copyright licences

### C.i Copyright licence for first paper



Involvement of Organic Cation Transporter 2 and a Na<sup>+</sup>-dependent active transporter in p-tyramine transport across Caco-2 intestinal cells

Author: Shreyasi Sarkar, Mark D. Berry

Publication: Life Sciences

Publisher: Elsevier

Date: 15 July 2020

© 2020 Elsevier Inc. All rights reserved.

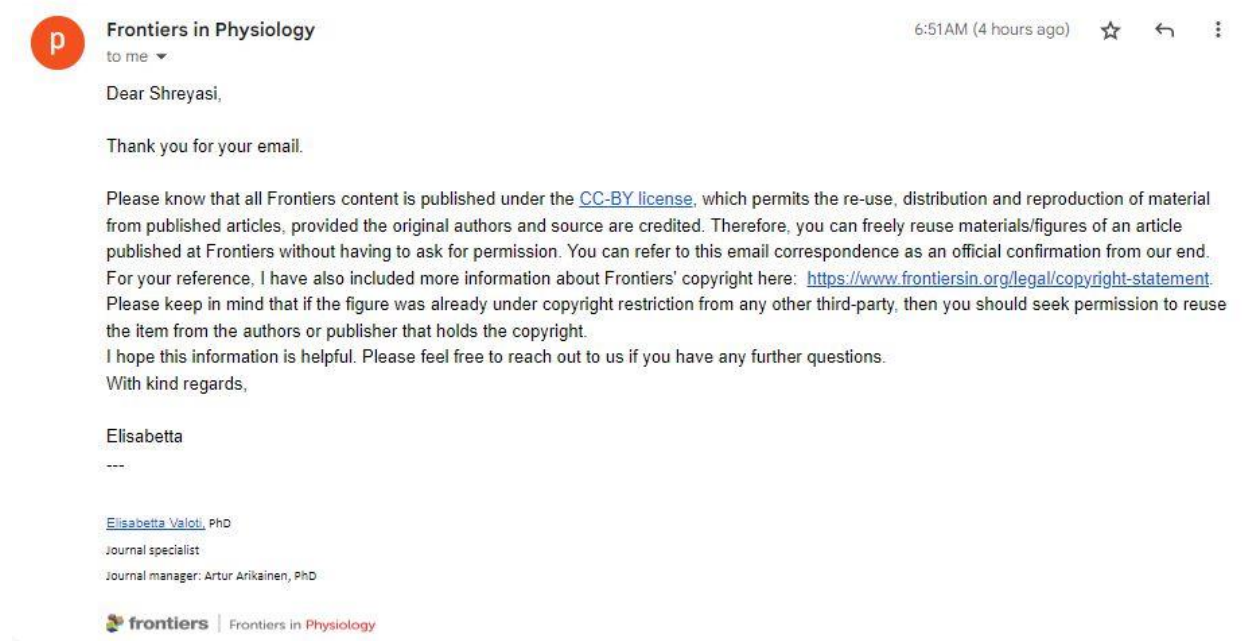
#### Journal Author Rights

Please note that, as the author of this Elsevier article, you retain the right to include it in a thesis or dissertation, provided it is not published commercially. Permission is not required, but please ensure that you reference the journal as the original source. For more information on this and on your other retained rights, please visit: <https://www.elsevier.com/about/our-business/policies/copyright#Author-rights>

BACK

CLOSE WINDOW

## C.ii Copyright licence for second paper



Link to Frontiers in Physiology copyright statement: <https://www.frontiersin.org/legal/copyright-statement>